

**Thermal Impact on the Damaged Zone Around a Radioactive Waste
Disposal in Clay Host Rocks**

TIMODAZ

Deliverable 2

STATE OF THE ART ON THMC

Technical annex 1

**This document (version 31/10/07) is a draft version of the document
"TIMODAZ Deliverable 2: STATE OF THE ART ON THMC"**

**This document should deliver the necessary background information to
the end users group for the review of the TIMODAZ project.**

Table of content

1	Introduction	4
2	Main issues related to the thermal impact	5
2.1	Boom Clay	5
2.1.1	Temperature evolution in the Host Rock in the Belgian repository designs	6
2.1.2	Thermal effects on the host rock	8
2.1.3	Thermal impact on the geochemical aspects	9
2.1.4	Thermal impact on the lining stability	9
2.2	Opalinus Clay	9
2.2.1	Near field temperature evolution in the Swiss repository design	10
2.2.2	Thermal effects on the host rock in the near field	11
2.2.3	Impact of thermal damage in the tunnel nearfield onto performance assessment	12
2.3	Callovo-Oxfordian Clay	12
2.3.1	Near field temperature evolution in the French repository designs	13
2.3.2	Thermal Effects on the hydro-mechanical behaviour of the disposal cells	14
2.3.3	Thermal Impact on the conditions of solute transfer	16
2.3.4	Thermal impact on geochemical processes	17
3	Terminology	19
4	State of the art for Boom Clay	20
4.1	Main characteristics	20
4.2	THM characterization in lab	22
4.2.1	Short term THM behaviour	22
4.2.1.1	WASUK project (EUR 10987)	22
4.2.1.2	WASI 380.83.7 (EUR 10924) and FI1W/0150 (EUR 13365) projects	29
4.2.1.3	INTERCLAY II project (EUR 16204 EN)	36
4.2.1.4	PhD thesis of N. Sultan	36
4.2.1.5	PhD thesis of D. De Bruyn	40
4.2.2	Time related THM behaviour	41
4.2.2.1	PhD thesis of G. Rousset	42
4.2.2.2	CEC contract FI1W/0049 (EUR 14438 FR)	44
4.2.2.3	Contract ONDRAF – G3S (Report G3S, n° 94-002)	45
4.2.2.4	EC SELFRAC project	47
4.2.3	Unsaturated hydro-mechanical behaviour	51
4.2.4	Main remarks on the performed laboratory works	52
4.3	THM characterization in-situ	54
4.3.1	CERBERUS test (EUR 18151 EN)	54
4.3.2	Mine – By test (EUR 13985 and EUR 15719)	57
4.3.3	ATLAS in situ test (part of INTERCLAY II project: EUR 16204)	60
4.3.4	BACCHUS 2 tests (EUR 16860 EN/FR)	62
4.3.5	PHEBUS test (EUR 17792 FR)	64
4.3.6	Shaft RESEAL test	64
4.3.7	CACTUS I & II (EUR 15482 and EUR 17558 EN)	67
4.3.8	CLIPLEX project (EUR 20619 EN)	70
4.3.9	SELFAC in situ experiment	72
4.3.10	General remarks on the realised in situ experiments in the URF of Mol	74
4.4	Modelling	74
4.4.1	Saturated elastoplastic models at ambient temperature (p'-q plan)	75
4.4.2	Unsaturated elastoplastic model at ambient temperature (p-q-s space)	76
4.4.3	Saturated thermo-elastoplastic models (p'-q-T space)	77
4.4.4	Saturated thermo-elasto-visco-plastic models	79
4.4.5	Applications (Validations – Simulations – Predictions)	80
4.4.6	Future modelling development	83

4.5	THM behaviour of Boom Clay – Synthesis	83
4.5.1	Hydro-Mechanical behaviour of the "intact" Boom Clay observed in labs	83
4.5.2	Construction phase – Effect of the excavation	85
4.5.3	Open drift phase	89
4.5.4	Early closure phase	89
4.5.5	Late closure phase	91
4.5.6	Open questions	91
4.6	Related chemical aspects	92
4.6.1	The geochemistry of the Boom Clay under natural conditions	93
4.6.1.1	The geochemistry of the Boom Clay at the reference site in Mol	93
4.6.1.2	Regional variations in the geochemistry of the Boom Clay	96
4.6.2	Geochemical perturbations in Boom Clay	96
4.6.2.1	Oxidation	96
4.6.2.2	Alkaline plume	97
4.6.2.3	Heat/Radiation	99
4.7	Discussion	104
5	<i>State of the art for the Opalinus clay</i>	110
5.1	Main characteristics	110
5.2	THM characterization in lab	113
5.2.1	Mechanical properties	114
5.2.2	Thermal properties	116
5.3	THM characterization in-situ – Experiment and modelling	120
5.4	Chemical aspects related to heating of the host rock	145
5.5	Discussion	145
6	<i>Thermo-hydro-mechanical behaviour of Callovo-Oxfordian argillite</i>	148
6.1	Main characteristics	148
6.1.1	Geological setting	148
6.1.2	Mineralogy and porewater chemistry of the Callovo-Oxfordian argillites	149
6.1.3	Mechanical properties of the Callovo-Oxfordian argillites	150
6.1.4	Thermal conductivity	151
6.1.5	Specific heat	153
6.2	Thermohydromechanical characterisation in laboratory	153
6.2.1	Observation of temperature impact on samples	153
6.3	In-situ thermo-hydromechanical characterisation	160
6.3.1	Monitoring of thermal disturbance during the REP experiment	160
6.3.2	The TER experiment	161
6.4	Related chemical aspects	166
6.4.1	Experimental characterisation of mineralogical transformations	166
6.4.2	Modelling of the geochemical evolution under temperature conditions	172
6.5	THM modelling	175
6.5.1	Analytical and numerical thermal calculations	176
6.5.2	Numerical modelling of the REP experiment	178
6.5.3	Numerical modelling of the TER experiment	180
7	<i>References</i>	195

1 Introduction

In all nuclear power generating countries, spent nuclear fuel and/or long lived radioactive-waste management is an important environmental issue today. Disposal in deep clay geological formations is one of the promising options to dispose of these wastes. An important item for the long-term safety of underground disposal is the proper evaluation of the Damaged Zone (DZ) in the clay host rock. The DZ is first initiated during the repository construction. Its behaviour is a dynamic problem that depends on the changing conditions during the open-drift period, the initial closure period and the entire heating-cooling cycle of the decaying waste. Other factors concern the even longer-term issues of chemical reactions and biological activities.

In recent years, there have been intense efforts to evaluate the extent and properties of the Excavation Damaged Zone (EDZ), the DZ initiated during the repository construction, involving field, laboratory, and theoretical studies (as in the recently terminated EC project SELFRAC). Performance assessment models for different repository designs in different clay formations have demonstrated that even for rather unfavourable EDZ conditions the overall performance of the repository system is not adversely affected and that dose rates remain well below regulatory guidelines.

The influence of the temperature on the clay host rock has also been studied in previous research projects. The THM characterization was mainly performed on samples in surface laboratory and from small/medium scale in-situ heater tests. At the same time, different THM models and numerical codes were developed to better understand the THM processes. However, the influence of the thermal load generated by the radioactive waste on the performance of the disposal system has only been studied at a limited scale of time and space compared to a real repository. This aspect is particularly important since the early transient THM (Thermo-Hydro-Mechanical) perturbation might be the most severe impact the repository system will undergo on a large spatial scale and in a relatively short period of time. Assessing the consequence of the thermal transient on the performance of the disposal system will be the main objective of the proposed TIMODAZ project. Even the full THMC (Thermo-Hydro-Mechanical-Chemical) coupling aspect will be studied, the effect of temperature on the chemistry will be investigated in a more limited extent. The TIMODAZ project will focus on the significance of THM processes, in the context of the safety case. Especially the combined effect of the EDZ and the thermal impact on the host rocks around a radioactive waste disposal. The influence of the temperature increase on the EDZ evolution as well as the possible additional damage created by the thermal load will be investigated.

The present report gives a synthesis of the relevant works previously performed on the three investigated clays (Boom Clay, Opalinus Clay and Callovo-Oxfordian Argillite) in surface laboratories and in in-situ facilities. It comprises a database and a reference document to optimise the testing procedures of the laboratory experiments and the in-situ experiments to be performed in the present project.

The first part of the report points out the main issues related to the thermal impact, which should reflect the viewpoints of end users. The second part is devoted to the state of the art for each investigated clay, including the main characteristics of each clay, the available THM characterisation, the related chemical aspects and the current development of the constitutive models. For each clay the report provides a discussion in order to:

- delineate the most important temperature-dependent material properties
- define the most important coupled processes and parameters
- assess the effect of discrete fractures and fracture connectivity on the effective hydraulic properties, to determine the importance of chemical impact

- derive/evaluate the most appropriate conceptual models and numerical codes as well as to notice the remaining uncertainties on the THM properties of the clays

This version is considered to be the technical annex of the synthetic version of Deliverable 2. State of the Art of the Laboratory Experiments on the THM Behaviour realised on the Opalinus Clay and the Callovo-Oxfordian Clay is given in annex separately too. The appendix will be integrated in chapter 5 & 6 in the final version of the document.

2 Main issues related to the thermal impact

The disposal of heat emitting radioactive waste will induce disturbances in the host rock. The impact of the thermal load is particularly important since it will affect the temperature and the stress in the host rock to a large spatial extent (depending on the repository design) around the repository.

The disturbances can be of different types and are often coupled: thermal (T), hydraulic (H), mechanical (M) and chemical (C). The THMC responses will highly depend on the initial and the boundary conditions imposed by the repository design, as for example:

- the hydraulic boundary conditions around the waste imposed by the repository design
- the pore pressures reached around the disposal gallery before the waste disposal
- the mechanical conditions imposed by the lining
- etcetera

The overpressure generated in the host rock by the temperature rising depends highly on the hydraulic boundary conditions of the disposal gallery. This will in turn be controlled by the hydraulic properties of the seal closing the disposal gallery and by the saturation of the engineered components reached before the disposal of the waste. The thermal induced pore pressure build-up will be much more pronounced if a rather impermeable hydraulic boundary condition is assumed (as revealed by the scoping calculations, see technical annex 2). The impermeable boundary condition constitutes therefore a more critical situation for the host rock.

During the open drift period, pore water will flow from the host rock towards and into the disposal tunnels. Depending on the different national concepts and especially on regulatory guidelines with respect to monitoring and reversibility, such open drift phases could range from one month to a few years. On the one hand, the long term drainage of the disposal gallery will enhance the hydromechanical coupling due to the pore pressure drop and induce contracting strains that are able to create additional plastic deformation and/or damage (micro-macro) and thus increase the DZ that may have been limited by tunnel support. On the other hand, this may constitute, from a purely thermohydromechanical point of view, a favourable factor (less thermal induced pore pressure build-up) for the safety of the repository system. Meanwhile, the open drift will be ventilated and suction (possibly partial de-saturation) could evolve in the rock close to the tunnel wall. This suction could improve the hydro-mechanical properties of the rock (decrease the permeability and increase the shearing strength). However, the excess desaturation may evoke additional damage through tensile failure and will affect the THMC coupled responses of the repository system (oxidation, etc.). The long term drainage also favours the sealing process as observed in Boom Clay around the URL HADES.

Consequently, the maximum thermal source term is not the only issue to be considered when assessing the thermal impact of heat emitting waste. Other design issues controlling the hydraulic conditions of the repository system are also important to be taken into account.

Hereafter more specific issues related to the three considered clays (Boom Clay, Opalinus Clay and Callovo-Oxfordian Argilite) are given.

2.1 Boom Clay

2.1.1 Temperature evolution in the Host Rock in the Belgian repository designs

In the Belgian disposal system for the vitrified High Level radioactive Waste and Spent Fuel, the Boom Clay host-rock is the main barrier for the long term isolation in the normal evolution scenario. The waste packages will be disposed of in a network of horizontal galleries in the Boom Clay host formation.

The safety function of the host rock is delaying and spreading the radionuclide release. The Boom Clay will slow down the migration of radionuclides towards the biosphere allowing radioactive decay within the disposal system. In order to prevent any alteration of the favourable physico-chemical properties of the repository components and those of the host rock, a criterion for the admissible maximum temperature in the different parts of the disposal system was established. In particular, the maximum temperature in the host rock must be kept below 100°C (NIROND 2001-05). A sufficiently long cooling time of the radioactive waste (intermediate storage), a suitable canister and gallery spacing are necessary.

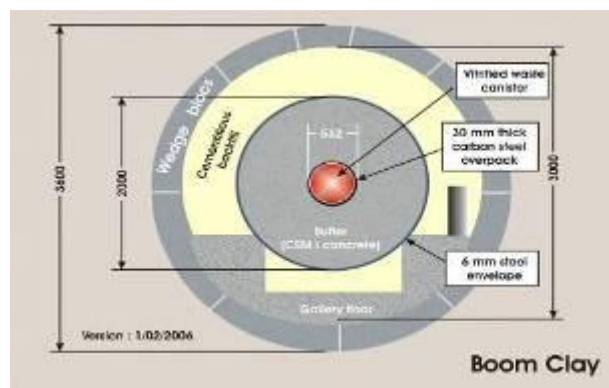
NIRAS/ONDRAF is now considering three alternative designs (NIROND 2003-01):

- the Supercontainer (SC)
- the Borehole
- the Sleeve

Based on a multi criteria analysis, the Supercontainer design was selected as the preferred option (NIROND 2004-03). However, NIRAS/ONDRAF considers the two other options as possible alternatives (borehole and sleeve).

The *Supercontainer* design for vitrified waste considers disposal of two vitrified Cogema canisters in a carbon steel overpack, surrounded by a concrete buffer (see Figure 2.1). The heat produced by the Supercontainers will increase the temperature in the near field, in the Boom Clay host formation and even in the aquifers during several hundred of years.

The *Supercontainer* design for spent fuel is very similar¹ to the design mentioned above but in this case four assemblies of spent fuel UOX (or one assembly of MOX) will be placed in a carbon steel container instead of a common overpack. The maximum heat flux (W/gallery length) produced by the *Supercontainer* for spent fuel is very comparable to the case of vitrified waste (about 240W/m) but the thermal period will extent to several thousand of years.



¹ The supercontainers for spent fuels have a length of about 6 m instead of 4 m for the supercontainer for vitrified waste.

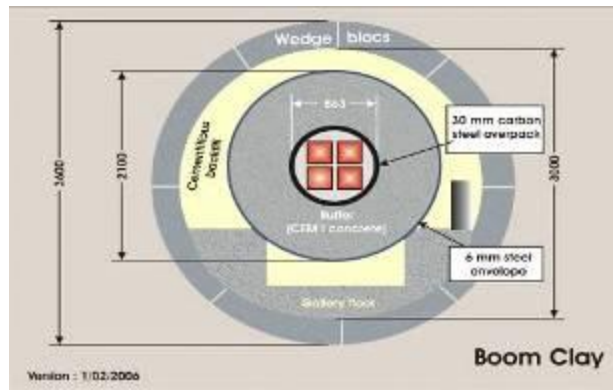
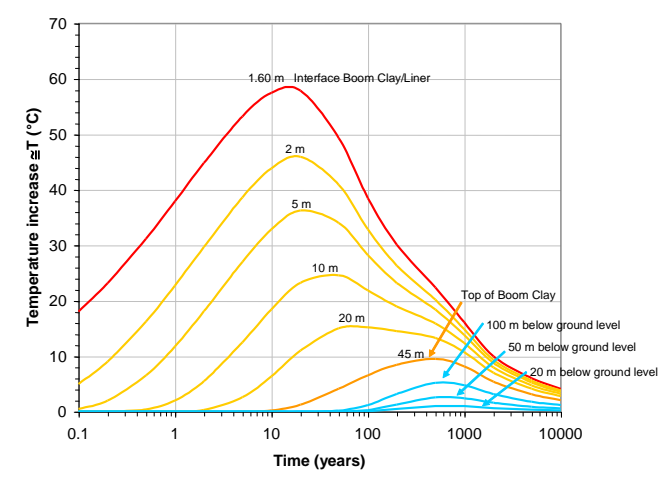


Figure 2.1: ONDRAF/NIRAS reference design (anno 2006) for vitrified waste (above) and spent fuels (below)

Different calculations have been made to assess the maximum temperatures in the engineered barriers and the Boom Clay for different cooling periods and the different waste types (vitrified waste, UOX and MOX), considering the Supercontainer designs (Weetjens & al. 2005). The disposal gallery spacing is about 50m for the galleries with vitrified waste while it is extended to about 120m for the galleries with spent fuels. This repository geometry (i.e. the gallery spacing) implies that, for the same cooling period², the maximum temperatures in the Boom Clay will be slightly higher (10% up to 15%) for spent fuel than for vitrified waste (Figure 2.2). For an OPC concrete buffer and a cooling period of 50 years, the maximum calculated temperature for vitrified waste at the interface Boom Clay/liner is 65°C ($\Delta T = 49^\circ\text{C}$) and 74°C ($\Delta T = 58^\circ\text{C}$) in the case of spent fuel. It is worth to note that the above calculations were based on the actual knowledge on the thermal properties of the Boom Clay on which uncertainty still exists. Especially the thermal conductivity will largely affect the final geometry of the repository (especially the gallery spacing).



² $t=0$ is defined as the time when the waste is produced in its final form, i.e. vitrification of the reprocessing waste and unloading from the reactor for the spent fuel.

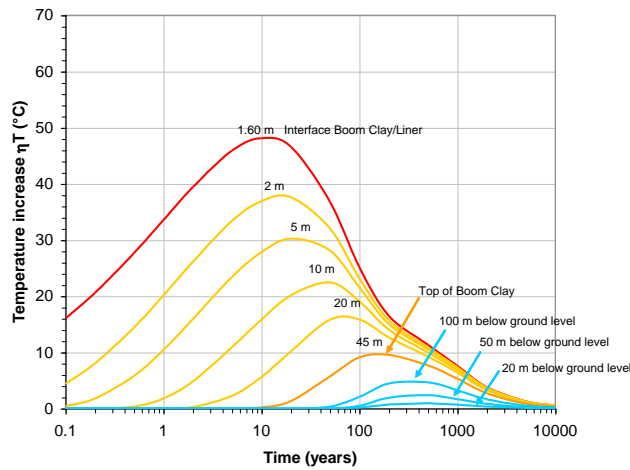


Figure 2.2: Maximum temperatures in Boom Clay for the supercontainer design for (above) spent fuel (50y cooling, 120m gallery spacing) and for (below) vitrified waste (50y cooling, 50m gallery spacing)

2.1.2 Thermal effects on the host rock

A good comprehension of the inter-related processes in the Boom Clay around the repository is an essential element of confidence building to assess to what extent the favourable properties of this clay are, temporarily or permanently, altered according to the safety function. These favourable properties are the low permeability, good sorption and retention capacity for radionuclides, the slow diffusive transport capability combined with the absence of preferential migration pathways for solutes and the sealing capacities.

The construction of the disposal infrastructure and the repository components (RC) will induce disturbances in the Boom Clay. The time and spatial evolution of the THMC disturbances around a disposal gallery are schematically represented on Figure 2.3.

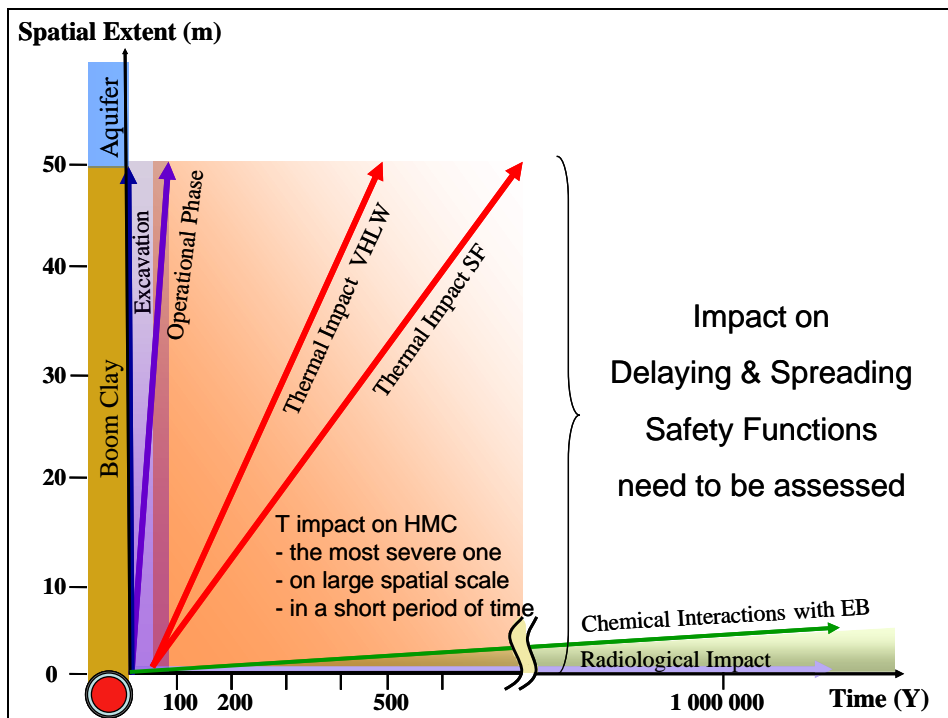


Figure 2.3: Time and spatial evolution of the disturbed zone (dZ) around a disposal gallery

Different sources of disturbances can be distinguished:

- disturbances created by the construction of the disposal infrastructure and by the operational phase: these disturbances will affect the hydro-mechanical conditions of the Boom Clay and concern the whole thickness of Boom Clay
- disturbances created by the large scale thermal load generated by the waste: these disturbances can affect a) the hydro-mechanical conditions of the Boom Clay at short term (0 to 500 years for the vitrified waste and 0 to 2000 years for the spent fuel) and concern the whole thickness of Boom Clay; b) the diffusion coefficient c) the chemical conditions in the near field, which could induce changes in the transport properties. However disturbances b) and c) are expected to be very limited for the considered temperatures and temperature gradients
- disturbances created by the chemical interactions with the repository components: these disturbances will be mainly limited to the near field and concern the long term (several thousand of years)
- disturbances created by the radiation of the waste: these disturbances can affect the near field when the thickness of the repository components surrounding the waste is small (this is the case for the borehole design, which consists in inserting the waste package directly into the lined borehole). The CERBERUS experiment demonstrated that the extent of these disturbances can be expected to be limited taking (Noynaert & al., 2000). Simple radiolysis calculations lead to a similar conclusion

Consequently the early THM perturbation created by the excavation, the operational phase and the thermal load might be the most severe transient that the repository will undergo on a large spatial scale and in a relatively short period of time. Given an identical thermal flux, the temperature profiles around the disposal galleries will be very similar independently of the considered design and are mainly determined by the thermal properties of the Boom Clay under saturated condition.

The repository design can significantly influence the disturbances in the Boom Clay. The major affecting factors are the HM conditions prevailing the heating phase: the pore water pressure and stress profiles in the Boom Clay, the saturation degree of the repository components and the hydraulic boundary conditions imposed by the repository design. These factors will have a direct impact on the maximum pore water pressure build-up reached during the heating phase. For example, the longer the drainage phase before the disposal of the waste, the lower the maximum pore pressure during the heating phase.

2.1.3 Thermal impact on the geochemical aspects

The temperature increase can also affect the chemistry of the host rock. Recent experimental work in collaboration with l'Institut Français de Pétrole (IFP) has shown the quick release of CO₂ from Boom Clay kerogen, even at a moderate temperature increase. H₂S release is also expected but to a smaller extent. This rising temperature will likely cause changes in clay mineralogy and pore water chemistry. These geochemical perturbations could have a potential impact on the integrity and the performance of Boom Clay as a geological barrier. Therefore they demand a further investigation.

2.1.4 Thermal impact on the lining stability

The thermal load can also affect the stability of the disposal gallery lining. Calculations show that the temperature increase can induce high stresses in the lining. The use of compressive materials between the concrete lining blocks could be a solution to limit these stresses. This issue is particularly important when the retrievability of the waste is considered.

2.2 Opalinus Clay

2.2.1 Near field temperature evolution in the Swiss repository design

The design of a possible geological repository for high-level radioactive waste that has been used to demonstrate the feasibility of such a repository at a potential site in NE Switzerland (Nagra 2002a) is based on a multiple barrier concept. Canisters containing radioactive waste are emplaced into tunnels drilled into the Opalinus Clay. The tunnels are backfilled with a mixture of bentonite and sand (Figure 2.4). In order to maintain the favourable chemical properties of the backfill material the peak temperature of a predefined part of the bentonite will be kept sufficiently low to prevent significant mineralogical or chemical alteration of the material. This is ensured by a sufficiently long intermediate storage time of the radioactive waste, an appropriate canister loading (mixing of MOX and UO₂ spent fuel elements) and a suitable canister spacing. These requirements for the backfill material also limit the thermal load on the surrounding rock.

Numerical simulations show that with an intermediate storage time of 40 years these requirements can be met (Nagra 2002b). The canisters, which have an average initial heat output of 1500 W, reach a peak temperature shortly after backfilling of 150 degree on their outsides (Figure 2.5). The temperature field in the surrounding bentonite material and the host rock depend strongly on the water content of the backfill material. This water content is controlled by the water flow rates towards the repository which are in turn limited by the permeability of the Opalinus Clay. Resaturation is expected to take a few hundred years. In the unsaturated case the bentonite has a low thermal conductivity and the temperature at the point midway between the spent fuel canisters and the bentonite / host rock interface will reach a maximum of 110 °C. Host rock temperatures remain below 90 °C in the base case. Rapid saturation of the near field occurs within decades and would lead to significantly lower temperatures (10 to 20 °C lower at the mid-bentonite position).

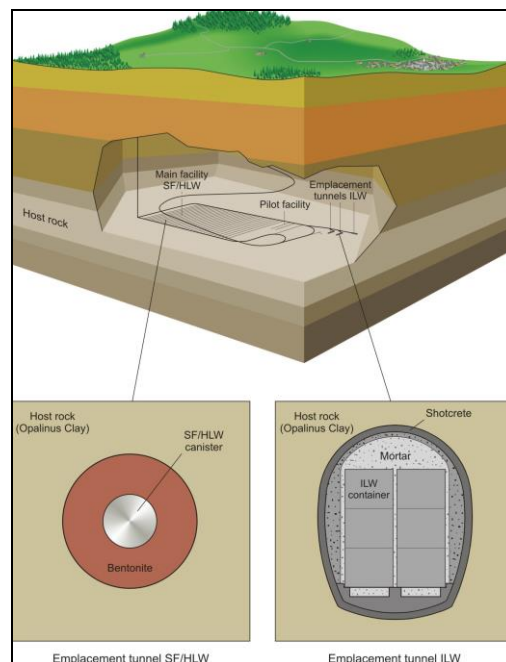


Figure 2.4: Possible layout for a deep geological repository for Spent Fuel, High Level Waste, Intermediate Level Waste (SF / HLW / ILW) in Opalinus Clay (Nagra 2002a).

The strong dependence of near field temperatures on bentonite thermal conductivity leads to some uncertainty in temperatures within the bentonite because groundwater inflow rates are uncertain. Smaller uncertainties in predicted temperatures (approximately 10 °C) arise from uncertainty in the values of thermal conductivity assumed for the host rock. In any case, there is relatively little uncertainty regarding the maximum projected temperatures at the bentonite-canister interface since the maximum temperature is reached within only 10 years, i.e. when this region is still dry.

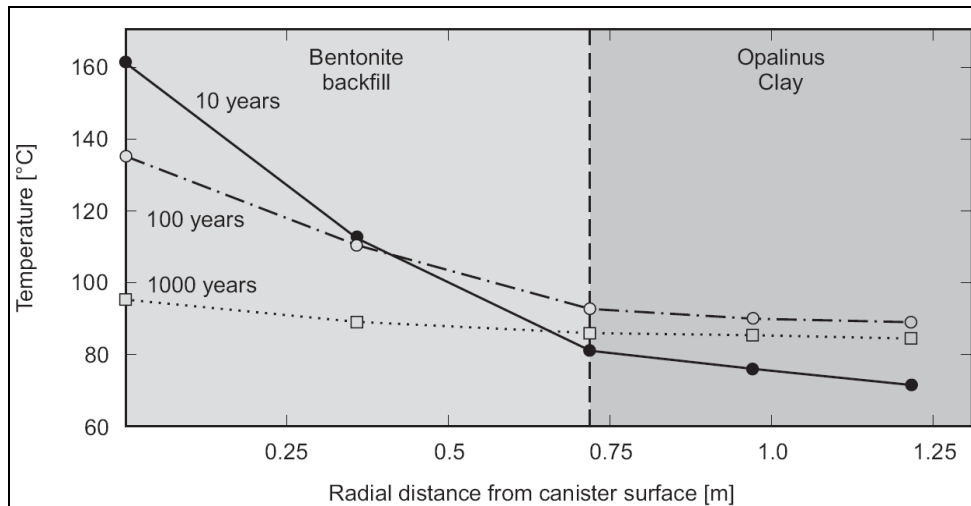


Figure 2.5: Time-dependent temperature evolution at various positions within the engineered barrier system and surrounding rock for canisters containing four spent fuel assemblies. The bentonite is assumed to have a thermal conductivity of $0.4 \text{ W m}^{-1} \text{ K}^{-1}$ and a heat capacity of $1.2 \text{ MJ m}^{-3} \text{ K}^{-1}$. The initial ambient temperature is $38 \text{ }^\circ\text{C}$. Canisters have a heat output of 1490 W at the time of waste emplacement in the repository (Nagra 2002b).

2.2.2 Thermal effects on the host rock in the near field

In indurated clays several heat sensitive processes may affect the state and the properties of the tunnel nearfield. These are for example damage caused by temperature induced stresses (crack growth), increased pore pressures, chemical and mineralogical changes in the host rock that affect its barrier function.

Investigations at the Aspo URL and the Canadian URL show that thermally induced damage on a micro scale is detectable in crystalline rock by acoustic emission (AE) monitoring. Analysis of AE time series shows that the damage accumulation depends mainly on (1) thermal gradients over time and (2) minimum stress (e.g. Read *et al.* 1997). Similar dependencies can be expected for indurated clays but the strong hydromechanical coupling introduces some additional complexities.

Thermal expansion of fluids is generally by an order of magnitude larger than that of solids. As a result fluid saturated porous rocks like the Opalinus Clay show a pore pressure increase during heating (Wileveau, 2005). The increased pore pressure reduces the effective stresses and may destabilize critically loaded regions around excavations and enlarge the damaged zone. Similar to crystalline rocks, the temporal and spatial gradients of heating are important. If the nearfield is already desaturated or drainage from the heated and pressurized region is possible and operates at similar rates as the heating, the pore pressure built-up may be considerably reduced. However, both lab data and field experiments relating pore pressures and heating rate in the Opalinus Clay are scarce. This highlights the need for new laboratory and field investigations of THM coupling in the Opalinus Clay.

Thermally assisted weakening of the Opalinus Clay has been postulated in a few studies. Tests with samples at natural water content show that the short term strength is significantly reduced by heating. In contrast, creep rates do not differ much between room temperature and $80 \text{ }^\circ\text{C}$. This may indicate that the increase of the pore pressure plays a more important role for the strength reduction than the temperature assisted growth of defects.

Chemical or mineralogical changes in the Opalinus Clay due to heating in the nearfield are unlikely. Possible effects would include (1) maturation of organic material that leads to the production of carbohydrates or changes in the pore water chemistry, (2) the transition of smectite to illite in the composite clay minerals that leads to an embrittlement of the material and a partial loss of the swelling capacity, (3) an acceleration of oxidation reactions ensuing from a change in porosity and pore water chemistry, (4) the re-adjustment of chemical equilibrium reactions. However,

experimental data, natural analogues and chemical model calculations show that heating of 85 to 95 °C for a few hundred years is insufficient to induce any significant impact by the above mechanisms (Mazurek 2002).

In the context of the entire repository system the potential for damage in the tunnel nearfield due to heating is considerably reduced. In the Swiss concept of a high level waste repository the nearfield will be desaturated during the excavation and operation of the tunnels. The resaturation is limited by the permeability of the host rock and will take several hundred years. This has several consequences. On the one hand the bentonite buffer will retain its low thermal conductivity throughout the rise of the canister temperatures in the first decades. Consequently the heating of the host rock will be slow, thus decreasing the likelihood of any thermal damage. On the other hand pore pressures that reduce the effective stresses cannot increase while the rock is not re-saturated. Hence, desaturation of the nearfield and thermal isolation of the canisters by the bentonite material protect the nearfield host rock from excessive thermal damage.

2.2.3 Impact of thermal damage in the tunnel nearfield onto performance assessment

In order to assess the importance of the host rock properties in the vicinity of the underground excavations the entire repository system has to be taken into account. Such an evaluation has been done in a performance assessment of the Swiss repository concept (Nagra 2002a). In this study all relevant components and properties of the repository system have been included and their performance has been evaluated in terms of the calculated radiation exposure for an individual of the most affected group living in the surface environment.

It shows that for rock masses with low hydraulic conductivity and no natural water-conducting features, the flow through the EDZ is mainly limited by the inflow from the undisturbed rock into the tunnels and partly by the effectiveness of the seals (Nagra 2002a). Even without seals, the flow along tunnels levels off at hypothetical effective conductivities of the EDZ of about 10^{-8} m/s, implying that higher conductivities would not result in an increase in flow through the repository. But flow is not the only parameter that controls transport and radionuclide release from a repository. The retention capacities of the buffer and the host rock are at least equally important. It has been shown that, especially in the case of long emplacement tunnels (long distance between radionuclide source and the end of the tunnel), radionuclides will be released from the EDZ into the intact host rock by matrix diffusion. Smith *et al.* (2004) conducted a sensitivity study to evaluate the effect of EDZ conductivity on dose for a repository in Opalinus Clay. Figure 2.6 shows that even for the hypothetical case of an EDZ conductivity of 10^{-8} m/s (flow levels off at this value, see above) the dose stays well below the regulatory guideline.

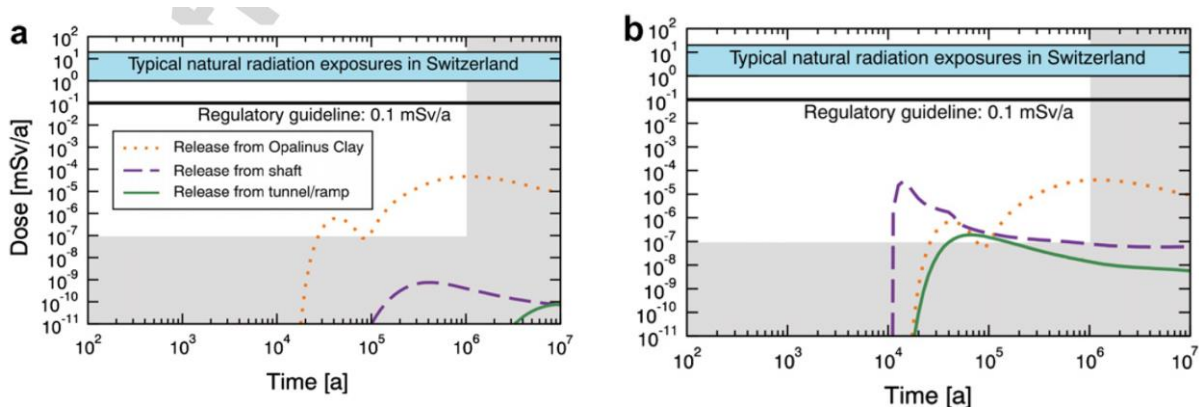


Figure 2.6: Dose curves calculated for a repository in Opalinus Clay for spent fuel (Smith *et al.*, 2004). (a) base case with an EDZ conductivity of 10^{-12} m/s. (b) “what if?” case with a hypothetical EDZ conductivity of 10^{-8} m/s.

2.3 Callovo-Oxfordian Clay

2.3.1 Near field temperature evolution in the French repository designs

The inventory of French radwaste contains exothermal packages: mainly high level vitrified wastes and to a lesser extent some intermediate level long-live (IL) wastes (and of course spent fuel if it were sent to the disposal).

The HL waste disposal cell is a dead-end tunnel (700 mm in diameter, 40 m long) with a steel casing as lining (see Figure 2.7).

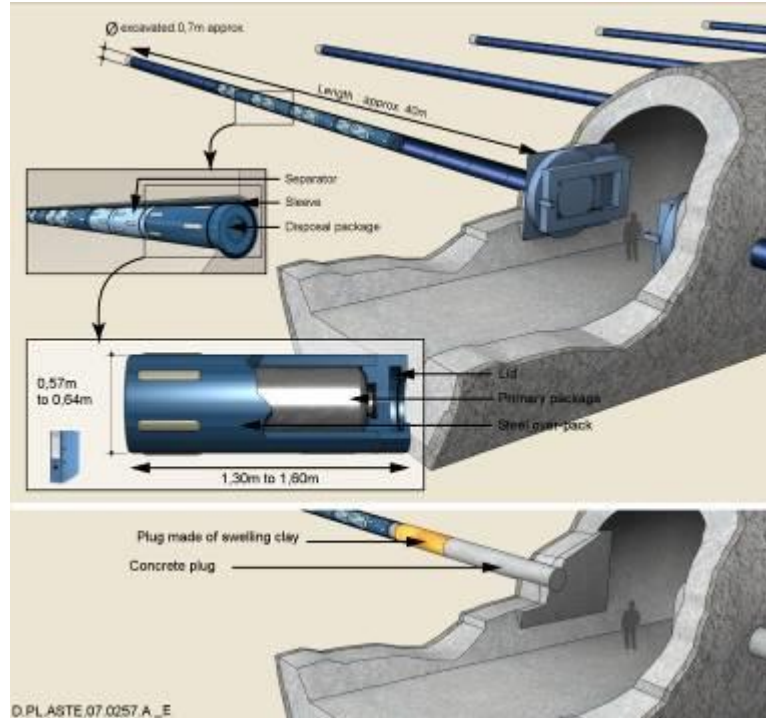


Figure 2.7:HL wastes cell while in operating configuration (up) and after sealing (down)

For IL wastes, the disposal cell is a dead-end horizontal tunnel with a useable length of 250 m and an excavated diameter of 12 m (see Figure 2.8).

The waste package emplacement in the repository induces a gradual but transient increase in temperature from the packages to the geological environment.

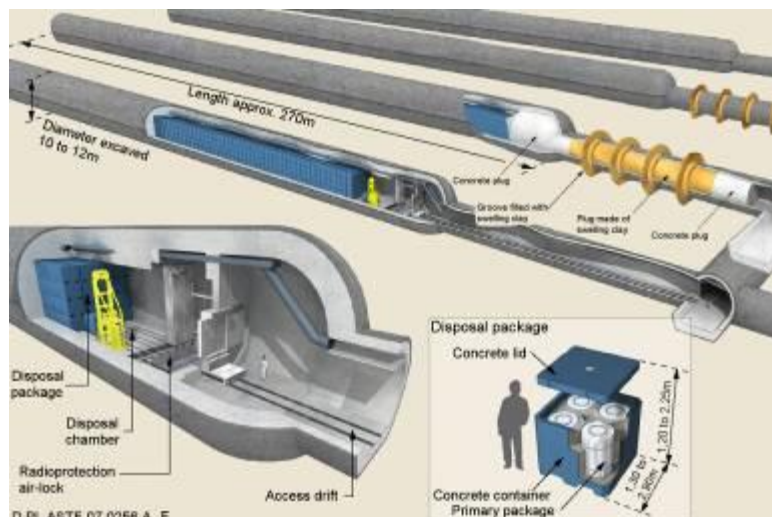


Figure 2.8:IL wastes disposal cell while in operation (foreground of the image) and after sealing (background of the image)

The chosen geologic formation in France is a thick layer of Callovo-Oxfordian argillites. Numerical simulations show that the temperature field linked to the thermal load is rapidly uniform in and around the disposal cell (from a few hundred to a thousand years). The temperature in the argillites reaches 90 °C in the first tens of years and remains in the order of 80 to 50 °C during the resaturation

of the EBS. A few meters away from the repository, the thermal profiles in the Callovo-Oxfordian show a rapid decrease in the temperature (weaker slope of the temperature profile) and the temperature does not exceed 60 °C. At the roof of the Callovo-Oxfordian, it reaches a maximum of 35 °C after about 1 000 years and descends again to less than 30 °C after about 10 000 years. Between 50 000 and 100 000 years are required to return to the geothermal temperature.

This thermal load affects the hydraulic, chemical or mechanical processes that govern the repository evolution, notably corrosion phenomena and release and transport of solutes.

In order to reduce impact of the heating the repository is subdivided in zones 250 m apart from each other. At this distance the thermal effects are negligible and the temperature is limited to 90 °C in the bulk of the host rock. As a consequence the main issues related to the thermal impact are limited to the near field³. In the far field (i.e. beyond the Callovo-Oxfordian formation) the stress increase due to the thermal loading is lower than 1 MPa. This cannot lead to a fracturing of the limestone overburden, but only to a very small uplift (some dm) above the disposal due to the thermal dilation of the rocks.

2.3.2 Thermal Effects on the hydro-mechanical behaviour of the disposal cells

The Callovo-Oxfordian argillites are characterized by strong water/mineral interactions due to its petrofabric. Free pore water probably only exists if the pore opening is larger than approximately 5 to 10 nm. Therefore the part of porosity occupied by bound water is estimated to make up 40 % of the total porosity.

The thermal cycle has different transient effects on the pore water:

- decreasing the viscosity of the water
- increasing the pore pressure
- weakening the bound of absorbed water on the external surface of clay particles (dipole-dipole and Van der Waals type interactions).

This is however only possible when water saturation and temperature rise are concomitant. This concomitance does not exist in exothermic IL waste disposal cells or their access drifts subjected to thermal load, because the temperature rise timescale (about a decade in the IL waste disposal cells and a few centuries in the access drifts) is much shorter than the time required to return to saturation inside these structures (Figure 2.9).

In the high level vitrified waste disposal cells the argillites are close to saturation after cell closure and during the thermal phase. A thermal load-induced hydraulic overpressure may thus be produced in the argillites around the disposal cells over several meters. It causes a divergent water flow because the overpressure is at its maximum at the disposal cell walls (4 MPa in ca. ten years). This overpressure lasts for a few centuries at the most. The created flow decreases more rapidly, within a few decades, as the temperature in the argillites evens out. Rises in temperature generate deformations and stresses in the repository components and argillites (Figure 2.10). The evolution of the mechanical behaviour of the repository engineered structures and surrounding argillites is then coupled to temperature evolutions in and around the engineered structures.

³ Following the definition given by « dossier 2005 », the near field refers to "the part of the geological disposal system of the radwastes including the Host Rock in the immediate surroundings, where the thermal, hydraulic, mechanical and chemical disturbances are induced by the presence of the wastes" - "Partie d'une installation de stockage géologique de déchets radioactifs, y compris la roche d'accueil en environnement immédiat, qui est généralement le siège de perturbations thermiques, hydrauliques, mécaniques et chimiques induites par la présence du stockage." It's worthwhile to note that the limit between near field and far field is not precisely defined. The near field is not only limited to the EDZ, but corresponds to a zone subjected to several sorts of perturbation that is able to modify the radionuclide migration and retention parameters. In the case of argillite, the hydric and chemical perturbations, as well as the modification of the transport properties are quasi limited to the EDZ. However, thermal field (temperature) as well as the hydraulic field (pore pressure) may be disturbed farther, but they only have a limited impact on the nuclides migration (comments from Patrick Lebon).

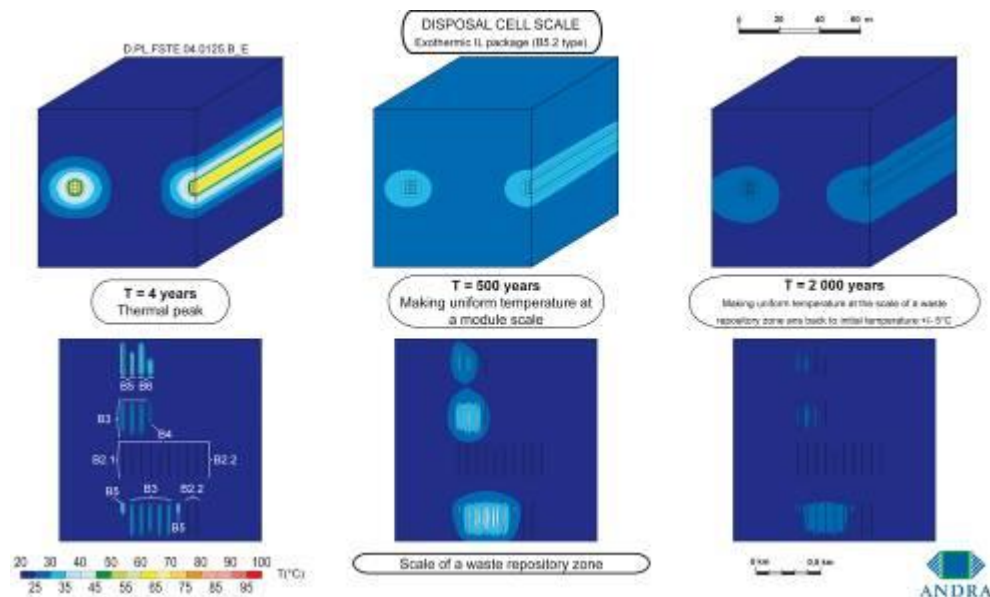


Figure 2.9: Representation of the thermal load of the IL waste repository zone at various times under the assumption that the disposal cells are closed immediately after emplacing the packages

The thermal effect on pore water causes (i) developing stresses within the argillites and (ii) accelerating the argillite creep. Consequently the convergence of the cell reaches 1.7 to 2.1 % of the excavation radius after a few years. It contributes to a gradual reduction of the gaps between the lining and the argillites at the disposal cell wall. 50 to 60 % of the initial gaps are closed at this time and all gaps are closed after ca. 100 to 150 years. Thermo-mechanical interactions between neighbouring disposal cells induce a slightly anisotropic fractured zone up and down the disposal cell, extending less than 0.1 times the cell radius (Su & Barnichon, 2005).

When the gaps between the argillites and the lining are filled, the total convergence of the argillites reaches 2.8 to 3.3 %. During these deformations the EDZ extends around the disposal cells: a fractured zone up to ca. 0.4 times the radius of the disposal cell (about 0.15 m) and a microfissured zone progressing up to ca. 1.4 times the radius of the disposal cell (about 0.50 m). A rapid installation of the swelling clay plug limits the convergence of the argillites and the evolution of the EDZ. The argillite creep rate is stabilised when thermal paroxysm is reached.

Hydraulic and thermal experiments conducted *in-situ* at Bure (TER experiment) and Mont-Terri (HE-D experiment) show strong thermo-hydro-mechanical couplings. The values of THM coupling parameters for argillites are the main input data when modelling of the mechanical behaviour of the argillites and components inside the cells during the thermal phase of the repository. Given the knowledge acquired in “Dossier 2005” (see Site reference document, Volume 2) the key questions to be addressed by the R&D program are:

- the reduction of the uncertainty in the THM coupling parameters that determines
- the induced interstitial overpressure, especially the coefficient of thermal expansion α and the coefficient of differential thermal expansion α_m
- the impact of this interstitial overpressure on damage (what is the threshold above which fissuring occurs?; is there a temperature effect on the rupture and damage thresholds?)
- a better understanding of the relationship between temperature and creep rate in argillites

To reach these objectives, additional tests will be performed under saturated conditions at temperatures lower than or equal to 90 °C. Furthermore some tests are performed at temperatures between 90 and 120°C to identify the major aspects of argillite behaviour at the limit of the repository operating domain and to obtain data for analysing hypothetical failure cases.

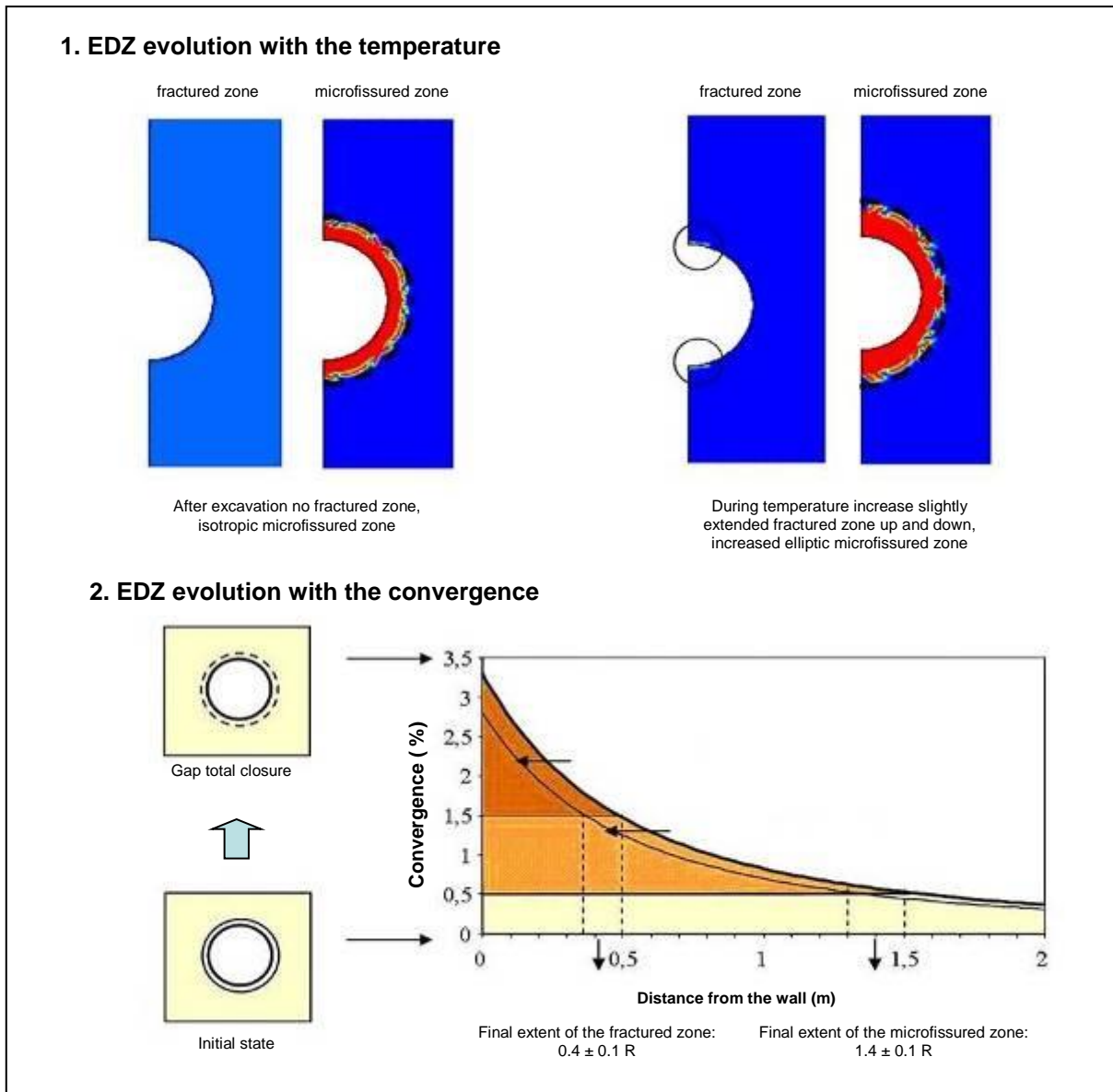


Figure 2.10: Effect of a temperature rise on the evolution of the EDZ and the deferred convergence around a vitrified waste disposal cell (hypothesis of maximum gaps)

2.3.3 Thermal Impact on the conditions of solute transfer

The overpressure developed around the exothermic waste cells provides higher gradients than the ones naturally occurring. The high thermal gradients in the near-field imply a significant Soret effect on solute transfer. Thermal load also increases the diffusion coefficient and permeability to water (Coelho, 2005).

However, according to the very slow corrosion rate of the steel overpack (a few microns per year), the period of the maximal thermal load persistence is much shorter than the leak tightness period of the waste package (e.g. a few centuries compared with 4000 years). Beyond 4000 years, the temperature rapidly decreases and is between 25 and 30 °C after approximately 10000 years. It has no effect on the transfer of radionuclides released by the vitrified waste. Furthermore, the hydraulic overpressure caused by the thermal load would not overlap the overpressures created by the hydrogen because it will have disappeared by the time the latter becomes significant. Nonetheless diffusion remains the dominant process. The relationship between temperature and anion effective diffusion coefficients is empirical and must be better understood. A same approach will be developed for cation diffusion.

2.3.4 Thermal impact on geochemical processes

Changes in degradation processes of waste package and overpack

During the thermal period, the corrosion kinetics under anoxic conditions are increased by a factor of 4 at 90 °C and a factor of 2 at 60 °C compared with those at the natural geothermal temperature of 22 °C. Given the decrease in temperature in the disposal cells after a few decades, the effects of the thermal load on the corrosion of the vitrified waste overpack are limited.

The dissolution kinetics of vitrified packages is controlled by the chemical composition of the glass and by the thermal and chemical conditions of the water in contact with the glass. The $\alpha\beta\gamma$ self-irradiation processes which begin from the moment that the vitrified packages are manufactured, do not influence the dissolution kinetics of the glasses, mainly because of the high self-healing ability of the glass matrix (Andra, 2005). In vitrified waste disposal cells the water comes into contact with the glass at least beyond 4 000 years. By then the temperature has dropped below 50 °C and dissolution kinetics are not significantly altered (Bauer, 2005).

Evolution of swelling clay and argillite properties

In the swelling clay heating can cause (i) precipitation of gypsum, (ii) dissolution of quartz, (iii) illitisation of smectite. But the quantity of quartz is small in swelling clays (< 3 %) (Andra, 2005g, Tome 1) and the available potassium in argillites is in very small concentration. The temperatures reached in disposal cells during the first thousand years (between 85 °C and 55 °C in contact with the containers) are insufficient to allow illitisation of the swelling clay plug in its mass⁴. Geochemical changes remain localised at the interface with the overpack. Modelling estimates the extent of the illitisation process into the plug to be less than a centimetre (Michau, 2005). It is accompanied by iron/clay disturbance developing in swelling clay in contact with the overpack. The reaction processes are only really effective when the plug is re-saturated (after about a hundred years) and are more intense at higher temperatures. Thus, the iron/clay disturbance develops mainly when favourable temperature and saturation conditions occur simultaneously, i.e. during the first thousand years. It develops more slowly after the thermal transient. The influence of iron/clay disturbance on illitisation has not been assessed so far, but is almost certainly negligible due to the mechanisms involved in the two disturbances.

The physico-chemical interactions between the Callovo-Oxfordian argillites and the repository materials are interface phenomena whose extent is limited to the initial EDZ.

It has been demonstrated that the temperature increase in the near field close to the exothermic waste disposal cells should not have any mineralogical consequences. The chemistry of the interstitial fluid also changes very little (Altmann & Jacquot, 2005; Cathelineau & Mosser, 1998). The iterative approach, with coupling between modelling and URL experiments on the pore water chemical composition, should ultimately weigh up if there is a need to precise the understanding of the regulatory mechanisms, notably of the influence of organic matter on fluid/rock equilibria and on speciation of elements in solution (in particular radionuclides). A main issue is to determine the type of “groupements fonctionnels” and their actual concentration, to assess their influence during the thermal load.

As for the swelling clay plug, the iron/argillite disturbance develops essentially during the thermal period. Beyond this period, it evolves very slowly. Furthermore, it ceases after several thousand years with the total corrosion of the metal components involved. It can therefore be considered that, over a million years, the extent of the disturbance remains close to that achieved at the end of the thermal period.

⁴ Numerous studies highlight the fact that illitisation process in sedimentary basins only starts at temperatures above 80 °C and does not become significant below 100 °C, as long as there is a potassium source.

The research programme aims at (i) determining the enthalpy and hydration energy to model the chemical changes with temperature and (ii) measuring the relation between ion exchange constants and temperature taking into account the solubility variations of mineral phases.

Significant experience has been gained concerning the chemical retention properties of swelling clays. The influence of temperature on sorption equilibria will be studied for temperatures until 100 °C to precise material reactivity with temperature (interaction with iron and alkaline fluids). Other effects (dissolution/precipitation processes, solute/surface interactions) will be examined to release the design constraints linked to the temperature (tight leak period). For that purpose thermodynamic data (e.g. the equilibrium constants for solids) and kinetic data (e.g. the dissolution/precipitation kinetic constants) will be measured for the clay minerals at low temperature (below 120 °C).

3 Terminology

Will be defined later in the project.

4 State of the art for Boom Clay

The R&D programme on geological disposal for high-level and long-lived waste (HLW) was initiated in Belgium at SCK•CEN in 1974. A deep tertiary clay formation, the "Boom Clay", present under the Mol-Dessel nuclear site, was selected as a candidate host formation for experimental purposes. An underground research facility (URF), called HADES, was constructed and has allowed large scale integrated tests close to real conditions. The facility consists then of one shaft and one horizontal gallery of 110 m length at 223 m depth.

In 1997, a second shaft was realised, followed in 2001 by the construction of the Connecting gallery (Figure 4.1). During the construction of the different parts, numerous samples were collected, allowing experimental campaigns devoted to the characterization of the thermo-hydro-mechanical (THM) behaviour of the Boom Clay. These ones were complemented by numerical studies in order to establish the constitutive laws and models to represent the Boom Clay. This chapter tries to give a global view of the state of the art of THM behaviour of the Boom Clay.

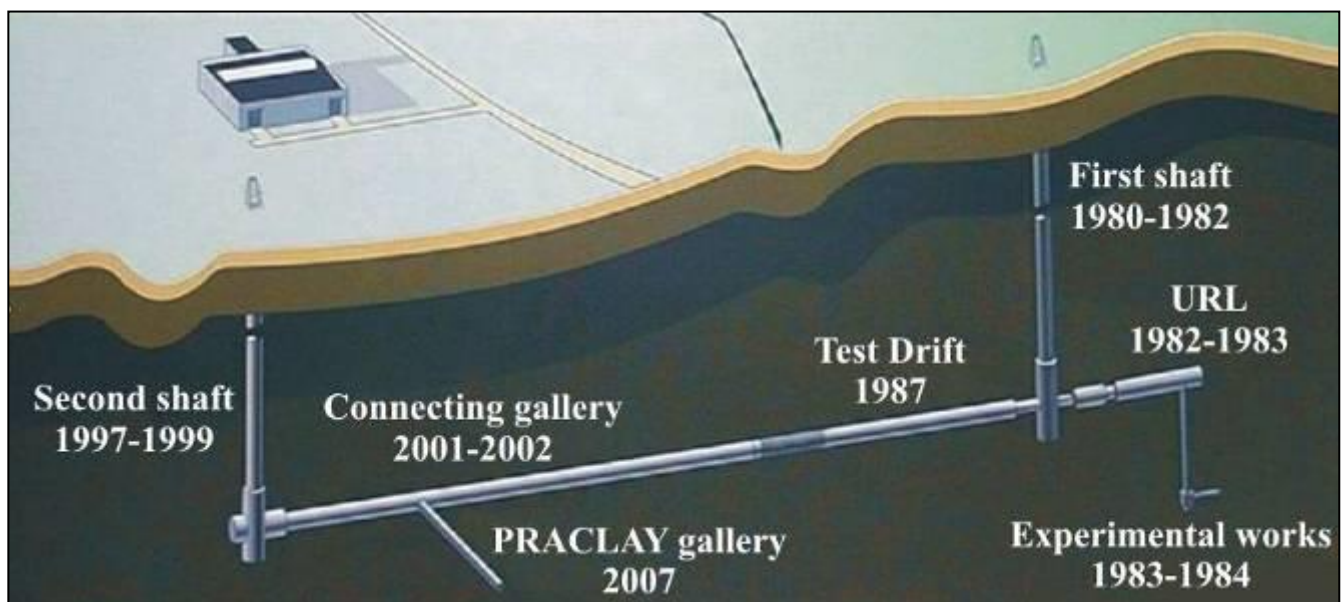


Figure 4.1: Underground Research Facility HADES at Mol

This chapter is guided by the report of Li (2004) and the document "EDZ development and evolution – State of the art" realised in the framework of the NF-Pro project (F16W-CT-2003-02389) (Alheid *et al.*, 2007). It begins with a summary of the main characteristics of the Boom Clay, including their initial state and their physical, thermal and geomechanical parameters. A more exhaustive evaluation of the THM behaviour is next realised, based on the work in lab and in situ. After, the chemical aspects are related. A study of the constitutive model is also carried out. To conclude, it will discuss about the incertitude, the most important thermal material properties and coupled processes as well as their parameters. The effect of discrete fractures and fracture connectivity on the effective hydraulic properties as well as the importance of the chemical impact will be assessed. From there, the most appropriate conceptual models and numerical code will be evaluated.

4.1 Main characteristics

The Boom Clay possesses numerous favourable properties to fill the function of geological barrier for radwaste disposal for different reasons. First, the layer that it forms has been steady for millions of years. Its permeability to fluid is very weak and it has a good retention capacity of the radionuclides. Its plastic behaviour has the advantage to close cavity and fractures in the more or less

long-term and then to favour the sealing/healing processes. Moreover, its swelling potential improves its self-sealing capacity (Picard, 1994; Coll et al., 2004; Bernier *et al.*, 2006).

Even if the samples of Boom Clay present inhomogeneity, especially in mineralogy and water content as it will be seen in the §4.2, Boom Clay is considered homogeneous. It is mainly constituted of clay minerals (30 to 70 % with an average of 55 %). This part is dominated by illite (50 % in volume), smectite (30 %), illite-smectite interstratifications and kaolinite (10 %). The non-clay part is mainly composed of quartz (25 %) and feldspar. It is also worthwhile to note the presence of pyrite concretion and the presence of calcite (Coll et al., 2004; Coll, 2005).

The Table 4.1 provides the basic geotechnical properties of the Boom Clay determined on the samples taken from HADES.

Table 4.1: Physical properties of the Boom Clay

Density	ρ	2026 [kg/m ³]
Water content	W	22 - 27 [%]
Plastic limit	w _P	23 - 29 [%]
Liquid limit	w _L	55 - 80 [%]
Plasticity index	I _p	32 - 51 [%]

The URF HADES is situated at about 225 m depth and the underground water level is situated more or less at the ground surface. At this depth, the initial state of the Boom Clay is given in the Table 4.2. There exist, however, open questions about the in-situ stress state tensor. K_0 value (ratio of horizontal to vertical effective stresses) was determined by laboratory methods and in-situ investigations. The in-situ investigations from HADES by means of Pressuremeter, Dilatometer, Self Boring Pressuremeter (SBP), Hydrofracturing tests, borehole breakouts analysis and back-analysis of the stresses in the liner gave some scattering K_0 values (0.3-0.9). Laboratory investigations indicated values for K_0 between 0.5 and 0.8. Deeper investigation of this subject is therefore necessary: a new set of in-situ tests including SBP and Hydrofracturing tests in different directions is planned in 2007 (Bernier *et al.*, 2007).

Table 4.2: Initial in situ state of the Boom Clay at HADES level

Initial total stress	σ_v	4500 [kPa]
	σ_H	3600 - 4500 [kPa]
Initial pore water pressure	u_w	2250 [kPa]

From a hydraulic point of view, the properties of the Boom Clay are listed in the Table 4.3. The permeability is weak and anisotropic.

Table 4.3: Hydraulic characteristics of Boom Clay

Porosity	n	0.39
Hydraulic conductivity	K _V	4 – 6 10 ⁻¹² [m/s]
	K _H	2 10 ⁻¹² – 4 10 ⁻¹² [m/s]
Water bulk modulus	K _w	2 [GPa]

Finally, the thermal parameters of the Boom Clay are summarised in the Table 4.4. The thermal conductivities obtained in laboratory (SAFIR2 project) and in situ (ATLAS) are significantly

different. This parameter value must thus be verified. It is actually in investigation in the framework of ATLAS III.

Thermal conductivity	λ	1.35 (ATLAS) [W/(mK)]
		1.70 (SAFIR2) [W/(mK)]
Volumetric heat capacity	ρ_c	$2.84 \cdot 10^6$ [J/(m ³ K)]
Linear thermal expansion coef. (drain condition)	α	10^{-5} [K ⁻¹]

All these parameters have been determined by the laboratory and in situ tests summed up here below.

4.2 THM characterization in lab

During the construction of the URF HADES, numerous Boom Clay samples in form of blocks or cores were taken and served for the different campaigns of laboratory tests. These were piloted in two main directions:

- Short term THM behaviour:
 - The elastoplastic *hydro-mechanical* behaviour in saturated condition and ambient temperature;
 - The *thermal* effects on the hydro-mechanical behaviour at saturated state.
- The time related behaviour at ambient and elevated temperature in saturated condition.

It is worthwhile to note that, until now, the majority of laboratory tests on Boom Clay were carried out in saturated condition. The work on the thermo-hydro-mechanical behaviour of natural Boom Clay at unsaturated or partially saturated state is very limited.

The most of laboratory realised tests were oedometer and triaxial tests on cylinder samples. Some hollow cylinder tests and thick tube tests were realised in different projects.

4.2.1 Short term THM behaviour

The different projects devoted to the characterisation of the short term thermo-hydro-mechanical behaviour of Boom Clay are here summarized in a chronological order.

4.2.1.1 WASUK project (EUR 10987)

The hydro-mechanical characterisation of Boom Clay at the URF HADES level began in 1987 with the WASUK project. This one was realised by the British Geological Survey of Nottingham, in collaboration with the European Atomic Energy Community (EAEC). The aim of laboratory tests carried out in the framework of this project was the study of the basic geotechnical properties of the Boom Clay.

The tests were performed on "undisturbed" samples come from the URL (small shaft or Experiments works on the Figure 4.1) at 247 m below the surface. Here is a summary of the different tests as well as their main results (Horseman *et al.*, 1987):

Oedometer tests with consolidation stresses up to 32 MPa

For example, the plot of void ratio versus the logarithm of effective stress of the one-dimensional consolidation test OCD/53/2 is given at the Figure 4.2.

From these oedometric tests the critical state parameters λ and κ can be determined:

$$\lambda = 0.178$$

$$\kappa = 0.046$$

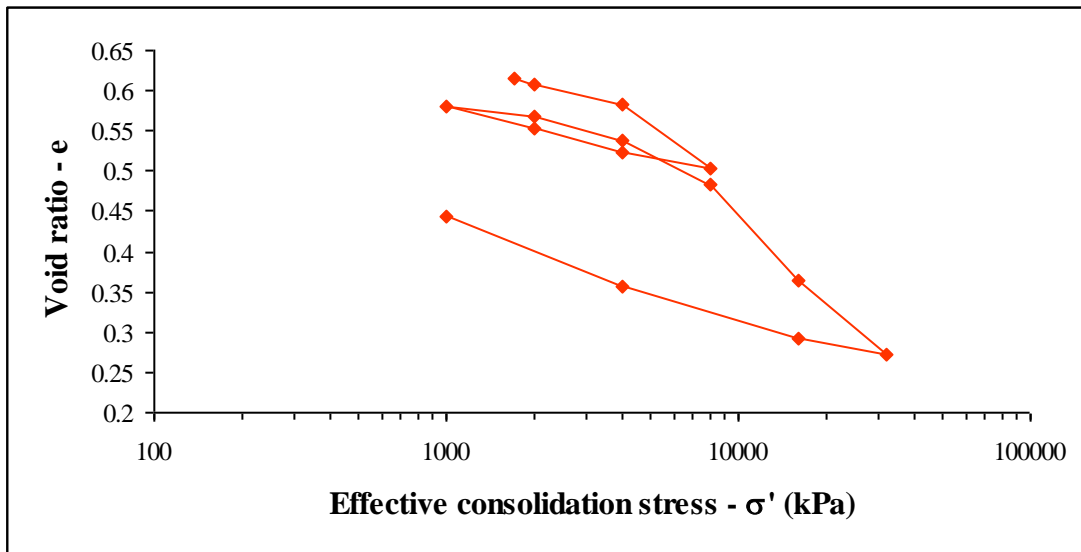


Figure 4.2: Consolidation results for Test ODC/53/2 (adapted from Horseman *et al.*, 1987)

The effective preconsolidation stress can also be established. The "most probable" value is 6.0 MPa. Taking the present in situ effective vertical stress at a depth of 247 m as 2.5 MPa, this gives an overconsolidation ratio (OCR) of about 2.4 for the Boom Clay at the elevation of the URF HADES.

$$p'_0 = 6.0 \text{ MPa}$$

$$OCR = 2.4$$

Taking the Terzaghi theory of the rate of consolidation as valid, the hydraulic conductivity K_w (m/s) of the clay may be estimated from consolidation data. As a first approximation the hydraulic conductivity decreases linearly with the logarithm of effective stress (Figure 4.3). Given the in situ effective vertical stress around 2.5 MPa, this figure suggests a vertical hydraulic conductivity K_{wV} at the elevation of the gallery in the range:

$$K_{wV} = 2.0 - 3.5 \cdot 10^{-12} \text{ m/s}$$

The specific storage, S_s , may then also be determined. For a saturated porous medium, specific storage is assumed to have two components, S_{sw} due to the elasticity of water and S_{sk} due to the elasticity of the soil and rock skeleton:

$$S_s = S_{sw} + S_{sk} = \rho_w g \left[\frac{n}{\chi_w} + \frac{1}{E'_k} \right]$$

where ρ_w is the density of water, g is the acceleration due to the gravity, n is the porosity, χ_w is the bulk modulus of water and E'_k is the (drained) constrained modulus of elasticity.

Under the in situ conditions at HADES level, χ_w can be taken as $2.2 \cdot 10^3$ MPa. Taking a porosity of 39 %, S_{sw} is about $1.7 \cdot 10^{-6} \text{ m}^{-1}$.

Since the constrained modulus defined for rebound and recompression varies with effective stress, then S_{sk} must also be stress-dependent. This relationship is most easily expressed in terms of recompression index C_s :

$$S_{sk} = \frac{0.000434C_s \rho_w g}{\sigma'_v(1+e_0)}$$

where ρ_w is the density of water, g is the acceleration due to the gravity and σ'_v is the vertical effective stress.

Taking C_s as 0.11 and e_0 as 0.646 and considering the in situ condition of Boom Clay with σ'_v equal to 2.5 MPa, S_{sk} is equal to $1.1 \cdot 10^{-4} m^{-1}$, giving:

$$S_s = 1.2 \cdot 10^{-4} m^{-1}$$

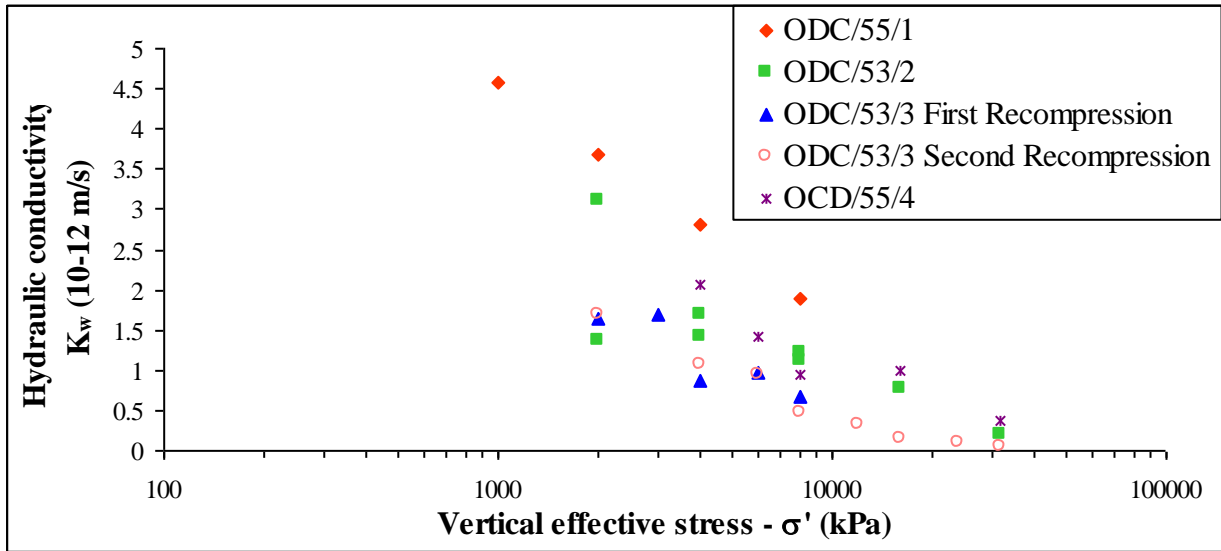


Figure 4.3: Hydraulic conductivity plotted against the vertical effective stress (adapted from Horseman *et al.*, 1987)

One-dimensional swelling pressure tests

In view of its clay mineralogy and its overconsolidated state, the Boom clay is likely to exhibit capacity for swelling. Figure 4.4 shows the swelling pressures plotted against time from a one-dimensional swelling test. The maximum value for the swelling pressures is then 0.92 MPa (Horseman *et al.*, 1987). Recent laboratory tests (Coll, 2003; Le, 2006) revealed that the procedure for determination of the swelling pressure is a delicate subject, which depends highly on the suction state of the samples and thus the saturation procedure for sample. This subject is under investigation in the frame of the PhDs study of Le and Alanice devoted to the THM behaviour of the Boom clay (Le, 2006; Alanice 2007).

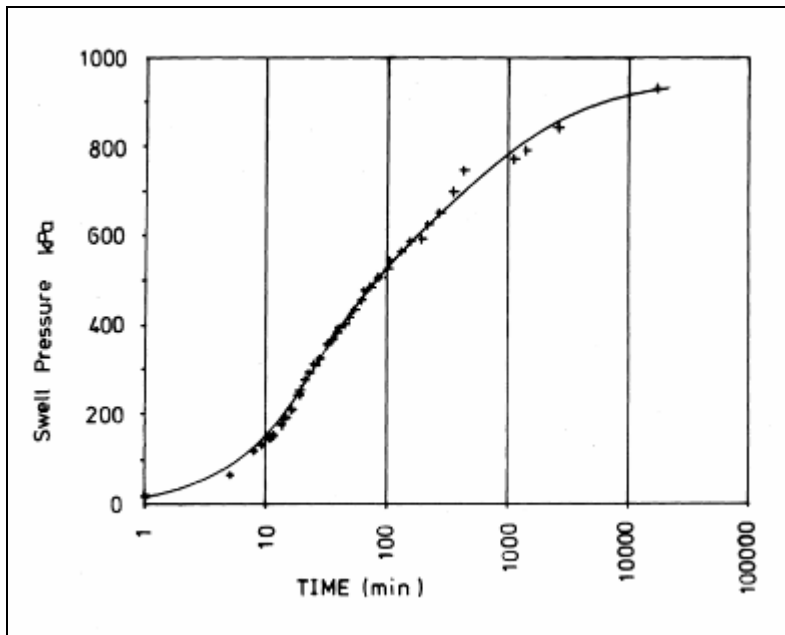


Figure 4.4: Swelling pressure in function of time of test ODS/53/1 (Horseman *et al.*, 1987)

Isotropical Consolidated and Undrained (CIU) triaxial tests with pore pressure measurement and Unconsolidated and Undrained (UU) triaxial tests

Adopting a critical state concept, the volumetric strain in overconsolidated domain can be expressed as:

$$\varepsilon_{ve} = \frac{\kappa}{(1 + e_0)} \ln\left(\frac{p'}{p'_0}\right)$$

where p' is the mean principal effective stress and p'_0 the strain-hardening parameter. The parameter κ can be determined from the isotropic consolidation (CIU) tests or odometer tests. Figure 4.5 presents the results of a CIU test which gives (Taking e_0 as 0.646)

$$\kappa = 0.029$$

This value is significantly lower than that inferred from the one-dimensional consolidation test data. An isotropic consolidation test with a rebound/recompression stage would provide a refined value for.

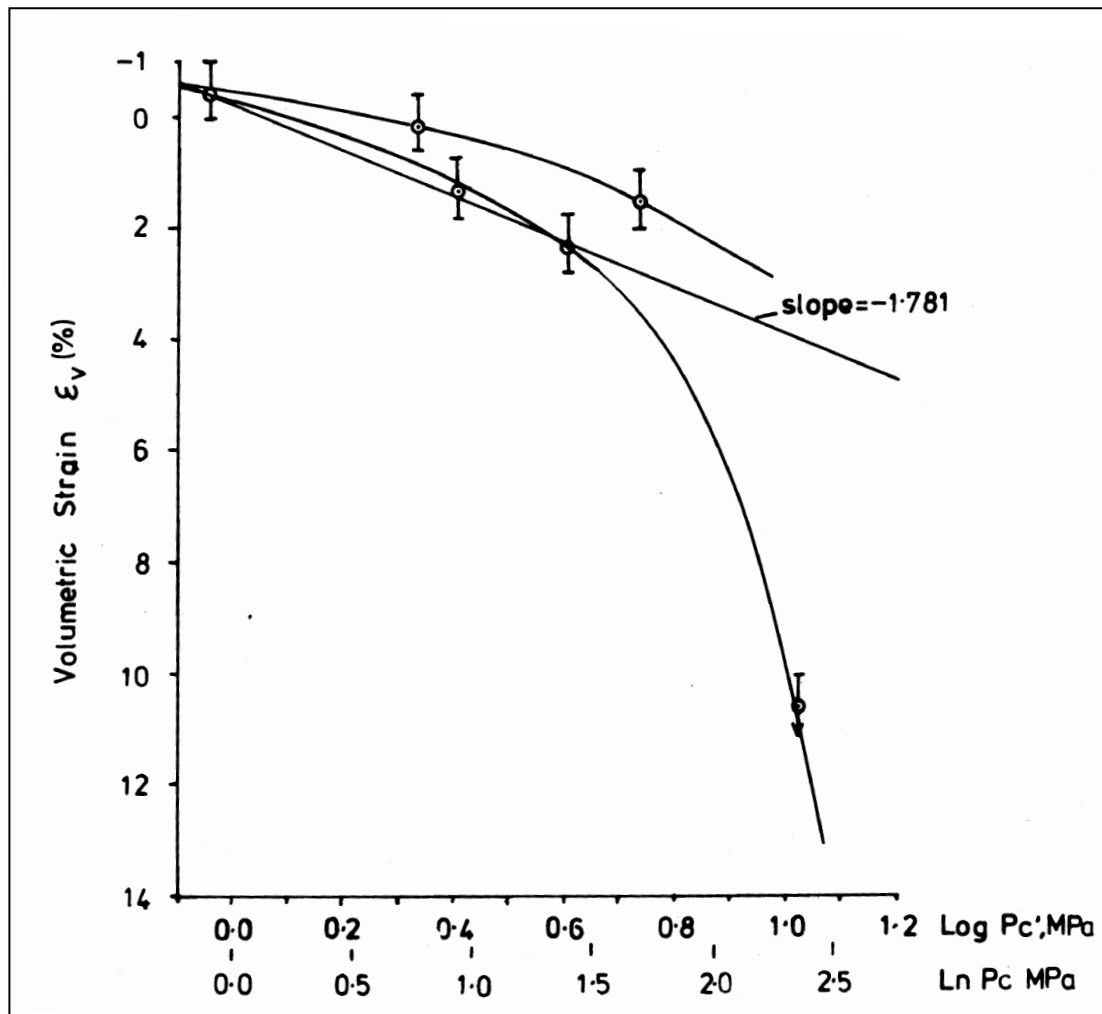


Figure 4.5: Volumetric strain plotted against the logarithm of isotropic consolidation stress (Horseman *et al.*, 1987)

Figure 4.6 shows the ambient temperature undrained stress-strain behaviour of the Boom Clay isotropically consolidated at various pressures in the range 0.89 to 5.42 MPa. The consolidation stage was effectuated according to following sequences: specimens were loaded in increment of approximately 0.5 MPa to the scheduled confined pressure and then, a valve is opened to apply a back pressure (nominally 50 % of cell pressure) to allow consolidation to commence. Once consolidation and pore pressure dissipation were completed, the specimens were sheared by the application of small increments in axial stress. The average shearing rate applied for different tests are given in Table 4.5.

Table 4.5: Rate of shear stressing (Horseman *et al.*, 1987)

Test N°	Average rate of shear stressing (MPa/min)
CIU/55/1	$4.5 \cdot 10^{-4}$
CIU/54/2	$8.3 \cdot 10^{-3}$
CIU/54/4	$1.1 \cdot 10^{-2}$
CIU/55/4	$1.8 \cdot 10^{-2}$
CIU/55/5	$8.3 \cdot 10^{-3}$
UU/51/1	$5.5 \cdot 10^{-2}$

The undrained Young's modulus, E_u , values can then be obtained from the stress-strain curves by graphical construction. Two modulus definitions have been selected, the secant at 1 % axial strain and the tangent at 50 % maximum shear stress (Table 4.6).

Table 4.6: Undrained Young's Modulus (E_u) (Horseman et al., 1987)

Test N°	Consolidation stress (MPa)	Young's Modulus (MPa)	
		Secant at 1 % strain	Tangent at 50 % q_{max}
CIU/55/4	0.89	112	82
UU/51/1	2.5*	163	157
CIU/55/1	2.5	159	111
CIU/54/2	2.85	223	179
CIU/54/3	5.42	282	203

* Confining stress for UU test taken as 2.5 MPa, the estimated in situ effective stress

Anyway, moduli E_u increase with increase of the isotropic consolidation stress, p'_c . The plots of the ratios of E_u to consolidation pressure, based on secant modulus at 1 % strain and tangent modulus at 50 % of q_{max} show following linear relationships:

Based on secant modulus at 1 % of strain:

$$\frac{E_u}{p'_c} = 37.2 + 43.4 \ln(OCR_i)$$

Based on tangent modulus at 50 % of q_{max} :

$$\frac{E_u}{p'_c} = 32.0 + 30.0 \ln(OCR_i)$$

If p'_c is taken as 2.5 MPa, stress in situ, the undrained Young's moduli become:

$$E_u(\text{secant at 1 \% strain}) = 197 \text{ MPa}$$

$$E_u(\text{tangent at 50 \% } q_{max}) = 152 \text{ MPa}$$

If it is assumed that stress paths for clay "wet of critical" terminate at the critical state line (CSL), the slope of this one, M , may be estimated thanks to the test CIU/54/3:

$$M = 0.81$$

The effective friction angle ϕ and the slope M of the critical state line are linked by:

$$\sin \phi = \frac{3M}{(6 + M)},$$

given a effective friction angle equal to:

$$\phi = 20,9^\circ$$

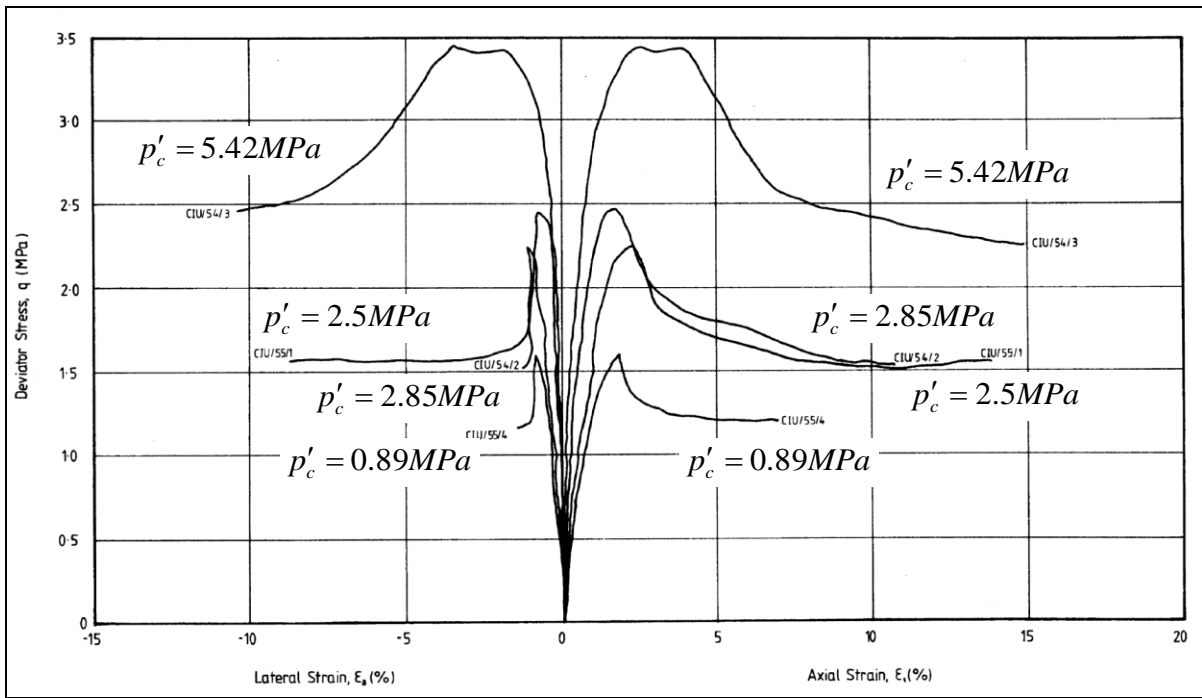


Figure 4.6: Stress/strain curves for specimens isotropically consolidated at various pressures in the range 0.89 to 5.42 MPa (Horseman *et al.*, 1987)

Limited Isotropical Consolidated and Undrained (CIU) tests at elevated temperature

Figure 4.7 shows the rise of the pore pressure produced by heating the clay under undrained conditions, from ambient laboratory temperature to 80 °C. Pore pressures are based on the average reading of the back pressure and pore pressure transducers. The initial rate of heating on both tests was approximately 0.5 °C per minute and the heating period was about 3 hours.

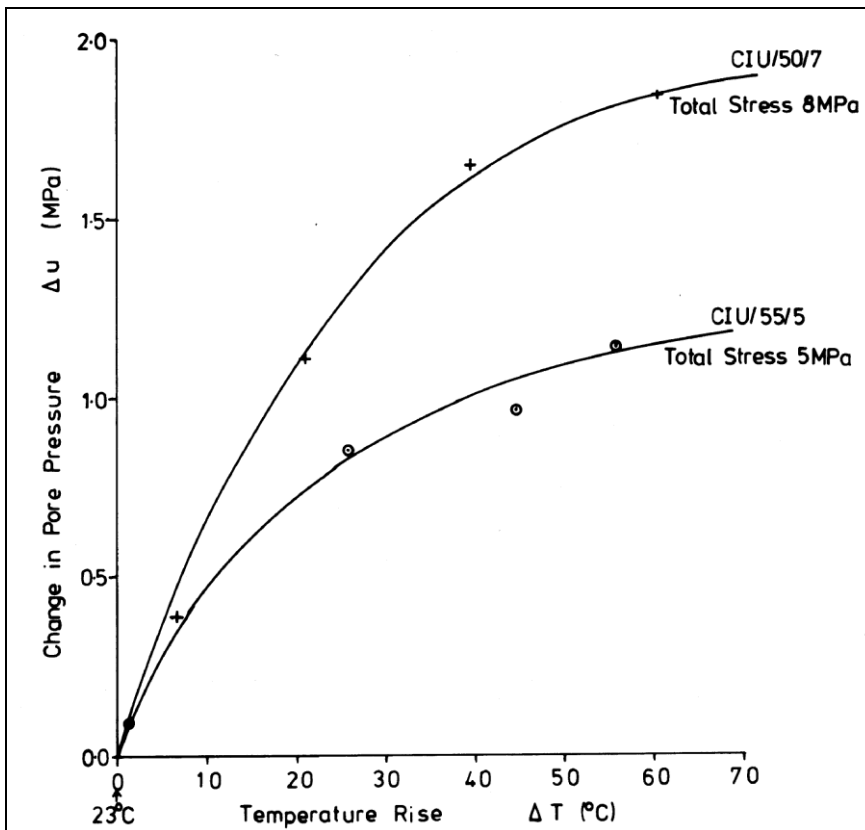


Figure 4.7: Change in pore pressure under undrained conditions plotted against temperature rise (Horseman *et al.*, 1987)

It is important to investigate the effect of the temperature on the pore pressure response, deformability and strength because the excess of pore pressure developed during the heating may significantly alter the near-field and, in the long term, the far-field ground water flow pattern. Moreover, an increase of pore pressure is accompanied by a reduction of the effective stress and the capacity of the clay to sustain the shear stress decreases. There is thus possibility that the thermal induced pore pressure triggers the shear failure.

The Figure 4.8 shows the volumetric strain in function of the temperature increase, based on an initial temperature of 22 °C. The rate of heating is such that the internal temperature of the specimen probably lags behind the surface temperature. The clay is heated under undrained conditions. It is possible to determine the coefficient of volume expansion of the solids α_s . Taking e_0 equal to 0.654, the fitted line on the Figure 4.8 uses a value of:

$$\alpha_s = 3 \cdot 10^{-5} \text{ K}^{-1}$$

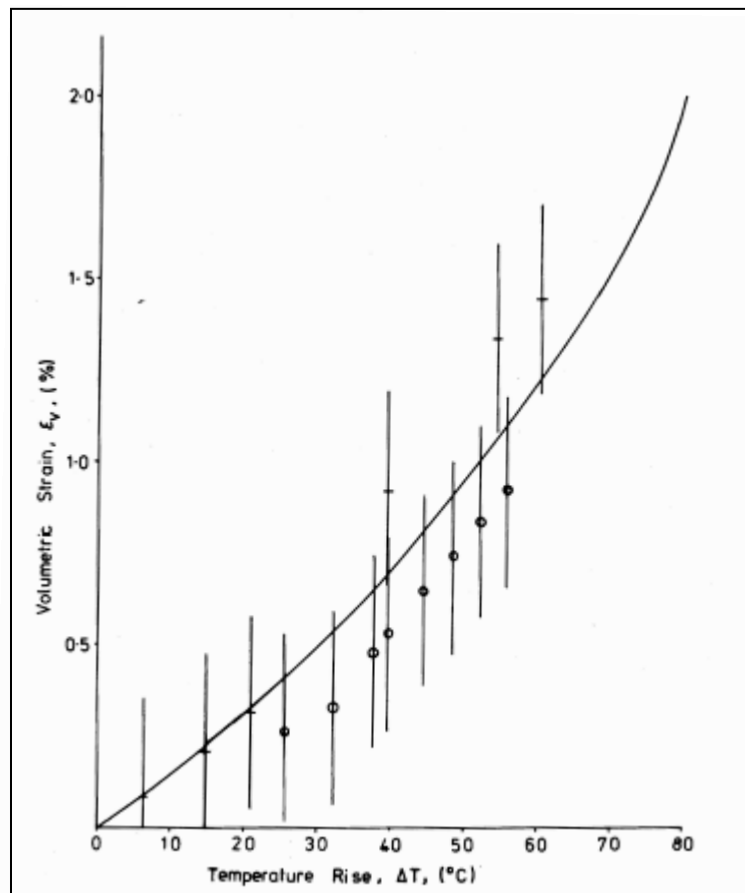


Figure 4.8: Volumetric strain during undrained heating in function of the temperature rise (Horseman *et al.*, 1987)

The test results obtained in this project permitted to obtain the BASIC hydro-geotechnical properties of the Boom Clay at the depth of HADES. Most of parameters obtained in this project have been served as the reference parameters of Boom Clay, such as the preconsolidation pressure, OCR, permeability, elastic and plastic stiffness, critical state line, etc.

The effect of the temperature on the pore pressure responses and deformability and strength under undrained or partially undrained conditions based on the limited CIU tests was also analysed.

4.2.1.2 WASI 380.83.7 (EUR 10924) and FI1W/0150 (EUR 13365) projects

Nearly at the same period as the WASUK project, a program of laboratory tests was commissioned for the WASI 380.83.7 project in order to study the thermal-hydro-mechanical behaviour of Boom Clay in saturated condition and to calibrate a method and mathematical model. This project was performed by ISMES Geotechnical Laboratory in 1987. In 1991, ISMES extended the project (CEC

contract F11W/0150) aiming to improve the knowledge on the thermo-deformational responses of clay samples putting emphasis on the role of adsorbed water and to develop models for numerical simulation. The first part of the project tries to lay the foundations of a comprehensive theoretical treatment of the interaction between water and soil skeleton during thermal dilatation. The second part of the research is devoted to the development (refinement) and the application of advanced constitutive modelling of mechanical behaviour of clay taking into account the extensive tests on Boom Clay realised in this project and in the frame of the contract of WASI 380.83.7.

The tests have been realised on Boom Clay samples taken from 223 m (Test Drift) and 240 m (small shaft for Experimental works, Figure 4.1) below the ground surface.

The tests performed in the frame of project WASI 380.83.7 and the corresponding main results are (Baldi *et al.*, 1987):

Oedometric and isotropic consolidation tests and CU triaxial tests in different consolidation pressures.

These tests allowed to determine the preconsolidation pressure p'_0 and the OCR:

$$p'_0 = 6.0 \text{ MPa}$$
$$\text{OCR} \cong 2.64$$

These results are consistent with the WASUK project's results (Horseman *et al.*, 1987).

Figure 4.9 represents the isotropic compression curves obtained from the consolidation tests, which give:

$$\kappa = 0.031$$
$$\lambda = 0.129$$

with:

$$p'_0 = 6.0 \text{ MPa}$$
$$e_0 = 0.589$$

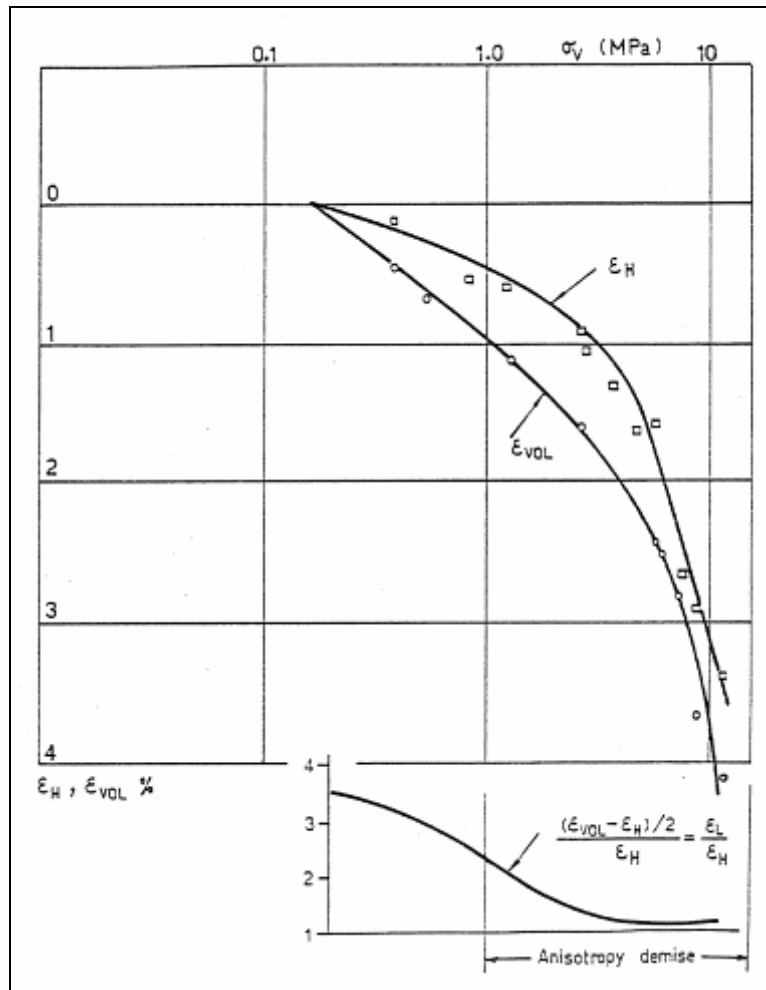


Figure 4.9: Isotropic consolidation tests results (Baldi *et al.*, 1987)

On the Figure 4.9, the difference between the curves of volumetric and vertical deformation (ϵ_{vol} and ϵ_H) shows clearly that Boom Clay presents anisotropy. Moreover, the small graph at the bottom of the figure shows that this anisotropy seems decrease with the increasing vertical stress (the ratio of lateral to vertical strain).

In order to determine the effective friction angle, a series of consolidation undrained triaxial tests with pore pressure measurement has been performed. The effective stress paths have been plotted in plane p' - q as shown in Figure 4.10. p' is the effective mean stress and q the deviatoric stress, allowing the determination of the critical state line and its slope M .

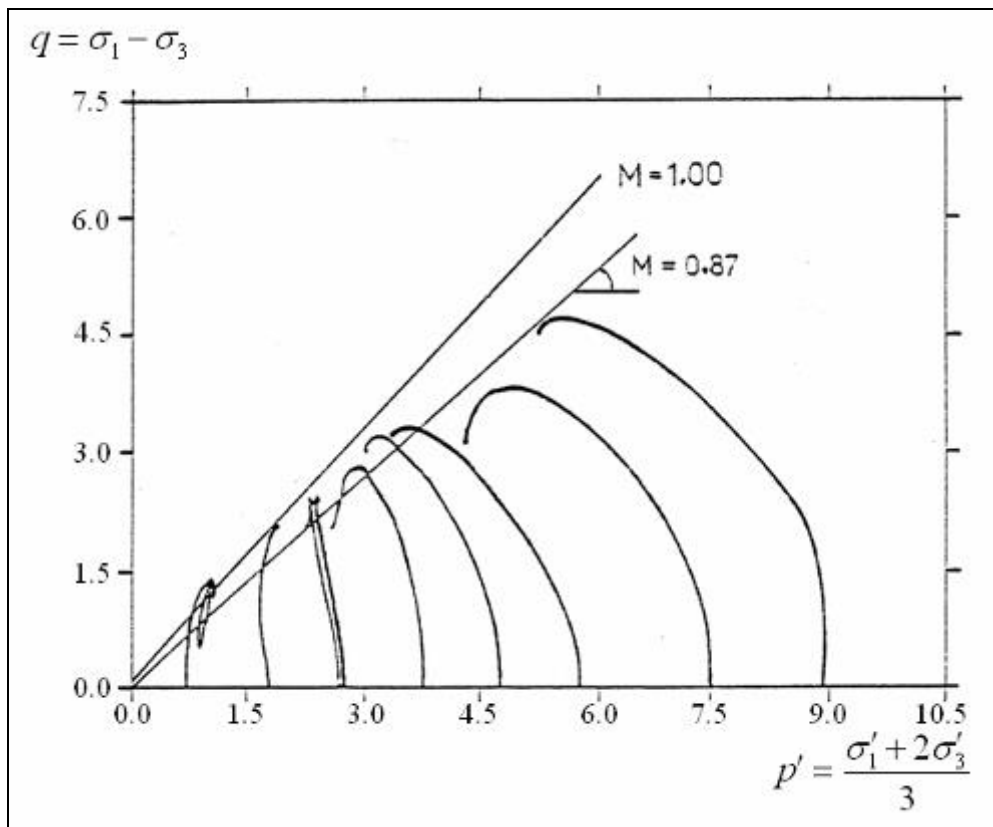


Figure 4.10: Stress paths in undrained, overconsolidated and normally consolidated tests (adapted from Baldi *et al.*, 1987)

M is ranged between 0.81 and 1 and thus gave the effective friction angle values (see § 4.2.1.1):

$$\phi = 22.3^\circ - 25.3^\circ$$

Thanks to shear tests, the elastic shear modulus was determined. The non linear elastic behaviour (shear modulus varies with the current effective isotropic pressure, p') is shown in Figure 4.11. The mean value for $p' \in [4 - 8.5] \text{ MPa}$ is about:

$$G = 100 \text{ MPa} .$$

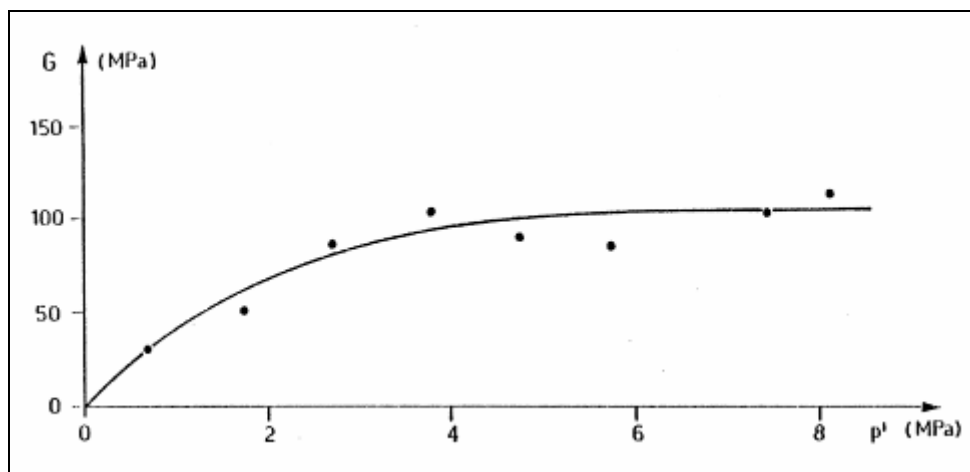


Figure 4.11: Shear modulus G variation with the effective mean pressure p' (Baldi *et al.*, 1987)

On the whole, the fundamental parameters of Boom Clay obtained are more or less consistent with the WASUK project's results (Horseman *et al.*, 1987).

Isotropic thermal consolidation tests : tests with controlled stress paths in a plan p' - T

The thermal consolidation patterns of Boom Clay have thus been characterized. The Figure 4.12 is an example of thermal consolidation curve at a normally consolidated state, in other words, heating is applied on a sample submitted to a pressure of 6 MPa (Baldi *et al.*, 1987).

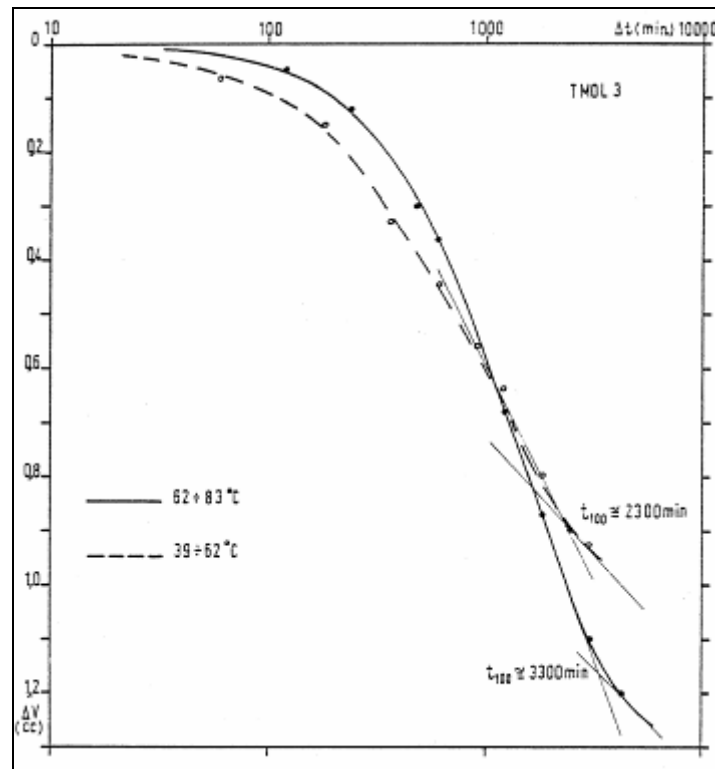


Figure 4.12: Thermal consolidation curves at a normally consolidated state (6 MPa), heating steps 39 – 62 °C and 62 – 83 °C (Baldi *et al.*, 1987)

Heating tests at controlled deviatoric stress state.

Conclusions drawn from these tests are, at constant total stress state, at normal consolidation state, in undrained condition, the failure of the Boom Clay during heating may occur due to the shear band since the pore pressure increases drastically. Moreover, it was put in evidence the stress dependence behaviour of the heating strain. Indeed, at higher deviatoric stress state, the soil failure may appear quicker during undrained heating (Baldi *et al.*, 1987).

In the frame of the FI1W/0150 project, an additional laboratory tests campaign on Boom Clay samples taken from URF of Mol has been performed. Tests were aimed at enlarging the data base on the volumetric responses of Boom Clay under shear at overconsolidated states, and on the heating-cooling effects.

In addition to the standard oedometer and triaxial tests, the triaxial HITEP apparatus was used to performed high pressure and high temperature tests (included heating-cooling cycles) and test paths include drained and undrained, compression drained tests at different OCR, at ambient and elevated temperature, heating at different constant pressure in drained conditions in over- and normally consolidate states, undrained heating at constant isotropic stress with back pressure corresponding to the in situ hydrostatic pressure, undrained constant deviator heating with elevated back pressures and different initial geostatic stress, etc.

It is interesting to present the following test with a mixed mechanical (isotropic) and thermal loading program (Figure 4.13). The specimen was saturated at 2 MPa, unloaded to 1 MPa, heated to 95 °C and cooled back to 21.5 °C, loaded at 21.5 °C up to 3 MPa, heated to 95 °C and cooled back, loaded to 6 MPa and again heated and cooled, and finally loaded from 6 to 8 MPa and unloaded back to 3 MPa.

The response during heating is different for different stress state: an axial expansion is seen for 1 MPa, initial expansion followed by compression at higher temperature for 3 MPa and finally compaction is obtained for the whole temperature range at 6 MPa (Figure 4.14). The Boom Clay behaviour resulting of heating depends thus on the overconsolidated ratio. This phenomenon is analysed in more details in the framework of the Sultan's thesis (1997).

Concerning the cooling branch of the experiment, the results are also remarkable (Figure 4.14). In all the tests, there is only compaction deems not depends on the stress state

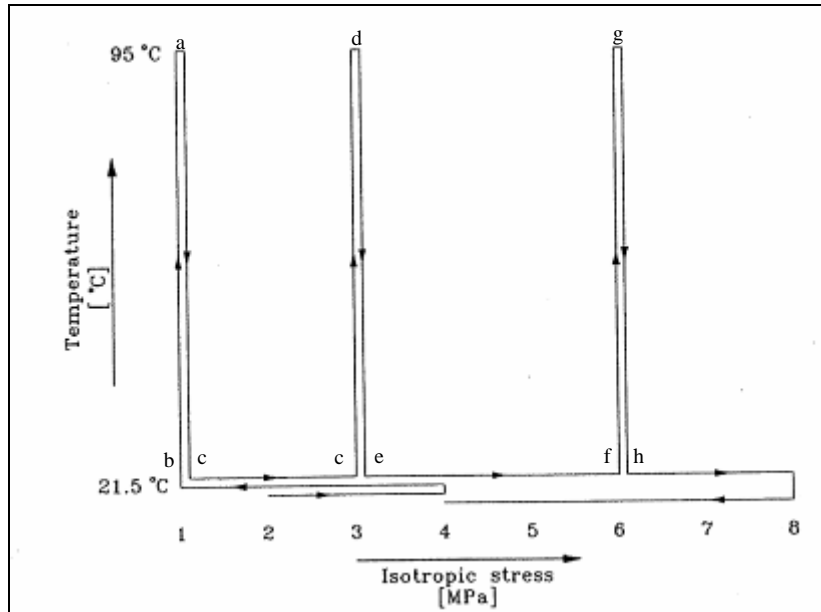


Figure 4.13: Mixed mechanical (isotropic) and thermal loading program (Baldi *et al.*, 1991)

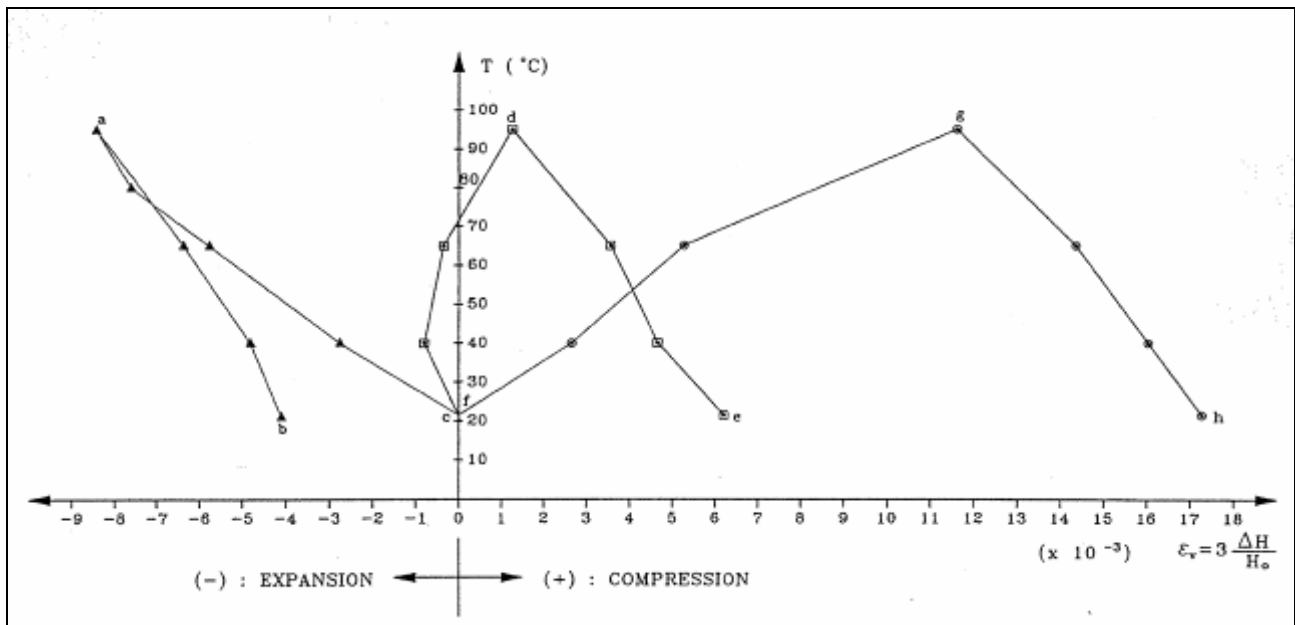


Figure 4.14: Volumetric thermal strain during heating/cooling at different pressures (Baldi *et al.*, 1991)

The set of tests realised in this project allowed to put in evidence the inhomogeneity of the Boom Clay. Indeed, the samples taken from 223 m were markedly different in physical and mechanical properties in comparison with the samples from 240 m level. Indeed, it is noted that an important difference in the mineral composition and in the water content, resulting in a difference in the physical properties such the liquid limit, plasticity index, etc. Moreover, it seems that the samples from different depth reveal different non linear elasticity. The shear modulus seems to be lower for the samples from 223 m depth than ones of 240 m depth (Figure 4.15). The peak and residual

resistance are also different. In more, the stress-strain relationship reveals a wider stress range of the softening responses for Boom Clay at 223 m depth in comparison with the Boom Clay at 240 m depth.

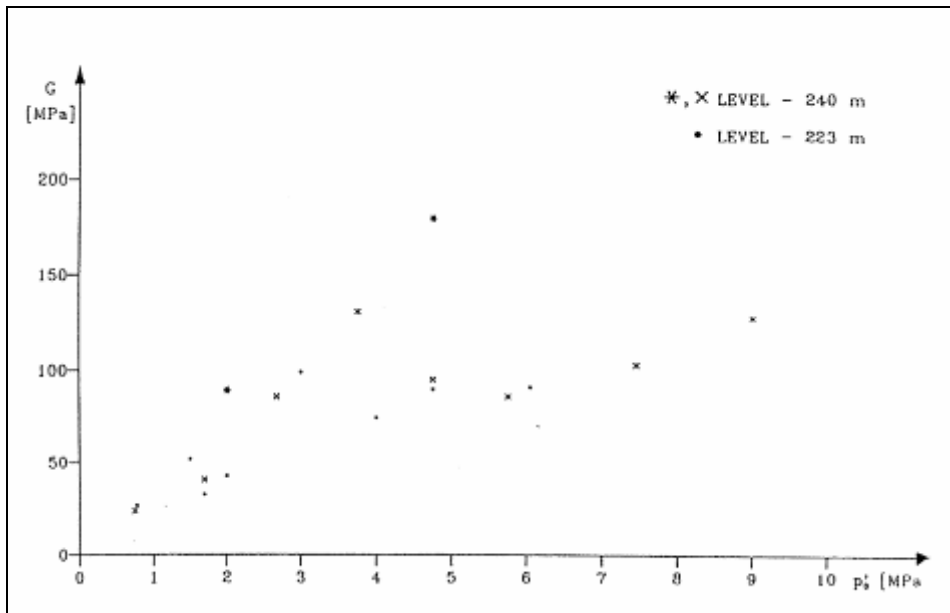


Figure 4.15: Secant shear modulus versus isotropic stress calculated from compression tests on samples from 223 m and 240 m depth (Baldi *et al.*, 1991)

Moreover, the set of oedometric and isotropic tests revealed anisotropy of properties of Boom Clay, which seems to decrease with the appearance of plastic strain.

In conclusion, these tests allowed to investigate aspects such the thermal consolidation patterns (through the controlled stress paths tests in a plan p' - T), the failure mode during heating under undrained condition (undrained heating tests at controlled deviatoric stress state), the influence of the temperature on the yield locus position, on failure conditions, on deformational pattern (non associated behaviour), on the compressibility (compression drained tests at different OCR and different temperatures, heating at different constant pressure in drained conditions at different OCR), etc. Moreover, they allowed to determine some mechanical constants. The value kept by Baldi *et al.* (1991) are presented in the Table 4.7:

Slope of the Critical State line (CSL)	M	0.87 - 1	
Friction angle	ϕ	22.3 - 25.3	°
Preconsolidation pressure	p'_0	≈ 6	MPa
Overconsolidated ratio	OCR	2.05 - 2.64	
Initial void ratio	e_0	≈ 0.5	

Slope of the elastic line	□	≈ 0.013	
Slope of the normal consolidation line	□	≈ 0.11	
Shear modulus	G	≈ 95	MPa

4.2.1.3 INTERCLAY II project (EUR 16204 EN)

A program of small scale laboratory tests on samples of Boom Clay was specially commissioned for the INTERCLAY II project and carried out by ISMES to provide the THM behaviour data base and boundary problems for the numerical benchmark exercises.

The tests performed were 5 hollow cylinder and 3 triaxial tests but one of them was not utilizable owing to the unexpected behaviour observed during the test. The triaxial tests were realised in different path in a p' - q - T space, including shearing loading – unloading cycles at a constant temperature of 90 °C and heating – cooling cycles at constant deviatoric stress. The temperature cycle ranged from 22 °C to 90 °C. The hollow cylinder tests were carried out using the samples from the Test Drift. The loading paths included the saturation under isotropic effective stress, decreasing of the inner cavity pressure under undrained conditions and heating of the samples in undrained conditions.

The main results of hollow cylinder tests were measurement of the internal volume change and vertical deformation with the temperature variation.

There are nevertheless some remaining questions in the program of tests. Indeed, the results obtained from various samples were significantly different and the difference increased rapidly with increase of temperature. It illustrated the difficulty to obtain consistent results and the uncertainty in interpretation and deduction of the material properties. In more, the questions about the natural inhomogeneity of the Boom Clay samples were raised again (Jeffries, 1995).

4.2.1.4 PhD thesis of N. Sultan

In 1997, N. Sultan realised his PhD thesis on the theme of the thermo-mechanical behaviour of Boom Clay including experimental campaign and model development. This one, entitled "*Etude du Comportement Thermo-Mécanique de l'Argile de Boom: Expériences et Modélisation* – Study of the Thermo-Mechanical Behaviour of the Boom Clay: Experiments and Modelling", is effectuated at the laboratory CERMES, "Ecole des Ponts et Chaussées" in Paris. His main objective is to establish a pertinent thermo-mechanical constitutive law for saturated Boom Clay with the help of a comprehensive laboratory test program, under stress and temperature controlled (Sultan, 1997).

The test program are realised on samples taken from the Test Drift at 223 m depth. It included two parts:

Saturated hydro-mechanical behaviour: oedometer tests and drained/undrained triaxial tests at different OCR and under isothermal conditions, at ambient temperature;

Thermo-hydro-mechanical behaviour: triaxial tests with very complex stress paths and temperature controlled in a space p' - q - T (p' is the effective mean stress, q the deviatoric stress and T the temperature) under drained/undrained conditions.

The test program allowed to characterize the main thermo-hydro-mechanical behaviour of saturated Boom Clay and to investigate the following aspects:

For high OCR, thermal loading induces first expansion resulting from the thermal dilation of the components and secondly contraction further to a rearrangement of the particles (Figure 4.16). The transition temperature between these behaviours increases with OCR. However, the slope of the volumetric strain curve in the cooling stage is independent of the applied mean effective stress, which is consistent with the result obtained by Baldi (§ 4.2.1.2). The cooling slope is parallel to the slope of the expansion heating phase.

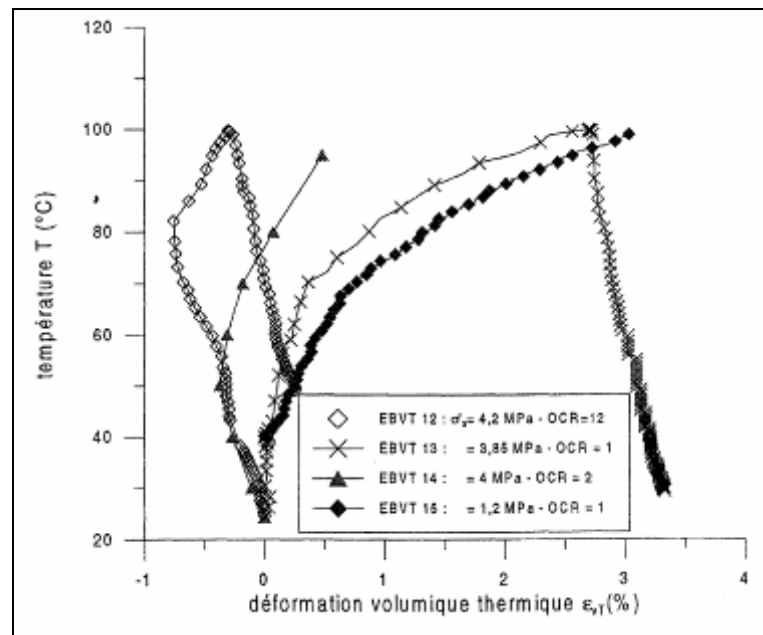


Figure 4.16: Thermal volumic deformation at different OCR (Sultan, 1997)

These observations confirm that the thermal behaviour of Boom Clay is elasto-plastic. In the case of high OCR, heating first produces elastic strain that corresponds to the thermal expansion of the soil particles, as demonstrated by the parallelism observed between the cooling slope and the expansion slope. Plastic contraction intervenes afterwards when temperature reaches a certain value. According to standard soil elasto-plastic behaviour, an irrecoverable volumetric strain commonly induces a hardening phenomenon that is characterised by an increased of the yield stress. This should also be observed with thermal induced plastic strains, what is investigated in the next point (Delage *et al.*, 2004).

In order to check the thermal induced plastic strains (hardening) of the Boom Clay, a series of tests was performed on 4 samples which were initially isotropically loaded to 4 MPa, next heated to 100 °C and finally submitted to temperatures equals to 23, 40, 70 and 100 °C respectively where they are then isothermally loaded. Heating up 100 °C would induce hardening of the sample that would be evidenced by subsequent loading at various lower temperatures. Figure 4.17 shows that the preconsolidation pressure (corresponding to the yield pressure) at various temperatures are all higher than 4 MPa, showing a thermal hardening which is more significant at lower temperature (Delage *et al.*, 2004).

Moreover, the lower part of the Figure 4.17 shows that the yielding points are aligned in a $\log(p'_{cT})$ -T plane. It can be thus concluded that the preconsolidation pressure decreases when temperature increases according to an exponential function.

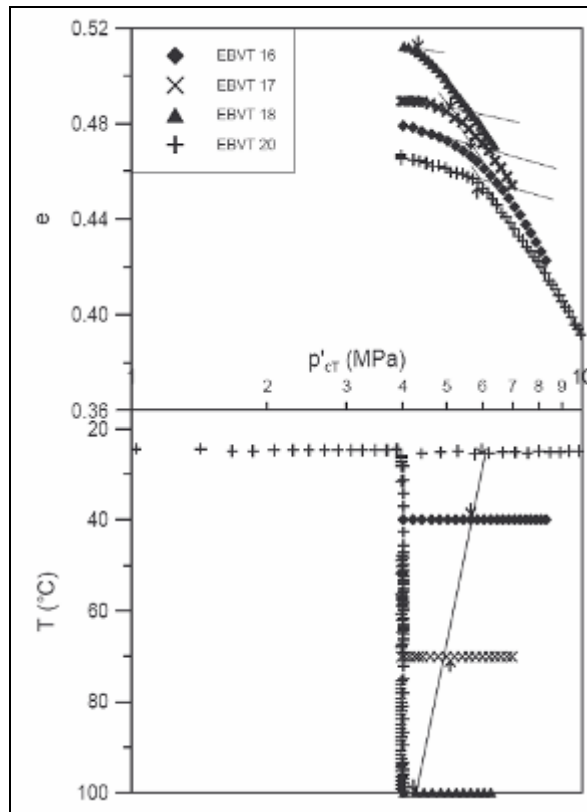


Figure 4.17: Isotropic compression tests at different temperatures (Delage *et al.*, 2004)

Boom Clay presents thermal consolidation. Indeed, thermal consolidation tests at different temperatures were carried out by applying 10 °C temperature increments from 20 °C to 95 °C to a natural Boom Clay sample saturated and at an overconsolidated state with OCR equal to 2. Figure 4.18 shows the curves giving the volume changes as a function of time at different temperature increment step. It is observed that a larger contraction takes place after an initial smaller thermal expansion. The expansion corresponds to the thermal expansion of the solid and water phases. In the contraction stages, the shapes of the curves are similar to that of standard consolidation curves, and show that the volume decrease is related to thermal induced excess pore pressure dissipation (Delage *et al.*, 2004).

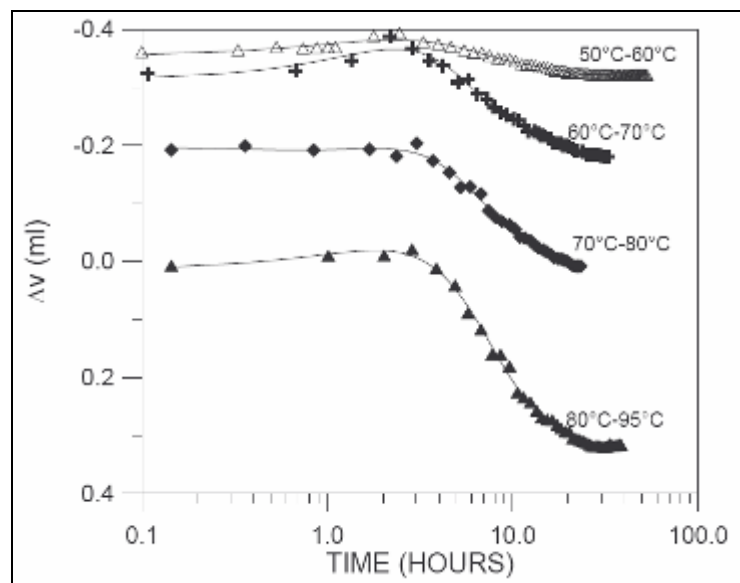


Figure 4.18: Thermal consolidation curves, highest temperature (Delage *et al.*, 2004)

Temperature has an effect on the permeability (Figure 4.19). However, it can be seen on this figure that the changes in permeability are due to the coupled effect of changes in temperature and porosity. It can also be noted on the Figure 4.20 (from Delage et al. 2000). To separate these two effect the intrinsic permeability values (K) were calculated according to:

$$k = \frac{K\gamma_w(T)}{\mu(T)}$$

where $\mu(T)$ is the water viscosity and $\gamma_w(T)$ the unit weight of water. The water viscosity in Pa.s is determined by the following relation, valid for free water:

$$\mu(T) = -0.00046575\ln(T) + 0.00239138$$

In this range of temperature considered (20 to 90 °C), there is no significant change in the value of $\gamma_w(T)$.

The results, presented in Figure 4.20 in a semi-logarithmic diagram, show that the relationship between the intrinsic permeability K and the porosity n is linear and appears reasonably independent of temperature. Consequently, the intrinsic permeability of a sample loaded at a given temperature is only dependent on its porosity, not on the thermo-mechanical path previously followed in a (p' – T) plane where p' is the mean effective stress. In other words, volume changes created by stress and/or temperature changes have the same effect on the intrinsic permeability of a sample.

It can be thus concluded that the changes in permeability k with temperature depends mainly on the variation of the viscosity.

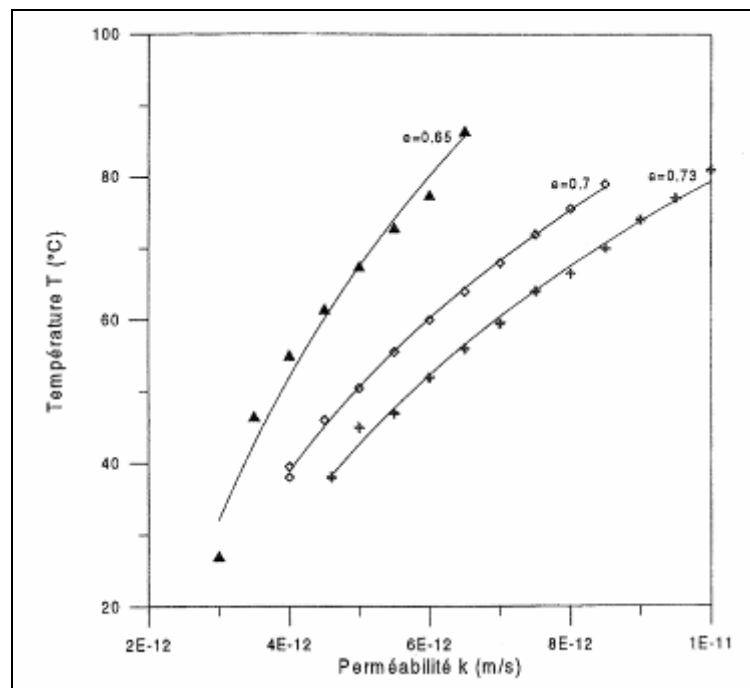


Figure 4.19: Temperature effect on the permeability (Sultan, 1997)

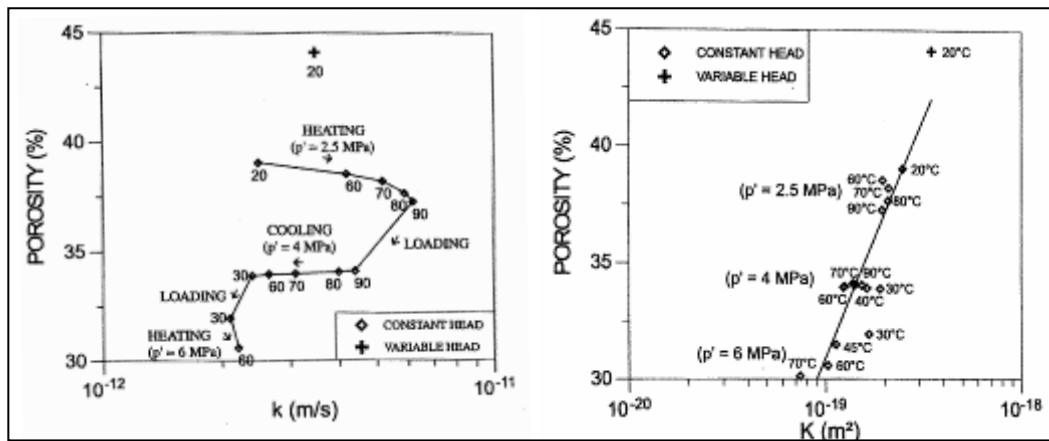


Figure 4.20: a) Permeability (k) tests performed on a sample of Boom Clay at various temperatures (values along the line in °C) and stresses; b) Results of permeability tests in terms of intrinsic permeability (K) (Delage *et al.*, 2000)

It is also worthwhile to insist here that, in case of undrained condition, heating induces pore water overpressures. Their influence on fracturation must be investigated in more details.

The analysis of the tests results indicated clearly anisotropy. This one is of two kinds, the inherent anisotropy and the induced anisotropy.

It is necessary to note that the saturated preconsolidation pressure at ambient temperature obtained within the campaign tests of Sultan' thesis is very low (0.37 MPa) with respect to those obtained in other projects where it is about 6 MPa. The loss of the preconsolidation pressure is explained by three factors:

- The age of samples;
- The swelling induced by the unloading during the sampling;
- The desaturation of the samples.
- The loss of preconsolidation pressure must be studied to check its effect on the tests results.

Moreover, the evolution of the anisotropy with the stress, the plastic deformation and the temperature needs more investigations.

4.2.1.5 PhD thesis of D. De Bruyn

In 1999, De Bruyn devoted his PhD thesis, "Influence d'une élévation de température sur le comportement physique et mécanique de l'Argile de Boom dans le cadre de la problématique de galeries d'enfouissement de déchets radioactifs – Influence of a temperature increase on the physical and mechanical behaviour of the Boom Clay in the framework of the storage gallery of radioactive waste", to the study of temperature influence on the physical and mechanical behaviour of Boom Clay.

He performed then several series of CIU triaxial tests at different temperatures on samples from the Tests Drift, at 223 m depth. In more, one series of tests were realised on samples taken around the ATLAS in situ experiment (Figure 4.21). The ATLAS large scale in situ test is a part of the INTERCLAY program, which consisted in the study of the admissible thermal loading for Boom Clay. These samples were thus submitted at a temperature of 40 °C during three years and of 65 °C during two years previously.

Compared to tests on samples not submitted to ATLAS, it can be concluded that the limited temperature level of ATLAS (65 °C, thus a ΔT equal to 55 °C) does not seem to have a significant effect on the samples.

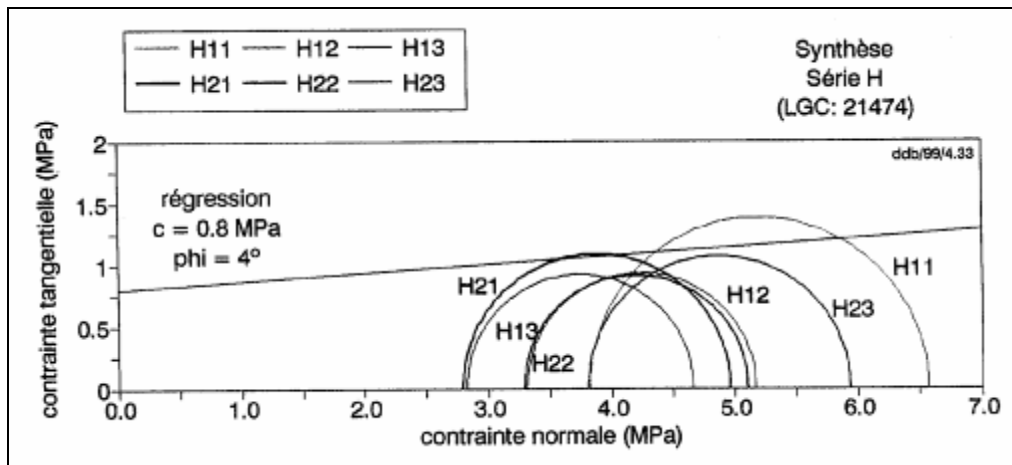


Figure 4.21: CIU tests on samples taken around ATLAS in situ experiment (Mohr-Coulomb circle in total stress) (De Bruyn, 1999)

Another series of tests was also carried out on samples taken around the CERBERUS in situ experiment (Figure 4.22). This one aimed to stimulate the near-field effects of a Cogema HLW-canister after 50 years cooling time in the Boom Clay. The samples were thus heated at about 85 – 90 °C and/or irradiated during a period of five years previously.

It must be noted that these samples have been submitted to the excavation of the Test Drift and to the drilling of the experiment itself, and next to the heating and irradiation. Taking into account this, it is remarked that a heating to 90 °C for 5 years has induced a significant loss in cohesion (30 %).

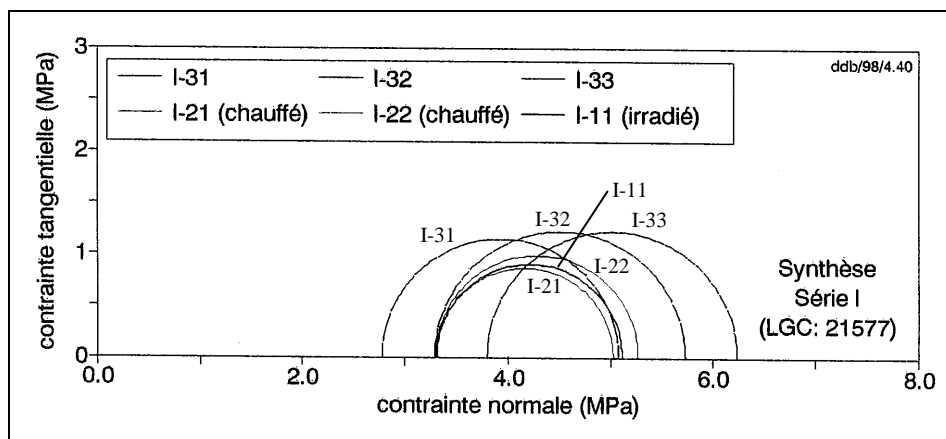


Figure 4.22: CIU tests on samples taken around CERBERUS in situ experiment (Mohr-Coulomb circle in total stress) (De Bruyn, 1999)

Moreover, attention was paid to the cutting orientation of each sample regarding to the natural stratification of the Boom Clay. Some samples were cut following the direction perpendicular to the stratification and the others following the parallel one. The anisotropy of Boom Clay was thus put in evidence (De Bruyn, 1999).

4.2.2 Time related THM behaviour

Some laboratory tests campaigns realised in different projects like these of the Rousset's PhD, the ONDRAF-G3S contract and the CEC contract F11/0049 were devoted at the study of the time related thermo-hydro-mechanical behaviour. A synthesis taken the different projects in a chronological order is realised here.

4.2.2.1 PhD thesis of G. Rousset

In 1988, Rousset realised his PhD thesis, "*Comportement Mécanique des Argiles Profondes: Application au Stockage des Déchets Radioactifs – Mechanical Behaviour of Deep Clays: Application to the Radioactive Waste Storage*" in order to establish an elasto-visco-plastic model for saturated Boom Clay. He effectuated this one at the Ecole Nationale des Ponts et Chaussées in Paris.

The samples used in the tests come from coring performed in the Boom Clay at 230 m depth.

In a first time, some undrained short term laboratory tests were realised. There were undrained triaxial tests with sometimes loading – unloading cycles. An example with loading - unloading is presented at the Figure 4.23.

Through the realised tests, following results can be put in evidence:

- Small softening (dilatation) at small deformation;
- The cohesions and the friction angles were determined respectively at the peak of strength and at the residual strength of the material:

$$c_{cu} = 1.3 \text{ MPa} \quad \phi_{cu} = 4^\circ$$

$$c_{res} = 0.8 \text{ MPa} \quad \phi_{res} = 4^\circ$$

- The elastic zone is very limited, nearly null;
- The Young's modulus E is very high. It decreases with the accumulated irreversible deformation;
- The volume of the sample is not very affected by the loading – unloading cycles. It signifies that the volume variations are induced by the piled up irreversible deformation and not to the stress.

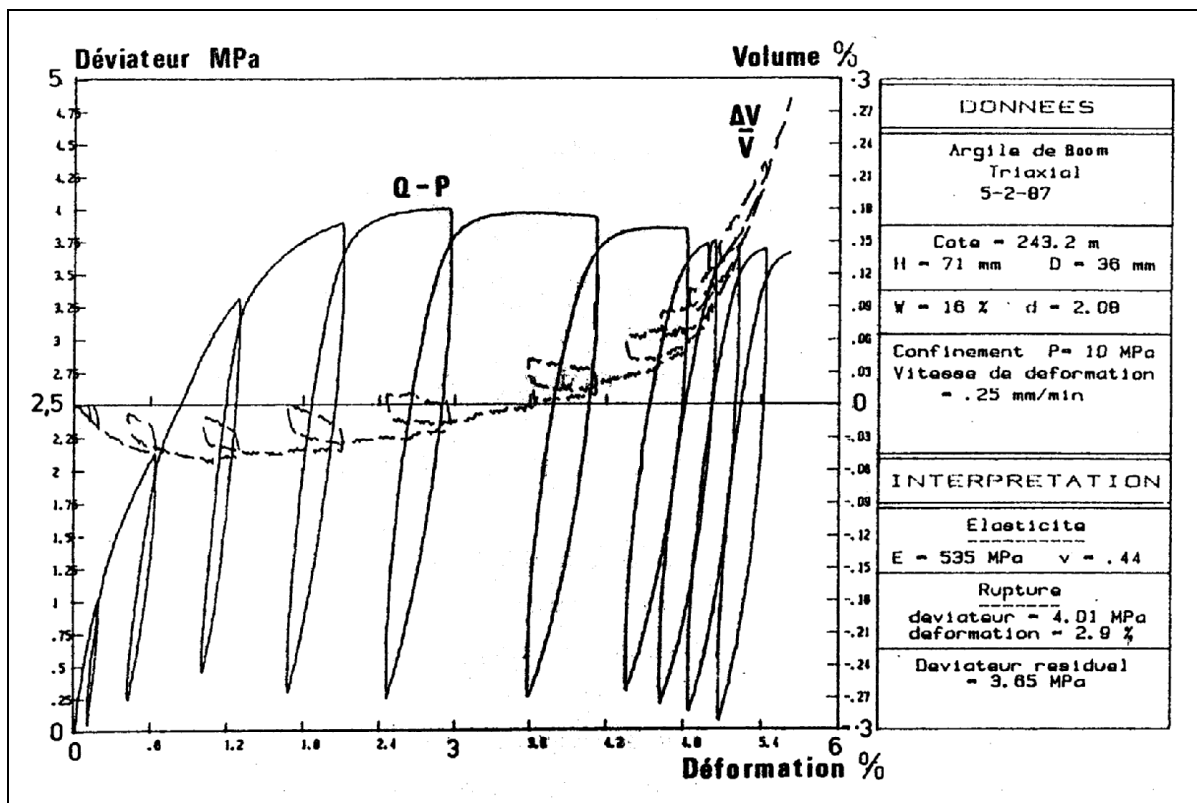


Figure 4.23: Undrained triaxial test with loading-unloading cycles (P=10 MPa) (Rousset, 1988)

Next, the laboratory tests were thus devoted to the time related behaviour of the Boom Clay. Triaxial creep tests at different deviatoric stress state as well as thick tube creep tests allows to simulate more closely the in situ conditions in controlling independently the internal pressure or convergence, the external pressure or the external volume and the axial force or displacement (plane stress or plane strain conditions).

The results of a creep test on thick tube are presented at the Figure 4.24.

The main conclusion of these tests is that the time related behaviour of the Boom Clay begins very early, in the same time as the plastic deformation (Rousset, 1988).

The Rousset's PhD thesis is the first work on the delayed behaviour of Boom Clay and it provides very interesting results. However, it is necessary to note that all tests were carried out in undrained conditions and the pore water pressure was not measured. The water effect is thus not taken into account and it is not yet possible to decouple the effect of the skeleton viscosity from the effect of the pore water.

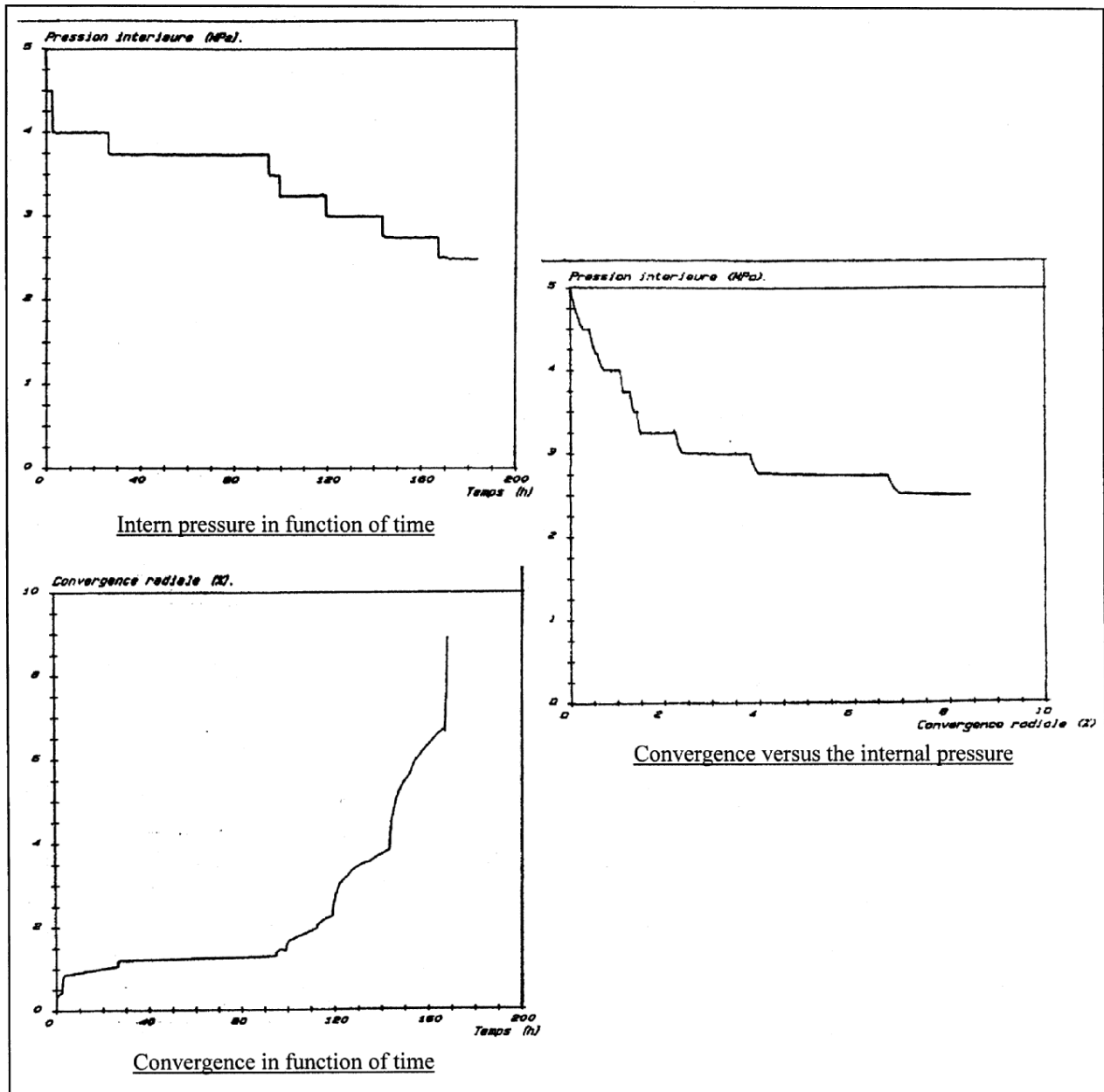


Figure 4.24: Creep test on thick tube (adapted from Rousset, 1988)

4.2.2.2 CEC contract FI1W/0049 (EUR 14438 FR)

In 1993, Rousset *et al.* carried out the studies on the delayed behaviour of Boom Clays in the framework of the CEC contract thanks to a campaign of laboratory and in situ tests. In order to facilitate the test results comparison and to study the scale effect, the laboratory tests were performed with the same geometry but with different scales.

The tests carried out were of two kinds:

- Thick tube tests. The creep at different stress state and the relaxation at different controlled convergences;
- In situ dilatometer tests. Both creep and relaxation aspects were studied over a period of three years.

It was observed and deduced that:

- The Boom Clay presents a pronounced time related behaviour;

- Both short and long terms shear strength depend largely on the water content;
- The borehole in Boom Clay presents important convergence;
- The scale effect is moderate for Boom Clay;

The results obtained in laboratory and in situ are comparable.

The tests also allowed to determine the short and long term convergence of Boom Clay.

Attention was paid on the inhomogeneity of Boom Clay. Indeed, the samples taken from the Test Drift at 223 m depth presented a very big scatter in water content, from 24.6 to 29.4 %. The tests were thus realised in three classes following the water content (25 %, 27 % and 29 %). The influence of the water content on short and long term resistance was thus clearly put in evidence.

The impact of the anisotropy of in situ stresses was also investigated and the in situ dilatometer tests were performed in boreholes drilled in different directions. The creep tests showed that the convergence of the Boom Clay depends on the borehole direction and the anisotropy of the in situ stress state was thus put in evidence (Rousset *et al.*, 1993).

A question remains always open concerning the representative and the quality of the samples in regard to the variable water content.

4.2.2.3 Contract ONDRAF – G3S (Report G3S, n° 94-002)

In 1994, the laboratory G3S studied the THM behaviour of Boom Clay, especially the temperature influence on its viscoplastic behaviour.

The tests were carried out on samples taken from a horizontal borehole drilled from the Test Drift. They were cut following the direction perpendicular to the borehole axis and came then from different distances from the Test Drift gallery.

Undrained triaxial tests under different deformation velocity, with loading – unloading cycle, at elevated temperature were realised. These tests allow mainly to characterise the short term TM behaviour (especially undrained) of the Boom Clay as well as the temperature influence on this behaviour.

The main conclusion of these tests is that the Boom Clay is a high plastic clay with an elastic zone very limited. Indeed, plasticity appears as soon as the beginning of the loading. It is consistent with the results of Rousset, in the framework of his PhD thesis (see Figure 4.23).

The inhomogeneity of the Boom Clay was again put in evidence in this project. Indeed, the samples presented a very big variation in physical properties, principally in the water content. The influence of this one was then analysed in the project.

Concerning the long term behaviour, the following tests were carried out:

- Drained and undrained triaxial creep tests in order to distinguish the time related behaviour due to the hydraulic diffusion (drained tests) from that caused by the viscosity of solid skeleton (undrained tests);
- Triaxial drained creep tests at different temperatures in order to study the influence of the temperature on the creep behaviour;
- Oedometer creep tests;
- Some particular tests with very complex stress paths;

It can be noted that the time related behaviour is an essential mechanical behaviour of the Boom Clay. Indeed, Figure 4.25 shows two triaxial creep tests at different constant deviatoric stresses, the first in drained condition (D) and the second in undrained condition (U). The comparison between these two experiments allows to distinguish the importance of the consolidation, in other words of the pore water dissipation, in the delayed deformation of the first stage of the drained test and to put in evidence the importance of the delayed deformation due to the viscosity of the skeleton for the undrained test (Djeran *et al.*, 1994).

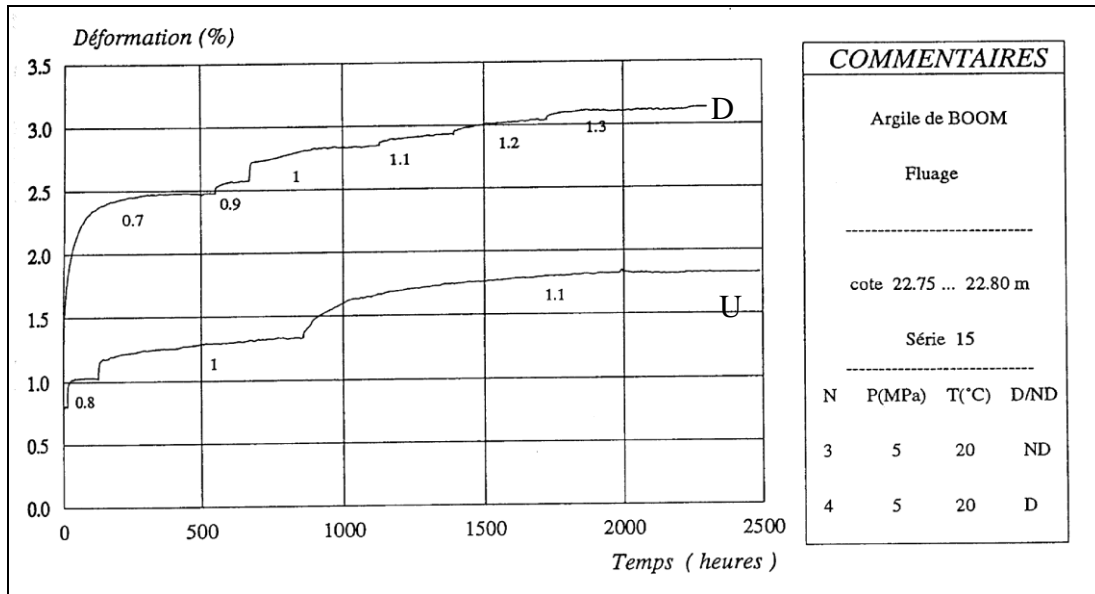


Figure 4.25: Creep at 20 °C – Drained (D) and Undrained (U) (Djeran *et al.*, 1994)

Figure 4.26 represents undrained creep tests realised at 100 °C on two different samples. Compared with the curve U on the Figure 4.25, it can be seen that the creep is highly raised for an elevated temperature and happens for smaller deviatoric stress. The tests being undrained, the creep depends only on the viscosity of the Boom Clay skeleton. It can thus be deduced that the temperature increases sensibly the viscosity of the material.

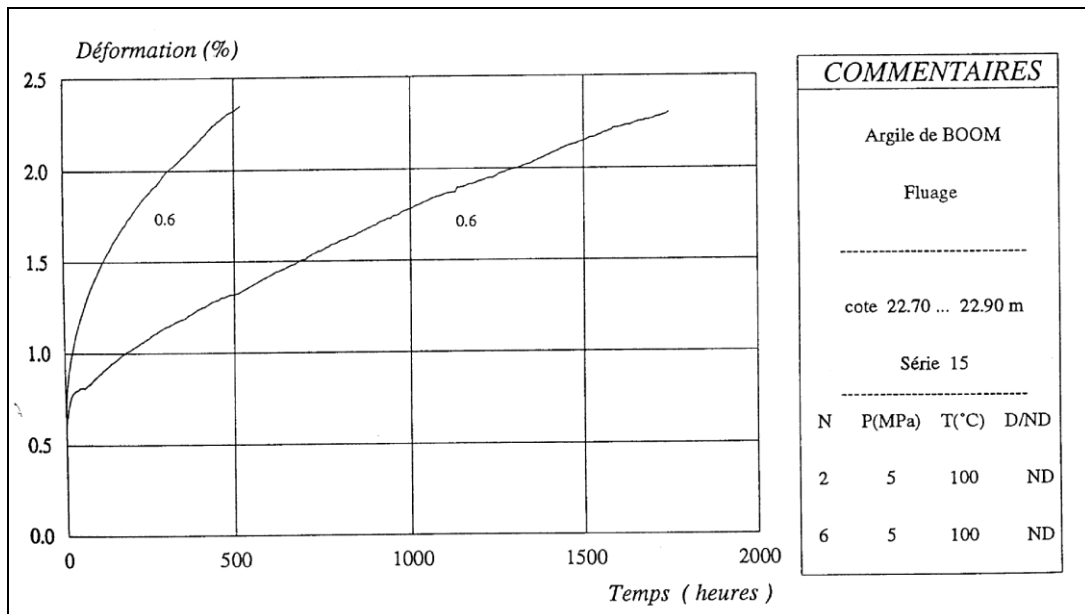


Figure 4.26: Undrained creep tests at 100 °C for 2 different samples (Djeran *et al.*, 1994)

Heating tests were also performed on the Boom Clay. The heating was performed on drained condition, the sample height was monitored during the heating phase. The curves of apparent extension of the samples in function of the temperature are mainly linear, the drained linear dilation coefficient α_m can thus be determined and it is on average equal to:

$$\alpha_m = 4.7 \cdot 10^{-5} \text{ K}^{-1}$$

It must be noted that the thermal loading are effectuated with two different velocities, 3.95 °C/min and 2.0 °C/min. The comparison of the thermal dilation values shows that a decrease of the velocity induces a decrease of the measured thermal dilation (Djeran *et al.*, 1994).

One more time, the samples presented a big variation in physical properties and principally in the water content. Unfortunately, the influence of this one on the long term behaviour could not be deduced due to the lack of tests results.

4.2.2.4 EC SELFRAC project

Recently, more attention was paid to the evaluation of both mechanical and transport properties in the Excavation Disturbed Zone around the underground storage gallery. The perturbation of the excavation may induce a significant increase of the permeability, related to diffuse and/or localised crack proliferation in the material (Process A). Self-healing properties of clays can in turn reduce the permeability with time (Process B).

In the frame of the project SELFRAC, additional laboratory tests to characterise Processes A and B were realised to give the necessary data to improve and calibrate constitutive models.

Triaxial tests, isotropic tests and biaxial tests as well as hollow cylinder tests on both damaged and undamaged samples (with or without artificial fractures) were performed at different stress states, different hydraulic boundary conditions in order to characterise the hydromechanical behaviour of the soil and the obtained data were used to calibrate the constitutive model. During the tests, the permeability was monitored to obtain the correlation between the diffuse and localised plastic strain and permeability as well as the self-sealing capacity. During the biaxial tests, deformation of the specimen was visualised using a stereophotogrammetric system.

Permeability tests on initially fractured core samples are being performed also. Some of these tests are followed up by means of non destructive microfocus X-ray computer tomography (μ CT) to analyse the evolution of the density of the sample. Consequently, these μ CT analyses can confirm if there is a closure of the fractures during the permeability tests.

Here is listed the main results obtained from the laboratory tests campaign, classified by kind of tests:

- Uniaxial, biaxial and triaxial tests – Diffuse and/or localised crack formation – Process A:
The Boom Clay exhibits two type of mechanical behaviour, depending on the mean effective stress (Figure 4.27):

At the in situ state of stress and in drained condition, the behaviour is ductile and contractant, i.e. the q - $\varepsilon_{\text{axial}}$ curve, where q is the deviatoric stress and $\varepsilon_{\text{axial}}$ the axial strain, shows a plateau. The hydraulic conductivity was found to slightly decrease from $7.15 \cdot 10^{-12}$ to 10^{-13} m/s due to the contractance of the pore space during the shearing phase, during these tests.

Conversely, at a low mean effective stress (0.4 MPa), the mechanical behaviour is characterized by the development of shear bands leading to the failure of the specimen. The q - $\varepsilon_{\text{axial}}$ curve shows a peak and the specimen exhibits dilatancy. In this case, the permeability is not influenced neither by the onset of localisation and the propagation of shear bands nor by the dilatancy before the peak stress.

We can note that to detect an important increase of the permeability, the porosity of the specimen (bulk porosity or discontinuities), has to change in a significant manner. Moreover, the discontinuities (if they exist) have to be interconnected to each other and to the hydraulic pore pressure lines. In our tests, the shear bands that we have observed were very thin indicating a low change of the bulk porosity. They were not always propagating from one end to the other end of the specimen and, due to their slope, they were not always connected with the pore pressure lines of the system. If the bulk permeability has not evolved, we can not conclude on the permeability in the shear band.

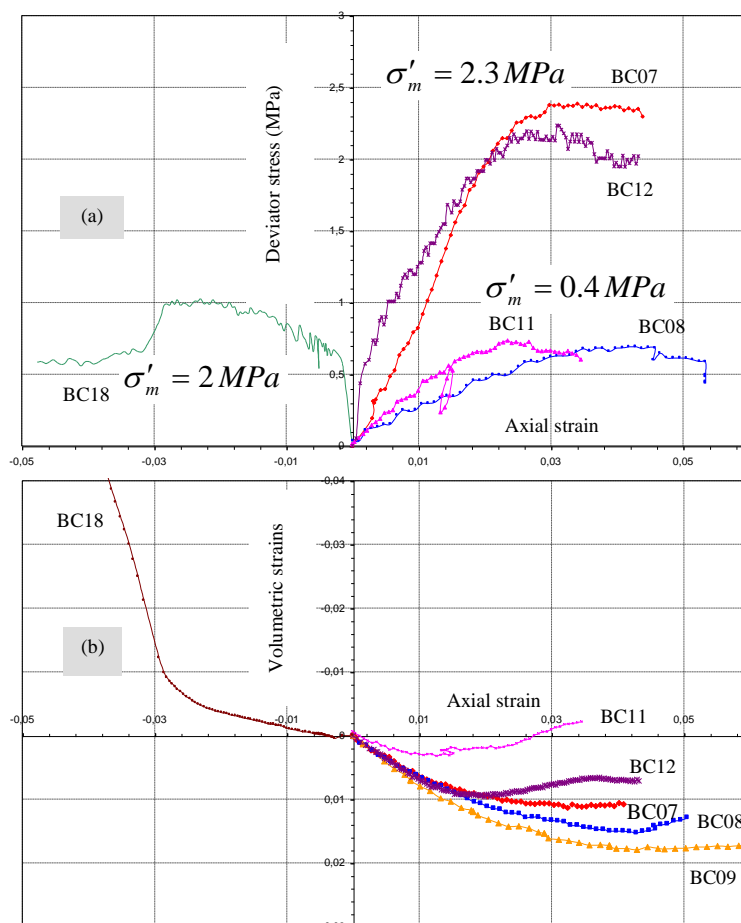


Figure 4.27: Shear tests on Boom Clay on samples consolidated at different effective isotropic stress: 0.4 MPa (BC11, BC08), 2 MPa (BC18), 2.3 MPa (BC07, BC12) - (a) deviator stress / (b) volumetric strains versus axial strain (Bernier *et al.*, 2006)

- Triaxial tests on hollow cylindrical samples:
These tests allowed to measure the increase of permeability related to localised crack proliferation (Process A), and to check the potential reduction in permeability with time and thus the sealing capability (Process B). The main conclusion of these tests is that fractures developing in Boom Clay can undergo a very fast sealing when subjected to an almost hydrostatic state of stress close to the in situ one (4.5 MPa total stress).
- Isostatic and permeameter tests with μ CT visualisation:
The specific objectives of these laboratory tests were:
 - To assess the modifications of flow properties due to the presence of a main single discontinuity in Boom Clay samples by monitoring the evolution of its hydraulic conductivity;
 - To test the influence of the chemical composition of the solution injected through the Boom Clay samples on their sealing properties;

- To establish a correlation between the discontinuity geometry and dimensions, the state of stress and the flow properties;
- To visually observe the evolution of the sealing process with a microfocus X-ray computer tomography technique.

The permeameter tests consisted in testing the influence of the injected fluid chemistry on the sealing capacity of the clay. An artificial planar fracture has been produced through the axis of a cylindrical sample prior its installation in a permeameter cell. The evolution of the samples hydraulic conductivity has been monitored. We used micro focus X-ray computer tomography (μ CT) as an imaging technique to visualise the sealing process of the fracture. The isostatic tests consisted in testing combined mechanical and chemical sealing. The principle was to drill a hole along the axis of a cylindrical clay sample and to submit it to an increasing confining pressure, while the evolution of the clay hydraulic conductivity was monitored by applying an axial hydraulic gradient. Mean pore water pressure and mean effective stress were kept balanced throughout the test.

The permeameter tests showed that a sealing phenomenon occurs for the Boom Clay. Indeed, a decrease in permeability is observed (Figure 4.28). The final measured hydraulic conductivity was comparable to undisturbed clay and the initial planar fracture was no longer discernable. Moreover, the artificial fracture is no longer continuous as observed in the μ CT images (Figure 4.29). Indeed, after 4 hours of permeability test, the fracture has nearly completely disappeared and even before starting permeability test, fracture has disappeared at some places.

The interstitial water chemistry had clearly an influence on the speed of the sealing process and on the recovered cohesion level. For the both parameters, the use of alkaline fluid was favourable.

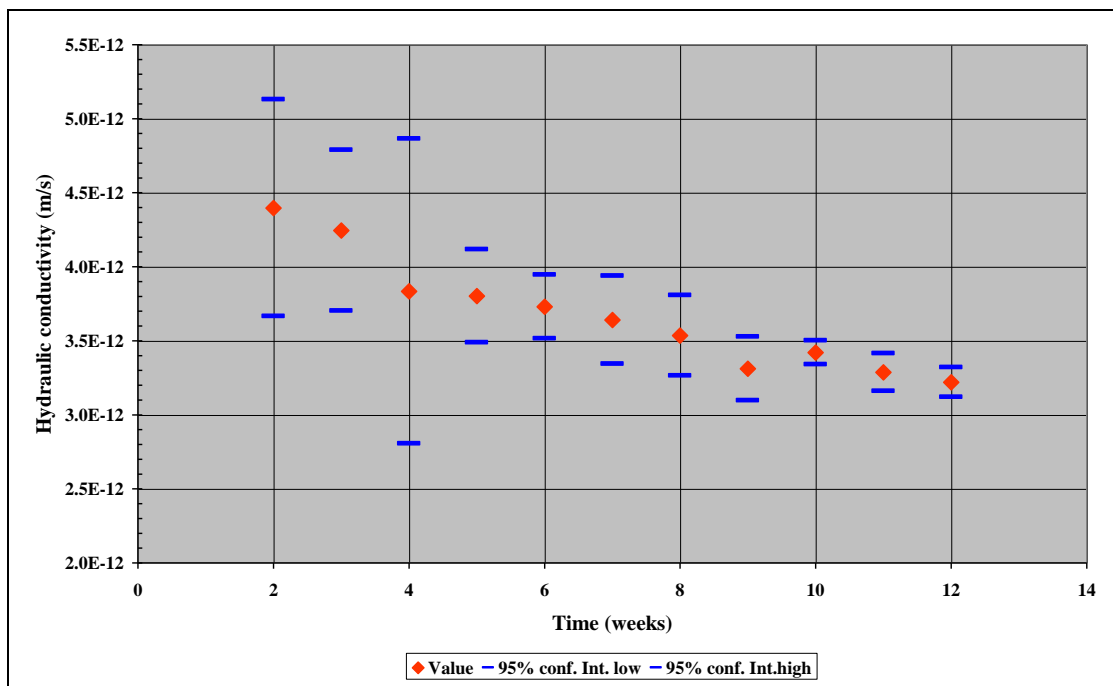


Figure 4.28: Weekly evolution of the hydraulic conductivity during a permeameter test on a Boom Clay sample with synthetic Boom Clay water as pore water solution (Selfrac – D2)

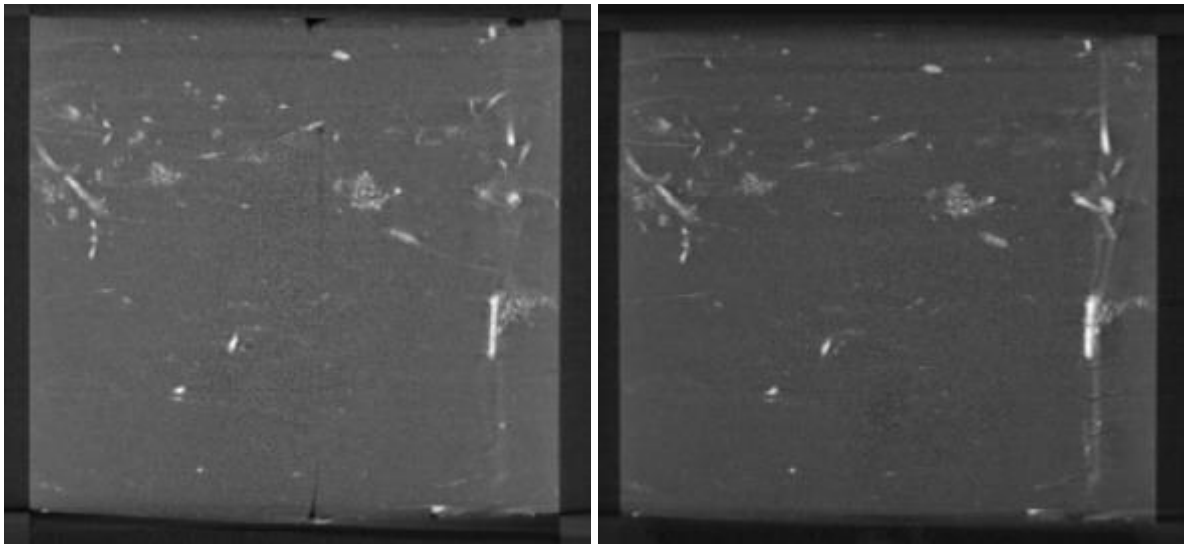


Figure 4.29: μ CT transects through Boom Clay sample in permeameter cell before permeability test (left) and after 4 hours of permeability test with synthetic Boom Clay water (Selfrac – D2)

The principle of the isostatic test was to drill a hole along the axis of a cylindrical clay sample and to submit it to an increasing confining pressure, while the evolution of the clay hydraulic conductivity was monitored by applying an axial hydraulic gradient. Mean pore water pressure and mean effective stress were kept balanced throughout the test.

A fast decrease in permeability (Figure 4.30) is observed for holes of 6 and 12 mm diameter, which show a similar evolution. Both permeabilities tend to the in situ measured value. After dismantling from the isostatic cell, a fracture developed, probably due to the confining pressure release. Within the μ CT analyses (Figure 4.31), both samples showed an eye-shaped zone of reduced density around the original position of the hole. The long edge of the reduced density zone is parallel to the bedding plane. The fracture created during the dismantling is fully located within the low density zone.

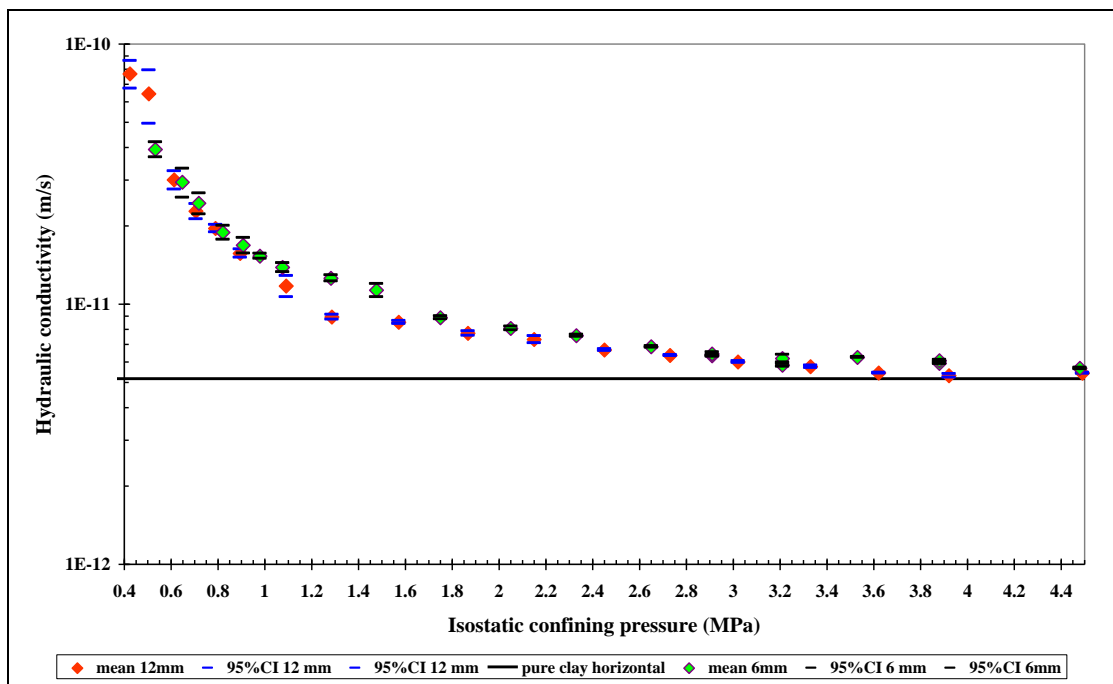


Figure 4.30: Evolution of permeability in Boom Clay sample with original artificial hole of 6 and 12 mm diameter analysed in isostatic cell (Selfrac – D2)

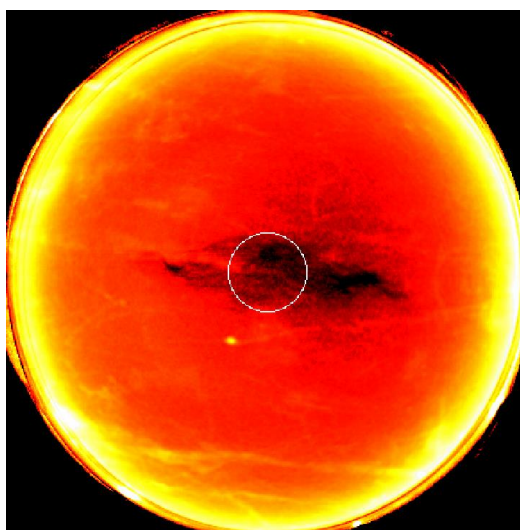


Figure 4.31: Mean μ CT slice, averaging the clay matrix while ignoring the fractures, through Boom Clay sample with original artificial hole of 12 mm diameter after permeability tests and dismantling from isostatic cell (Bernier *et al.*, 2006)

In conclusion, the fast self-sealing capacity of Boom Clay has been clearly demonstrated with permeability tests in permeameter and isostatic cells and visualised by means of μ CT. Alkaline fluids seem to enhance the sealing process. Even disturbances of 15 % of the original sample surface/volume, show the sealing. Moreover, a density decrease around the original fracture/hole is noticed due the self-healing process. On the total surface/volume of clay analysed, the permeability recovers the permeability of undisturbed Boom Clay (Bernier *et al.*, 2006).

4.2.3 Unsaturated hydro-mechanical behaviour

Few tests were devoted to the study of the unsaturated hydro-mechanical behaviour of the Boom Clay. They are listed here:

In the framework of the Reseal project, two suction controlled oedometer tests were performed by SCK;

PHEBUS project:

The objective of this project was to study the hydraulic behaviour of the massif around a ventilated underground gallery (desaturation, suction generation, etc.). Some sorption – desorption tests were carried out on natural Boom Clay samples, on Boom Clay mud samples and on compacted artificial Boom Clay samples. Moreover, a mock up test was realised in laboratory to study the possibility of desaturation of Boom Clay due to the ventilation. The principle of this one was to cycle a controlled humidity air in an orifice drilled in a cylinder sample and to measure the hydric exchange between the air and the Boom Clay. After dismantling, the moisture profile of the mock up was measured and the test showed that a suction field develops around the orifice inducing consolidation. However, the desaturation zone is limited. It is also necessary to underline that the air entry value may be very high in intact Boom Clay, at least 1 or 2 MPa. But, in the EDZ, the host rock may possess a double porosity, composed of micro-pores and of micro-fractures. Air entry value could then be lower due to the presence of the micro-fractures. In such case, the desaturation in the EDZ could become significant.

MEGAS project:

In the framework of this project on the gas migration in the clay, some meaningful laboratory tests were realised on artificial Boom Clay samples to determine the relative gas permeability, and on both natural and remould Boom Clay samples to determine the gas

breakthrough pressure. Very interesting results were obtained by the gas breakthrough experiments carried out under different conditions. Moreover, the comparison between the natural Boom Clay and the clay plug showed a very good repeatability of both hydraulic conductivity and breakthrough pressure. It would mean that the hydraulic properties measured from the artificial clay plug compacted from Boom Clay powder to the same dry density as natural Boom Clay are closed to the properties of the natural Boom Clay. However, the experiments provided very limited data or parameters related to the hydro-mechanical coupling behaviour. In fact, experiments did not give information on the mechanical effects (deformation) on the two-phases flow behaviour.

A lot of tests in unsaturated condition were realised on artificially prepared samples made from Boom Clay powder like compacted plug, pellets, powder or pellet/powder mixture, in the framework of the CEC project (EUR 16744), the CATSIUS clay project (DOC XII/158/99) and in the PhD thesis of Enrique (1999). But, the validation of these results to the natural Boom Clay is not straightforward. Different parameters must be taken into account like the fact that the natural Boom Clay samples and the artificial ones had not been submitted to the same stress paths or the microstructure, which plays an important role in the THM behaviour. Some properties are of course intrinsic under some conditions but not enough researches can say clearly which ones are intrinsic and which ones not. Consequently, it is difficult to extent directly the tests results obtained on artificial samples to the natural Boom Clay (Li, 2004).

4.2.4 Main remarks on the performed laboratory works

Although a lot of work was performed on Boom Clay, in many directions, with many partners and though a lot of results are available, there is a lack of coherent and systematic THM characterization program due to:

The inhomogeneity of the samples. Moreover, the origin of this inhomogeneity is unclear and there is no sensitive analysis to study its influence on the THM behaviour of the Boom Clay;

The tests results present a big dispersion. Some uncertainties and a lack of precision remain on some aspects of the behaviour and some parameters of the Boom Clay also. Indeed, the tests were realised in different laboratories, with different test equipments, following different test procedures, different protocols, etc.

Most of tests were realised in undrained conditions but the pore pressure was not measured, making difficult the interpretation of the tests results, the Boom Clay being highly hydro-mechanical coupled. The knowledge of the effective stress is thus essential for the constitutive law building.

Although all samples were initially assumed saturated, most of tests were realised without application of a back pressure to assure the saturation throughout the test. The saturation is thus discussible according to a lot of factors like the sampling procedure, the samples conservation and the unpacking which can provoke the desaturation of the samples. A small lack of saturation may alter the hydro-mechanical response of tests and make difficult the interpretation of tests results and parameters determination.

A global interpretation of these tests results is thus difficult, as well as the comparison of total tests results. In 2004, in the framework of his PhD thesis, P. Gourmel had assembled the most important laboratory tests results, and showed that the dispersion of the tests results realised in different project is significant and it is difficult to discern the reasons of this dispersion. Indeed, many factors may influence the tests results like the state of the samples (desaturation, fissures, etc.), the rigidity of the test system, the test procedure (consolidation phase, saturation process, stress or strained controlled condition, loading rate, etc.) or the inhomogeneity of the samples, etc. Another difficulty was that all information was not related in the reports.

Globally, the thermo-mechanical behaviour observed by Sultan and ISMES (WASI 380.83.7 project and FI1W/0149 contract) are consistent and the tests program was rather complete. The difference obtained between the parameters may due to the inhomogeneity and the ageing of the material itself. The Sultan's results merit thus to be checked by some identical tests with fresh specimens. A parametric sensibility analysis would be thus necessary, on the influence of the water content for example.

The majority of the laboratory works on Boom Clay were devoted to the saturated behaviour. Very few tests were realised to characterize the thermo-hydro-mechanical behaviour at unsaturated or partially saturated state of Boom Clay at natural state. Even if numerous hydro-mechanical tests were performed on artificial samples prepared from Boom Clay powder, the results can not be extended directly to the natural Boom Clay, as it was said in the previous paragraph.

So, the main uncertainties revealed by several tests are:

- ***Inhomogeneity of the samples*** and mainly the big variation related to the water content:
Visibly, the water content seems not influence fundamentally the global tests responses, and in other word, the behaviour, but well some parameters such as the cohesion, the friction angle, the elastic modulus, the shear strength, etc. This aspect needs to be checked more deeply and the spatial variation of the physical properties around the gallery should be investigated;
- **Anisotropy:**
The anisotropy of the Boom Clay was revealed in several projects but there are not yet enough investigation allowing to evaluate quantitatively this aspect;
- ***Ageing of samples:***
Although the samples used by Sultan presented a serious problem of ageing, the thermo-mechanical behaviour obtained by the tests under stress and temperature controlled paths seems however to be consistent with the responses realised in the framework of the WASI 380.83.7 project and FI1W/0149 contract;
- ***Tests procedures:***
The tests procedures used in the different studies are not always reported. It makes more difficult the interpretation and the comparison of the different tests;
- ***State of saturation:***
Mainly in the first campaigns of tests, no attention was paid on the state of saturation of the samples resulting in an uncertainty in the interpretation of the tests.

Anyway some aspects still remain to be investigated more deeply:

- The tests realised by Sultan showed that the velocity of the cooling may influence the mechanical responses but no quantitative conclusion were drawn on this subject. The hydro-mechanical behaviour under a very slowly cooling phase needs more investigation;
- The temperature and suction effects on the shear strength;
- The temperature and suction effects on the anisotropy;
- The failure mode under heating at different deviatoric stress state under drained or partially drained condition. Indeed, the tests realised in the framework of the WASI 380.83.7 project and FI1W/0149 contract showed that the heating at constant deviatoric stress will drive earlier failure of the Boom Clay due to the excess pore pressure generation but the hydraulic boundary condition around the disposal gallery in Boom Clay will be much more complex. It depends on the design of the repository and its evolution. The hydraulic boundary conditions may thus evolve with the different repository phase. It is important to investigate this aspect because the excess of pore pressure during the heating may significantly alter the near-field

and in the long-term the far-field ground water flow pattern. In addition, an increase of pore pressure induces a reduction of the effective stress and thus the capacity of the clay to sustain the shear stress will be reduced. It is thus possible that the thermal loading induces shear failure.

- The time related behaviour for the stress state when the loading is volumetric dominant because the available tests results were mostly devoted to the creep behaviour at high deviatoric stress where the viscosity is usually more pronounced. However, time related behaviour may also appear at lower deviatoric stress state. It is for example the case during the thermal loading due to the waste disposal which generates strong mean stresses in the near field of the gallery and induces irreversible deformation, or the swelling due to the backfilling, under swelling pressure which may induces volumetric viscoplastic deformation in the Boom Clay.
- Sampling disturbance effect on the test responses and the effect of the sampling procedure, in other word, the difference between blocks sampling and borehole coring.
- The desaturation – resaturation effect on both short term and long term THM behaviours of Boom Clay. This aspect stays nearly unknown for the natural Boom Clay. Moreover, the suction effect on the long term behaviour needs to be investigated because the vaporisation and desaturation in the massif after excavation may persist long time due to the ventilation and heat waste disposal (Li, 2004).

4.3 THM characterization in-situ

Since the construction of the HADES, a lot of in situ experiments have been performed. Here only the in situ tests related to the THM behaviour of natural Boom Clay will be cited.

4.3.1 CERBERUS test (EUR 18151 EN)

The CERBERUS test aimed to stimulate the near-field effects of a Cogema HLW-canister after 50 years cooling time in the Boom Clay. These properties were simulated during 5 years from 1989 to 1994.

The test was designed to collect experimental in situ data about thermo-hydro-mechanical couplings in Boom Clay under thermal loading. In situ experiments were also performed to determine the thermal and hydraulic transfer parameters, to measure the pH/E_h-values and to detect the presence of gases produced by radiolysis as H₂ and CH₄. At the end of the heating phase, the behaviour of engineered barrier, i.e. backfill material and the behaviour of the Boom Clay were studied on the samples taken after test and compared to the initial samples taken before test.

A thermo-hydro-geochemical modelling (THG) of the CERBERUS test has been developed and the results gained with the THG model were compared with the observations.

From the point of view of THM behaviour, the main results are summarised here:

The maximum temperatures reached during the test were 120 °C in contact with the canister wall at the mid height of the heaters (Figure 4.32 and Figure 4.33), 106 °C in contact with the canister wall at the mid height of the ⁶⁰Co-sources and 50 °C at 1 m distance from the axis of the canister at the mid height of the ⁶⁰Co-sources (Figure 4.32 and Figure 4.34).

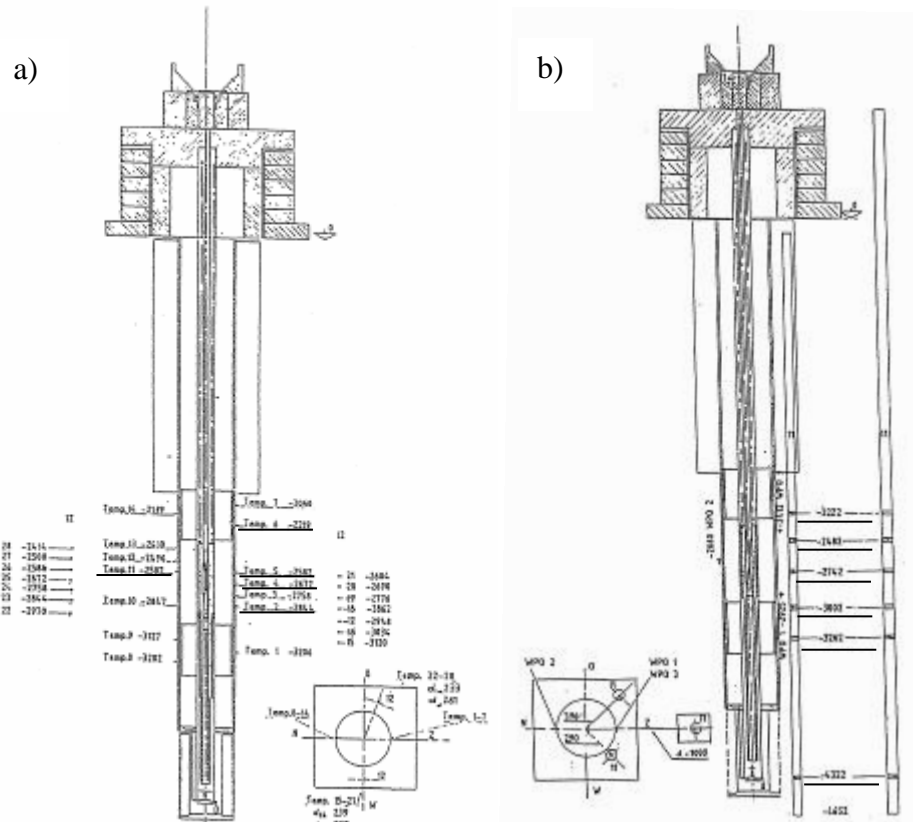


Figure 4.32: Cerberus Test – a) Situation of the Thermocouple at the canister wall ('CS' Figure 4.33); b) Situation of the Thermocouple and piezometer at 1 m from the canister axis ('PSS' Figure 4.34 and Figure 4.35) (Noynaert *et al.*, 1998)

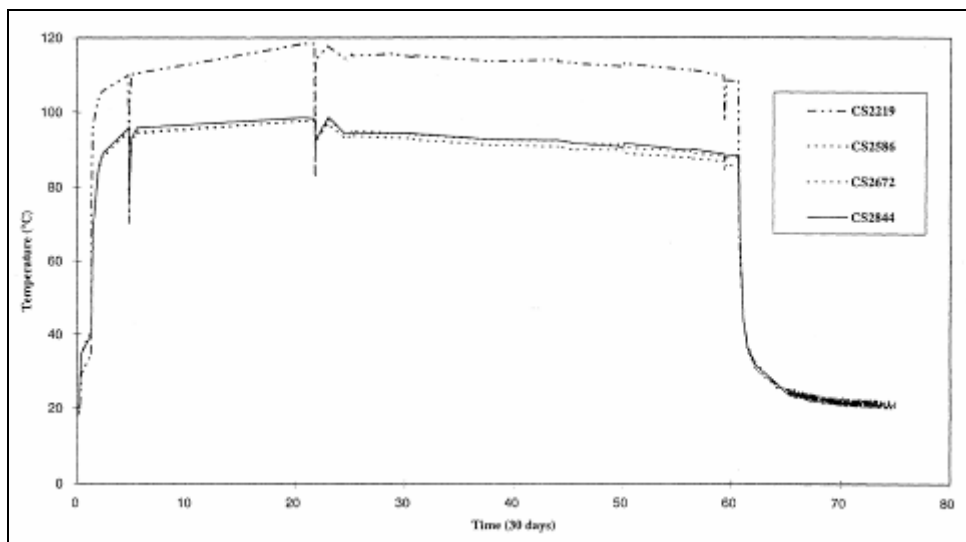


Figure 4.33: Temperature at the canister wall (Noynaert *et al.*, 1998)

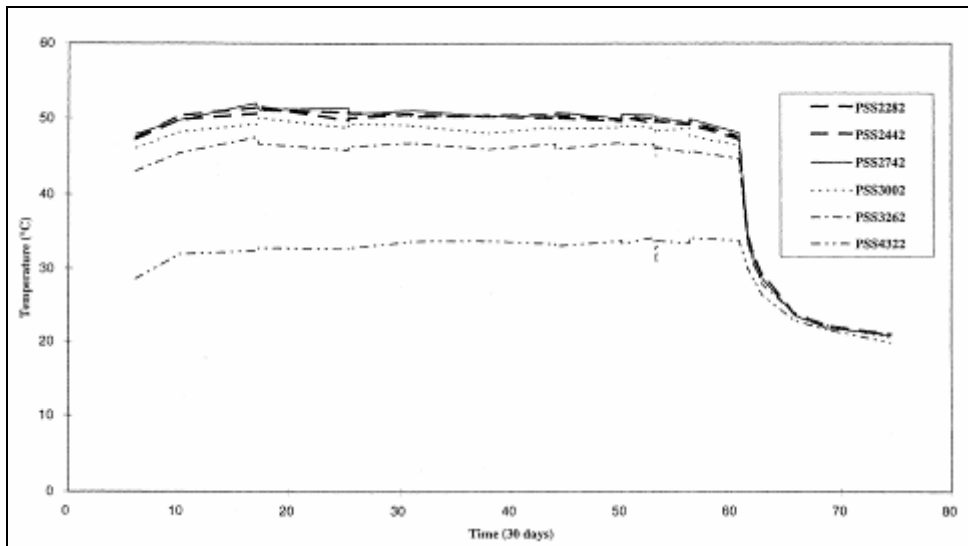


Figure 4.34: Temperature at 1 m from the canister axis (Noynaert *et al.*, 1998)

The temperatures, total pressures and pore water pressures measured at the different sensors during the heating test provided additional information on Boom Clay THM behaviour.

The pore water pressure (Figure 4.35) response of the heat transfer depends on the location and, in particular, on the distance to the heating elements. The evolution of the pore pressure was found to be related to the varying way of the hydraulic conductivity during the heating phase at different place.

The micro-cracks are created around near field of main borehole. Indeed, the hydraulic conductivity measured at the closes sensor after 1 year thermal loading has increased by almost 50 % above what can be expected by the temperature increase.

The hydraulic conductivity measured from the nearer sensor at the end of the thermal loading was very close to the value measured before the start of the test. This indicates that Boom Clay remains plastic and has a self sealing/healing capacity after fissuring.

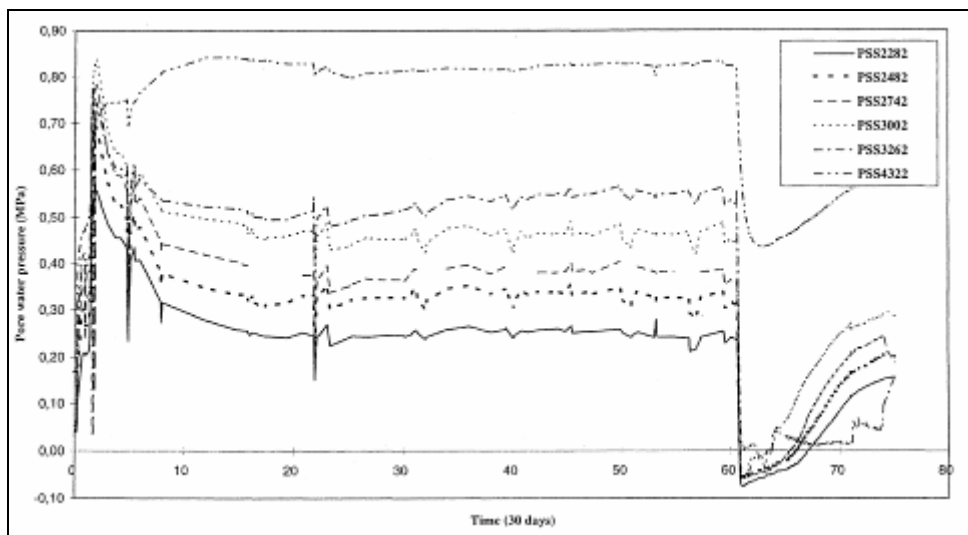


Figure 4.35: Pore water pressure at 1 m from the canister axis (Noynaert *et al.*, 1998)

The hydraulic characteristic time is smaller than the thermal characteristic time. The hydraulic perturbation due to heating power variation propagates thus faster than the temperature front.

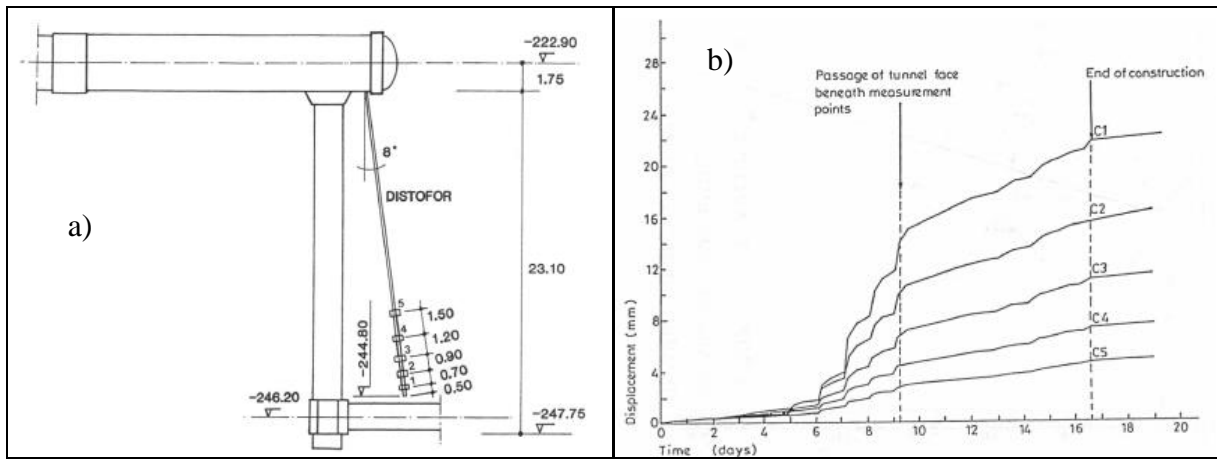


Figure 4.37: Displacements above the experimental drift; a) Position of the extensometers – b) Displacements during the excavation (Bastiaens *et al.*, 2006)

Figure 4.38 shows the displacement profile beneath the Test Drift at different moments. We can see that 7.5 years after construction of the gallery, the displacements are still increasing in the host rock as deep as 5.8 m into the clay.

As for the Figure 4.39, it is a plot of the diameter reductions of 4 sections from the central part of the Test Drift. The decrease of the lining diameter is fastest during the first year after construction. It slows down afterwards but still goes on, at a rate of 0.5 mm/year some 18 years after construction.

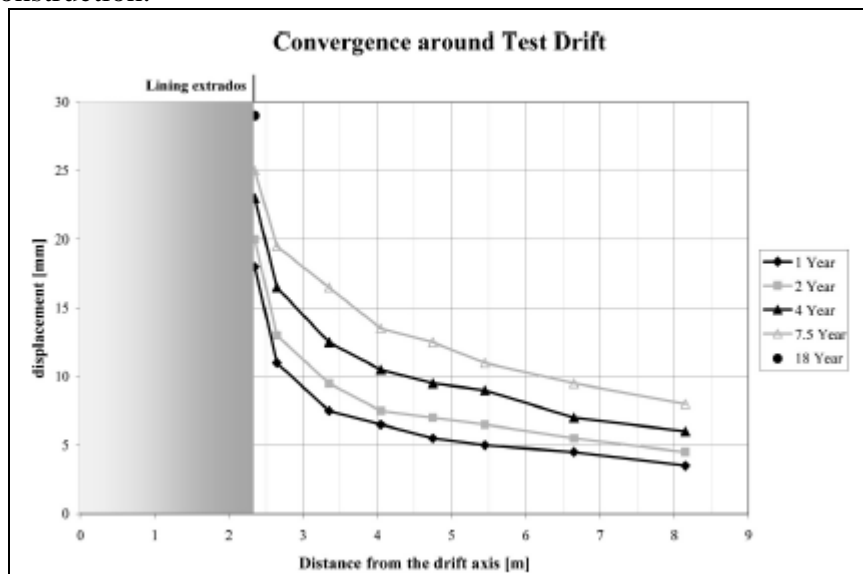


Figure 4.38: Displacement profiles beneath the Test Drift at different moments (Bastiaens *et al.*, 2006)

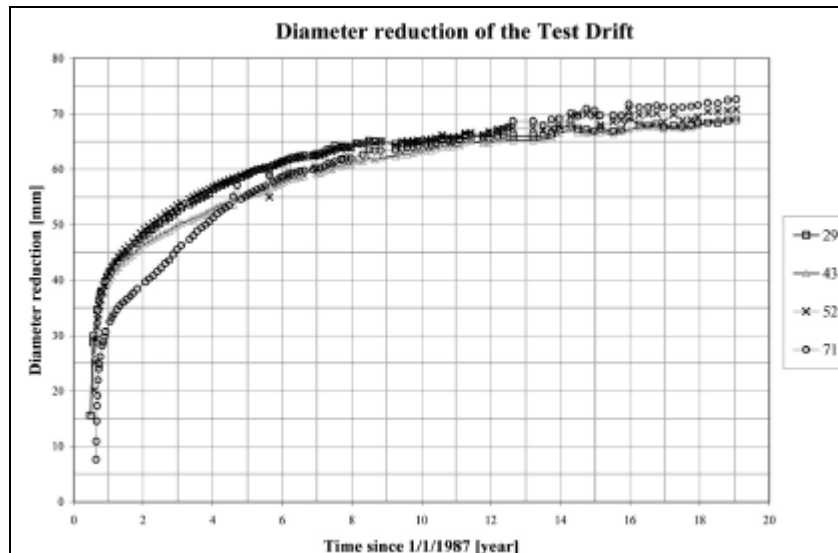


Figure 4.39: Diameter reduction of the Test Drift (Bastiaens *et al.*, 2006)

Pore pressure evolution around the gallery:

Figure 4.40 shows the measurements of the most inclined piezometer of the Mine-by Test. After installation an increase of pore water pressure is measured due to re-equilibrium of the instrument with the surrounding host rock. The influence of the first shaft is visible: higher values are measured with increasing distance to the shaft. The excavation of the Test Drift induced a pore water pressure drop. For each sensor, pore pressure starts to increase again once the gallery under construction has passed above the sensor. Several months later, the increase slows down but gradually continues for several years.

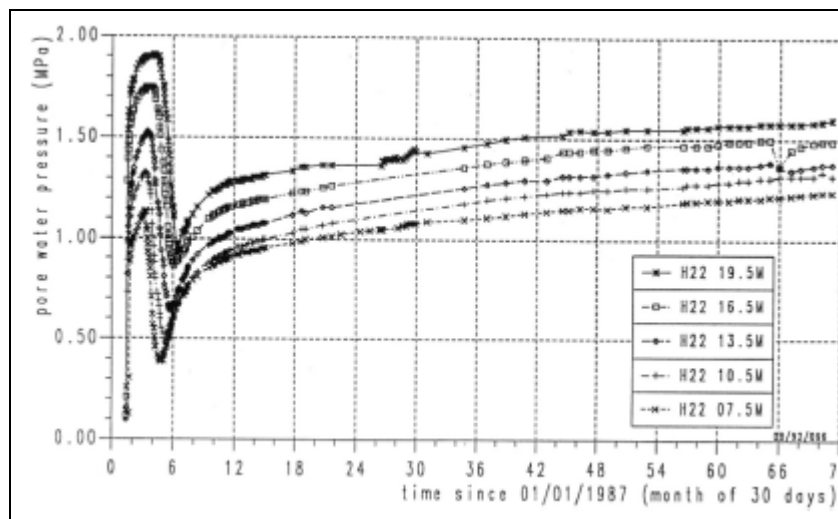


Figure 4.40: Pore pressures measured during the Mine-by Test. The depths of the filters in the borehole are given; the radial distances between the filters and the Test Drift extrados are respectively 9.5, 8.4, 7.3, 6.1 and 5.0 m (Bastiaens *et al.*, 2006)

Figure 4.41 shows the results of piezometers installed in vertical and horizontal boreholes around the Test Drift. To be able to compare these results, they are expressed as a percentage of the undisturbed in-situ pore pressure. Some 2.5 years after excavation, pressures measured in horizontal boreholes are relatively higher than those in vertical boreholes but this relation is inverted with time. It is explained by the fact that the short-term evolution of pore pressures during and after excavation results from the undrained behaviour of the clay. However, the hydraulic disturbed zone (HdZ) does not become isotropic during the re-

equilibrium phase, but the "anisotropy" is inverted. This effect is attributed to the anisotropy of the hydraulic conductivity in Boom Clay ($k_H \approx 2k_V$) which causes a larger draining effect horizontally. In conclusion, the HdZ profiles are dominated in the short-term by the anisotropy of the initial stress state (undrained instantaneous response) and in the long-term by the anisotropy of the hydraulic conductivity.

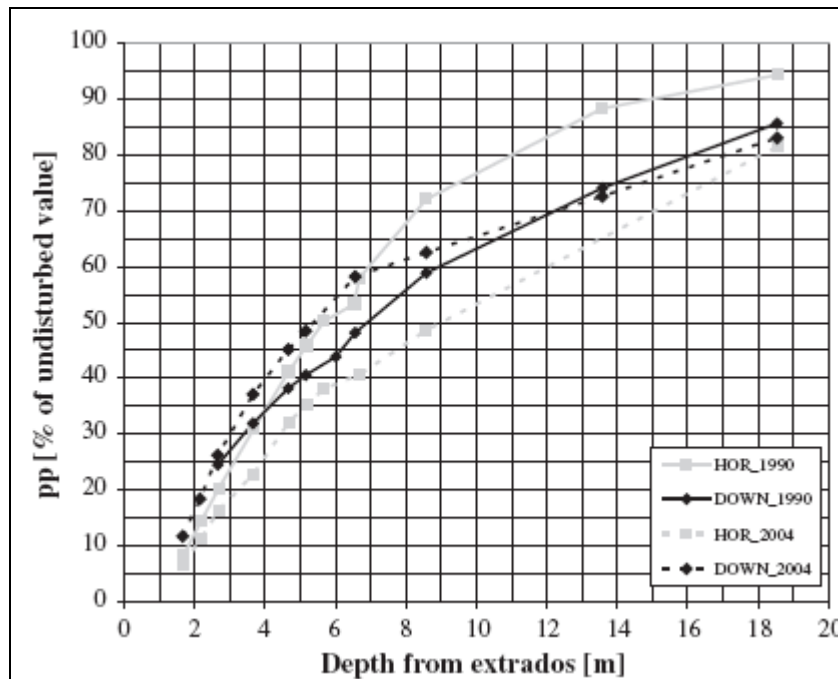


Figure 4.41: Pore pressure profiles horizontally and vertically to the Test Drift (Bastiaens *et al.*, 2006)

Convergence, stress and strain of the Test Drift lining. Long term measurements exist, for example, the displacement of the Test Drift front

Self boring pressuremeter tests in the Test Drift in order to be used to calibrate the Boom Clay law, to evaluate the EDZ and to compare with the self boring pressuremeter tests of the connecting gallery.

4.3.3 ATLAS in situ test (part of INTERCLAY II project: EUR 16204)

The ATLAS large scale in situ test (Figure 4.42) is a part of the INTERCLAY program, which consisted in the study of the admissible thermal loading for Boom Clay.

A first heating phase started in July 1993 with a power of 900 W up to late 1995. Since no shutdown of the heat power occurred at the end of the INTERCLAY II programme, a second phase of heating was carried on in doubling the power to 1800 W. In May 1997, after almost 1 year of supplementary heating, ATLAS was cooled down (Jeffries, 1995).

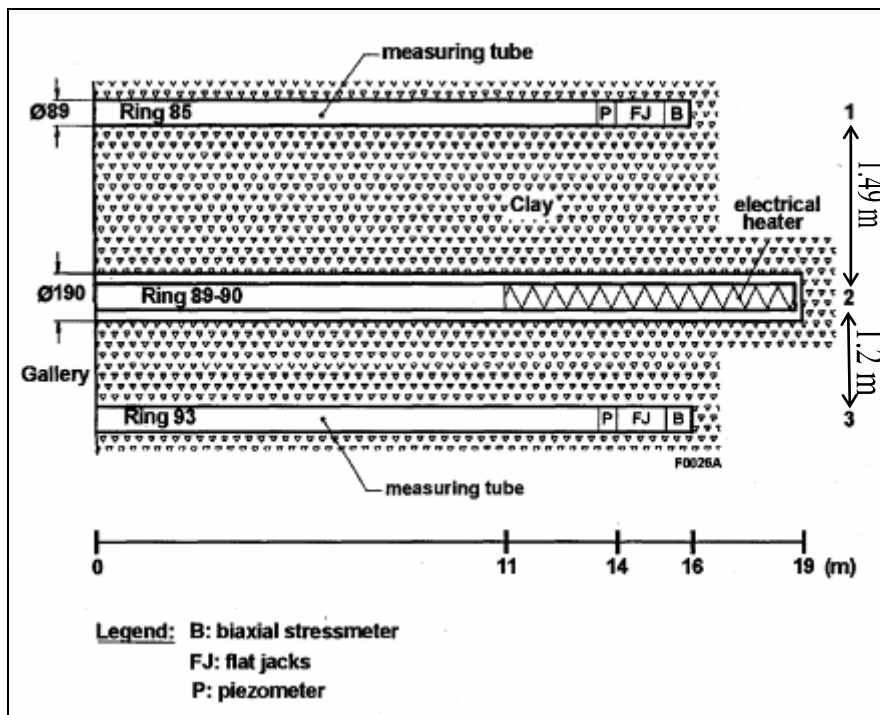


Figure 4.42: General layout of the ATLAS experiment (De Bruyn & Labat, 2002)

This test simulated the thermal loading of a typical high level waste canister in Boom Clay and included measurements of temperature, total stress and pore pressure distributions in the clay mass around the heater. In view of the THM behaviour assessment of Boom Clay, there is no backfill between the heater and the host clay, the thermal loading is thus applied directly on the Boom Clay which facilitate the validation of the chosen model for Boom Clay. The long period of measurement (5 years of heating and several years of cooling) allows to study the long term THM behaviour of the Boom Clay.

The evolution with time of total pressure σ , pore pressure u and temperature T , is shown in Figure 4.43.

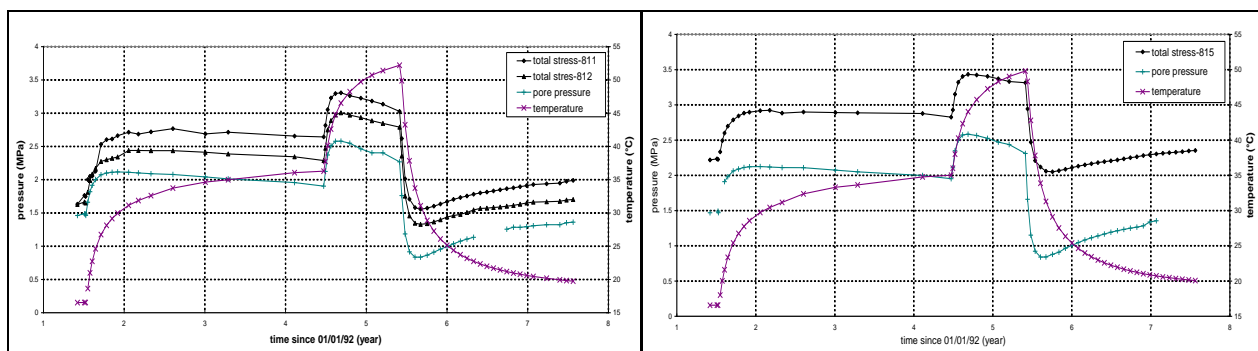


Figure 4.43: Evolution with time of total pressure, pore pressure and temperature; a) ring 93 – b) ring 85 (adapted from De Bruyn & Labat, 2002)

The first phase of heating induces:

- An increase in total stress σ . This increase stabilises while the temperature raises still. In the case of ATLAS, the maximum is obtained after 1 year of heating. The decrease, with 2 more years of constant heating, remains limited (0.1 MPa);
- A rapid increase in pore pressure u , followed by a slight decrease when the temperature increase velocity decreases. The decrease due to dissipation amounts to 0.2 MPa and is larger than for σ . Apparently, the hydraulic characteristic time of Boom clay is smaller than the thermal one.

Despite the fact that the second temperature increase is in the same range as in the first heating phase, the behaviour of total and pore pressures is quite different:

The increase is faster (2 to 3 months), the maximum occurs almost simultaneously and is followed for both type of measurements by a marked decrease, significantly larger than in the first phase, resulting from the higher pressure gradient.

During cooling, a large and rapid decrease of pore pressure is observed together with a total pressure decrease. This behaviour is just opposed to what has been recorded in the first heating phase. After a minimum, pore pressure and total pressure increase again to the value recorded before the first heating phase. The total stress reaches the initial values before the pore pressure which is still slowly increases in 2002 (De Bruyn & Labat, 2002).

During the tests, there are no measurements on the deformation, the density and the water content of the Boom Clay around the heater. This is a disadvantage for the validation of the THM model, even though the deformation may be very limited under the range of temperature.

4.3.4 BACCHUS 2 tests (EUR 16860 EN/FR)

The BACCHUS 2 tests (Figure 4.44) aimed to investigate the thermo-hydro-mechanical behaviour of the Boom Clay and to optimize and demonstrate an installation procedure for a clay based backfill material. It was instrumented to be used as a validation experiment for the hydro-mechanical model developed. The experiment aimed to study the natural and artificial hydration processes of the Backfill and interaction between the backfill and Boom Clay. There is not thermal loading in the test (Volckaert *et al.*, 1996).

The demonstration consists in the sealing of the large borehole (50 cm diameter) left after the retrieval of the BACCHUS 1 mock-up (investigation of the thermal behaviour of the host clay as well as the thermal and hydraulic transfers through a highly compacted material). The granular backfill material was installed around a central filter tube which is used as support and access tube for the instrumentation. It consists of a mixture of Boom Clay pellets and Boom Clay powder where the ratio powder/pellets and the density, size and water content of the pellets are used as the controlled parameters to optimize the backfill material.

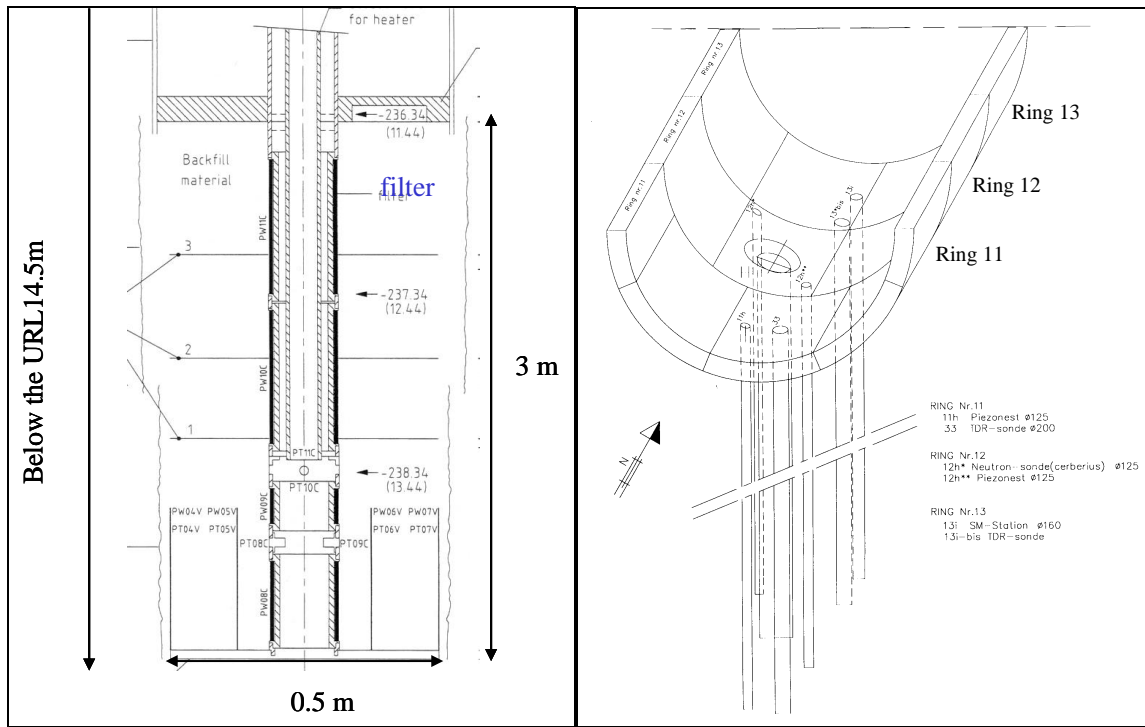


Figure 4.44: BACCHUS 2 in situ test

Concerning the hydro-mechanical behaviour of the host clay, the pore pressures (Figure 4.45) and the total stresses were recorded during the natural and artificial hydration process. The effect of the artificial hydration phase (start at 516 days) can be clearly observed.

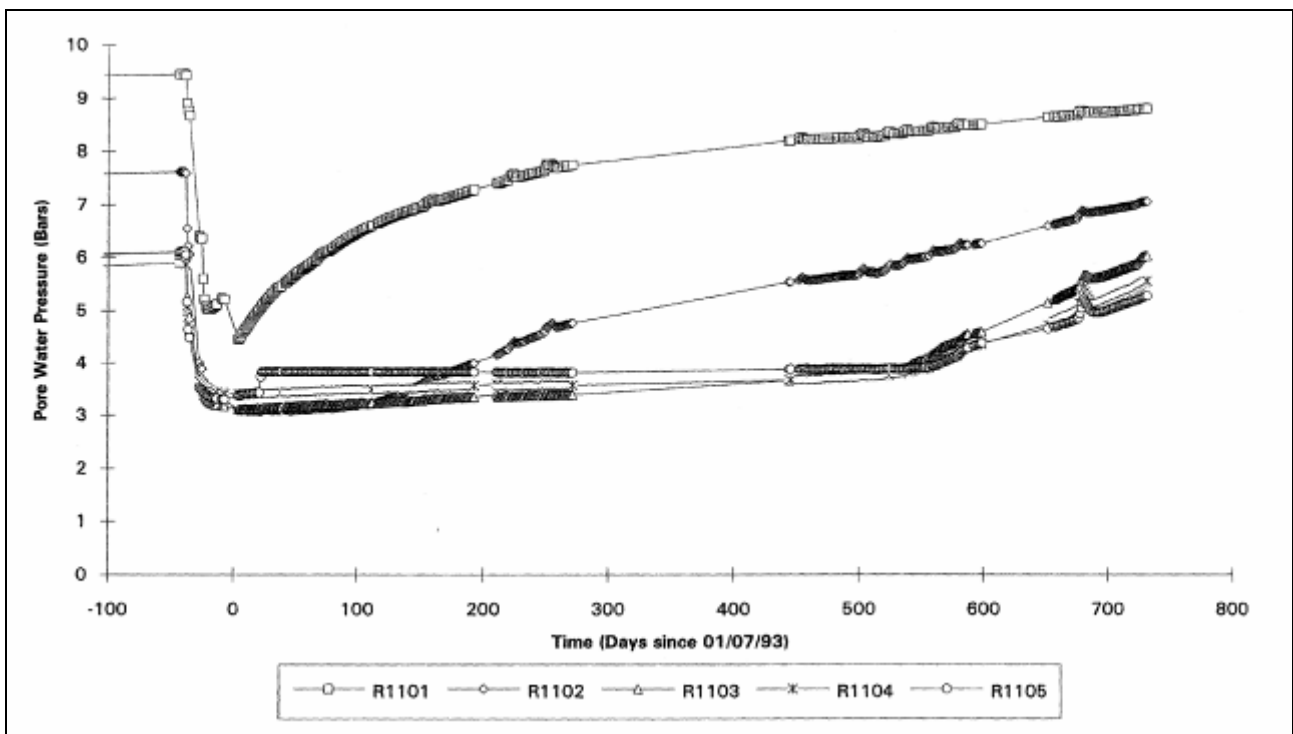


Figure 4.45: Pore water pressure evolution (ring 11) around BACCHUS 2 (Volckaert *et al.*, 1996)

The measurements provided a good database for the determination of the HM parameters by back-analysis.

Due to the high suction of the backfill, the Boom Clay close to this one may be desaturated. However, the pore pressure measurement in the massif showed that the desaturation is extremely limited when it is put in contact with a high unsaturated backfilling material. On the one hand, there lacks a characteristic program for assessing the unsaturated hydro-mechanical behaviour of Boom Clay. On the other hand, the modelling benchmark exercises realized in the frame of the Catsius clay project revealed that the hydro-mechanical contact behaviour at interface between host clay and backfill was an important issue for understanding the HM responses of the Boom Clay during the hydration processes (Volckaert *et al.*, 1996; Catsius clay, 2000).

4.3.5 PHEBUS test (EUR 17792 FR)

The objective of the PHEBUS project (Robinet *et al.*, 1998) was to study the hydraulic behaviour of the massif around a ventilated underground gallery (desaturation, suction generation, etc.).

During the open drift phase, the drift is ventilated. However, hydro-mechanical properties of host rock are sensitive to moisture content and thus, ventilation influences these ones, it reduces drift humidity and eventually dehydrates the rock near the drift surface. Consequently, ventilation of a plastic clay may change its hydro-mechanical properties (strength, permeability, etc.) and retarding self-sealing.

The principle of the test is to cycle a controlled humidity air in a large borehole drilled from the test Drift gallery and measure the hydric exchange between the air and Boom Clay. Two instrumented sections were installed on the porous tubing to measure the stress applied by clay, respectively in the ventilated and unventilated zones. Around the test room, three instrumented borehole were drilled to monitor clay changes in pore pressure, stresses and water content.

This in situ test showed that:

- the desaturation zone is limited and the massif stays saturated during the ventilation phase, the hydraulic gradient was hardly affected;
- the suction generated by ventilation around the gallery induces a consolidation;
- the ventilation enhances the anisotropic stress state in the massif (decreasing of K_0).

The 32 % of relative humidity of the ventilated air corresponds to a total suction of 150 MPa and under a such high suction, the desaturation zone is still very limited. This fact merits to be analysed more in details.

So, the future research should be concentrate not only on the water retention property of the Boom Clay itself but also on the hydro-mechanical properties at the interface.

Moreover, as it was said in the paragraph about the laboratory tests under unsaturated conditions, the air entry value may be very high in intact Boom Clay but, in the EDZ, the host rock may possess a double porosity, composed of micro-pores and micro-fractures. Air entry value could then be lower due to the micro-fractures and in such case, the desaturation in the EDZ could become significant (Li, 2004).

4.3.6 Shaft RESEAL test

The objective of the RESEAL project was to demonstrate on a large scale the possibility to seal a shaft in plastic clay with a mixture of bentonite pellets and powder and to test its efficiency. In addition, laboratory characterization of the bentonite and modelling exercises were realised to better understand the swelling and migration behaviour of the bentonite.

The lining of the experimental shaft (Experimental work on Figure 4.1) of the HADES facility (Figure 4.46) has been removed over 3.45 m (-12.90 m to -16.35 m below the Underground Research Laboratory). Then a mixture of bentonite pellets and powder has been put in place together with several instrumentation equipment. The experimental gallery and shaft underneath the seal had been filled with concrete earlier.

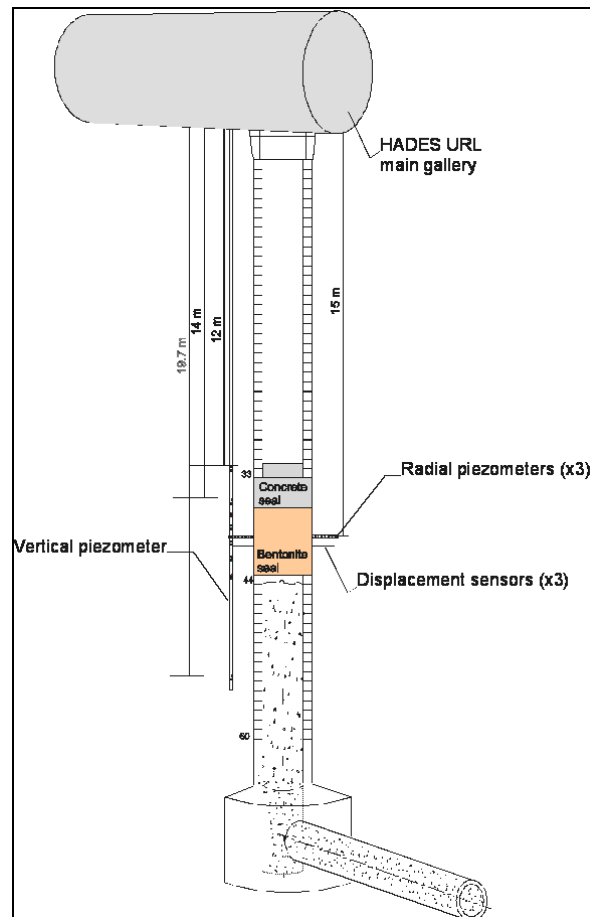


Figure 4.46: Schematic view of the RESEAL experiment and the position of instrumentation used throughout the text (Volckaert *et al.*, 2000)

Thus, the main objectives of the project are:

- To demonstrate the installation technique(s) for the backfilling and sealing of a shaft on a representative scale, i.e. a 2 m diameter shaft in HADES;
- To demonstrate that using a low permeability seal to avoid preferential migration of water or gas along or through the shaft lining or even through the EDZ of the host clay formation can be realised;
- To validate models for the transfer of gas and water through the sealing system including geomechanical aspects;
- To demonstrate the mechanical stability of the seal under accidental overpressure conditions.

The coring of the host rock around the experimental shaft before the removal of the shaft lining showed that fractures created during the excavation of the shaft 14 years before (if any) were closed at the moment of the installation of the seal. Moreover, the permeability measured in these clay cores were in the range measured for undisturbed Boom Clay samples and cores taken close to the shaft and at 1 m yielded similar values of permeability (Volckaert *et al.*, 2000).

After removal of the lining, a decompression occurred. Consequently, fractures in the Boom Clay have been observed, but it is impossible to distinguish between reactivation of existing and newly formed fractures. During the installation of the seal many clay blocks have fallen off the shaft wall, clearly indicating the important mechanical disturbance.

Apart from these visual observations, piezometers installed radially into the host rock from the shaft (Figure 4.46) provide some additional quantitative data (Figure 4.47). These piezometers show, after installation and before removal of the lining, a quite constant pore water pressure. It illustrates an equilibrium state. As a result of the removal of the lining a sudden decrease in the pore water pressure is noticed. The pore water pressure drops to a value lower than the detection limit of the measurement set-up (0 bar absolute). It signifies that suction appears in the massif, around the experimental shaft. A more detailed view (Figure 4.48) of the pore water pressure evolution shows a pressure increase following this sudden decrease. The pressure evolution after this step and the curve of the air atmospheric pressure are qualitatively the same. The sensors connected to the filters of the piezometer measure thus the atmospheric pressure. This means that there is a direct connection between the filter and the atmosphere. In other words, fractures have been developed through the host rock due to the decompression of the host rock around the shaft where the lining has been removed. The instrumentation was limited to 1 m around the shaft, showing that fractures occur at least up to 1 m distance from the shaft/clay interface (Van Geet *et al.*, 2003).

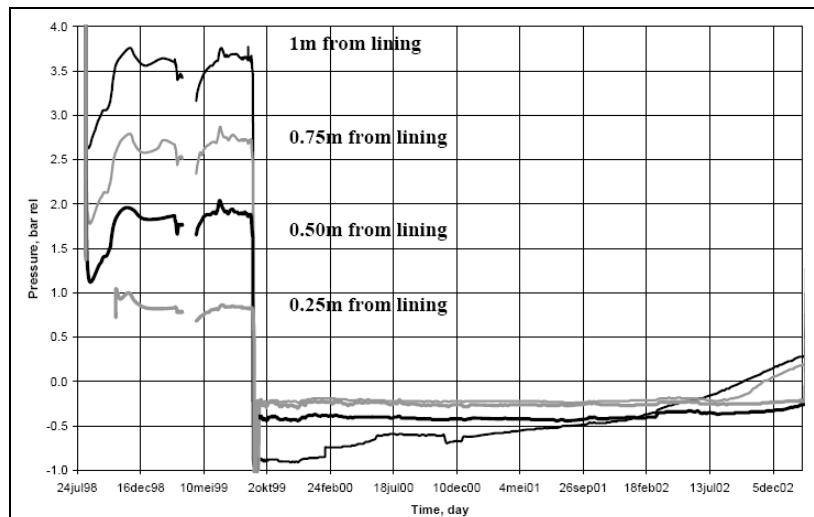


Figure 4.47: Pore water pressure evolution in the filters of a radial piezometer into the host rock (Van Geet *et al.*, 2003)

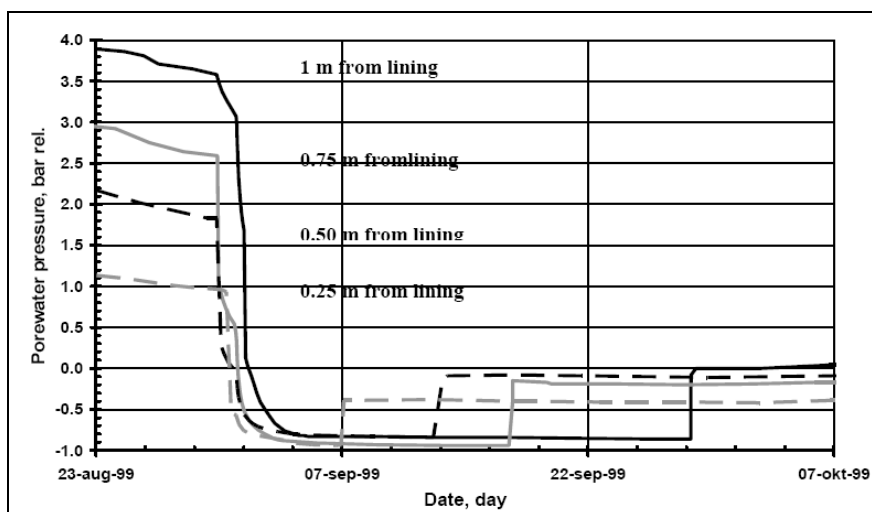


Figure 4.48: Detail of Figure 4.47 (Van Geet *et al.*, 2003)

In a vertical piezometer parallel with the shaft at a distance of one meter (Figure 4.49), the sensors positioned relatively next to the seal emplacement (there where lining is removed; filters 4, 5, 6 and 7) show also a sudden decrease in pore water pressure followed by an increase to atmospheric pressure. However, the filters above and below the relative position of the seal do show a sudden decrease in pore water pressure, but remain at a pressure well above atmospheric pressure. Consequently, a decompression of the host rock took place, but fractures in direct contact with air do not occur in these zones. In other words, fissuration seems to develop radially around the shaft where the lining has been removed (Van Geet *et al.*, 2003).

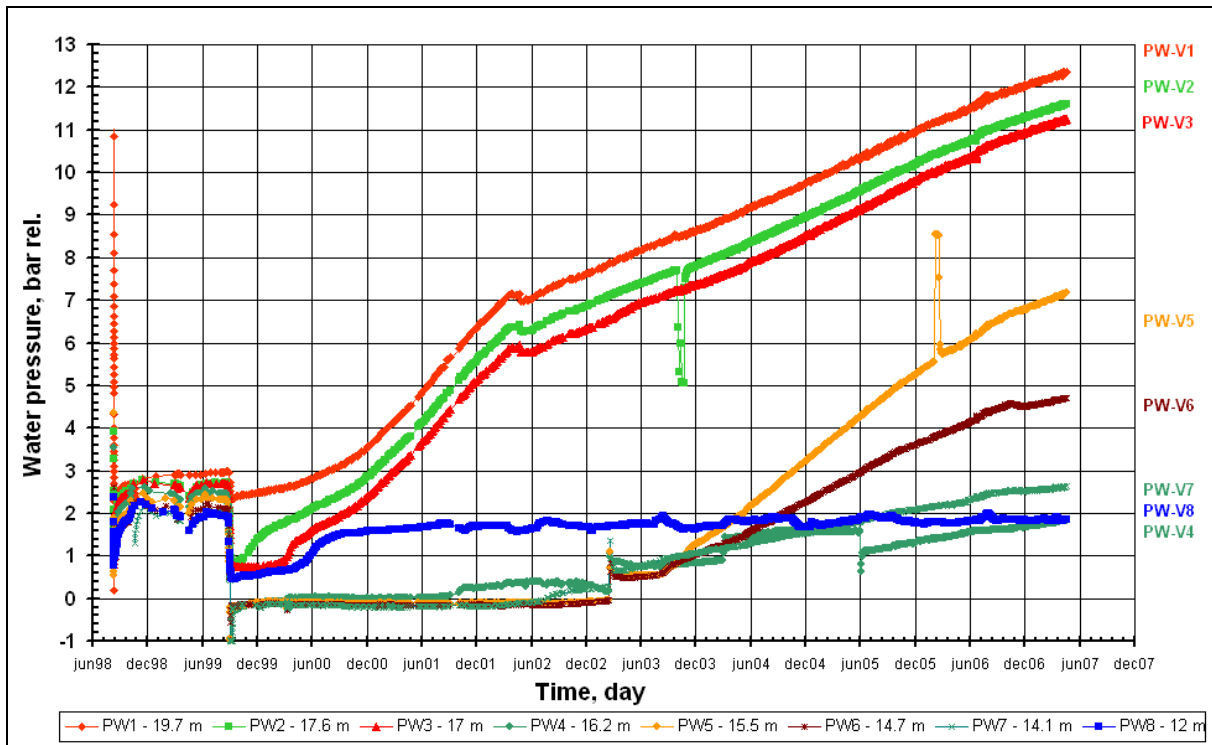


Figure 4.49: Pore water pressure evolution in the filters of the vertical piezometer (Bastiaens, report in prep.)

After the installation of the bentonite seal, saturation of the seal takes place. This saturation is performed by natural drainage from the host rock and by artificial hydration. The relative humidity sensors inside the seal show that the seal is near saturation after 4 years of artificial injection. Actually (2007), the saturation is considered completed. As a consequence, a re-establishment of hydraulic pressure (Figure 4.49) in the host rock happens, due to self-sealing of the fractures (Van Geet *et al.*, 2003, Bastiaens, report in prep.).

4.3.7 CACTUS I & II (EUR 15482 and EUR 17558 EN)

The CACTUS experiment (Figure 4.50) was aimed to study the thermo-hydro-mechanical coupling developed in the Boom Clay massif. They provided a series of measurements at different phases: drilling of the borehole, plugging operations, heating – cooling, etc.

The "CACTUS" programme is composed of two in situ tests. The first test (CACTUS 1) served as preliminary approach. Each test is composed, in addition to a thermal probe placed in a large diameter central borehole, of a peripheral instrumentation located in six small diameter boreholes. The peripheral instrumentation has been installed first, in order to record stabilized the hydro-mechanical parameters prior to the drilling of the central borehole. The physiognomy of the instrumentation is identical for both tests.

The tests were realised during a significant period, i.e. totally three years of measurements including a year of heating and a year of cooling. The measurements obtained put in evidence some

particularities of the THM responses of the Boom Clay under the same conditions as the waste storage.

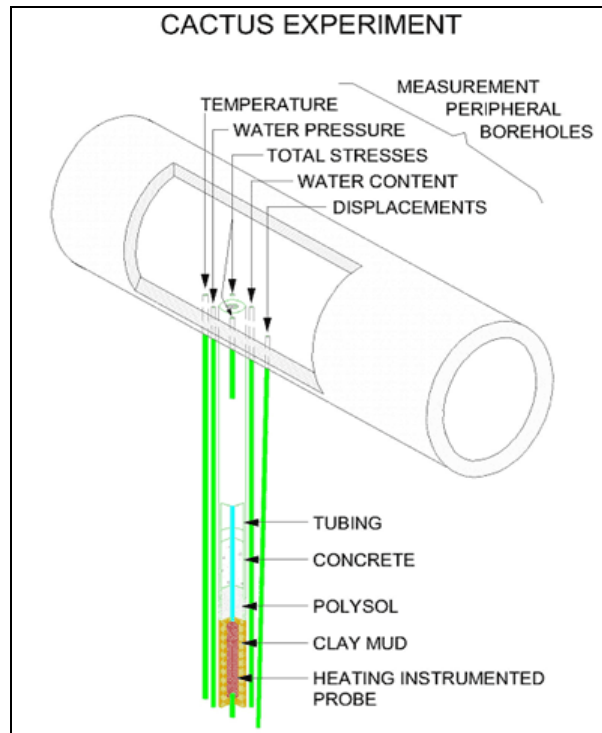


Figure 4.50: Schematic view of the CACTUS experiment

Before the excavation, it seems that the mechanical influence zone of the access gallery on the clay host rock has an extension that is larger than seven times its radius. During the excavation of the first central borehole, that lasted two days, a brutal response is observed: a drop of the interstitial pressure around the excavation, a drop of radial stress and an increase of the orthoradial stress. An increase of the water content is observed, while the density does not vary a lot. During the excavation of the second central borehole (CACTUS 2), an increase of the radial and orthoradial stresses are first observed during the drilling prior a decrease in the following days. In both cases, the deviatoric stress, defined by the difference between radial and orthoradial stresses has increased during the excavation. According to analytical calculations, the deviatoric stress is proportional to the excavation radius, and inversely proportional to the square of the distance from the borehole axis.

After the excavation, the interstitial pressures and the total stress components tend to their original values. In CACTUS 2, the equilibrium of the interstitial pressures was not reached yet when the heating phase was started. A re-consolidation of the clay host rock is observed after the excavation.

The power applied during the different phases of heating and cooling for the 2 tests are summarised in the Table 4.8.

*Table 4.8: Heating and cooling phases of both CACTUS tests –
N° of days counted from the 01/01/1990*

CACTUS 1				
	Date of begin	Length (in day)	Power	Loss
1 st Heating	26/09/1990	47	400 to 1200 W	10 %
1 st Cooling	12/11/1990	122	0 W	
2 nd Heating	14/03/1991	298	1200 W	14 to 17 %
2 nd Cooling	06/01/1992	> 700	0 W	
CACTUS 2				
1 st Heating	10/02/1992	378	1200 W	4 %
1 st Cooling	04/03/1993	216	0 W	
2 nd Heating	7/10/1993	33	1200 W	4 %
2 nd Cooling	08/11/1993	≈ 100	0 W	

During the heating phase, the temperature measurements are coherent. The temperature field has an axisymmetric configuration around the probe. The temperature rapidly decreases with the distance from the heat source. After one year of heating, the temperature increase is equal to 130-140 °C on the probe, while it does not go beyond 20 °C at a distance of 1.5m. The thermal analysis is made independently from the hydro-mechanical analysis, for the principal heat transfer process is conduction. By back-analysis, the thermal conductivity λ and the thermal diffusivity D_T of the Boom Clay were estimated:

$$\lambda = 1.7 \text{ W.m}^{-1}.\text{K}^{-1}$$

$$D_T = 6 \cdot 10^{-7} \text{ m}^2.\text{s}^{-1}$$

Three phases are observed for the THM parameters evolution:

Initial phase:

The heating phase is started, but due to the thermal inertia, no temperature variation is observed at this point. As for the hydro-mechanical behaviour, the response is limited. We note a decrease of the orthoradial stress, an increase of the radial stress and of the interstitial pressures.

Transient phase:

The temperature rapidly increases and both radial and orthoradial stresses raise also, as well as the interstitial pressures. A decrease of the water content is observed. The thermal dilation of the hot zone is hampered by the surrounding clay massif producing compressions in this zone. The thermal dilation coefficient of water is much higher than the constitutive minerals of Boom Clay. In an undrained situation, the interstitial water is overpressurized. A hydraulic gradient appears between the warm and cold zones leading to the dissipation of the overpressures.

Near equilibrium phase:

The temperature slowly and steadily increases near the probe. There is almost no variation of the total stress components. The interstitial pressure decrease and stabilize. The compressions appeared during the transient phase are maintained, even after the dissipation of the interstitial overpressures. Considering the water content and the strain, they are evolving towards the original state. The strain evolution is elapsed over a long period of time, which might indicate a creep due to the visco-plastic properties of Boom Clay.

During the cooling phase, the THM parameters inversely evolve in comparison with the heating phase, on a very similar way. It was also observed in the ATLAS experiment. This observation tends to indicate that an important part of the observed variations are reversible. Nevertheless, it is essential to identify the irreversibilities that subsist, like a modification of the water content during the first heating phase of CACTUS 1, the displacements in the massif of low amplitude and a slight increase of the density. An interesting observation is that the water content variation established during the first heating phase does not appear during the next heating/cooling cycle.

4.3.8 CLIPEX project (EUR 20619 EN)

The aim of the CLIPEX project is to assess and characterize the EDZ and short term HM responses of Boom Clay to the excavation around a gallery similar in size to that of a disposal gallery for radioactive waste. The CLIPEX project was realised in the frame of the extension of the underground research facility HADES (Figure 4.1). The extension consisted of a second shaft, and the excavation of a gallery connecting this shaft with the existing facility. The connecting gallery was realised with a tunnel machine allowing an excavation rate about three meters per day, and minimising perturbation of the host rock. A unique and original opportunity was then given, within the CLIPEX project, to monitor the hydro-mechanical parameters ahead of the face of the connecting gallery (Figure 4.51). An important part of the project was also devoted to blind predictions and their comparison with the in-situ measurements.

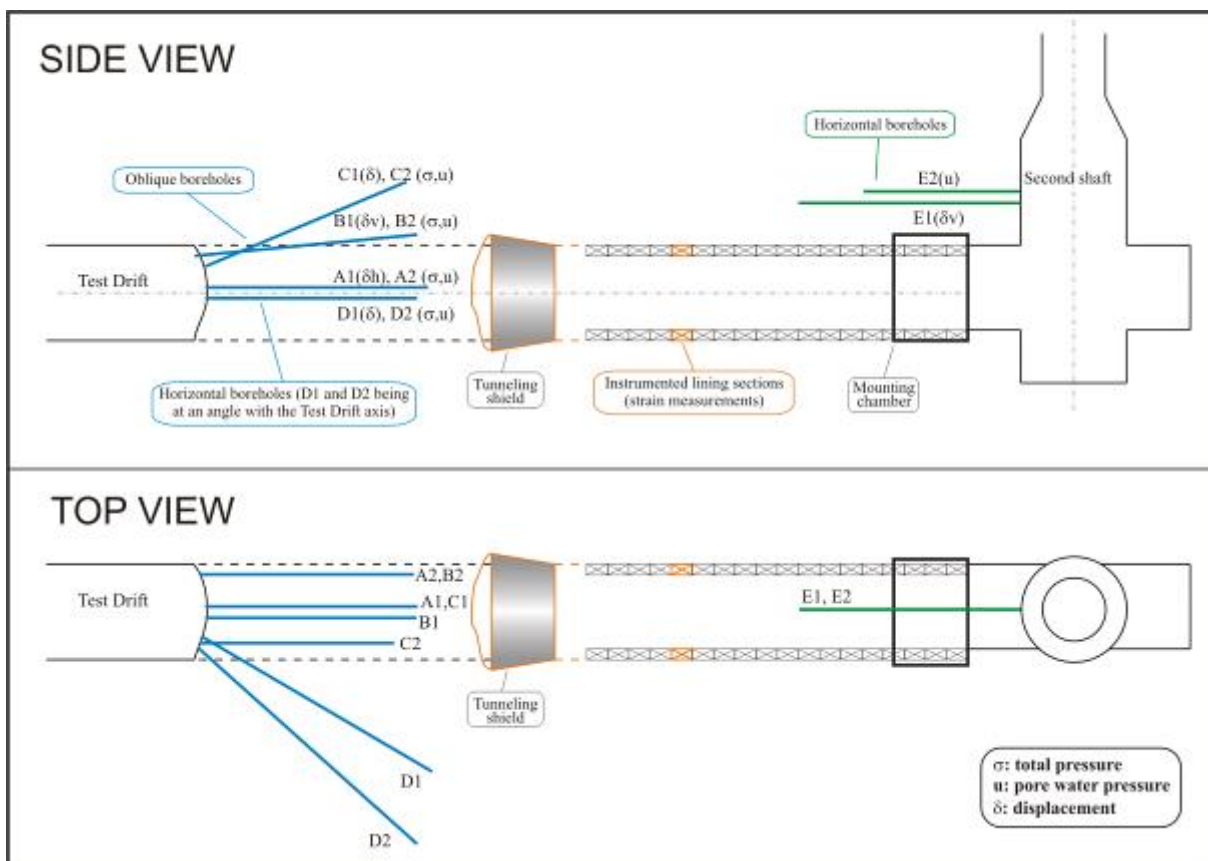


Figure 4.51: CLIPEX instrumentation program (Bernier *et al.*, 2007)

The new data obtained during the connection of the connecting gallery has put in evidence the following hydro-mechanical behaviour of the Boom Clay:

Highly hydromechanical coupling behaviour (Figure 4.52);

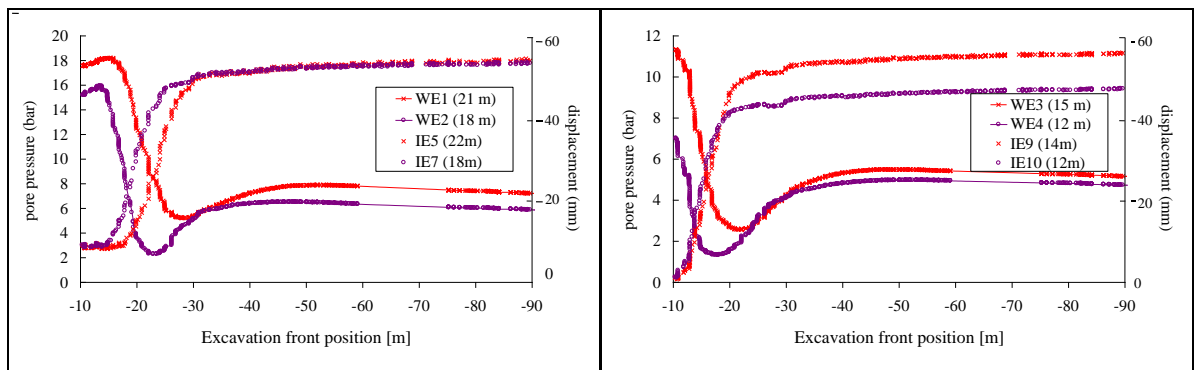


Figure 4.52: HM coupling evidence – Pore water pressure and displacement evolution measured from the second shaft (Bernier *et al.*, 2003)

The hydro-mechanical coupling can easily be visualised on the Figure 4.52 with the measurements of the borehole E from the second shaft and parallel to the gallery axis, measurements of the deformation (IE_x) from the inclinometer E1 and of the pore pressure (WE_x) from the piezometer E2 (Figure 4.51). The close relationship between the deformation and pore pressure is clearly put in evidence: the inclinometers show a large displacement up that the excavation front passes by the sensors corresponding to a strong decrease of the pore pressure.

Fracturation development and suction generation around gallery and ahead of the front;

Time related behaviour (Figure 4.53): the continual increasing of the external pressure on the linings of gallery by Boom Clay embodies the time-related behaviour of Boom Clay through hydraulic diffusion process and viscosity of skeleton.

The outside pressures exerted on the lining are calculated based on the mean stress inside each segment assuming a thin wall approximation.

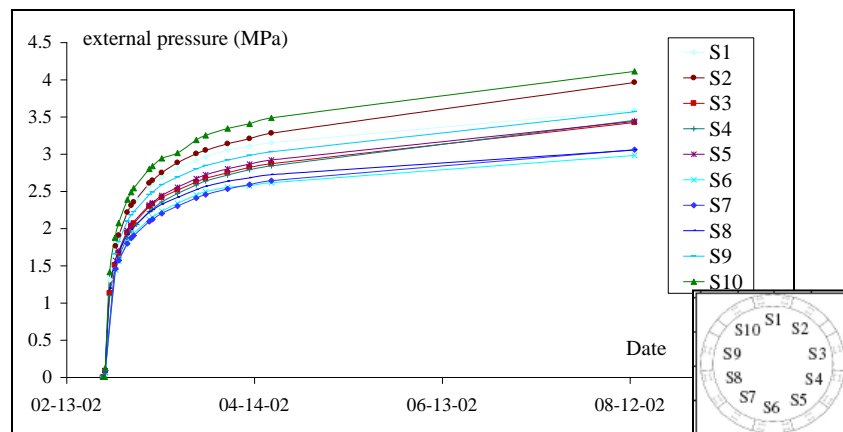


Figure 4.53: Time related behaviour: Outside pressure exerted on the lining (Bernier *et al.*, 2003)

Very extended Hydraulic Disturbed Zone (HdZ) and Excavation Disturbed Zone (EdZ) which remain very difficult to explain. It was likely partly associated to the effect of the fracturing around excavation face and to the viscosity skeleton.

Indeed, all pore water pressure sensors begin to increase when the excavation front is still 60 m before them (Figure 4.54). It implies that the hydraulic disturbed zone due to the excavation extends at least 60 m.

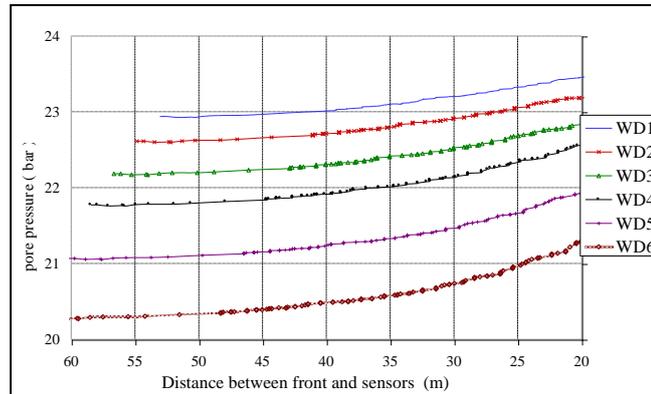


Figure 4.54: Far field reaction to excavation – Pore pressure – HDZ (Bernier *et al.*, 2003)

As for the EdZ, the detail view of the Figure 4.55b shows clearly the immediate reaction of sensors: the sensors began to react as soon as the excavation debuted. It means that the EdZ extends at least about 75 meters ahead of front.

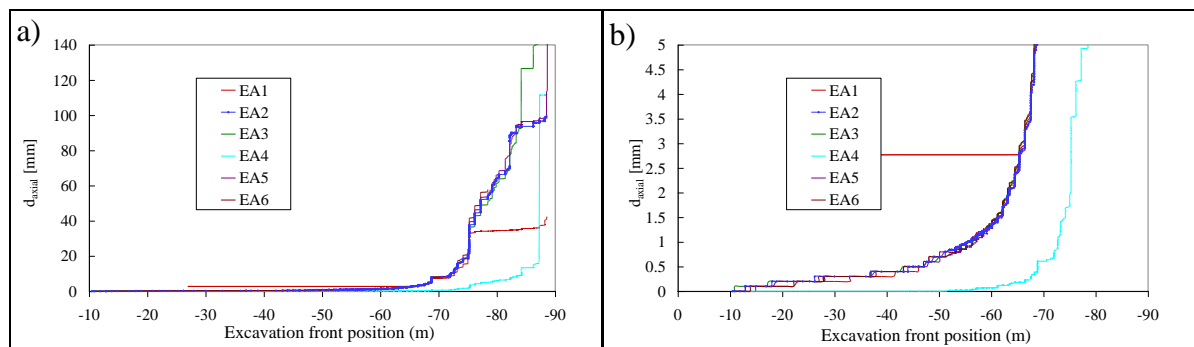


Figure 4.55: Displacement evolution during the excavation of the Connecting Gallery from the Test Drift – a) Global view; b) Detail view (Bernier *et al.*, 2003)

After excavation, the pore pressure distribution around the gallery is anisotropic. This anisotropy depends on both the anisotropy of the stress state and the anisotropy of the hydraulic conductivity (Bernier *et al.*, 2003).

Unfortunately, the total pressure measurements are failed due to technical difficulties. Moreover, in terms of displacement, most of inclinometers and deflectometer installed from Test Drift failed to give quantitative measurements due to the difficulty to fix a reference point and the bending of the chain. The interpretation is thus only qualitative (Bernier *et al.*, 2003).

Moreover, it is worthwhile to mention here that many phenomena observed by CACTUS tests are equally observed in the frame of CLIPEX project like the fracturation and desaturation in the near perturbed field. These consistent observations in different scale are important to characterize the hydro-mechanical behaviour of Boom Clay (Li, 2004).

4.3.9 SELFRAC in situ experiment

Within the EC project SELFRAC, two in situ experiments were realised. The first aimed at studying the hydro-mechanical properties of Boom Clay around a freshly excavated gallery and their

evolution with time and the second studied the influence of borehole drilling and closure (collapse) on the host rock, using seismic and acoustic emission measurements (Bernier *et al.*, 2006).

The in situ experiments in Boom Clay have allowed to follow the evolution with time of the hydro-mechanical behaviour of Boom Clay around a gallery excavated by industrial technique and to quantify the effect of the sealing processes on the hydraulic conductivity evolution.

The main results of these in situ experiments are that the radial extent of the fracture zone around the gallery is about 1 m. Moreover, the pore pressure evolution around the connecting gallery was measured. The results of the 6th December 2004, i.e. about 2 years and 9 months after gallery construction, were presented at the Figure 4.56. To make a meaningful comparison between the measurements at different locations, pore pressure is expressed as a percentage of the original undisturbed value at each location.

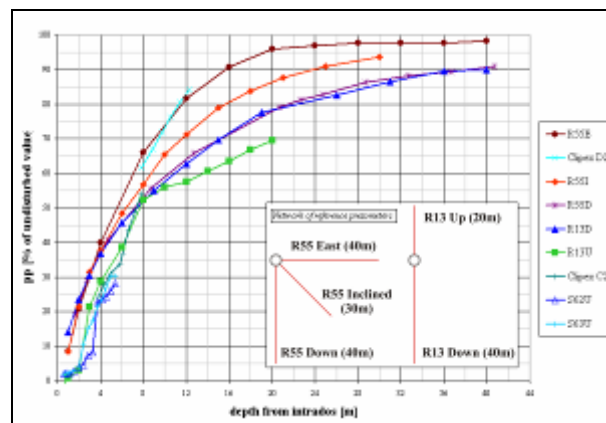


Figure 4.56: Overview of pore pressure measurements around the connecting gallery on 6th December 2004, expressed as a percentage of the original undisturbed value at each filter location (Bernier *et al.*, 2006)

It is clear that the pore pressure distribution around the connecting gallery is anisotropic. This can be explained by stress anisotropy (on the shorter term) and by anisotropic hydraulic conductivity of the host rock (on the longer term). Indeed, due to the low hydraulic conductivity, the immediate response of the host rock can be considered as undrained and because $K_0 < 1$, the response of the host rock upon excavation will be different in a vertical plane than in a horizontal one and the mean stress will be higher in a horizontal plane than in a vertical one, resulting in a pore pressures increase left and right of the gallery, and decrease above and below it. Re-equilibrium of pore pressures (dissipation of over- and underpressures) takes several years and depends mainly on hydraulic diffusivity. On this time scale (several years), the influence of hydraulic conductivity (cf. $k_H \sim 2 \cdot k_V$) becomes important: the drainage by the gallery is larger horizontally than vertically.

Pore pressure could be measured as little as 40 cm into the host rock. This indicates that any fracture network existing beyond (at most) a few decimetres into the host rock is sealed. Moreover, since no packers are used, the filters are sealed off by natural convergence of the borehole walls around the instrument. This result confirms that Boom Clay has important sealing properties.

Hydraulic conditions around the Connecting Gallery were derived from constant head tests in steady state flow regime. An increase of the hydraulic conductivity up to 1 order of magnitude (Figure 4.57) was measured up to 6-8 m into the host-rock. The values outside this influenced zone are about $6 \cdot 10^{-12}$ m/s for the vertical piezometer and $4 \cdot 10^{-12}$ m/s for the horizontal piezometer. About 1 year after the first measuring campaign, some filters were tested again. The obtained values were systematically lower, although not much.

The values outside the influenced zone are consistent with in situ data obtained in previous experiments, although slightly higher. When measuring on a vertical piezometer, k_H is dominant; when measuring on a horizontal piezometer, k_H and k_V are more or less equally important. This

explains the larger values of k obtained from the vertical piezometer. It is important to notice that even at the measuring points closest to the gallery; k is still only one order of magnitude larger than the undisturbed value.

Based upon these results and literature, it is concluded that effective stress variation alone can account for the variation of hydraulic conductivity measured around the connecting gallery and that fractures do not play an important role in this case (cf. sealing); almost all measurements were performed further than 1 m into the host rock and thus well beyond the fractured zone (Bernier *et al.*, 2006).

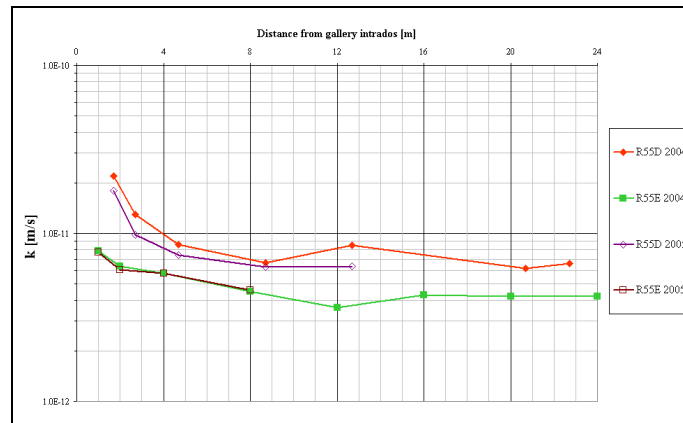


Figure 4.57: Hydraulic conductivity (k) around the connecting gallery (Bernier *et al.*, 2006)

4.3.10 General remarks on the realised in situ experiments in the URF of Mol

The in situ experiments realised up to now in the URL provided without doubt a valuable data base for the calibration and validation of the developed/to be developed models. A lot of (T)HM in situ responses of Boom Clay were observed thanks to the realised in situ tests (ATLAS, CACTUS, BACCHUS, PHEBUS, CERBERUS). Excavation of connecting gallery (CLIPLEX) provided indeed a valuable data base for validation of the developed/to be developed constitutive laws.

However, a global examination of the performed in situ tests revealed that many test were conceived for observing THM phenomenon and not for calibrating models. Moreover, in most of the tests, there is a lack of information on the in situ deformation, saturation and in situ stresses. Despite of the extensive testing, there is still considerable uncertainty regarding the anisotropy of the stress profile around the gallery. This is a generic problem which needs further attention when considering the characterisation of a possible repository site. More extensive site characterization tests are needed.

As result, it is difficult to validate the developed/to be developed constitutive laws with the help of a single test and a global interpretation and back analysis of ensemble of tests is needed (Li, 2004).

4.4 Modelling

The modelling development works included two parts, the constitutive laws building and the validations – simulations – predictions, they were carried out in parallel with the laboratory and in situ test programs.

Two approaches were adopted up to now to build the mechanical constitutive laws of the Boom Clay, either the interpretation of the test results in terms of well known constitutive laws or, based on the test results obtained by well established program, determination of the yielding points in a stress space following certain yielding criterion, flow rule, hardening rule, etc. to establish the constitutive law and corresponding parameters.

This paragraph gives firstly a global view on the constitutive laws that have been considered/developed for Boom Clay in different projects. Then, some application examples of certain models, as well as their capacities and limits will be introduced.

4.4.1 Saturated elastoplastic models at ambient temperature (p'-q plan)

Mohr-Coulomb and Cam-Clay models

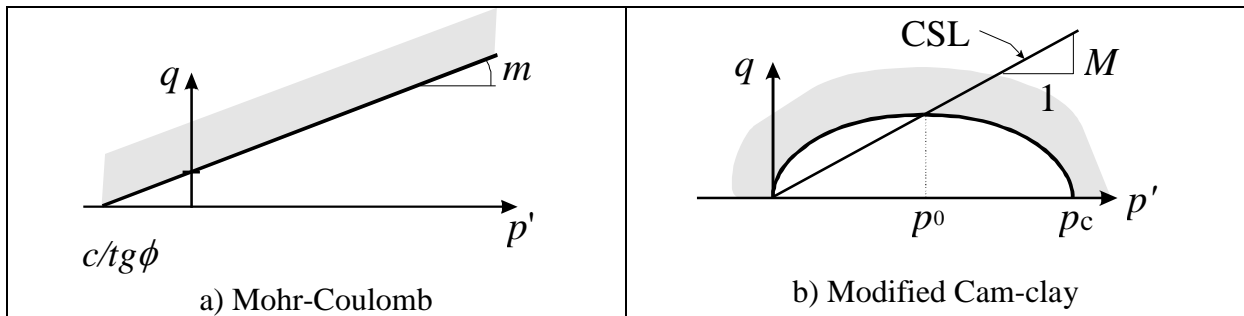


Figure 4.58: Mohr-Coulomb and Modified Cam-Clay saturated elastoplastic models (Li, 2004)

The mostly used models are the classical elastoplastic Mohr-Coulomb and Modified Cam-Clay models. These ones present a sharp transition between elastic and plastic responses. Unfortunately, the test results revealed that the Boom Clay presents a very limited elastic zone and that the viscoplasticity is an essential mechanical behaviour. This pattern of behaviour can not be reproduced by this kind of classical model. Moreover, although these classical models can usually reproduce the tendency of the evolution of pore water pressure in the massif, they can not produce its amplitude (see hereafter) (Li, 2004).

Dafalias-Kaliakin and "Two bubbles" models

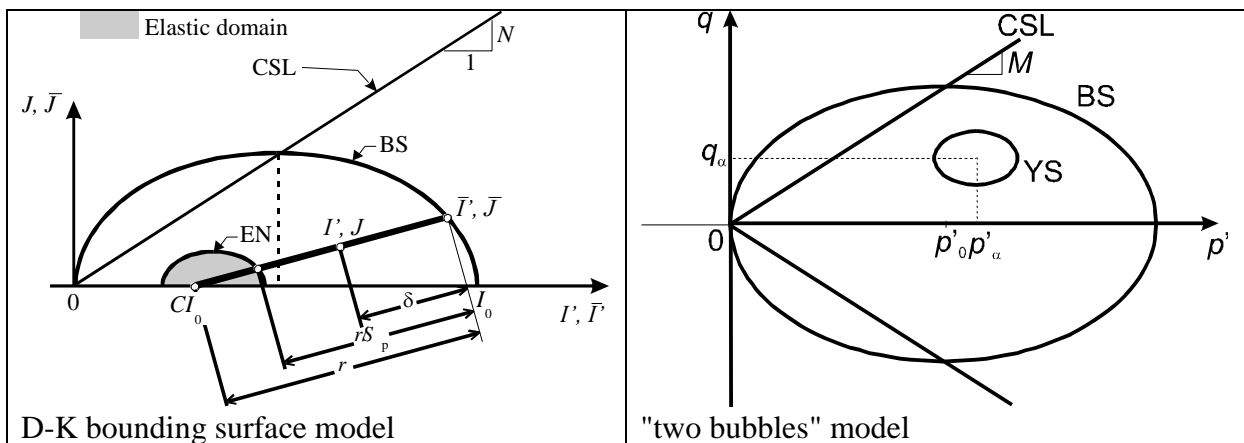


Figure 4.59: Dafalias-Kaliakin and "Two bubbles" saturated elastoplastic models (Li, 2004)

In order to reproduce the water pressure evolution during the Test Drift and 2nd shaft excavation, Barnichon and Labiouse tried to apply two more sophisticate models to Boom Clay: the Dafalias-Kaliakin bounding surface and the "Two bubbles" models. These two models allow a better representation of the plasticity and a progressive transition of elasto-plasticity. In addition, they can present the hysteresis of the loading-unloading pattern. But these models demand a lot of parameters and they are not all determined for the Boom Clay (Li, 2004).

Sultan's model

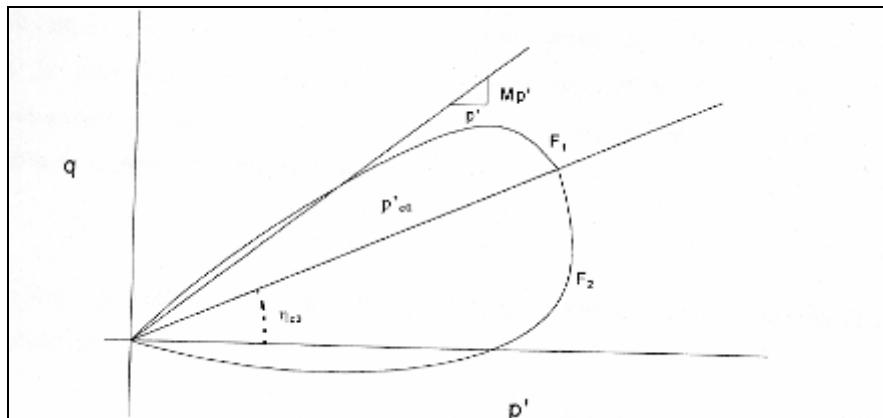


Figure 4.60: Sultan anisotropic saturated elastoplastic model (Sultan, 1997)

Another model for Boom Clay is proposed by Sultan, based on the test results realised in the framework of his PhD thesis. This model can take into account the inherent anisotropy of Boom Clay by inclination of the yield surface with respect to the K_0 line and the anisotropy induced by external mechanical loading by a rotation of the yield surface around the loading path.

The simulation of some laboratory tests showed that this model could produce correctly the test results. However, it is worthwhile to note that this model was build only based on the axisymmetric triaxial test where $\sigma_2 = \sigma_3$ and the transition between elastic and plastic responses is also sharp as in a classical model (Li, 2004).

4.4.2 Unsaturated elastoplastic model at ambient temperature (p-q-s space)

Barcelona Basic Model

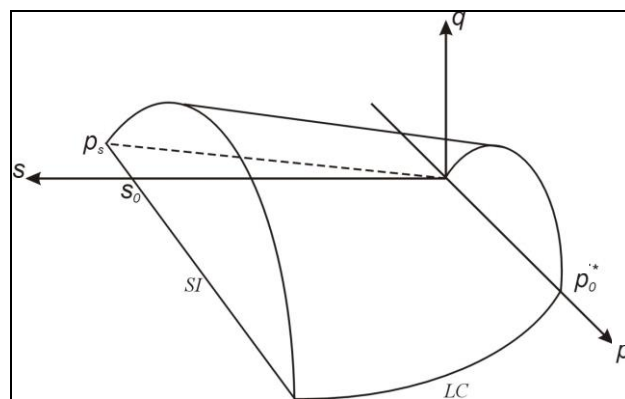


Figure 4.61: Barcelona Basic unsaturated elastoplastic model (Alonso *et al.*, 1990)

The interactions between mechanical stresses and fluid flow needs to be taken into account in a model. A lot of effort has been put into the development of constitutive laws describing the phenomena. The Barcelona Basic Model (BBM) model proposed by Alonso *et al* (1990) is probably most used up to now for the simulations of the in situ tests realized in HADES in different projects by different institutions (BACCHUS 2 test simulations performed by ULg and UPC in CATSIUS clay project, RESEAL test simulations by UPC and CEA in RESEAL project).

This model is based on the well-known CamClay model. It is written within the framework of the independent stresses state variables through which the suction effect on the mechanical behaviour is incorporated. The plastic yield surfaces are written in a three-dimensional stress space p - q - s where p is the net mean stress and q refers to the net deviatoric stress and s indicates the suction (Figure 4.61).

In the p - s plane, the Loading Collapse (LC) curve represents the dependence of the preconsolidation net mean stress on the suction. This curve allows also to model the collapse during the wetting under an elevated mechanical load. As for the Suction Increase (SI) curve, it is the plastic yield in suction, which depends certainly on the confinement stress but it is considered constant and note s_0 .

It is then necessary to use a diffusive model to determine the multiphase flows in a porous deformable medium. Different numerical codes such as CODE_BRIGHT (developed by UPC) and Lagamine (developed by ULg) can take into account the multiphase flows and heat transport. They have been applied to Boom Clay for the simulations of different in situ tests such that RESEAL and BACCHUS 2 tests.

4.4.3 Saturated thermo-elastoplastic models (p' - q - T space)

It is necessary that the saturated thermo-elastoplastic models can represent the temperature effect on the irreversible part of the clay behaviour, particularly the thermal induced plastic strain, which are very complex and depends on the stress state (see § 4.2.1.4 and 4.5.4).

Hueckel and Borsetto (1990) and Hueckel and Baldi (1990) model

Hueckel and Borsetto (1990) and Hueckel and Baldi (1990) proposed a thermo-elastoplastic model for the saturated Boom Clay which is an extension of the modified Cam-Clay model to thermal variations. It is able to reproduce the decrease of p_c under heating and its increase during cooling. However, it is only able to predict plastic thermal contraction in the normally consolidated states and elastic thermal strains in the overconsolidated states until yielding, whereas some plastic thermal expansion usually observed at these states can not be reproduced.

In 1994, Picard (1994) proposed also a thermo-elastoplastic model for the saturated Boom Clay. It used the same assumption as Hueckel and Borsetto (1990) and Hueckel and Baldi (1990) but he simplified the evolution law of p_c , decoupling the temperature effects from ones of the effective mean stress which allows to better present the thermal plasticity at higher OCR.

Sultan's model

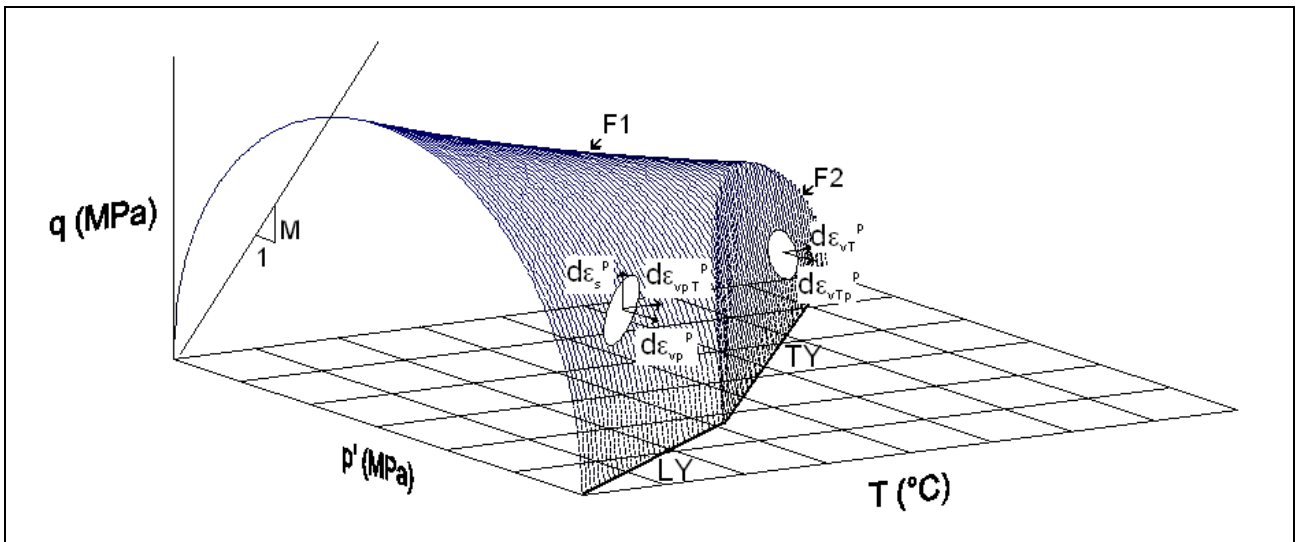


Figure 4.62: Sultan Saturated thermo-elastoplastic model (Li, 2004)

Inspired by the unsaturated elastoplastic models developed by Alonso and Gens (BBM models, see before), Sultan developed a very promising thermo-mechanical model by addition of a second plastic mechanism that allows a prediction of the effect of the OCR on the irreversible volume change. This model is based on both his own test results and those from the literature.

At constant temperature, the yield surface F1 is defined by the modified Cam-Clay model. The preconsolidation pressure and thus the elastic zone decrease with the temperature raising and this evolution is represented by the Loading Yield (LY) curve. When a temperature greater than maximum temperature know by the soil is applied, it induces a hardening. This one is defined in the p' - T plane by the Thermal Yield (TY) curve. It is thus only activated by temperature increase. The resulting yield surface F2 in the p' - q - T as well as F1 is represented at the Figure 4.62, where p' refers to the effective mean stress, q is the deviatoric stress and T the temperature.

As for the soil overconsolidation effect, it is considered thanks to the Heating Contraction (HC) curve. This curve represents the transit temperature between the dilating volumetric behaviour and the contracting one. This transit temperature grows with the OCR.

All the parameters (12) required for this model have been identified for the Boom Clay, and they appear to match very closely some experimental results carried out on the Boom Clay by Baldi *et al.* (1991) in terms of volumetric strain as a function of OCR and temperature (Sultan, 1997).

However, the use of the modified Cam-Clay model at constant temperature is a weakness of the model. It implies that the model can not correctly represent the isothermal elastoplastic behaviour, at least for the elastoplastic behaviour at ambient temperature. In addition, the yielding surface F1 at a constant and elevated temperature is still a subject that is never investigated up to now. Moreover, the influence of the temperature on the critical state line is still a subject to deal with because there is not enough information to draw the conclusion for Boom Clay.

Anyway, this thermo-mechanical model can be considered as a reference model for saturated thermo-mechanical model. Further developments can be devoted to:

Improvement of the yielding surface F1 to enable the model to present correctly the elastoplastic behaviour at a constant temperature. For example, incorporating concepts of the Dafalias Bounding surface or two bubbles taking into account at the mean time the inherent/induced anisotropy. The prominent feature of the concept of the bounding surface is the fact that inelastic deformation can occur for stress points within the bounding surface. This concept has been used in a variety of constitutive laws for material such as metals, isotropic/anisotropic cohesive soils, sands and concrete. As a result, it allows to better presenting the short term viscoplasticity and progressive

transition of elasto-viscoplasticity. This should be the continuation of the development of a saturated elastoplastic model.

Introduction the suction effect in the model in combining the BBM model with this thermo-mechanical model.

Nevertheless, it's worthwhile to note that the cited future development of constitutive model for Boom Clay requires a very extensive and consistent laboratory or in situ characterization program, since it should take into account not only the temperature effect but also the desaturation of the massif (Li, 2004).

4.4.4 Saturated thermo-elasto-visco-plastic models

The first viscoplasticity model was developed by Rousset based on a series of undrained test results. The model developed in such way was written in terms of "total stress" and not "effective stress". In other words, the effect of water is not taken into account. This model was thus later on extended to the "effective stress" in the framework of the ONDRAF-G3S contract. At the same time, temperature effect on the viscosity behaviour was introduced in the model via the dependence of the viscosity parameters and hardening parameters on the temperature.

The model was written in a classical way in introducing the viscosity deformation contribution into a classical elastoplastic constitutive model through the Perzyna theory. The hardening and softening are expressed in function of the accumulated total irreversible deformation, i.e. the viscoplastic deformation. The yielding surface is taken as Mohr-Coulomb's model where the cohesion C_f evolves with the hardening parameter ζ according to the curve on the Figure 4.63. The potential surface was that of Tresca's model. The temperature effects were introduced through the decrease of the cohesion with the temperature and the dependence of the viscosity related parameter η on the temperature.

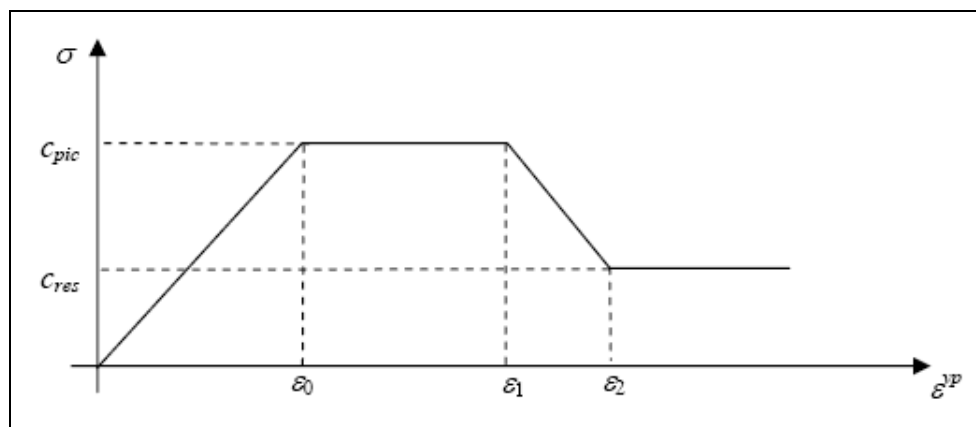


Figure 4.63: Viscoplastic threshold in function of the hardening parameter (Rousset, 1988)

The viscosity related parameters were identified by the triaxial creep tests at ambient and elevated temperature.

However this model has two limitations. Indeed, the yielding criterion of Mohr-Coulomb is only well adapted to the cases where the loading is essentially deviatoric, such as the excavation of the gallery. In addition, the model is suitable to present the long term delayed behaviour, but not to present the short term delayed behaviour. Especially when the loading rate is very high, the dash pot prevents the viscoplastic deformation development, the responses of the model is mainly elastic and the yielding point is so high, this is not in reality.

To withstand two above cited weakness of the developed model, two improvements would be helpful.

First, it may be interesting to introduce the cap model concept. The yield surface is then split into two parts, the Mohr Coulomb criterion for the high deviatoric stress state and the Cam-Clay model

for the mean stress dominate region. The cap means then that the yielding surface is closed on the side of the compressive mean stresses. In such way, the model can present the viscoplasticity deformation in all direction of stress path (Figure 4.64).

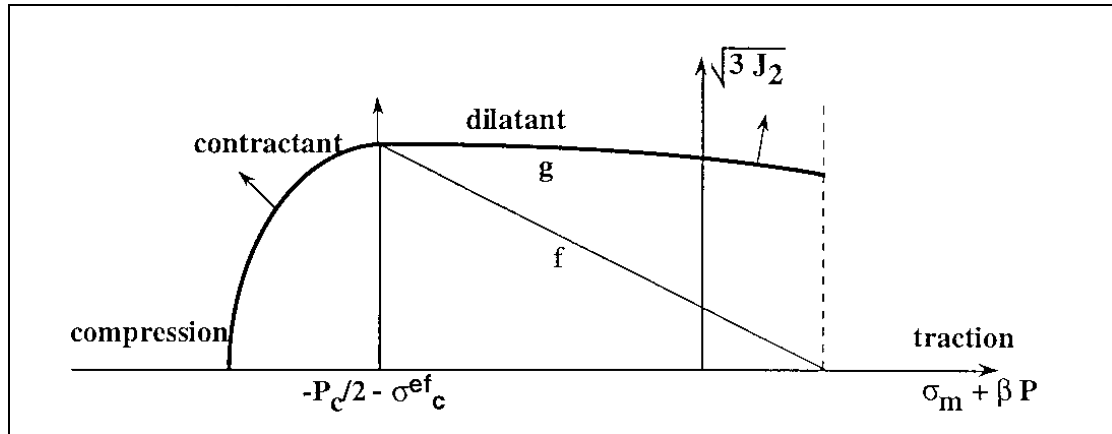


Figure 4.64: Cap model concept

Secondly, it is considered to introduce the notion of "bounding surface" as in the Dafalias-Kaliakin model or "two bubbles notion" as in the "two bubbles" model.

It's worthwhile to note that the composite form of the Dafalias-Kaliakin bounding surface can be converted easily as the "cap" model (Li, 2004).

4.4.5 Applications (Validations – Simulations – Predictions)

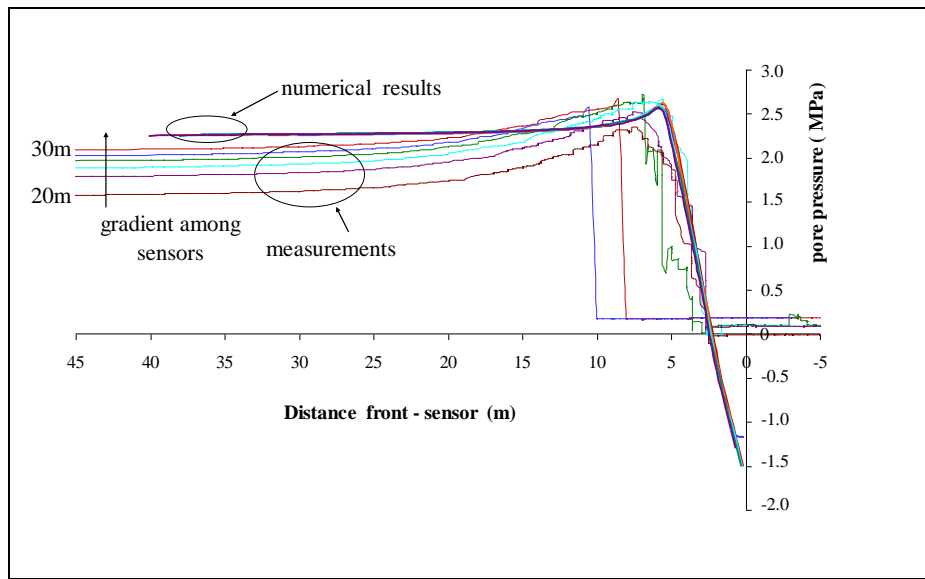
In the framework of numerous projects (INTERCLAY II, ATLAS, CACTUS I and II in the thesis of Picard, CLIPEX, BACCHUS test in the CATSIUS-clay project), simulations and validations of the developed models were realised. This chapter is a brief synthesis revealing the weakness and shortness of the developed constitutive laws for Boom Clay and highlighting thus the necessity for the further development and associated characterisation tests program.

First, regarding the simulation of laboratory tests from INTERCLAY II, it is worthwhile to note that a model calibrated from only a kind of tests can not represent the whole behaviour of the material, resulting from a lack of information. In addition, the thermo-hydro-mechanical behaviour depends on the prior loading and stress path. Thus, the data obtained from a kind of tests may not be applicable to the other test scenario. Large scale and in situ tests are then needed to get a global thermo-hydro-mechanical characterization. It allows also to avoid the differences arising from the inhomogeneity of the Boom Clay.

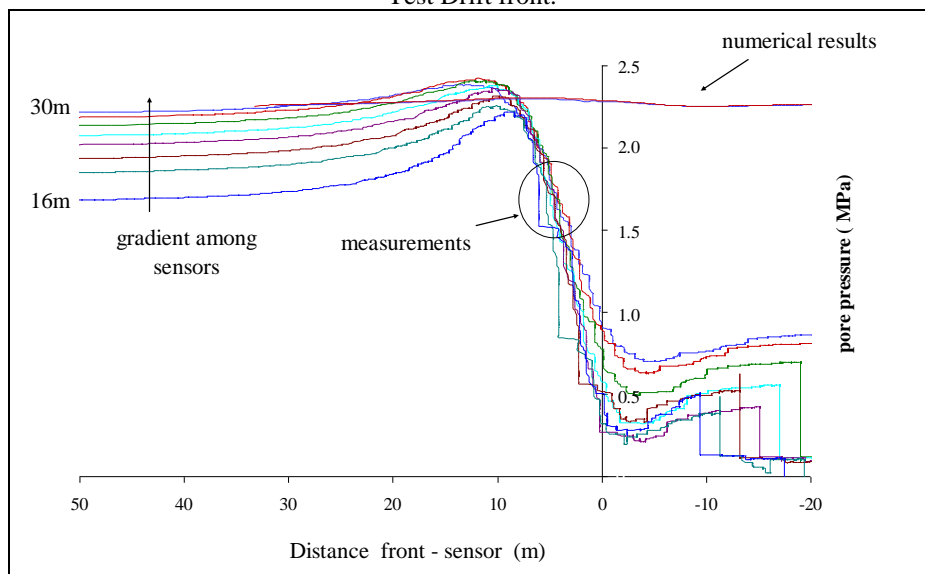
Another observation is that the classical models like Mohr-Coulomb and Modified Cam-Clay models are not able to replicate the thermo-hydro-mechanical behaviour of the Boom Clay. Even the short term hydro-mechanical behaviour is not completely modelled. The major differences appear in the prediction of the excavation effects. All the modelling of CACTUS, CLIPEX and ATLAS projects underestimate the variation of the pore pressure and of the total stress either in the excavation phase or in the thermal-cooling phases (Li, 2004).

For instance, in the framework of CLIPEX project, numerical prediction of the pore water pressure evolution at the points of the piezometers installed in the boreholes A2 and C2 (Figure 4.51) are given in Figure 4.65, in which the in situ measurements are presented also for comparison. It can be seen that the pore water pressure evolution obtained by the Mohr-Coulomb model agrees well with the general tendency of the in situ measurements. The pore pressure increase is due to the undrained contractant behaviour of the clay (Biot coefficient $\alpha=1$), while the drop phenomenon results from the high decompression of the formation (volumetric dilatations). However the numerical simulations

did not produce the extended hydraulic disturbed zone and underestimated the radial variation of the pore pressure (Li *et al.*, 2006).



a) Borehole A2 (installed horizontally along the axis of the gallery), sensors are located between 20 and 30 m from the Test Drift front.



b) Borehole C2 (installed in a vertical plan), sensors are located between 16 and 30 m from the Test Drift front.

Figure 4.65: Pore water pressure evolution ahead of excavation front (comparison between numerical predictions and in situ measurements) (Li *et al.*, 2006)

Modelled total axial displacement agrees with the in-situ measurements (Figure 4.66). But again, the far-field behaviour was not reproduced numerically, since the sensors react very late compared to the in situ measurements (Li *et al.*, 2006)

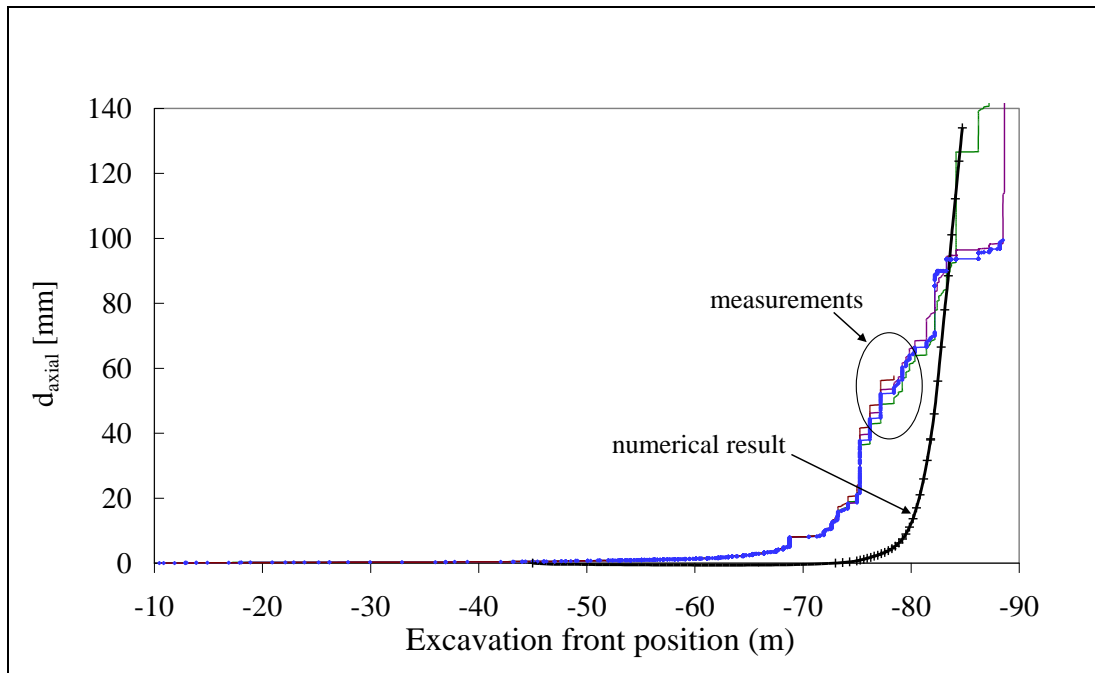


Figure 4.66: Axial convergence prediction (Bernier *et al.*, 2007)

As for the thermal responses predicted by most participants of the ATLAS simulations, they were in reasonable agreement with the measured response.

It is also worthwhile to note that, according to the modelling results, the initial conditions measurement is very important. This is a lesson should be learned for the coming heater test in order to get most credible information for the calibration of the THM model.

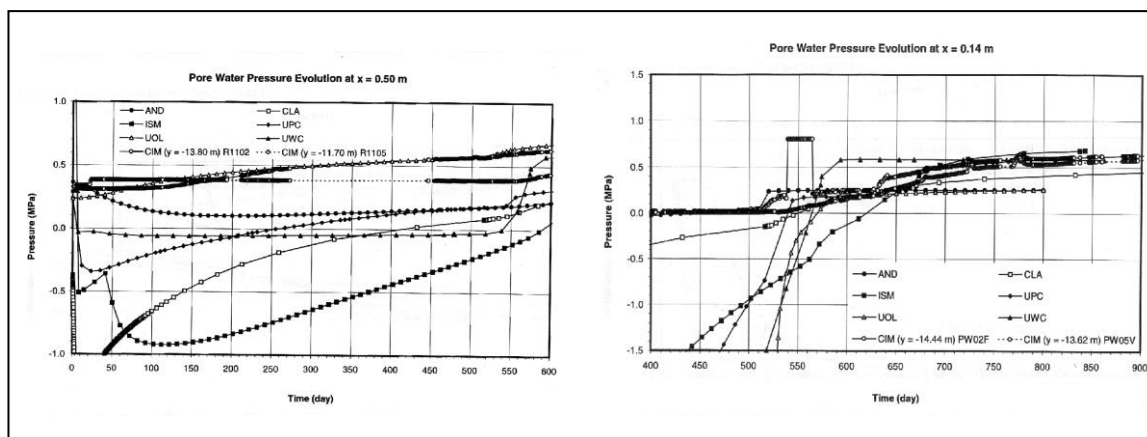


Figure 4.67: Pore pressure predictions by different partners in the framework of Bacchus project (Volckaert *et al.*, 1996)

Resulting from the simulations of PHEBUS, BACCHUS and RESEAL tests, the complexity of the THM behaviour on the interface of the Boom Clay is put in evidence, for example, the contact surface between the backfill and the Boom Clay as in the BACCHUS and RESEAL tests. Moreover, the thermo-hydro-mechanical responses of massif are often affected by the interface behaviour. Figure 4.68 shows the finite element modelling of Bacchus 2 test realised in the frame of Catsius clay using Lagamine Code developed by Liège University of Belgium, which put in evidence the importance of the interface HM behaviour.

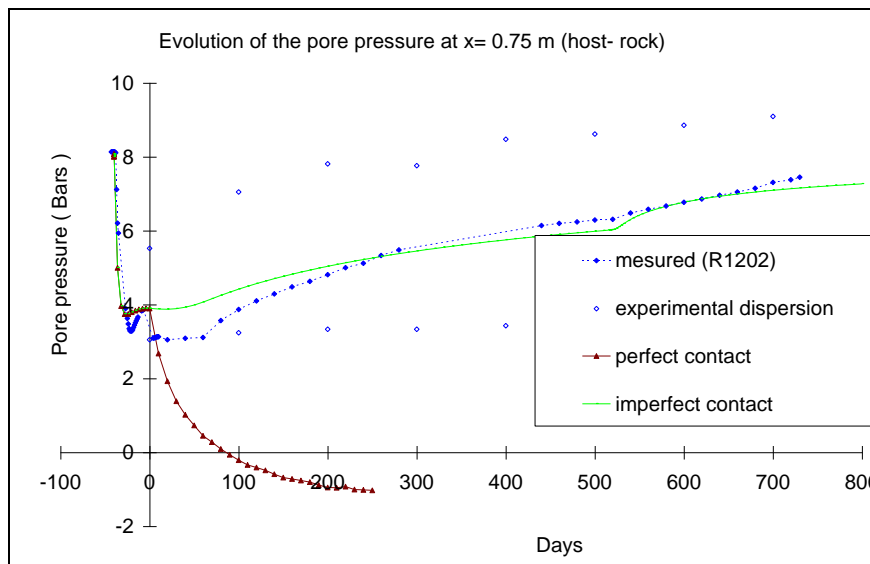


Figure 4.68: Numerical modelling of BACCHUS2 test - considering interface behaviour (imperfect contact) allowing better produce the pore pressure evolution in the massif

Finally, another conclusion from the CACTUS, CLIPEX and ATLAS project is that the possible desaturation of the massif, the EDZ and the viscosity of the clayey skeleton may influence the thermo-hydro-mechanical responses of the Boom Clay during excavation and under thermal solicitations. So, they should be taken into account by the models (Li, 2004).

4.4.6 Future modelling development

First, it is necessary to improve the saturated elasto-visco-plastic models at ambient temperature, i.e. in the p - q plane. The notion of "Bounding surface" or "two bubbles" seems to be promising for several reasons. Indeed, it can take into account the very early appearance of the viscoplasticity (micro-damage) and thus allow a progressive transition of the elasto-plasticity.

It is maybe also interesting to take the anisotropy, natural or induced, into account in the models at ambient temperature.

Secondly, it may be interesting to introduce the temperature and the suction effects into this well calibrated and validated saturated isothermal elasto-visco-plastic model adapted from the Sultan's thermo-plastic model for the temperature effect and from the BBM model for the suction effect and combine both together. The temperature and suction effect on viscosity should be taken into account in the meanwhile.

The model will be then validated with the help of existing in situ tests and simulate the heater test. The latter will provide a good support to understand the physical phenomena that may take place in the system (Li, 2004).

4.5 THM behaviour of Boom Clay – Synthesis

Based on the knowledge obtained through laboratory tests and in situ experiments as well as constitutive modelling studies described above, this paragraph tries to make a synthesis on the THM behaviour of Boom Clay, but in connection with different repository phases.

4.5.1 Hydro-Mechanical behaviour of the "intact" Boom Clay observed in labs

The laboratory tests summarized above have allowed to determine the mechanical behaviour of the "intact" Boom Clay.

Oedometric and triaxial tests provided that the elastic zone of the Boom Clay is very limited and plastic deformation appears early. Moreover, the Young's modulus is very high but it decreases with the accumulated irreversible deformation as shown in Figure 4.69.

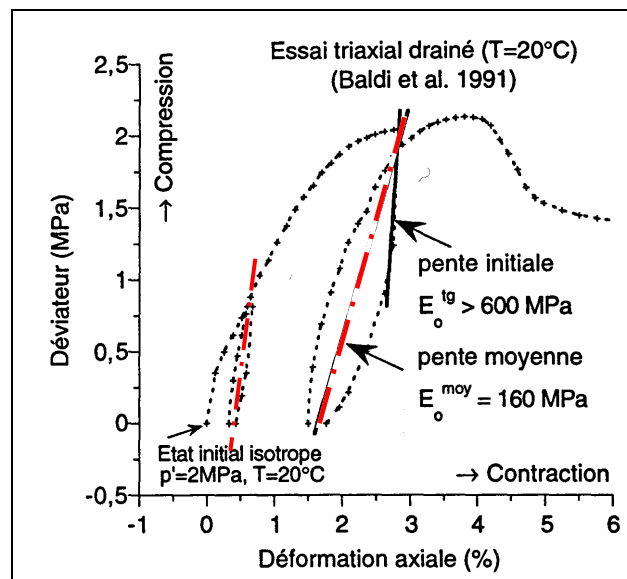


Figure 4.69: Drained triaxial test – Determination of the Elastic modulus (adapted from Picard, 1994)

At in situ state, Boom Clay is overconsolidated. Indeed, its preconsolidation effective pressure p'_c is around 6 MPa. The overconsolidation ratio (OCR) of the rock is then about 2.5. The consolidation state influences the mechanical behaviour of Boom Clay. Indeed, in the laboratory tests effectuated in the SELFRAC project, the stress-strain relation has been established under various states of stress ranging from the overconsolidated domain to the normally consolidated domain and on the basis of the results obtained, Boom Clay exhibits two types of mechanical behaviour depending on the mean effective stress (see Figure 4.27, § 4.2.2.4).

At the in situ state of stress and in drained condition, the behaviour is ductile and contractant, i.e. the q - ε_{axial} curve, where q is the deviatoric stress and ε_{axial} the axial strain, shows a plateau. The hydraulic conductivity was found to slightly decrease from $7.15 \cdot 10^{-12}$ to 10^{-13} m/s due to the contractance of the pore space during the shearing phase, during these tests.

Conversely, at a low mean effective stress (0.4 MPa), the mechanical behaviour is characterized by the development of shear bands leading to the failure of the specimen. The q - ε_{axial} curve shows a peak and the specimen exhibits dilatancy. In this case, the permeability is not influenced neither by the onset of localisation and the propagation of shear bands nor by the dilatancy before the peak stress.

We can note that to detect an important increase of the permeability, the porosity of the specimen (bulk porosity or discontinuities), has to change in a significant manner. Moreover, the discontinuities (if they exist) have to be interconnected to each other and to the hydraulic pore pressure lines. In our tests, the shear bands that we have observed were very thin indicating a low change of the bulk porosity. They were not always propagating from one end to the other end of the specimen and, due to their slope, they were not always connected with the pore pressure lines of the system. If the bulk permeability has not evolved, we can not conclude on the permeability in the shear band (Selfrac –D2).

To represent the mechanical behaviour of the Boom Clay, the most used models are these ones of Mohr-Coulomb and Modified Cam-Clay. As it was seen before, numerous campaigns of tests were realised to determine the needed parameters and the 'best' sets of parameters for these two

constitutive laws usually considered at EURIDICE and SCK•CEN for the Boom Clay around 225 m depth are listed in Table 4.9 and Table 4.10.

Table 4.9: Mohr-Coulomb model parameters for Boom Clay

Young's modulus	E'	300 [MPa]
Poisson's coefficient	ν'	0.125
Cohesion	c'	0.3 [MPa]
Friction angle	ϕ'	18 [°]
Dilatation angle	ψ	0 - 10 [°]

Table 4.10: Modified Cam-Clay model parameters for Boom Clay

Slope of the normal consolidation line	λ	0.13
Slope of the elastic swelling line	κ	0.02
Preconsolidation pressure	p'_0	6 [MPa]
Shear modulus	G	134 [MPa]
Bulk modulus	K'	134 [MPa]

4.5.2 Construction phase – Effect of the excavation

HM responses to excavation were intensively studied in the frame of the CLIPEX and SELFRAC project. During the excavation, stress readjustments take place and clay fracturing occurs and thus creates Excavation Damaged Zone (EDZ) and Excavation disturbed Zone (EdZ) and modifies both mechanical and transport properties around the underground storage gallery. Indeed, the perturbation of the excavation may induce a significant increase of the permeability, related to effective mean stress variation and to diffuse and/or localised crack proliferation in the material (Process A). Self-healing properties of clays can in turn reduce the permeability in time (Process B).

During the extension of the URL HADES, a unique and original opportunity was given, within the CLIPEX project, to monitor the hydro-mechanical parameters of the Boom Clay. The extension consisted of a second shaft, and the excavation of a gallery connecting this shaft with the existing facility. Then the EDZ and EdZ around the second shaft and the connecting gallery may be characterized. Indeed, the excavation of the connecting gallery started from the second shaft and evolved towards the existing Test Drift, from which instrumentation was foreseen in the frame of the CLIPEX programme (see Figure 4.51).

It should be noted that during the excavation of the second shaft, wall convergence was important and induced an important extent of the EdZ. On the other hand, an excavation technique minimising the EDZ was used during the construction of the connecting gallery which was realised with a tunnel machine allowing an excavation rate about three meters per day. Moreover, convergences are controlled during construction of the gallery by placing the lining as soon as possible behind the excavation front.

To avoid the risk of blocking and to ensure a well-controlled and continuous excavation process, the excavation technique has to present enough flexibility to allow an easy driving of the tunnel machine. To that effect, some convergence is unavoidable. In the case of a gallery with a radius of about 2.4 m, a radial convergence of about 9 cm was found to be a good compromise. This value is the sum of 35 mm on the radius at the level of the rear end of the shield, 10 mm on the radius in the unsupported zone and 45 mm on the radius ahead of the front. Using that excavation technique, the

opening of the fractures could be kept smaller than 1 mm at the excavation wall. Fractures remained closed deeper in the host-rock. Moreover, a wedge block concrete lining has been used (Bastiaens *et al.*, 2003).

The fractures were thus characterized throughout the construction connecting gallery. Indeed, the front and excavated profile of the gallery were observed as systematically as possible during excavation. The fractures were photographed, characterised, and mapped. The obtained fracture map, which covers the entire gallery, reveals a fracturation pattern (Figure 4.70) that is constant along the gallery, except in its first and last metres, because of the influence of, respectively, the second shaft and the existing facility (Test Drift).

The fracturation pattern consists of two conjugated fracture planes: one in the upper part, dipping towards the excavation direction (north); the other in the lower part, dipping towards the opposite direction (south). The distance between the fractures is a few decimetres, and they originate at about 6 metres ahead of the front (Figure 4.70). Nevertheless, pre-existing fractures were not observed at the Mol site, though it is impossible to prove their absence. Two cored borings performed shortly after the construction of the connecting gallery to assess the radial extent of the fractures revealed the presence of fractures up to about 1 metre into the clay. If the fracturation pattern is simplified to two flat fracture planes, having their strike perpendicular to the gallery axis, the theoretical trace on the excavated profile in the unsupported zone can be calculated. The observed fracture traces in this zone are quite similar.

The shape and orientation of the observed fracture planes can be explained by the high level of the stresses ahead of the excavation front and by the differential stresses.

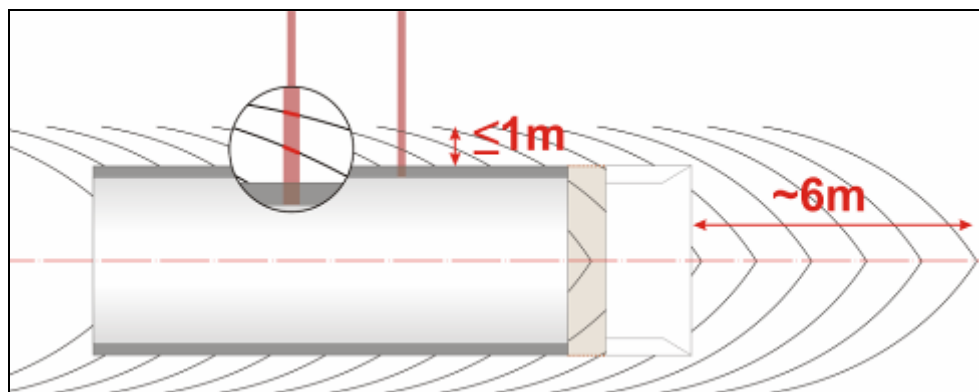


Figure 4.70: Vertical cross section through the Connecting Gallery showing the fracturation pattern around it, as deduced from the observations (Bernier *et al.*, 2003)

From the Clipex and SELFRAC programmes, following major observations can be drawn.

First, the measurements during the construction of the connecting gallery, especially those of the evolution of the pore water pressure, have clearly shown the strong hydro-mechanical coupling behaviour of the Boom Clay as it can be seen on the Figure 4.52.

Secondly, the presence of fractures around the connecting gallery can be confirmed by measurement of pore pressure. Indeed, the suction occurred at about 3 metres ahead of the excavation front because of the strong hydromechanical coupling has been followed by an abrupt recovery of the pore water pressure up to the atmospheric pressure as the front was coming closer, i.e. fractures that are connected to the front.

The zone disturbed by excavation extended much further in the Boom Clay than expected: both piezometer sensors and displacement sensors reacted almost instantaneously to the excavation in spite of their distance from the front, with variations of the pore water pressure and displacements being recorded (Figure 4.71) at, respectively, more than 60 metres and more than 75 metres from the front.

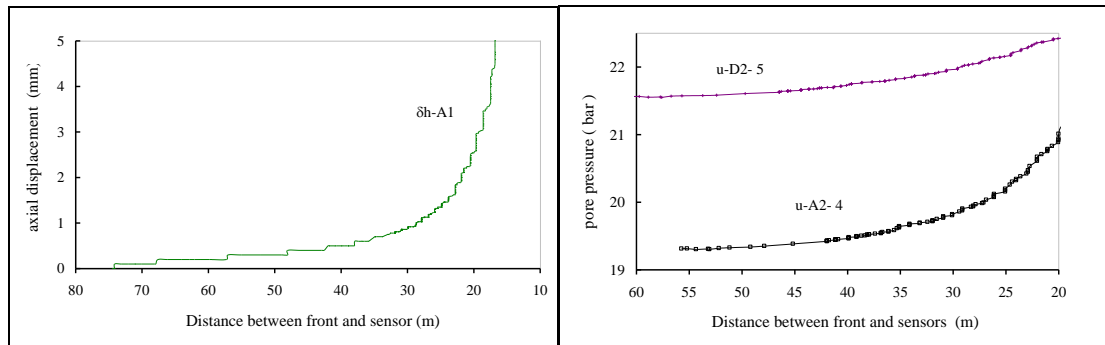


Figure 4.71: Evidences of the extent of the disturbed zone. a) Very early reaction of the extensometer; b) Very early reaction of the piezometers (Bernier *et al.*, 2003)

The Boom Clay presents a time-dependent behaviour through hydraulic diffusion processes and viscosity of the skeleton. It is shown by the increase of the external pressure exerted on the lining segments since their installation. In reality, due to the structure of the lining, the lining – host rock interface can be considered as a drained hydraulic boundary. The reconsolidation of the Boom Clay, caused by both the drainage of the pore water and the creep of the massif, results in an increase of the pressure on the lining. This pressure builds up quite rapidly and to a relatively high percentage of the in-situ lithostatic pressure, soon after the installation of the liner and then evolve slowly with time towards the initial in situ lithostatic pressure (see Figure 4.53 § 4.3.8).

The pore pressure distribution around the connecting gallery is anisotropic (see Figure 4.56). The short-term anisotropy can be explained by stress anisotropy whereas the long-term one by anisotropic hydraulic conductivity of the host rock (see § 4.3.9)

Concerning the hydraulic conductivity around the connecting gallery, it was derived from constant head tests in steady state flow regime. An increase of hydraulic conductivity is observed up to about 6-8 m into the host rock. The values outside this influenced zone are about $6 \cdot 10^{-12}$ m/s for the vertical piezometer and about $4 \cdot 10^{-12}$ m/s for the horizontal piezometer. About 1 year after the first measuring campaign, a new one is realised and the obtained values were systematically lower, although not much. The variation of hydraulic conductivity measured around the connecting gallery was likely related to the effective stress variation and the fractures do not play an important role in this case.

Finally, the total stresses are influenced at least 6-8 m into the host rock (Figure 4.72) and after 2 years, we can see that the total stress close to the gallery wall have increased, indicating stress build-up (re-equilibrium) around the excavation. Moreover, the material parameters (e.g. shear strength and shear modulus) were only slightly influenced and variations are restricted to a limited zone around the gallery (2-3 m). No significant change with time was observed (Bernier *et al.*, 2006).

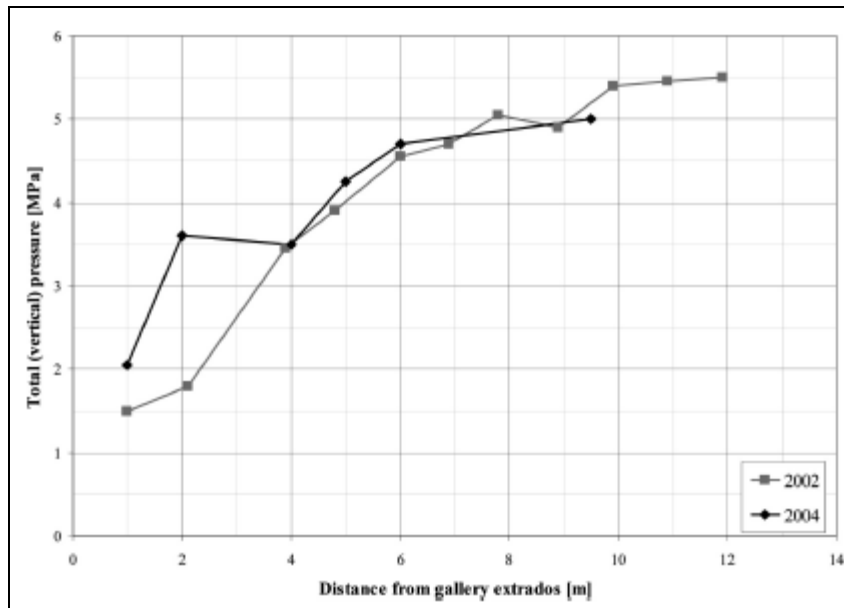


Figure 4.72: Best estimate of total (vertical) stress based upon two series of self-boring pressuremeter tests conducted from the connecting gallery in 2002 and 2004 (Bastiaens *et al.*, 2006)

The results of SELFRAC in situ tests confirm that Boom Clay has important sealing properties. It was shown that, two years after the excavation, the interconnected fractures zone was reduced from 1 m to less than 60 cm around the gallery. The hydraulic conductivity in the sealed zone and beyond in the host-rock remains lower than $2.5 \cdot 10^{-11}$ m/s. Moreover, it was concluded in the RESEAL project that the self-sealing might be enhanced by swelling of the backfill material (Bernier *et al.*, 2006).

In conclusion, gallery construction in Boom Clay at an important depth (223 m in the case of the URF HADES) will always induce fractures. Fracturation is caused by stress redistribution which is inherent in tunnelling. Fracture extent can however be limited by using appropriate excavation and lining techniques. Nevertheless, it was observed that these fractures seal but only heal partially.

From the point of view of the modelling, it is worthwhile to note that the comparison between the prediction results, considering classical constitutive laws like modified Cam-Clay and Mohr-Coulomb model, and in-situ measurements showed a very good agreement for the instantaneous radial convergence and total axial displacements at near field. The simulations can only reproduce the tendency of the pore water pressure evolution, but cannot explain the large extent of hydro-mechanical disturbance. Improvements are needed in the future. Indeed, a correct consideration of plasticity behaviour may certainly improve the quality of prediction, especially the evolution of the pore water pressure. A first tentative simulation with a more sophisticated constitutive law (Bounding surface elastoplastic law) has brought some hope of improvement on the far-field behaviour. It however requires more laboratory work for the calibration of parameters. It is also necessary to consider the time related effects through hydraulic diffusion process and viscosity of skeleton. Finally, the Damaged Zone around the gallery has to be considered because it can influence significantly the hydro-mechanical response. Indeed, the generation of fractured zone around the gallery increases the apparent excavation diameter from hydraulic point of view and so extends probably the hydraulic perturbation zone (Bernier *et al.*, 2003). In addition, consideration of the degradation of the physical properties in the Damaged Zone, like Young's modulus, cohesion, etc. could improve the far-field behaviour prediction (Mair *et al.*, 1992).

4.5.3 Open drift phase

During this stage, the ventilation of the drift and the creep process of plastic clay are the most important processes related to the host rock behaviour.

Ventilation of the drift

During this open drift phase, the drift is ventilated. In general, ventilation is an important factor in clays whose hydro-mechanical properties are sensitive to moisture content. Ventilation reduces drift humidity and eventually dehydrates the rock near the drift surfaces (depending on the air-entry value of the rock). For plastic clays, ventilation changes moisture level, in turn changes its hydro-mechanical properties (strength, permeability, etc) and retarding self-sealing.

In the framework of the PHEBUS project, a laboratory mock up as well as an in situ test consisting in a ventilated borehole have been realized to study the possibility of desaturation of the Boom Clay due to ventilation. The principle of the test is to cycle a controlled humidity air in an orifice drilled in a cylinder sample and measure the hydric exchange between the air and Boom Clay.

After dismantling, the moisture profile of the mock up was measured. This test showed that the desaturation zone is limited and that a suction field around the orifice is created inducing a consolidation (Robinet *et al.*, 1998).

It's necessary to underline that the air entry value may be very high in intact Boom Clay, at least 1 or 2 MPa. But in the EDZ, the host rock may possess a double porosity, composed of micro-pores and of micro-fractures. Air entry value could be lower due to the presence of the micro-fractures. In such case, the desaturation in the EDZ could become significant.

Creep of the Boom Clay

Boom Clay presents a strong time-related behaviour, which comes from both the viscosity of the skeleton (creep) and hydraulic diffusion. This feature of viscoplasticity constitutes a favourable factor to the healing of the fracture.

Different laboratory tests were performed in order to characterize the creep of the Boom Clay. It was put in evidence that the elastic limit is very small and that the viscoplasticity is an essential mechanical behaviour of the Boom Clay (Figure 4.25, Figure 4.37, Figure 4.41 and Figure 4.53).

The viscous behaviour of clays together with early observations performed during and after the excavation of the connecting gallery at Mol suggest that after the initiation of the damaged zone during repository construction, the geological barrier might not be further mechanically damaged, the open fractures should close and parts of the EDZ could even partially recover the characteristics of the undamaged material. However, this potentially important input to PA has to be confirmed by additional observations and explained using convincing models.

4.5.4 Early closure phase

At this stage, the hydromechanical behaviour of the host rock will be much more complex due to the heat released from the waste: it will be a Thermo-Hydro-Mechanical coupling problem. This complexity of THM processes will be further increased when dealing with the interaction between host rock and EBS.

Due to the strong coupling among transient flow, consolidation phenomena and thermal variations, the complexity is also increased by the important influence of temperature on the hydro-mechanical properties of low permeability clay.

The main process during the early closure phase include thus the temperature effect on the host rock, including the damaged and undamaged zones, and the interplay between the host rock and EBS for the phenomena of resaturation – desaturation – temperature variation. Water phase change, in other words vaporisation, can occur too.

Temperature effects on the behaviour of the saturated host rock

The main thermo-hydro-mechanical properties of Boom Clay are characterised in the frame of Sultan's PhD thesis (1997), projects WASI and FI1W/0150 in laboratory and ATLAS and CACTUS as well as CERBERUS in situ.

First, it is important to note that the heat transport is done mainly by conduction and the convection transport is practically inexistent due to its extremely low hydraulic conductivity. The thermal analysis can thus be considered independent of the hydro-mechanical results. Conversely, the thermal conditions influence strongly the hydro-mechanical behaviour.

It is observed that the heating induced hydro-mechanical responses of Boom Clay depend highly on the consolidation state (OCR). For high OCR, thermal loading induces first expansion resulting from the thermal dilation of the components and secondly contraction further to a rearrangement of the particles. The transition temperature between these behaviours increases with OCR. In the case of a normally consolidated state, the thermal loading generates immediately an irreversible contraction. As for cooling, it induces contraction, which seems not depend on the stress state (see Figure 4.16).

Secondly, it is observed that Boom Clay is undergone to a thermal hardening (thermal plasticity). It is shown on the Figure 4.17. Indeed, samples initially isotropically loaded to 4 MPa, heating to 100 °C and next cooled present a preconsolidation pressure higher than 4 MPa. The preconsolidation pressure decreases when temperature increases according to an exponential function.

It is observed too that Boom Clay presents thermal consolidation. From the triaxial heating tests in drained condition, the curves that express the volume changes are similar to that of standard consolidation curves, the volume decrease is related to thermal induced excess pore pressure dissipation (Delage *et al.*, 2004).

The main temperature effect on the hydro-mechanical and physical properties of the Boom Clay is also considered.

First, elevation of temperature induces a decrease of the water viscosity and has consequence on some properties of the clay. For instance, it induces a decrease of the Atterberg limits and an increase of the hydraulic conductivity (see Figure 4.19). Indeed, the temperature augmentation induces a reduction of the friction intervening in the ground flow.

The ATLAS and CACTUS as well as CERBERUS in situ experiments allowed to study the response of Boom Clay to the heating directly in situ and in a medium-large scale. In the CACTUS in situ tests (§ 4.3.7), the measurements obtained put in evidence some particularities of the THM responses of the Boom Clay.

In the massif, the response to heating appears first by an increase of the pore pressures which happens before the temperature increase. However, it is explained by a modification of the mechanical state which is transmitted instantly in the massif. Next, pore pressures and temperature increases simultaneously resulting from the discrepancy of thermal dilation between water and solid skeleton. In a third time, the pore pressures decrease because the hydraulic flow becomes significant. The hydraulic characteristic time is shorter than the thermal one for Boom Clay.

During the cooling phase, the THM parameters inversely evolve in comparison with the heating phase, on a very similar way. This observation tends to indicate that an important part of the observed variations are reversible. Nevertheless, it is essential to identify the irreversibilities that subsist, like a modification of the water content during the first heating phase of CACTUS 1, the displacements in the massif of low amplitude and a slight increase of the density.

Interplay among resaturation – desaturation – temperature

Very limited laboratory tests on unsaturated and high temperature conditions have been realized on natural Boom Clay. Only in the frame of BACCHUS and RESEAL projects, some effort was devoted to the determination of the unsaturated hydraulic properties in laboratory at ambient temperature such as the retention curves, relative permeability, etc. But it is worth to note that most of the laboratory tests were realized on remoulded samples. There is not yet a consistent laboratory THM characterisation program realised on natural Boom Clay (intact or damaged), at unsaturated or partially unsaturated state. A PhD thesis is on-going in UPC to study this aspect.

Moreover, the saturation – desaturation of the massif depends on the interaction between the host rock and the Engineered Barrier System (EBS) and in particular with the backfill material. For that, the BACCHUS experiment focused on the hydro-mechanical behaviour of the backfill material and the Boom Clay and their interaction.

4.5.5 Late closure phase

The evolution of the EDZ around the experimental shaft of the HADES URL, after emplacement of a bentonite seal is followed within the RESEAL project since 1999. At this moment (2007), all fractures close. Nevertheless, the RESEAL is still watched in order to obtain additional information about the evolution of the EDZ on a longer period of time. However, it is not actually planned to study the effects of heat within the RESEAL set-up.

Nevertheless, although the self-sealing carries on, we can not say what will be the mechanical and hydraulic behaviour of the fractures on the long term. Moreover, the chemical effects will evolve in the long term and the support system may be degraded. What will be its effect on the EDZ? Gas can then appear. It is therefore important to study its transport in the massif and its effect on the radionuclide transport along the EDZ.

4.5.6 Open questions

The state of the art on THM (c) behaviour of Boom clay revealed that there still some open question to be clarified.

First, during the excavation of the connecting gallery of the URL HADES, hydraulic pressure evolutions were measured far from the excavation front what is not predicted by classical elastic – perfectly plastic models. More efforts should be put in the modelling, taking into account the fracture development under shear loading, the viscous effects, the anisotropy and the suction effects.

During the open drift phase, the evolution of the geochemical changes has not yet been studied and is not clear so far. It is studying within the EC project NF-PRO.

The role of the suction in the creation of fractures must also be evaluated. The suction has two origins. First, during the excavation of the gallery, the dilatant behaviour of the host rock will induce a decrease of the pore pressure and possibly suction near the gallery wall, where the higher deviatoric stresses are obtained. Secondly, during the open drift phase, suction may appear resulting from the ventilation of the gallery. The suction will increase the host rock apparent strength by a

suction based cohesion. On the other hand, suction development implies an isotropic contraction of the soil. With regards with a low traction strength, traction fractures may appear, in relation with excavation dilatant behaviour and the gallery ventilation.

While the waste installed, the heat decayed from the waste has to be dissipated through the engineered barrier to the host rock. The quick increase of temperature in the EDZ will induce a thermal expansion of the porous media (solid and liquid phases), and thus some effective stress changes. In plastic clays, it is currently unclear whether these changes will induce fracturing or EDZ sealing. In other words, it is not yet clear if the THM transient will further reduce the thickness of the undamaged geological barrier or improve the sealing of the EDZ. All these constitute main objective project TIMODAZ.

Heating clay induces strength modification of intact material (Cui, 2000; Delage, 2000; Laloui, 2001; Romero, 1999; Baldi et al, 1985 & 1988; Hueckel and Baldi, 1990). Only very few experiments have been performed in order to evaluate these strength modifications. Sign and amplitude have still to be confirmed. Especially deviatoric strength (cohesion, friction angle) has been poorly investigated. If heating increases the Atterberg limits (liquid limit LL and plasticity index PI), it generally implies a friction angle decrease and a (viscous-) plastic strain increase, which help sealing. However, one has seen brittle fractures in heated clay, which could mean a kind of material "embrittlement", of loss of plasticity. Interaction between damaged clay and heating has never been investigated, but should be in the TIMODAZ project.

Partial saturation during heating may modify the clay behaviour. The effect of water vapour flowing through fractures should be clarified.

On a long term time scale creep rate and viscous strains could be enhanced by temperature increase, which could in turn improve self-sealing. However, experimental results are lacking on this subject.

The thermal phase should last a few hundreds to a few thousands of years depending on waste type. The engineered barrier system is designed in such a way that no radionuclide releases occur while a significant part of the host formation is hot. However, the reversibility of thermally-induced changes should be checked.

The evolution of the geochemical changes when returning to anaerobic/anoxic conditions has not been studied yet. Is a geochemically disturbed zone (GDZ) created? If so, what is the extent, what is the fate and how should it be treated in PA studies. Finally, interactions with the engineered barrier system have to be considered: corrosion, degradation, alteration of concrete of canister steel envelope and of the swelling backfill material (Gérard, 2001; Coussy, 2001; Le Bellego, 2000).

Gas production (corrosion processes) could enhance radionuclide transport along the EDZ. Could the gas pressure gradient induce significant advective transport? What is the threshold for gas migration through the EDZ compared to intact clay? How does it move? The air entry value is very high in intact Boom Clay, at least 1 or 2 MPa. But there may be a double porosity in EDZ, composed of micro-pores and of micro-fractures. Air entry value could be lower because of micro-fractures. Gas may dissolve in water and then move by diffusion. On the other hand, gas fracturing could be possible (Olivella & Alonso, 2003). Is the gas flow a diffuse quasi-homogeneous phenomenon or is it an unstable process?

Finally, in the long term, a lot of questions remain. First, how does the self-sealing evaluate, do fracture close and what is their mechanical and hydraulic behaviour on the long term? What is the long term evolution of chemical effects? Does degradation of the support system take place and what is its effect on the EDZ? And how does the gas problem evolve?

4.6 Related chemical aspects

4.6.1 The geochemistry of the Boom Clay under natural conditions

4.6.1.1 The geochemistry of the Boom Clay at the reference site in Mol

The geochemistry of the Boom Clay has been studied in general at the reference borehole Mol-1. A more detailed study on the Boom Clay composition and its pore water chemistry has been performed on the borehole HADES 2001/4 and associated MORPHEUS piezometer (De Craen et al., 2004) and the borehole HADES 2003/9 and the associated reference piezometer R13U (De Craen, 2005). The borehole HADES 2001/4 was drilled from HADES URF vertically downwards to a depth of 40m below the HADES URF and the borehole HADES 2003/9 vertically upwards to a depth of 20 m above the HADES URF. Mineralogical analyses were carried out and, within the scope of the geochemical characterization, the major (Si, Al, Fe, Mg, K, Ca, Na), trace elements (Mn, Rb, Sr, Cs, Y, Zr, Ba and lanthanides) and radionuclides of U, Th and Ra have been analyzed. The organic carbon content (TOC) was derived from Rock-Eval analysis.

4.6.1.1.1 Mineralogy

The Boom clay is a polyphasic sediment composed of non-clay and clay minerals, fossil remains, organic matter and pore water. The quartz, K-feldspar, Na-plagioclase, pyrite and carbonates were identified as the most abundant non-clay mineral constituent. The carbonate composition may vary from calcite to dolomite, siderite and ankerite respectively. The clay mineralogy is dominated by the mixed-layered illite-smectite, illite, kaolinite, chlorite and vermiculite. The mineralogical composition is very homogeneous in the vertical profile of the Boom Clay from qualitative point of view. However, the significant variations exist in the quantitative mineralogy, which is related to different grain-size distributions in silt-dominated and clay-dominated layers. The total non-clay content was found to vary between 41-77 wt%, the total clay content in the range of 23-59 wt% in the studied profile. The reference mineralogical composition of the Boom Clay is given in the Table 4.11.

Table 4.11: The quantitative mineralogical composition of the Boom Clay at the reference site in Mol. All values are expressed as weight % and should be considered as indicative.

Clay minerals	23-59 %
Kaolinite	5-15 %
2:1 clays and micas	35-50 %
Vermiculite/chlorite	1-4 %
Non-clay minerals	41-77 %
Quartz	23-57 %
K-feldspar	6-11 %
Na-plagioclase	0-3 %
Carbonates	1-5 %
Pyrite	1-5 %
Organic matter	1-5 %

The present-day mineral assemblage of the Boom Clay is considered to represent more or less the mineral assemblage of the Boom Clay shortly after deposition (30Ma ago). No evidence of important mineral transformations is found in the Boom Clay. Nevertheless, several diagenetic products are recognised, the most important being pyrite and carbonates, the latter forming septarian carbonate concretions. These are the result of early-diagenetic processes taking place in the shallow burial environment. Since then, the mineralogy of the Boom Clay probably remained the same.

4.6.1.1.2 Organic matter

The TOC contents in the sediment of the Boom Clay at the reference site in Mol vary between 0.78 and 4.13%, the highest values being found in the organic-rich layers at the base of the Putte Member. The Tmax values of the Rock-Eval analysis indicate low maturity of the analyzed kerogen, the oxygen (OI) and hydrogen index (HI) point to a Type III or the terrestrial kerogen. Important to note is that the Boom Clay kerogen exhibits an unusually high oxygen content (O/C ratios of 0.27 from the Putte Member), which is about twice the value generally observed for low maturity kerogens in clay formations. In contrast, relatively low nitrogen and sulfur contents (N/C ratios ~ 0.035 and S/C ratios ~0.025) were observed in the Boom Clay kerogen (Deniau et al., 2001, 2004).

4.6.1.1.3 Pore water composition

The pore water composition was determined from squeezing and leaching of clay cores and *in-situ* from MORPHEUS and R13U piezometers. The pore water was analyzed for TIC (Total Inorganic Carbon), dissolved organic carbon (DOC), major cations (Ca, Mg, Na, K, Si, Fe), anions (F⁻, Cl⁻, Br⁻, SO₄²⁻, S₂O₃²⁻ and HCO₃⁻), trace elements (Mn, Rb, Sr, Ba, Cs, Al, Y, Zr and I), lanthanides (La, Ce, Pr, Gd, Tb, Dy, Ho and Hf) and radionuclides of the U and Th.

At the reference sit in Mol, the Boom Clay pore water is NaHCO₃ type water with NaHCO₃ content of 15 mmol/l, containing an important amount of dissolved organic matter (about 115±15 mg C / l).

Its pH ranges from 8.3-8.6 and the maximum redox potential Eh is about -270 mV (De Craen et al., 2004). The reference Boom Clay pore water composition and the measured MORPHEUS pore water composition are indicated in the Table 4.12.

Vertical variations in pore water composition are present, but are very small. The only remarkable difference was found in the chlorine concentration in the pore water, which was 10-20 mg/l above the HADES URF and 20-30 mg/l measured below the HADES URF.

Table 4.12: The reference Boom Clay pore water composition and the measured MORPHEUS water composition. The major ion concentrations of the reference water are calculated by cation exchange and mineral dissolution reactions that are calibrated against the measured

composition	reference water	MORPHEUS water -217~ -235 m TAW
--------------------	------------------------	--

	mg/l	mmol/l	mg/l	mmol/l
Na	359	15.6	348-431	15.1-18.7
K	7.2	0.2	6.7-8.3	0.17-0.21
Ca	2.0	0.05	1.5-2.9	0.04-0.07
Mg	1.6	0.06	1.3-2.6	0.05-0.11
Fe	0.2	0.003	0.10-0.68	0.002-0.012
Si	3.4	0.1	4.2-5.5	0.1-0.2
Al	0.6E-3	2.4E-5	0.03-0.06	1.1-2.2E-3
HCO ₃ ⁻	878.9	14.4		
TIC (mg C/l)	181.3	15.1	173-206	14.4-17.2
alkalinity (meq/l)	15.12		14.9	
Cl	26	0.7	24-30	0.7-0.8
total S	0.77	0.02	na	
SO ₄ ²⁻	2.2	0.02	0.63-2.31	6.5E-3-0.02
HPO ₄ ²⁻			na ^s	
NO ₃ ⁻			~0.4	6.4E-3
F			2.6-3.3	0.13-0.17
Br			~0.6	7.5E-3
B			~7	0.6
DOC (mg C/l)			120-200	
Cs			<0.5 (µg/l)	<4E-9 (M)
Sr			46-90 (µg/l)	5-10 E-7 (M)
U			0.3-1.2 (µg/l)	1-5 E-9 (M)
pH	8.5		na	
pCO ₂ (atm)	10 ^{-2.62}		na	
E _h (mV)	-274		na	
temperature (°C)	16		~16	
conductivity (µS.cm ⁻¹)			1700	
ionic strength	0.016			

4.6.1.1.4 Natural U-Th in Boom Clay

The radiochemical study of the Boom Clay, in particular the application of uranium-thorium series disequilibrium studies, indicates that, in general, **the Boom Clay is in a state of secular radioactive equilibrium**. This means that over the geological history no preferential leaching and/or precipitation of U occurred. This observation points to the fact that the Boom Clay can be considered as a stable geological system. On the other hand the radiochemical studies performed on the pore waters systematically showed the state of radioactive disequilibrium. The fractionation between ²³⁴U and ²³⁸U can be explained as a result of α -recoil.

In general, the Boom Clay can be considered as a rather homogeneous sediment. Depth profiles of mineralogy and geochemistry are generally very flat, although some small variations can be recognised. These variations in mineralogy and geochemistry can be related to grain size variations in the Boom Clay.

4.6.1.2 Regional variations in the geochemistry of the Boom Clay

The geochemical characteristics of the Boom Clay at the reference site in Mol have been compared to the data from the borehole Zoersel, Doel and Essen. This comparison was performed in order to assess the lateral homogeneity of the geochemistry of the Boom Clay.

The qualitative mineralogy is comparable in the vertical profile of the Mol and Essen boreholes (De Craen et al., in prep.) However, the relative contents of the minerals may vary from site to site for a given layer. These differences stem from variations in the distance to the paleocoastline and to the detrital source areas.

The most important lateral variability is seen in the pore water chemistry. A general trend of increasing salinity is present from the east (Mol) to the northwest (Doel and Essen). **The water composition varies from a NaHCO₃ – type water in Mol over a Na(SO₄-HCO₃-Cl) – type water in Zoersel, and a NaCl – type water in Doel and in Essen** (De Craen et al., 2006). Moreover, an increasing salinity with depth was recognised in pore water chemistry in the Essen samples. No such a trend exists in porewater geochemistry at the Mol site.

4.6.2 Geochemical perturbations in Boom Clay

The geochemical perturbations of the Boom Clay occur, e.g. as a result of the engineering activities related to the construction of the shafts and galleries. During the excavation, the Boom Clay becomes inevitably oxidized. The cement, commonly used for lining, as a waste matrix and as a component in the recent belgian super-container design, is known to emanate hyperalkaline fluids after saturation. These high-pH solutions will interact with the Boom Clay and will alter its geochemical characteristics. Additional perturbations are expected after disposal of the HLW generating heat and radiation. Correspondingly, the most important geochemical perturbations include oxidation, the alkaline plume and heat/radiation effects.

4.6.2.1 Oxidation

The in-situ experiments have been performed in HADES URL in the Test Drift (ventilated for ~20 years) and Connecting Gallery (ventilated during ~4 years) in order to assess the extent and the degree of oxidation induced by the excavation and ventilation of the Boom Clay. Within this scope, two N₂ drillings were performed in order to avoid any additional oxidation caused by drilling, and a piezometers were installed with filters at different depths from the concrete/clay interface. The pore water chemistry was analysed to study the extent of oxidation in both galleries in the Boom Clay.

The main process occurring is the oxidation of pyrite (FeS₂), resulting in an increase of sulphate in the pore water and a precipitation of iron oxy-hydroxides. In the in-situ experiment, in the deepest filters, background concentrations of sulphate were measured in the pore waters, indicating the successful use of nitrogen during drilling. Increasing sulphate contents were measured in the first two filters located within one metre from the concrete lining / host rock interface. This trend of increasing sulphate contents in the direction of the gallery was also measured in the pore waters obtained by the batch leaching experiments of clay samples, sampled within the first cm's to dm's of clay, close to the concrete lining. Besides the high sulphate content, these pore waters also have increased contents of major cations. The observed changes in pore water chemistry as a result of oxidation, and within the first meter of clay, are explained by geochemical modelling as the result of cation exchange and mineral precipitation/dissolution reactions.

Also, the mineralogy was studied on micro-scale from cutting edges taken from Test drift and Connecting Gallery respectively. In both cases, gypsum was observed, most likely as a result of

pyrite oxidation. The presence of gypsum is limited to first few centimeters from the concrete/clay interface. Interestingly to note is that the region of the most intensive gypsum precipitation is connected with calcite depletion. Therefore, it is suggested that the dissolution of calcite is an important mineralogical change accompanying the oxidation of the Boom Clay. The calcite is an important mineral phase in Boom Clay to buffer the pH decrease as a result of pyrite oxidation.

Based on the experimental and modelling results performed on Boom Clay the following conceptual model of oxidation was developed (Van Geet et al., 2006): (i) excavation of galleries results in the creation of fractures around the gallery and the exposure of clay to oxygen. At that moment, an important instantaneous oxidation of the clay occurs limited to a depth to which the fractures are formed. (ii) oxidation products are created and will be transported (mainly towards gallery). (iii) during ventilation a continuous diffusion of oxygen from the gallery towards the clay body is maintained.

During excavation, fractures are created in the surrounding host rock to a depth of about 1 m. Therefore, in the first stage the oxidation is limited to the first 1 meter. Due to the fast sealing of the Boom Clay after emplacement of the lining, the oxidation products will remain entrapped within the first meter around a gallery. A substantial hydraulic gradient exists around an open gallery and the oxidation products will be redistributed by advective-diffusive transport. Scoping calculations illustrated that the diffusion of the oxidation products further into the undisturbed Boom Clay is negligible even after 50 years and that the majority of the oxidation products are transported towards the gallery. Consequently, the extent of the oxidized zone remains limited to about 1 m. During ventilation, the Boom Clay is fully saturated. Thus, the only way to oxidise the clay is by dissolution of oxygen into the pore water and diffusion into the Boom Clay. However, it needs to be reminded that a combined diffusion-advection regime is present.

To conclude the results, **the experimental and modelling data suggest that oxidation of the host rock is limited to about 1m, even after 20 years. The scoping calculations are rather conservative since only pure transport and no reactive transport (oxygen sink) has been taken into account.**

4.6.2.2 Alkaline plume

Highly alkaline solutions might be generated under natural conditions (e.g. Maqarin site, Smellie, 1998), or as a result of engineering activities related to emplacement of concrete. Concrete in combination with clay barrier as a host rock and/or as a back-fill material is currently considered in the disposal concepts of high-level radioactive waste in Belgium. During saturation phase, the concrete will emanate large quantities of chemically aggressive, highly alkaline solutions, which will interact with the surrounding rock medium. The pore fluid of cement is not in chemical equilibrium with Boom Clay, and therefore tends to react with clay and causes perturbation.

Two types of synthetic cement pore fluids – young cement water (YCW) and evolved cement water (ECW) were used in percolation and through diffusion experiments on Boom clay cores running for up to 6 years. The YCW is K and Na – dominated solution with an initial pH of 13.2 and represents the fluid emanated by cement at the early stages of repository evolution. The ECW is Ca – dominated, has a pH of 12.5 and represents later stages of cement pore water evolution (Wang et al., 2004, 2007). The experimental results can be summarized as follows: (i) the alkaline front progresses faster in the case of young cement water than in the case of evolved cement water, (ii) dissolution of aluminium silicates by high pH alkaline plume were observed by the increased concentrations of Al and Si in the effluents; dissolution of smectite by the YCW was evidenced, but mineralogical analysis did not detect any alterations in clay cores percolated by the evolved cement water; dissolution of natural organic matter was observed by the YCW, but not by the ECW (iii) hydraulic conductivity increased in the cores percolated by the young cement water and decreased in

the cores percolated by the evolved cement water, (iv) pyrite in Boom Clay was not altered by cement waters suggesting that the initial reducing capacity of the Boom Clay would remain unaffected, (vi) significant retardation of H_2CO_3^- was illustrated in the ECW experiment. This might be caused by precipitation of calcite as a result of ECW-clay interaction. This may also be linked to the observed decrease in hydraulic conductivity in the ECW experiments.

The effect of the alkaline interstitial water on the self-sealing capacity of the Boom Clay was studied within the framework of the SELFRAC project (Bernier, 2004). The alkaline solution was injected through the artificially induced fracture in the Boom Clay core in the permeameter cell. The hydraulic conductivity was measured as a function of time and applied confining pressure. In case of the experiment performed with calcium hydroxide saturated Boom Clay water a steady-state hydraulic conductivity was already reached after only two days of pore water injection. The initial fault was clearly visible, but the cohesion was much stronger compared to the other tests indicating the precipitation of neoformed mineral phase(s) in the fracture. This observation points to the importance of the porewater chemistry on the qualitative and quantitative degree of selfsealing processes in clays.

In situ tests were conducted by putting Ordinary Portland Cement (OPC) in contact with the Boom Clay at the HADES underground laboratory for a period of 18 months. Results of these tests and modeling were reported by (Adenot et al., 2001; Read et al., 2001; Sneyers et al., 2001). From the experiments, obvious dissolution of portlandite in cement was observed in conjunction with porosity increase in the zone where leaching of Ca and/or Si occurred. Also noted was the formation of calcite within a reaction zone in cement where apparent porosity decreased. At the clay side, Mg-Al-Si rich zone was evidenced and the formation of hydrotalcite and sepiolite like minerals was found probable. Very importantly, a disturbed zone of 100-250 μm into both the cement and the clay was evidenced indicating the magnitude of an alkline plume perturbation within the experimental time of 18 months.

Common patterns of mineralogical alterations in a clay under alkaline plume are (i) ion exchange reactions resulting in an increased CEC until pH around 12 (ii) dissolution of swelling clays in high $\text{pH} > 13$ and phyllosilicates at pH of 12.5 and (iii) precipitation of zeolites, C(A)SH phases, calcite, and portlandite.

Numerical modeling with coupled transport and simple mass balance constraints were applied to assess the extent of an alkaline plume in a host rock (Wang et al., 2007). Despite the different levels of details incorporated, all models predict a very limited extent of perturbation with a maximum of a few meters disturbed zone into a clay barrier and all models predict a potential self-sealing of the porosity in the vicinity of the interface suggesting a significant decrease of diffusion in the disturbed zone. Since repository concepts in clay normally rely on a thick layer of the host formation (much thicker than the alkaline plume perturbed zone), the effects of an alkaline plume can be neglected in PA and strong arguments are available to support this approach. However, it should be mentioned that the issue of natural organic matter was highlighted as it may play against an ignorance of an alkaline plume in PA. This may indicate that the migration of natural organic matter and the complexed radionuclides in an alkaline plume disturbed zone could be a major uncertainty and a subject of future studies.

All information available suggests that an expected impact of an alkaline plume on the Boom Clay as a repository formation should be very limited. **Laboratory experiments and modeling indicate that an alkaline plume disturbed zone in Boom Clay is about 2.5 meters at maximum** (Wang et al., 2007). This range is in good agreement with the conclusions made from studies on similar type of clays considered in France and Switzerland.

4.6.2.3 Heat/Radiation

The heat induced by the waste and its effects on the clay material when combined with fluid migration is an important issue for deep repository of HLW. The increase in temperature in a repository is considered to be a function of the thermal gradient of the waste package, the thermal conductivity of the engineered and geological barriers and the storage geometry (Performance Assessment of Geological Isolation Systems, PAGIS, 1988). The integrated modeling reports that temperatures should not exceed 100-150°C in the nearfield environment of waste packages, that the maximum temperatures will be reached in the first 10 years and may decrease slightly over 100-600 years (Poinssot et al., 1996). In Belgium, the temperatures calculated for the present repository concept (Weetjens and Sillen, 2005) are expected to be around 65-75°C for several hundreds (vitrified HLW) to thousands (spent fuels) of years. In this respect, the study of the processes which might alter the physical-chemical properties of the clay barrier within the temperatures of 50--100°C are of the prior importance.

The structure and composition of clay minerals and organic matter are modified by heating. The clay minerals and organic matter are considered to be the most active constituents of the clayey barriers from the radionuclide retardation point of view. The mixed-layer illite-smectite (I-S), illite, kaolinite, chlorite and/or chlorite/vermiculite have been recognized as the major clay mineral phases present in Boom Clay. The alteration of smectite to illite via intermediate mixed-layer I-S as a response to the increasing thermal gradient is the most extensively studied mineral reaction occurring in buried sediments. The sketch below (Figure 4.73) features the most important chemical changes during the illitization.

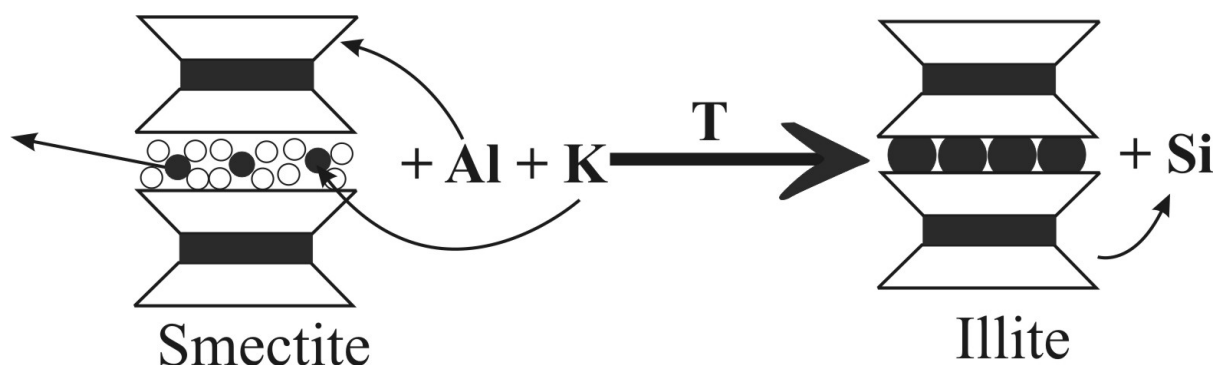


Figure 4.73: The most important chemical changes during the illitization

This reaction has been documented during burial diagenesis (e.g. Perry and Hower, 1970; Velde and Vasseur, 1992; Awwiller, 1993, Sucha et al., 1993), contact metamorphism (Nadeau and Reynolds, 1981; Horton, 1985), or hydrothermal alteration (Inoue et al., 1988; Bouchet et al., 1988 and Inoue et al.; 1992). In the course of the illitization, the illite is formed at the expense of smectite. The illite content typically increases as a function of burial depth/temperature. The onset of the illitization reaction starts at ~50°C and is terminated at 200°C under diagenetic conditions (reference?). Although, smectite illitization is affected by several other parameters (availability of K, porosity, time), the temperature is by far the most important factor controlling the reaction progress. Smectite illitization represents one of the greatest concerns with respect to the long-term stability of the clay barriers as it might influence significantly the chemical and physical evolution of the near field by controlling the water release and overpressure and affects the chemical budget of elements such as Si, Ca, Na and K. Chemical changes in I-S include an increase in K and Al, and a decrease in Si, Fe, Mg, Na, Ca and H₂O (Środoń et al., 1992). The layer collapse and correspondent transformation of expanding clay to non-expanding one is accompanied by the decrease in the sediment porosity, specific area, cation-exchange capacity etc.

During illitization, the K is incorporated in the mineral structure of illite, which makes the K-Ar method a convenient tool for dating duration of the illitization process. The temperature, burial history and the illitization mechanism are the most important factors affecting the K-Ar system in the illite. Notwithstanding some successful studies (e.g. Elliott et al., 1991), the omnipresence of the detrital illite in shales and claystones renders the K-Ar dating of the true duration of the illitization a frustrating problem. The presence of detrital illite gives K-Ar ages systematically higher than the stratigraphic age of the sediment even in the finest technically separable fractions (Clauer et al., 1997).

Nevertheless, the K-Ar dating can be successfully applied to constrain the timing of the illitization in bentonites, which are believed to be detrital-free. The Figure 4.74 (Honty et al., 2004) and Figure 4.75 (Clauer et al., 1997) illustrate two different burial models with corresponding K-Ar apparent ages of the illite fundamental particles separated from bentonites of the same sedimentary basin. The degree of the illitization in the sample from borehole Trhoviste is 18 % and that of Senne borehole 15%. The first model shows the burial model of the sample, which is characterized by slow tectonic subsidence throughout the geological history. The K-Ar dates record the time of the illitization between 10.3 and 2.2 Ma. The second model is typical for the area with the rapid tectonic subsidence followed by very slow or no tectonic subsidence. In this case, the K-Ar dates from bentonites lag behind the onset of the illitization (the time where the burial curve crosses $\sim 50^{\circ}\text{C}$ isotherm). The K-Ar apparent ages indicate $\sim 10\text{Ma}$ as the beginning and $\sim 8\text{ Ma}$ as the end of the illitization process. However, the theoretical illitization spreads over broader time interval. These examples demonstrate the effect of the burial history on the resultant K-Ar record of the illitization. It is evident from the abovementioned examples that the burial-induced illitization is a slow process lasting over several 10^6 of years. Also, there exist studies documenting the hydrothermally induced illitization with K-Ar data being the same within the analytical uncertainty tracing a single rapid crystallization event (e.g. Clauer et al., 1997, Honty, unpublished data on Lesne borehole in the East Slovak Basin). In such case, the K-Ar data of varied size fractions of the single sample plot on the $^{40}\text{K}/^{36}\text{Ar}$ vs. $^{40}\text{Ar}/^{36}\text{Ar}$ isochrone. The Lesne sample is completely illitized despite the fact that it was never deeply buried (max. depth of 1046 m). Important to mention is that in these cases the temperature must have been high enough to reset a K-Ar clock in the illite, i.e. at least 250°C , which is a minimal temperature for Ar retention in the illite-like minerals (Odin and Bonhomme, 1982). Besides temperature, the increased fluid/rock ratio probably also played an important role in the hydrothermally induced illitization. Due to the analytical uncertainty of the method, the estimated time frame of the non-diagenetic illitization can be several tens or hundreds of 10^3 years.

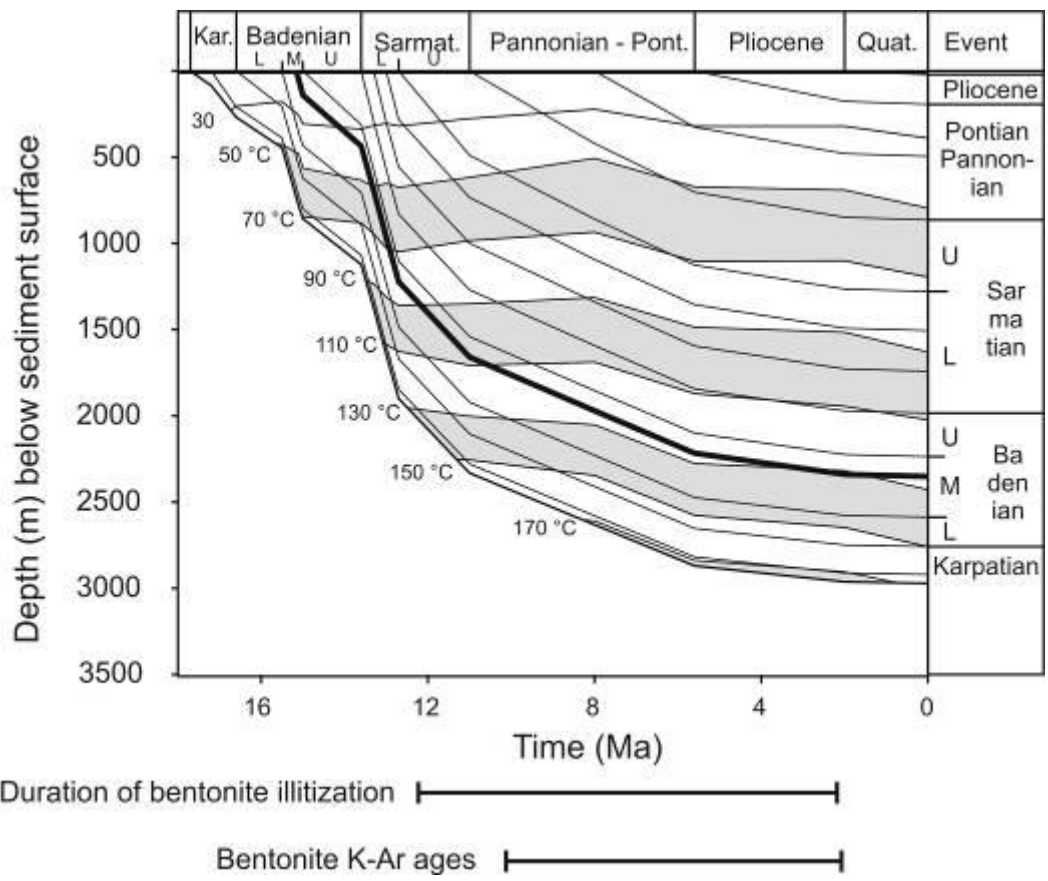


Figure 4.74 : Time-temperature burial history model of the borehole Senne (the East Slovak Basin)

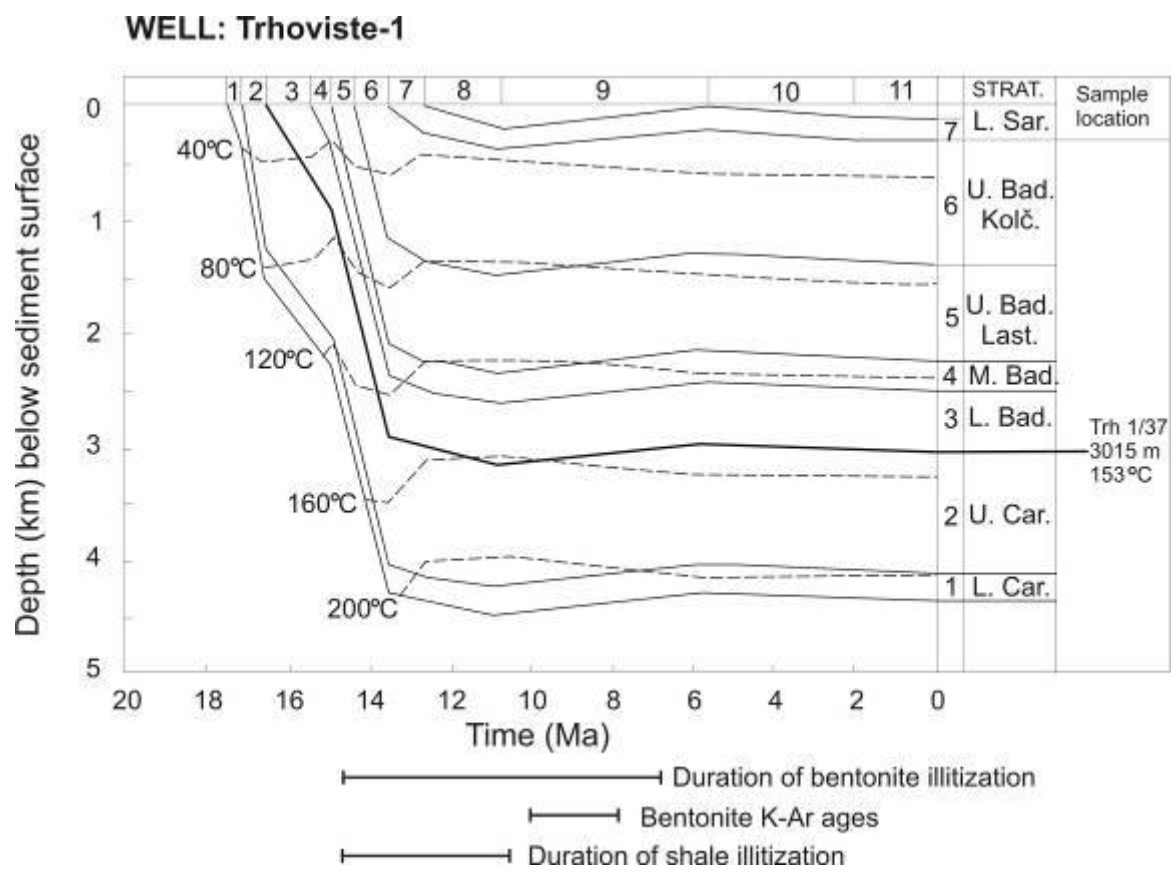


Figure 4.75: Time-temperature burial history model of the borehole Trhoviste-1 (the East Slovak Basin).

The reaction mechanism of the smectite-to-illite conversion might also play an important role in assessing the reaction kinetics in terms of the long-term chemical and physical stability of the clay host formation. The abrupt increase in temperature, naturally observed as a result of hydrothermal or contact metamorphic events, usually leads to the dissolution-recrystallization mechanism, followed by the sudden chemical changes in the system. On the other hand, the gradual increase in temperature typical for burial diagenesis would favour solid-state (layer-by-layer) transformation and related gradual changes in chemistry (see e.g. Altaner and Ylagan, 1997). Also, the fluid/rock ratio and permeability seem to greatly influence the reaction mechanism of smectite illitization. Clays and shales considered as a potential host rocks for disposal of HLW have relatively low permeability and low water content. From this viewpoint, the gradual chemical changes and solid-state transformation should be determining if any changes occur during the thermal phase of the repository. However, it should be noted that Boom Clay has relatively high water content (~20 wt%), therefore some deviations from abovementioned rules can be observed.

In situ and laboratory experiments have also been performed to simulate the impacts of thermal gradients on argillaceous materials and related chemical aspects (Bouchet et al., 1992; Pusch et al., 1993; Noynaert et al., 2000; Kolaříková et al., 2005). Moreover, the natural analogue studies of argillaceous formations that were subject to thermal impact (e.g. due to a magmatic intrusion) give a good opportunity to evaluate the short-term thermal behaviour of clays (Chapman, 1994; Techer et al., 2001; Techer et al., 2006).

Techer et al. (2006) used the Toarcian shale of the Perthus pass (France) penetrated by the basaltic dike as a natural analogue for the study of the behaviour of argillaceous material in a deep storage for high-level long-lived nuclear waste. These shales were subjected to temperatures close to those expected in the near field of the waste packages. The estimated temperatures based on the ^{40}Ar loss from clay fraction were 260-300°C on the basalt/shale contact and $50 \pm 10^\circ\text{C}$ 2 m away from the dike. **The data suggest that the mineral composition of the shales was not significantly disturbed at temperatures below 100-150°C.** Closer to the dike at 150-300°C, changes such as progressive dissolution of chlorite and kaolinite, increased content of the mixed-layers illite-smectite with more illite layers, complete decalcification and subsequent increased content of quartz, were found. Based on the K-Ar data combined with vitrinite reflectance (R₀) measurements it was estimated that the temperature increase lasted over a few hundreds of years. This time span is relevant compared to a typical time duration of the heat phase in the repository. From a chemical point of view, the changes were especially evident in the decreasing Ca and Sr contents and the increasing Rb and K contents. These variations are directly linked to mineral changes with a decreasing content in the carbonates (even disappearing at the dike contact) and an increasing content of I-S with increasing illite component. Also, the development of shrinkage cracks appeared in the so-called thermally-disturbed zone at a temperature of about 250°C accompanied by thermally-induced recrystallization effects. These structural discontinuities might become pathways for preferential fluid circulation.

The mineralogy and kinetics of alteration of a mixed-layer kaolinite-smectite was studied in-situ at Stripa site in Sweden by Bouchet et al. (1992). The FoCa (dominated by the mixed-layer kaolinite/smectite) clay cylindrical core was placed in granite and heated along its central axis at 175°C for 4 years. In the direct contact, a hardened black coating was formed. The original mixed-layer kaolinite/smectite was replaced by pure smectitic material. The kaolinite, quartz and calcite disappeared while anhydrite and gypsum crystallized. In the less altered regions of the core, both the original minerals and the reaction products were found. The concentration of free kaolinite decreased only above 130°C and went to zero at around 180°C while the variation of the K/S became detectable above 100°C. **The transformations occurring between 100 and 130°C remained limited**, then became greater when the kaolinite started to disappear. However, the oxidation must have also taken place because of the corroded heater at the end of the experiment.

Another in-situ heater test has been performed in HADES URL within the framework of the CERBERUS project (Noynaert et al., 2000). The CERBERUS (Control Experiment with Radiation of the Belgian Repository for Underground Storage) was aimed to simulate the combined effects of heat and radiation on the near field of a HLW repository. For this purpose, a ^{60}Co -source was installed with the activity of 397 TBq and 6 heating elements with a nominal power of 500W each. The effect of heat on the pore-water chemistry was followed in the near field of CERBERUS test with the aid of the piezometers. The Boom Clay samples selected for the mineralogical characterization were either irradiated and heated (100-120°C/0.1-11MGy) or just heated (50-120°C/0MGy). The results of the pore water chemistry study showed that after a short period of oxidation (reflected in the increase of sulphates and pH drop), the chemical parameters of the pore water chemistry have been reestablished. Fluids remained Na-HCO₃ type, with a pH close to the neutrality, and a reducing redox potential (-280 mV). The oxidation might have been caused by the water gamma radiolysis and/or due to the installation of the experiment. The redox conditions were found to be controlled by the mineral assemblage pyrite-siderite-goethite at high temperature as well as at low temperature. Important to note was the enrichment in CO₂ and oxalate in the pore water during the experiment. The enrichment in CO₂ could be the result of the dissolution of the carbonates and/or the decomposition of the organic matter. The presence of oxalate was most likely the result of the thermal degradation of the organic matter. **The heating/irradiating of the Boom Clay samples for 5 years did not induce any significant changes in either clay or non-clay mineralogy.** The differences observed between the samples at the end of the experiment are more related to the heterogeneity of the Boom Clay rather than to the experimental conditions itself.

The Boom Clay contains a substantial amount (average value around 3 wt %) of organic matter. From this organic matter, over 90% corresponds to a complex insoluble macromolecular organic fraction, termed kerogen. The study on the thermal stability of the kerogen isolated from Boom Clay was performed by Deniau et al. (2005a) and Deniau et al. (2005b). It was documented that kerogen can already undergo a significant degradation under mild to moderate thermal stresses. This degradation mainly releases heteroatomic polar compounds, especially oxygen-containing ones, due to the relatively low stability of chemical bonds with heteroatoms. By mild thermal stresses, one understands here the temperature/time couples typically relevant for the present repository design (80°C for decades or hundreds of years dependent on the type of waste). The most important results of the study of the kerogen subjected to mild/moderate thermal loads may be summarized as follows:

- (1) CO₂ is by far the most abundant gas generated under the various sets of temperature/time conditions
- (2) important amounts of “early” CO₂ (up to cca 50 mg/g of kerogen, representing about 1/5 of the total oxygen content of the kerogen) can be generated under mild thermal stress. A part of this “early” CO₂ corresponds to a “flash” production, representing 8-9 mg of CO₂/g of kerogen, taking place under very mild thermal stress.
- (3) a kinetic model predicts that (i) CO₂ would start to be formed in the near field of the waste 1 year after disposal (ii) CO₂ generation near the limits of the formation would become significant only after 100 years (iii) most of the CO₂ would be produced within the same period of time.
- (4) a variety of soluble oxygen-containing compounds dominated by monocarboxylic acids are also generated under mild thermal stresses. The quantity of the released monocarboxylic acids is negligible compared to total CO₂ production. However, this value (30 mg/kg clay) is important if compared to the organic acids naturally present in the Boom Clay pore water (30 mg/kg).

All together, these observations indicate that the release of oxygen-containing compounds from Boom Clay, especially CO₂ and carboxylic acids may significantly disturb the geochemistry in the near field of the radioactive waste due to the acido-basic, redox and complexing reactions. This physico-chemical disturbance of the clay-water system may result from the changes in pCO₂ in acidification of the pore water, in dissolution of carbonate minerals, in cation exchange, in

modification of pore water ionic strength, in changes of clay surface properties, and finally in radionuclide complexation.

The radiation is known to induce the structural defects in clay minerals, which are accompanied by the changes in cation exchange capacity, specific surface area, sorption capacity, mineral solubility etc. The effect of various doses of γ -irradiation (10^5 , 10^6 , 10^7 , 3×10^7 Gy) on types and concentration of radiation-induced defects, deuteration, changes in specific surface and solubility of clay minerals irradiated in D_2O solution was studied by Pushkareva et al. (2002). The concentration of radiation-induced defects in tetrahedrons (Si-O \cdot) and octahedrons (Al^{VI}-O—Al^{VI} bonds) was examined after irradiation in kaolinites, montmorillonite (dioctahedral Mg-smectite), palygorskite and muscovite by Electron Spin Resonance (ESR). The deuteration degree resulting from interaction of deuterium water with clay minerals was determined by IR-spectroscopy, the specific surface was measured by the standard methods. The solubility of initial and irradiated samples was determined by the mineral component contents (SiO₂ and Al₂O₃) in the distilled water. The most important finding of this study is that the accumulation of the radiation-induced defects is a function of the Al-Si substitution degree in the tetrahedral sheets. In silicate minerals, in which the tetrahedral structural cell is [Si₄O₁₀] tetrahedron (e.g. kaolinites), the Si-O \cdot defects are easily formed. In aluminosilicates, in which the Al/Si ratio in the tetrahedral position is $\sim 1:3$ (AlSi₃O₁₀ – e.g. muscovite), only slight dependence was observed between the intensity of radiation dose and the number of radiation-induced defects. Montmorillonite takes up an intermediate position between silicates and aluminosilicates regarding the substitution in the tetrahedral cell ($\sim Al_{0.5}Si_{3.5}O_{10}$). Accordingly, the formation of radiation-induced defects was intermediate between kaolinite and muscovite, respectively. Besides the structural chemistry, the formation of defects is considerably influenced by the presence of mobile water molecules on the surface and in the interlayer space of minerals. In general, the higher the water content, the less structural defects were formed.

The increase of the irradiation dose and, accordingly, the amount of the defects in the irradiated samples of clay minerals leads to the increase of their specific surface and change of solubility. The maximal irradiation dose applied to perfectly-ordered kaolinite results in the increase of the outgoing Al³⁺ from structure by 1.44 times, but one of Si⁴⁺ ions decreases by 1.5-2 times in comparison with an initial sample. An opposite situation has been observed in the case of montmorillonite – irradiation resulted in the decrease of outgoing Al³⁺ (11%) and increase of outgoing Si⁴⁺ ions (38%).

The increase of the irradiation dose from 0 to 3×10^7 Gy is followed by the specific surface increase: in kaolinite – 9%, in montmorillonite – 8% (sorption capacity growth 15%).

Important to note is that due to the current supercontainer design in Belgium, the radiation effects on the mineral stability of the Boom Clay can be neglected. The radiation from supercontainer is very low corresponding to the dose of 25 μ Sv/h. The radiation on the contact with the host rock will be further decreased by the backfill and the concrete lining.

4.7 Discussion

Uncertainties

The review on the past works (laboratory and in situ tests as well as models development) related to the THM behaviour of natural Boom Clay allowed to identify the main uncertainties on the THM behaviour (parameters) of the Boom clay. The important issues for the future research in terms of the THM behaviour as well as the constitutive study are equally identified.

Laboratory tests

The analysis of the existing laboratory tests pointed out the following **general** aspects that imply the uncertainties on the past test results and consequently on the parameters derived:

- The samples for the tests present a strong **inhomogeneity**, the origin of this inhomogeneity is unclear. Very little of sensitivity analysis to study its influence on the THM behaviour of Boom clay was performed.
- The **initial state** of the tested samples: The on-going study by CERMES in the frame of PhD thesis on the thermal mechanical behavior of natural Boom clay reveals that the tested samples present an **initial matrix suction** induced by the decompression of the massif followed by the gallery excavation (for bloc samples) or sampling procedure. Additional matrix suction can exist due to some water loss during the long-term storage of the samples. Consideration or not of this initial suction in the tested samples during the tests has certainly multi-influence on the test results. A proper test protocol needs to be defined in order to account for the impact of this initial suction of samples. Moreover, the **ageing** of tested samples influences equally the test results.
- The test **procedures**, test **boundary conditions** : the obtained test results present large **dispersion**. There exists consequently certain uncertainties on the test results which in turn induce the uncertainties on the behaviour observed and parameters obtained. Indeed, recent laboratory researches reveals that the test procedures, test boundary conditions, etc. have important influences on the test results. There is indeed lack of a **consistent, systematic** test program on natural Boom clay.
- **Anisotropy**: the anisotropy of the Boom clay were revealed in several projects through different aspects. But, there are not yet enough investigation allowing evaluating this aspect quantitatively.

Modelling

During the excavation of the connecting gallery of the URF HADES, hydraulic pressure variation and displacements were measured far from the excavation front that are not predicted by classical elastic – perfectly plastic models using the "average parameters" of Boom clay. Moreover, modellings show equally the variation of pore pressures in the near field were generally underestimated. The uncertainties existed thus in the models for accounting for the HM coupling process. The fractures development under shear loading; the damage and/or plastification processes due to high decompression of the massif; the HM coupling parameters (damage and/or volumetric plastic deformation induced hydraulic conductivity increasing, for example); the mechanical behaviour in small strain (Young's modulus) and associated coupling effect on the hydraulic aspect (for example, pore pressure variation in the far field); transition of elasto-plastic behaviour, effect of the viscosity; suction effects; as well as the anisotropy properties of the massif (Young's Modulus for example), etc. need to be investigated and accounted for in the model. Finally, the uncertainty on the initial stress state around the gallery (K_0 value) may have consequence on the modelling results.

Modellings of ATLAS in situ heater tests showed that there exists uncertainty on the thermal conductivity of Boom clay, values ranged from 1.35 to 1.7 w/m.°C were evoked, moreover, its nonlinearity with temperature and/or saturation, its anisotropy are not clear yet. The new test ATLAS III and future large scale Praclay heater test will provide more precision on these aspects.

Issues to be further studied

Concretely, following aspects of the Boom clay need to be reviewed:

THM characteristic :

- Thermal conductivity as well as its anisotropy
- Young's modulus value at low strain as well as its anisotropy
- Swelling pressure;
- Air entry value of Boom clay

THM coupling process :

- variation in hydraulic conductivity with temperature: recent limited tests performed by CIMNE on Boom clay revealed that the permeability increases significantly with the temperature under the prescribed test conditions (more than 5 times). This increase can't be explained only by the viscosity variation effect. The modification of the microstructure may play a role. Delage et al (2000) have however identified a single relationship between the intrinsic permeability and the porosity considering the temperature effect on the water viscosity and concluded that the temperature effect on the permeability is linked to the variation of the viscosity. More tests are required to detect the effect of temperature on water permeability.
- Variation of the thermal conductivity with temperature as well as the saturation.
- Modification of the stiffness (Young's modulus) and strength (internal friction angle and cohesion) induced by temperature
- Temperature effects on the evolution of EDZ as well as on the sealing/healing process of EDZ.
- Possibility and pattern of the additional damage/failure induced by temperature : more laboratory tests under well controlled boundary conditions.
- Creep rates (viscosity related parameters) as well as its/their dependence on the temperature
- Suction related THM behaviour: there are a number of laboratory results concerning thermal effects on saturated natural Boom clay under drained condition. In contrast, experimental information concerning thermal effects on unsaturated Boom clay is very limited. There is a need, therefore, to examine more systematically the combined effects of temperature and partial saturation on the hydro-mechanical behaviour of natural Boom clay under controlled conditions. Basic questions concerning its sensitivity to thermal impact under quasi-undrained conditions, its thermal sensitivity to the enhancement of creep and anisotropy effects, remain largely unanswered.

All these aspects constitute main objective of the present project TIMODAZ. Specific laboratory tests will be performed. In particular, the effects of the temperature on damaged clay as well as on the clay properties will be investigated. Special attention will be given to study the possibility of the creation of an irreversible damage. The tests include the study of the desaturation/resaturation processes on ambient and at different temperatures. These laboratory tests will provide the necessary data for the numerical models to be used in TIMODAZ.

Delineate the most important temperature-dependent material properties

The following temperature-dependent material properties are considered to be important:

- Temperature induced variation in hydraulic conductivity
- Temperature induced variation in thermal conductivity

- Temperature induced stiffness and strength modification
- Temperature dependence of creep rates.
- Thermal sensibility on anisotropy

Define the most important coupled processes and parameters

The strongly hydromechanical coupling process has been put in evidence during the excavation of the connecting gallery and by the long term in situ measurements : evolution of the total stress on the liner, pore pressure variation around gallery and convergences of the test drift. The dependence of permeability on the irreversible deformation is an important parameter for the short term HM coupling behaviour. However, recent research realised by Ulg on the viscosity of Boom clay highlighted that the long term coupling behaviour deals with the superposition of at least two mechanisms: creep and consolidation, which are difficult to differentiate. An important issue is to perform test with very low loading rate and creep tests in very long term (Coll, et al. 2007, in preparation).

The heat transport is mainly by conduction due to its extremely low hydraulic conductivity. The coupling effects of HM process to heat transport can be considered very weak. Conversely, the thermal conditions influence strongly the hydro-mechanical process.

The most important parameters are the relative importance of the characteristic time of mechanical process, of fluid diffusion process and thermal diffusion process.

The new laboratory tests and in-situ tests performed within the TIMODAZ project will allow to increase the knowledge on these processes and parameters.

Asses the effect of discrete fractures and fracture connectivity on the effective hydraulic properties

The majority of in-situ measurements of hydraulic conductivity of Boom Clay around HADES URF were made beyond the extent of excavation induced fractures, being about 1 m radially. However, the available results inside the fractured zone only show a limited increase of hydraulic conductivity of about one order of magnitude (Bastiaens et al., 2007). Furthermore, in-situ measurements around the HADES URF indicate that no interconnected fracture network is present beyond (at most) some decimetres into the clay host rock.

These results were confirmed by laboratory experiments, in which the hydraulic conductivity of (artificially) fractured Boom clay samples was measured (Bernier et al. 2007). For all the Boom Clay samples tested, the measured hydraulic conductivity was comparable (within the same order of magnitude) to undisturbed clay. The sealing process was visualised by μ CT imaging (Figure 4.76).

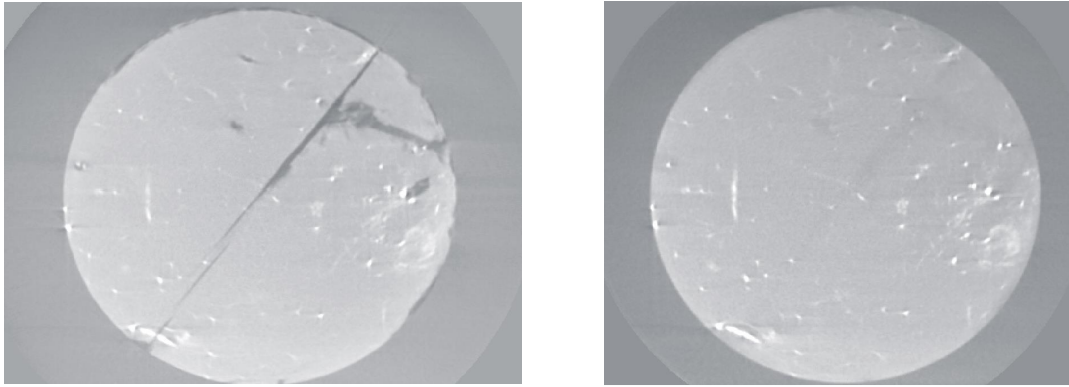


Figure 4.76: μ CT images of a (artificially) fractured Boom Clay sample before (left) and after (right) measurement of hydraulic conductivity. The sealing process is visualised.

In conclusion, the influence of excavation induced fractures in Boom Clay on hydraulic conductivity is limited due to sealing phenomena. These phenomena were evidenced in previous laboratory tests as well as in in-situ experiments.

The influence of the thermal impact on sealing will be studied within TIMODAZ.

Importance of chemical impact

Based on the literature review, the temperature increase in the range as expected in the near field of the PRACLAY gallery should not have a significant impact on the geochemical stability of the Boom Clay. However, the significance of the heat may become important if coupled with geochemical perturbations, e.g. the oxidation and the alkaline plume. The oxidation and alkaline plume perturbations will take place in the near field of the PRACLAY gallery and, if coupled with the increased temperature, may trigger the irreversible changes in the host rock properties. These changes might have both the positive and negative effects on the selfsealing and radionuclide retention.

The oxidation of the pyrite will produce sulfates and thiosulfates. The released protons (H^+) will decrease the pH. The pH drop will be buffered to certain extent by carbonates, which are naturally present in the Boom Clay. Other processes involve the ion-exchange reactions and protonation of the clay mineral surfaces. As a result, the negatively charged clay minerals may become positively charged; they will lose the potential to sorb positively charged radionuclides, but can effectively sorb anions (e.g. I^- , IO_3^- , TcO_4^-). Also, the Fe oxihydroxides are formed as a product of pyrite oxidation and they are known to have a large potential to sorb radionuclides. Little is known about the oxidation of the organic matter present in the Boom Clay, but the effects can be similar to those observed under mild thermal stresses – i.e. the production of CO_2 . Since CO_2 tends to increase the pore water pressure, its production will probably have a negative impact on the sealing of the voids.

Most of the expected alteration processes taking place in an alkaline plume disturbed zone of Boom Clay are expected to be in favor of self-sealing capacity of the clay. Cement- clay interactions in general tend to decrease the porosity of clay thus will enhance the consolidation of the temperature-induced openings. However the changes in the mechanical properties from plastic to more brittle behaviour can be expected in the area of the recrystallization. The Young Cement Water (YCW) has a great potential to dissolve the kerogen present in the Boom Clay. The release of the dissolved organic species will boost the complexation reactions, but their effect on the hydro-mechanical properties of the Boom Clay is so far unknown. The role of Boom Clay natural organics in a general term is difficult to assess because they also play a positive role by coating the surfaces of clay minerals hence protecting them from dissolution.

Carbonates, CSH and zeolite phases as a main product of the alkaline plume and sulfates as an oxidation product are less soluble at elevated temperatures, so these mineral phases might decrease the porosity and enhance the self sealing.

The potential threat resulting from the alkaline plume could be the dissolution and/or illitization of smectite at high pH, mainly in the presence of the Young Cement Water (YCW). The illitization is the process of the irreversible K-fixation in the interlayer space of smectite. This mineralogical alteration is accompanied by the loss of swelling potential, the decrease in the total surface area, decrease in the cation-exchange capacity and increased permeability. The illite formation might alter the sorption properties and the selfsealing capacity of the Boom Clay.. A positive effect might be expected in case of the Evolved Cement Water (ECW) where the newly formed precipitates contribute to the sealing of the pores.

In TIMODAZ project, some laboratory tests dealing with sealing/healing process will be complemented with a radionuclide migration test, in order to evaluate any possible relict of preferential migration along the sealed fracture. Different chemical conditions will be considered: chemical undisturbed, oxidised and alkaline environment. Mineralogical analyses will be performed and linked to the hydromechanical observations.

Derive the most appropriate conceptual models and evaluate the most appropriate numerical code

Based on the discussion above, it's thought that the following developments should be strengthen in the future:

- The damage and/or plastification processes: the mechanical behaviour at low strain (Young's modulus), transition of the elastoplastic deformation, degradation of the mechanical properties (Young's modulus, cohesion, etc.) with viscoplastic (irreversible) deformation, etc.
- The fractures development under shear loading;
- The HM coupling parameters (damage and/or volumetric viscoplastic deformation induced hydraulic conductivity increasing, for example);
- effect of the viscosity as well as its dependence on temperature
- suction effects;
- thermal-mechanical behaviour : Sultan's model needs more tests for validation and calibration.

The new lab tests to be performed in the TIMODAZ project, the short term and long term measurements around HADES, the new in situ test (ATLAS III) should provide a good data base allowing establishing an appropriate concept model.

The modelling work together with the results of the lab and the in-situ tests should allow to validate the numerical code to be used.

5 State of the art for the Opalinus clay

5.1 Main characteristics

Geological setting

The Opalinus Clay was deposited some 180 million years ago by the sedimentation of fine clay, quartz and carbonate particles in a shallow marine environment. It is part of a thick sequence of Mesozoic and Tertiary sediments in the Molasse Basin (Table 5.1, Table 5.2 and Figure 5.1), which overly Palaeozoic sediments and crystalline basement rocks. The overlying Tertiary sediments thicken considerably towards the Alpine Front. The Mesozoic sediments containing the Opalinus Clay are of uniform thickness over several kilometres, almost flat-lying (dipping gently to the south east) below the Molasse Basin and in NE Switzerland and little affected by faulting. Miocene Deformation has affected this sedimentary pile in the Jura Mountains that form an arc shaped foreland fold-and-thrust belt around the Molasse basin to the south.

Table 5.1: Hydrogeological classification of the stratigraphic units in the Mont Terri region (Thury & Bossart 1999). Hydrogeological conditions during construction of the motorway tunnel between 1989 and 1999

Stratigraphy	Hydrogeological classification
Limestones of the Upper Malm (Oxfordian / Kimmeridgian / Thionian)	Regional aquifer (karstified): fissured and karstic limestones; inflow rates > 1 l/s
Malm Marls (Lower Oxfordian / Callovian)	Aquitard: (shaly) marls, limestones, marly clay; impermeable
"Lower Dogger" (Lower Aalean / Lower Bajocian)	Local aquifer (karstified): sandy limestones, fissured and karstic; inflow rates 12 – 200 l/s
Opalinus Clay (Lower Aalenian)	Aquitard: silty and sandy shales; impermeable
Jurensis Marls and Posidonia Shales (Upper Toarcian)	Hydrogeological unit with localised water circulation (weakly karstified): Marls and limestones; spontaneous water inflows into the tunnel of 1 – 5 l/s
Triassic marls / anhydrite / dolomites / limestones	Aquitard: Marls, anhydrite, dolomites, limestones; partly fissured and karstic; tight rock with localised inflow rates << 1 l/min

Table 5.2: Definition of principal stratigraphic components overlying and underlying the Opalinus Clay host rock in NE Switzerland (Nagra, 2002c)

System component	Stratigraphy	Barrier function
Malm aquifer (Regional aquifer)	Malm limestones, Plattenkalke to Hornbuck beds	No barrier function, but dilution
Upper confining unit	Effingen beds to Wedelsandstein Formation Sequence of low permeability beds with intercalations of potentially water-conducting units of limited inter-connectedness	Upper supplementary geological barrier
Host rock	Opalinus Clay and Murchisonae beds in Opalinus Clay facies Sequence of low permeability beds	Primary geological barrier
Lower confining unit	Lias to Keuper Sequence of low permeability beds partly with minor aquifers of limited interconnectedness	Lower supplementary geological barrier
Muschelkalk aquifer (Regional aquifer)	Upper Muschelkalk (including dolomite of anhydrite group)	No barrier function, but dilution

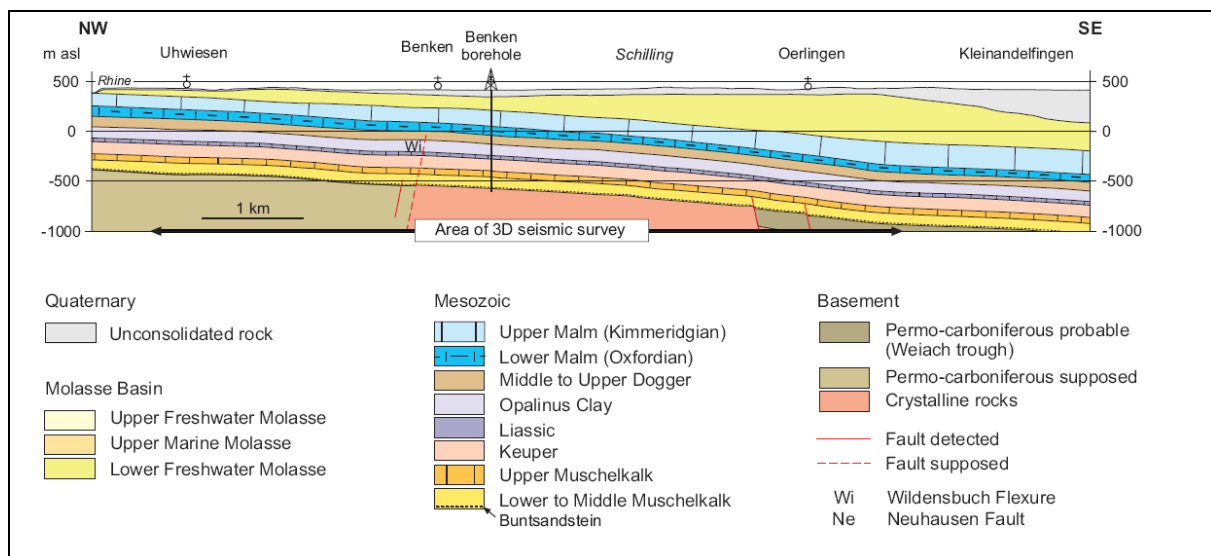


Figure 5.1: Schematic geological profiles from NW to SE through the sedimentary rocks of NE Switzerland (Nagra, 2002c)

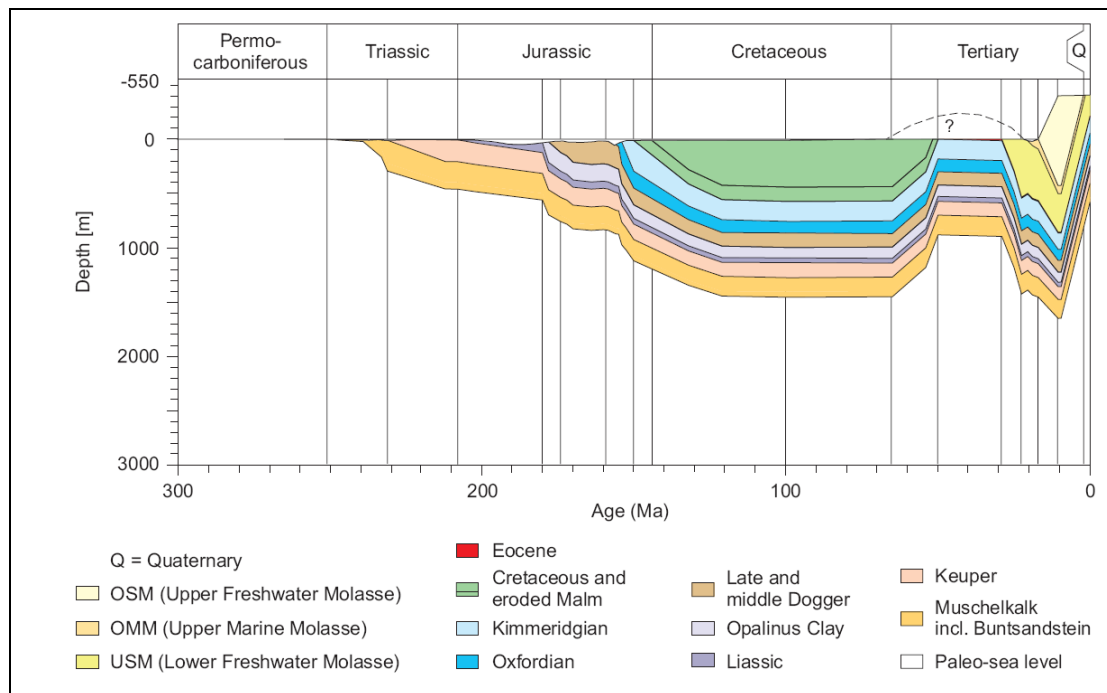


Figure 5.2: Burial history of the sedimentary formations in NE Switzerland (Nagra, 2002c)

The burial and compaction history of the sedimentary formations in NE Switzerland is shown in Figure 5.2. It can be seen that the Opalinus Clay reached a burial depth of about 1000 m during the Cretaceous, between about 65 and 120 million years ago.

Northern Switzerland was affected by the rifting of the Rhine Graben (starting about 40 million years ago) and by differential vertical movements that resulted in considerable uplift of the area in the mid-Tertiary, followed by down-warping and burial under late Tertiary sediments (Nagra, 2002c). This resulted in the Opalinus Clay reaching its greatest burial depth, of about 1700 m below the surface, in the Miocene stage of the Alpine orogeny, the last major tectonic event to affect the region. From about 10 million years ago, Alpine uplift and erosion brought the Opalinus Clay progressively up to its present burial depth of about 600 to 700 m in the region of interest. The most recent stage of the orogeny involved the thrusting and folding of the Jura Mountains, which, along with the uplift of the Alps and the updoming of the Black Forest massif, continues today. The present temperature of the Opalinus Clay at 650 m at Benken drillsite is 38 °C; during its burial and compaction history it has experienced maximum temperatures of about 85 °C.

Mineralogy and porewater chemistry of the Opalinus Clay

The average mineralogical composition of the host rock is presented in Table 5.3. The presence of pyrite and siderite, which show no signs of oxidation, indicate the reducing nature and the high redox-buffering capacity of the Opalinus Clay. The mineralogy in shear zones does not differ from that of the rock matrix (Nagra, 2002c).

Table 5.3: Average mineralogy of the Opalinus Clay (Nagra 2002c)

Mineral	wt % (average)	Standard deviation (1σ)wt%
Illite	18	6
Kaolinite	17	6
Illite/smectite mixed layer	14	4
Chlorite	5	2
Quartz	20	5

Calcite	16	10
Dolomite/ankerite	1	0.4
Siderite	4	2.4
Feldspar	3	1.3
Pyrite	1.1	1
Organic carbon	0.6	0.3

Due to its marine origin, the porewater of the Opalinus Clay is relatively saline and sodiumchloride dominated. Based on investigations on cores from Benken, extensive studies at Mont Terri and geochemical modelling, Pearson (2002) derived the so-called reference porewater chemistry for Opalinus Clay (see also Nagra, 2002c). This composition is given in Table 5.4 and it corresponds to the most probable water composition based on current understanding. The pH conditions are expected to be near-neutral but the uncertainties are rather large mainly because the partial pressure of CO₂ cannot presently be precisely constrained. Bounding pH values of 6.9 to 8.2 have been proposed (Pearson, 2002). Redox conditions are reducing as evidenced by the large amounts of unoxidised pyrite and siderite. From mineralogical observations, Eh measurements performed at Mont Terri and geochemical modelling, redox potentials of about -170 mV (SHE) for the reference water and bounding values of about -140 to -240 mV were derived. The derivation is based on the assumption of thermodynamic equilibrium between pyrite, sulphate and siderite.

Table 5.4: Reference water chemistry of the Opalinus Clay at the Benken site (Pearson, 2002)

pH	7.24
Eh [V]	-0.167
temperature [°C]*	25.0
log pCO ₂	-2.2
concentrations [mol l ⁻¹]	
CO ₃ (tot)	2.70 × 10 ⁻³
Na	1.69 × 10 ⁻¹
K	5.65 × 10 ⁻³
Mg	7.48 × 10 ⁻³
Ca	1.05 × 10 ⁻²
Sr	3.04 × 10 ⁻⁴
S(VI)	2.40 × 10 ⁻²
S(-II)	1.41 × 10 ⁻¹¹
F	1.67 × 10 ⁻⁴
Cl	1.60 × 10 ⁻¹
Br	2.40 × 10 ⁻⁴
Fe (II)	4.33 × 10 ⁻⁵
Mn	2.42 × 10 ⁻⁵
Si	1.78 × 10 ⁻⁴

* The temperature refers to the model water composition of Pearson (2002); the actual temperature of the formation at 650 m at Benken is 38 °C

5.2 THM characterization in lab

The current knowledge on the THM properties of the Opalinus Clay relies on data from two different sites in Switzerland. The Benken drillhole in NE Switzerland (Zürcher Weinland) has given access to the Opalinus Clay where the rock has experienced deeper burial and higher temperatures. This has led to relatively lower water contents and a slightly higher density than at the second sampling site, the Mont Terri URL in NW Switzerland. In addition at the Benken Site the sandy facies dominates while the Mont Terri URL is mostly within the clay rich facies. Laboratory and in-situ testing in the frame of TIMODAZ will be done with the Mont Terri variant of the Opalinus Clay. Hence, in the following, we focus this report on the properties of the Mont Terri material.

5.2.1 Mechanical properties

The influence of temperature on the short term behaviour becomes visible in relatively rapid triaxial shear experiments. These have been performed by the BGR in a true-triaxial and conventional triaxial tests (Schnier, 2005; Göbel *et al.*, 2006) and by the GRS in conventional triaxial experiments (Zhang *et al.*, in prep.). The latter experiments show a significant decrease of the failure strength along the bedding planes with increasing temperature (Figure 5.5). Tests parallel to bedding by Schnier (2005) indicate only a very minor decrease in failure strength (Figure 5.4). Finally the true triaxial tests in the frame of the HE experiment (Göbel *et al.*, 2006) may indicate that failure strength normal to bedding and parallel to bedding even increases with temperature (Figure 5.3).

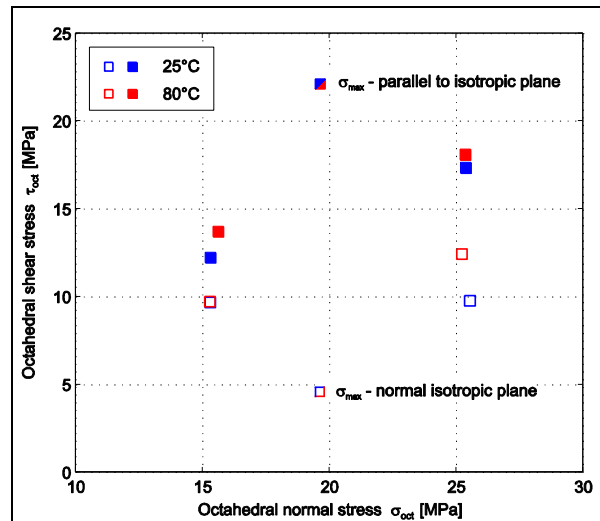


Figure 5.3: Failure strength in true triaxial tests at 25°C and at 80°C (Göbel *et al.*, 2006). Samples are stronger parallel to bedding than normal to bedding and strengthen with increasing temperature

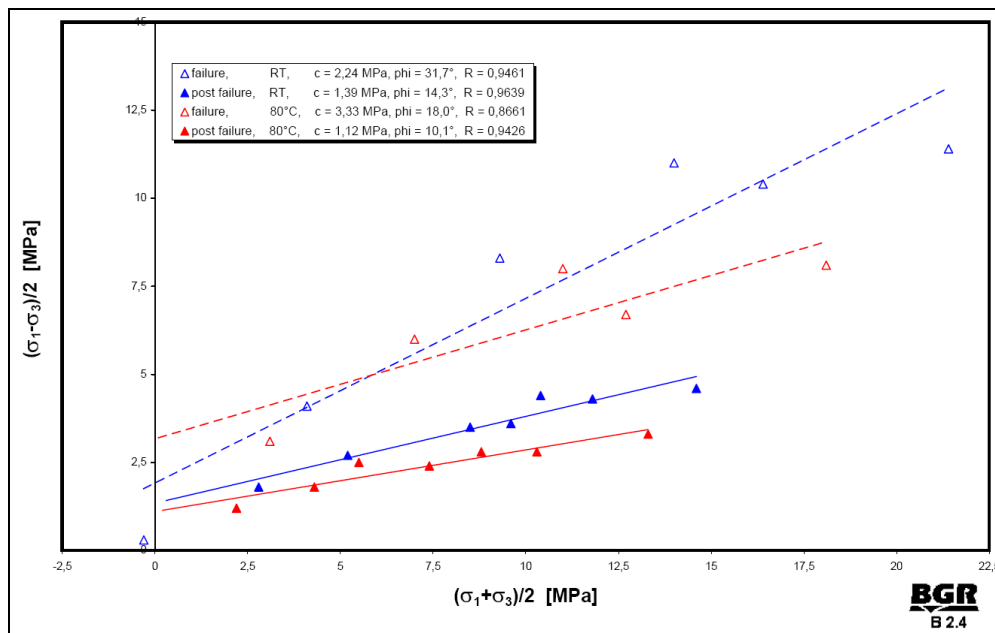


Figure 5.4: Linear fit of strength values in p-q plot for loading parallel to bedding. Fitted coefficients for a linear Mohr Coulomb criterion are given in the legend. Note that the failure strength decrease at 80°C largely depends on the two samples tested at higher confining stresses (Schnier, 2005).

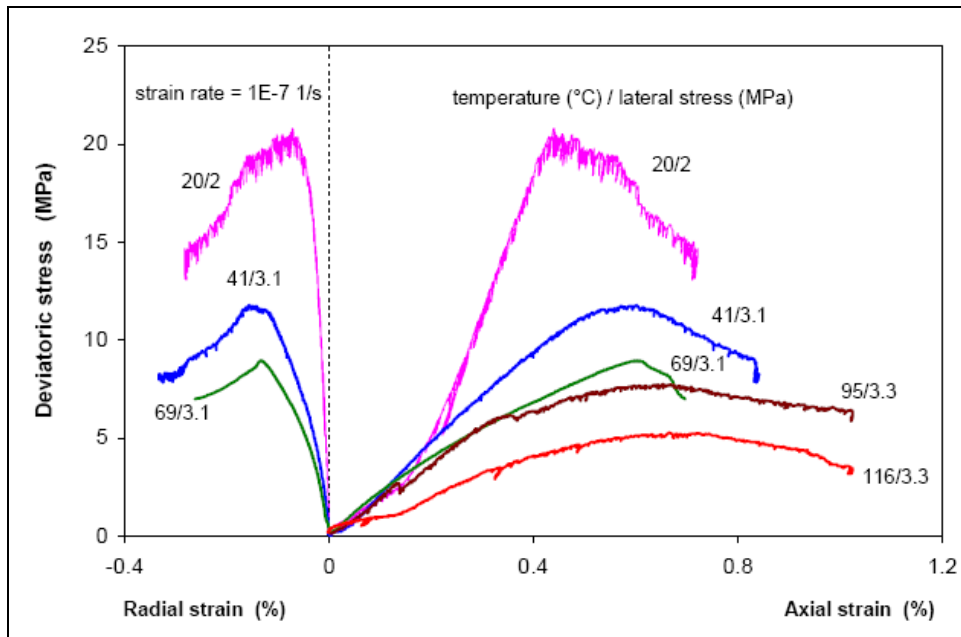


Figure 5.5: Triaxial tests on Opalinus Clay performed at 40° to bedding. Samples were first isotropically loaded, then heated to the desired temperatures and subsequently tested at a constant strain rate of 10⁻⁷/s (Zhang *et al.*, in prep.)

Long term deformation: creep rates

The impact of temperature on the long-term deformation has been studied in a couple of creep tests. These tests highlight the complex nature of the material (Figure 5.6). In the example shown in Figure 5.6 the sample is first loaded with an uniaxial stress of 0.74 MPa at 24 °C and 30 % relative humidity. Upon loading the sample did not contract but expand. Subsequent heating steps (28 °C and 38 °C) each resulted in initial expansion followed by contraction. Surprisingly, creep rates at 38 °C appear to be lower than at 28 °C. When the temperature was decreased and humidity increased to 85% the sample expanded again at half the contraction rate of 38 °C and 30 % relative humidity. Heating to 58 °C re-started contraction and increased loading at the same temperature subsequently also increased the creep rates. However, inspection of the deformation curve shows that it is unsure if stationary creep was reached during the first loading phases (Figure 5.6). Finally the sample was cooled to 23 °C at constant load of 5.6 MPa. The cooling reduced deformation rates to extremely low values.

The complex evolution of deformation rates cannot be explained by conventional temperature activated rock creep mechanisms (crack propagation, dislocation creep) alone. It has been suggested that the free and the adsorbed pore water play a key role in the process. Heating reduces the viscosity of the water and thus increases its mobility in the pores. Drainage of the sample interior and resulting volume reduction thus may be temperature assisted. However, the drainage will ultimately increase the grain contact area and thus increase shear resistance within the rock. Thus the test can be interpreted to indicate that at least at comparatively low stress levels temperature mainly affects the pore water that in turn controls deformation.

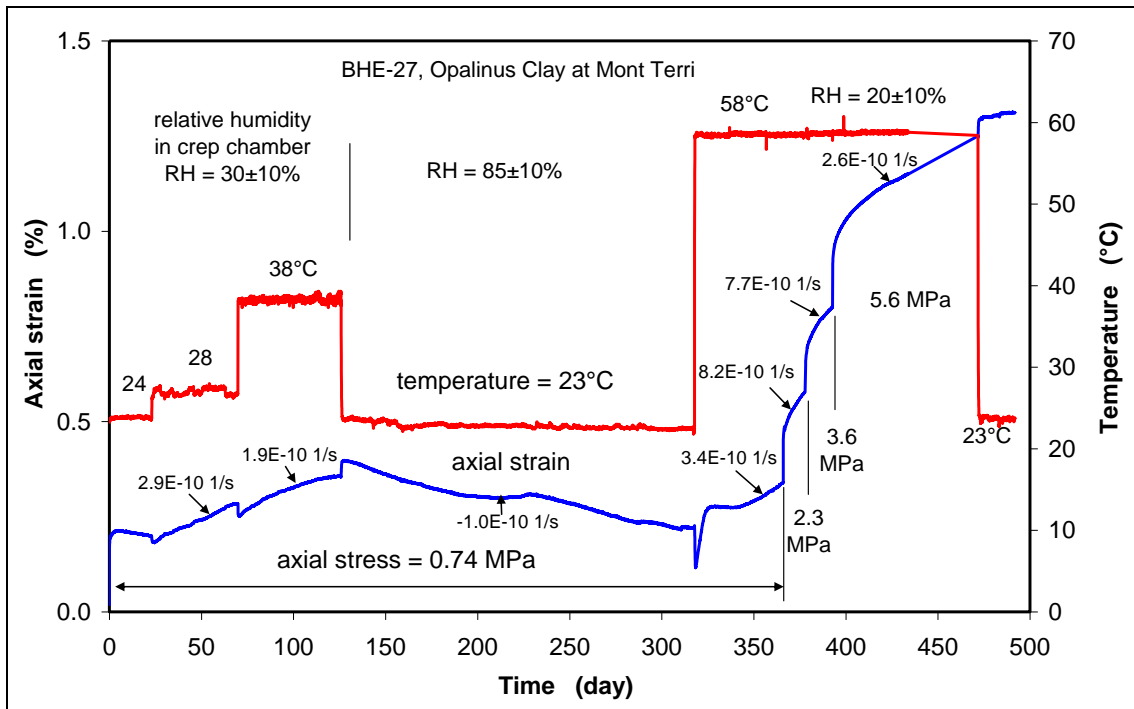


Figure 5.6: Uniaxial creep test on Opalinus clay sample at elevated temperatures and different loads (Zhang *et al.*, in prep)

5.2.2 Thermal properties

Thermal conductivity

Thermal conductivity was measured in the frame of the HE-D and HE experiments. The values are listed in Table 5.5.

LAEGO measured thermal diffusivity normal and parallel to bedding at 20 and 80 °C samples resulting in thermal diffusivity of $8.22 \cdot 10^{-7} \text{ m}^2/\text{s}$ to $9.27 \cdot 10^{-7} \text{ m}^2/\text{s}$ parallel to bedding and $4.13 \cdot 10^{-7} \text{ m}^2/\text{s}$ to $5.32 \cdot 10^{-7} \text{ m}^2/\text{s}$ parallel to bedding, whereby the values at 80 °C were $10^{-7} \text{ m}^2/\text{s}$ lower than at room temperature. The resulting conductivities (see Table 5.5) have an anisotropy factor of about 2. It should however be noted that the samples for the two orientations were prepared from two different cores originally several meters apart.

The tests by DBE were performed normal and oblique to bedding (Figure 5.7). The values show no significant temperature dependence. Anisotropy was derived value from the oblique and normal thermal conductivities as depicted in Figure 5.7. Based on this anisotropy the bedding plane parallel thermal conductivity was deduced. The measurements also indicate that thermal conductivity is independent of confining pressure between 0.8 and 7 MPa.

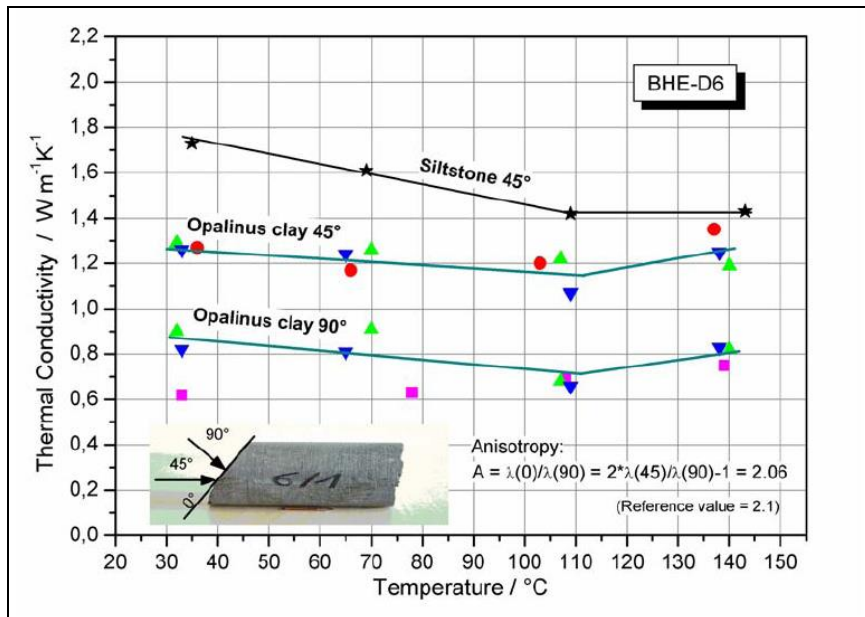


Figure 5.7: Thermal conductivity measurements by DBE (Wilveau, 2005)

Specific heat

Specific heat measurements are listed in Table 5.5. Early measurements of specific heat by Delacre *et al.* (2000) in the frame of the HE experiment are in the range of 780 to 820 J/kgC. However, these samples have only 4.5 % water content which is about 1.5 % lower than the normal value in Mont Terri.

Further determinations have been done in the frame of the HE-D experiment. Here, LAEGO tested samples during heating and cooling and showed that the pore water loss has a profound effect on the heat capacity of the rock (Figure 5.8).

Values by DBE (Wileveau, 2005) show a difference smaller than 10 % between the initial state at 20 °C and dried samples at 140 °C. DBE values are higher by about 20 % than the results by the other labs.

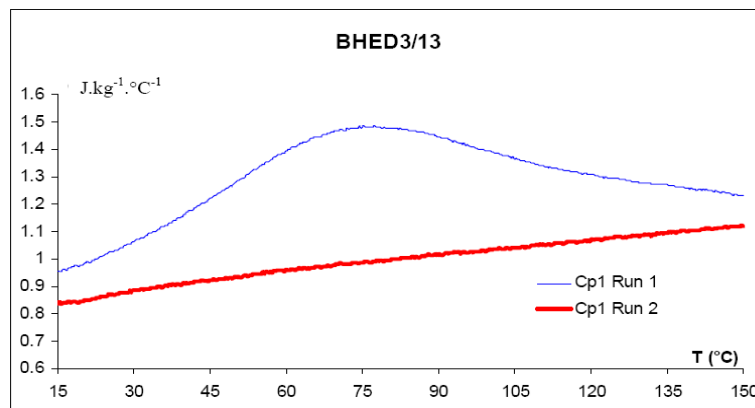


Figure 5.8: Heat capacity measurement by LAEGO (values /1000) and reported by Wileveau (2005). Heating values (blue) are higher due to the presence of water in the rock. The subsequent cooling phase (red) shows the specific heat of the matrix

Thermal expansion

The available thermal expansion measurements for the Opalinus Clay are listed in Table 5.5.

The measurements show a wide range, mainly due to variable test conditions (containment, drainage, etc.) and possibly also variable sample quality (desaturation and disturbance).

The unconfined measurements resulted in a generally smaller values for thermal expansion. The reason for that may be the competing contraction by progressive drying of the sample at rising temperatures. This effect is also evident in the experiments by DBE at 90° and 45° to bedding (Figure 5.11). The anisotropy factor of the determinations by DBE reaches a value of 10, however, most other tests suggest that it is in the range of 1.5 to 3.

It must be noted that these data need careful consideration as the subsequent THM modelling in the frame of the HE-D experiment showed that the observed deformations require significantly higher values for thermal expansions.

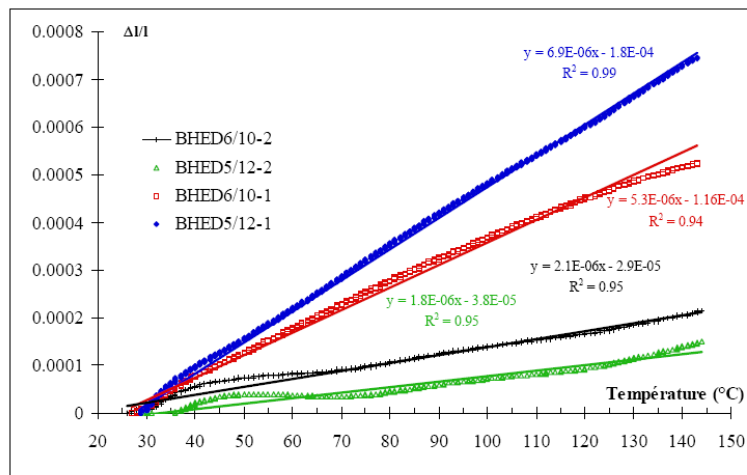


Figure 5.9: Dilatometer tests for thermal expansion (unconfined) by LAEGO reported in Wileveau (2005).

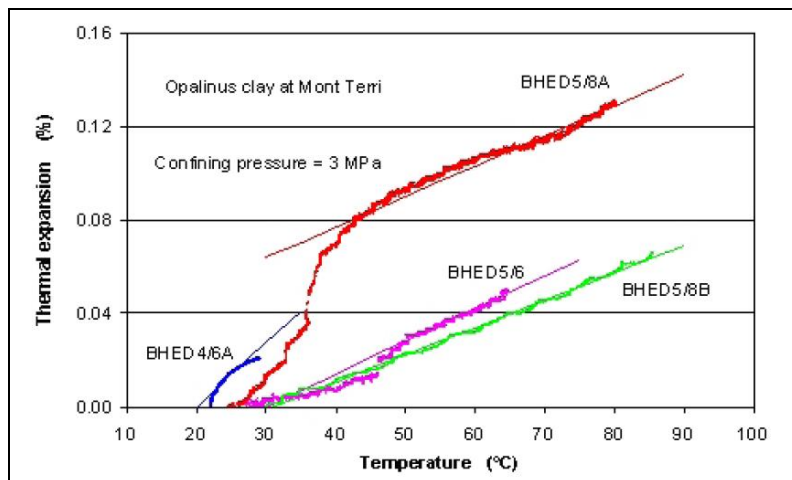


Figure 5.10: Linear thermal expansion experiment in a triaxial cell under 3 MPa confining pressure with bedding at 45°. Experiments performed by GRS and reported in Wileveau (2005)

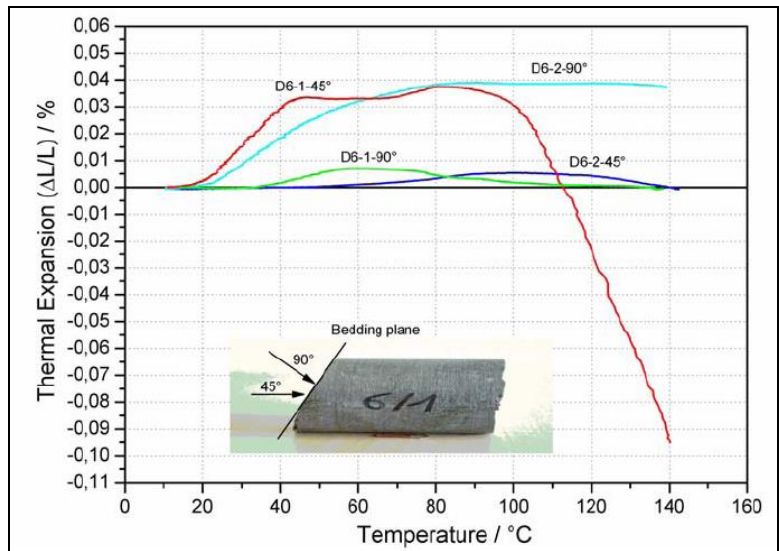


Figure 5.11: Thermal expansion by DBE (Wileveau, 2005), showing the effect of pore water loss at higher temperatures

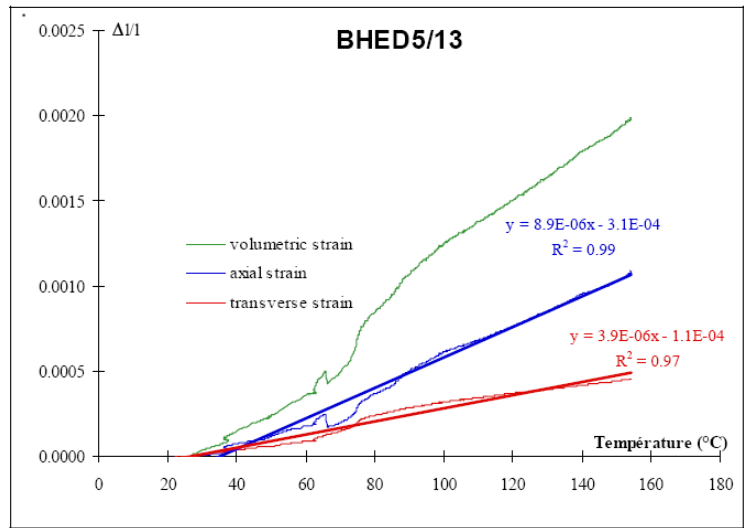


Figure 5.12: Example triaxial cell test for thermal expansion at 2 MPa by LAEGO reported in Wileveau (2005)

Table 5.5: Thermal and thermomechanical properties of the Opalinus Clay

Property	angle to bedding	Source	Value	Unit	Remarks
Thermal conductivity λ	0	DBE	1.60	W/mK	
	90	DBE	0.75	W/mK	
	45	DBE	1.55	W/mK	carbonate layer
	0	LAEGO	2.26	W/mK	20°C
	0	LAEGO	2.29	W/mK	20°C
	90	LAEGO	1.17	W/mK	20°C
	90	LAEGO	1.21	W/mK	20°C
	0	LAEGO	2.40	W/mK	80°C
	0	LAEGO	2.45	W/mK	80°C
	90	LAEGO	1.10	W/mK	80°C
	90	LAEGO	1.22	W/mK	80°C
Specific heat C_p		DBE	1230	J/kgK	20°C
		DBE	1360	J/kgK	20°C
		DBE	1140	J/kgK	20°C
		DBE	1390	J/kgK	140°C
		DBE	1380	J/kgK	140°C
		LEAGO	852	J/kgK	20°C, dry
		LEAGO	912	J/kgK	20°C, dry
		LEAGO	994	J/kgK	80°C, dry
	LEAGO	1078	J/kgK	80°C, dry	
Thermal expansion α	45	DBE	2.00E-05	1/°C	
	90	DBE	1.40E-05	1/°C	
	45	DBE	1.00E-05	1/°C	
	90	DBE	1.50E-06	1/°C	
	45	DBE	1.00E-05	1/°C	
	90	DBE	2.00E-06	1/°C	
	45	UPC	3.47E-05	1/°C	Unconfined, wrapped, heating path
	45	UPC	2.65E-05	1/°C	Unconfined, wrapped, cooling path
	0	LAEGO	5.30E-06	1/°C	unconfined
	0	LAEGO	6.90E-06	1/°C	unconfined
	0	LAEGO	8.90E-06	1/°C	Pc=2MPa
	0	LAEGO	9.80E-06	1/°C	Pc=2MPa
	0	BGR	2.1E-05	1/°C	
	0	BGR	2.0E-05	1/°C	
	0	BGR	2.1E-05	1/°C	
	0	BGR	1.9E-05	1/°C	
	0	BGR	1.1E-05	1/°C	
	0	BGR	1.6E-05	1/°C	
	90	BGR	2.5E-05	1/°C	Cooling path ("more reliable"), mean stress 0.4 MPa
	0	BGR	1.2E-05	1/°C	Cooling path ("more reliable"), mean stress 0.4 MPa
	90	BGR	1.8E-05	1/°C	Heating path, mean stress 15 MPa
	0	BGR	1.4E-05	1/°C	Heating path, mean stress 15 MPa
	90	LAEGO	2.10E-06	1/°C	unconfined dilatometer
90	LAEGO	3.90E-06	1/°C	Pc=2MPa	
90	LAEGO	5.70E-06	1/°C	Pc=2MPa	
45	GRS	1.70E-05	1/°C	weak temperature dependence	

5.3 THM characterization in-situ – Experiment and modelling

HE experiment in the Mont Terri URL

The description of the HE experiment was slightly shortened and rearranged modified from the final report of the experiment published by the EC. Details can be found in the original version (Göbel *et al.*, 2006).

The objective of the HE experiment was to improve the understanding of the coupled thermo-hydro-mechanical (THM) processes in a host rock-buffer system, based on experimental observations and numerical modelling. In detail, the basic objectives were:

Long-term monitoring in the vicinity of the heat source during hydration and heating phases, particularly observation and study of coupled THM processes in the near-field, i.e. continuous measurement of temperatures, pore pressures, displacements, electrical conductivity, and analysis of gas and water released into the rock due to the effects of heating.

Determination of the properties of the barrier and host rock using results from laboratory and in situ experiments, i.e. general mechanical and mineralogical properties, in-situ stress state, and changes induced by the experiment.

Study of the interaction between the host rock and the bentonite buffer, as well as validation and refinement of existing tools for modelling THM processes.

Study of the reliability of instrumentation and measuring techniques, e.g. inspection of sensors after dismantling the experimental set-up.

To achieve the defined objectives, the experiment was accompanied by an extensive programme of continuous monitoring, experimental investigations on-site and in laboratories and numerical modelling of coupled thermo-hydro-mechanical processes. Finally, the experiment was dismantled to provide laboratory samples of post-heating buffer and host rock material.

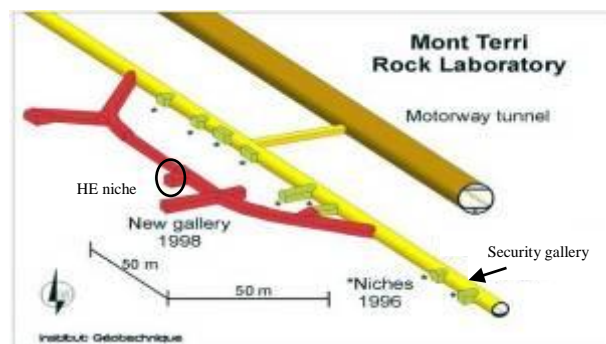


Figure 5.13: HE niche at the Mont Terri Rock Laboratory

The HE experiment was performed at the Mont Terri Rock Laboratory in a niche excavated for this purpose in the shaly facies of the Opalinus Clay formation (Figure 5.13). A central vertical borehole (BHE-0) 300 mm in diameter and 7.5 m long was drilled in the niche floor. Heat-producing waste was simulated by a heater element with 10 cm diameter, held at a constant surface temperature of 100 °C. The 2 m long heater element was placed in the vertical borehole at a depth of 4 to 6 m. It was embedded in a barrier of ring-shaped compacted bentonite blocks with an outer diameter of 30 cm and a dry density of 1.8 g/cm³. A total of 19 boreholes were drilled in the niche floor for instrumentation purposes (Figure 5.14). Sensors for measuring the most relevant rock parameters, such as temperature, humidity, stress state, pore pressure, displacement, and electric resistivity, as well as devices for determining gas and water release, were installed in the boreholes. To simulate long-term behaviour, and due to the absence of free water in the Mont Terri Rock Laboratory, an artificial hydration system was installed to accelerate the saturation process in the buffer prior to the heating phase (Figure 5.15).

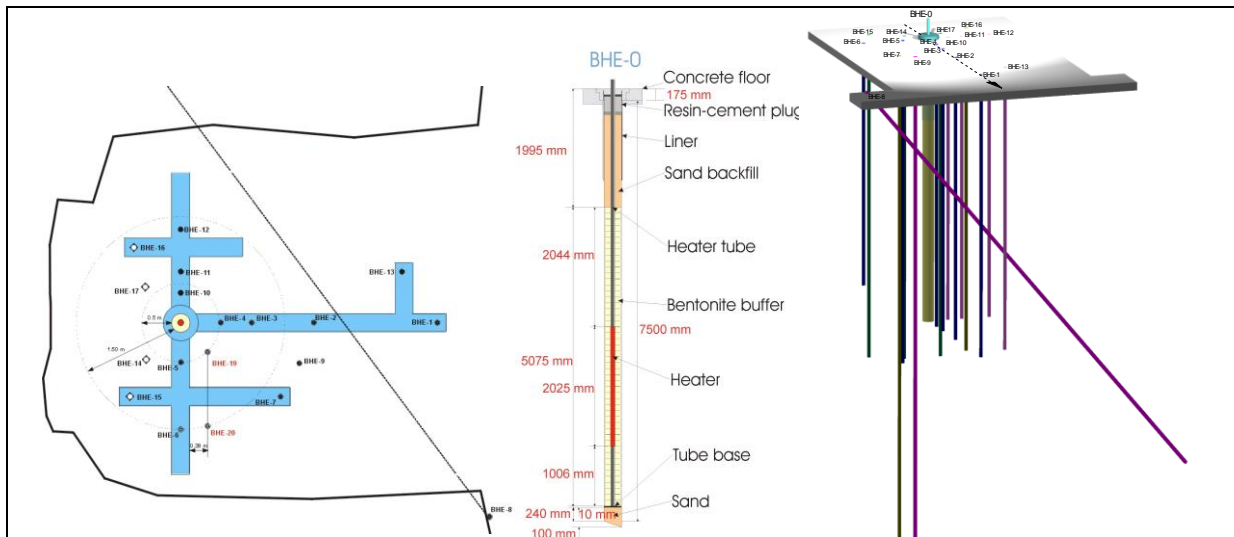


Figure 5.14: Layout of the HE experiment (plan view), description of the central borehole BHE-0 and 3D view of the HE boreholes

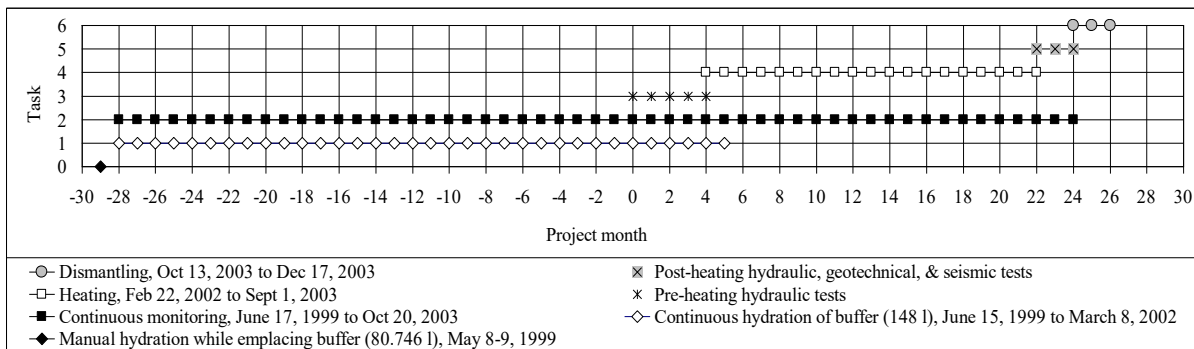


Figure 5.15: Time-table for the HE experiment: negative numbers for project months indicate the installation period and positive numbers the operational and post-operational phase

The water used was synthetic experimental water, which is chemically similar to the water in the Opalinus Clay formation. The artificial saturation lasted for 35 months before the heating phase (duration 18 months) began.

The first heating phase (Figure 5.16) was carried out in different constant power steps, to allow adjustment of the parameters of the temperature control loop, reaching a maximum temperature in the bentonite blocks of about 68 °C. The temperature control loop was then adjusted using the data obtained. The power applied to the heater was automatically regulated to a constant temperature of 100 °C at the contact between the heater and the bentonite buffer. After the heater was switched off, the system cooled down rapidly. After about one month, the maximum temperature of 40 °C allowed access for dismantling work.

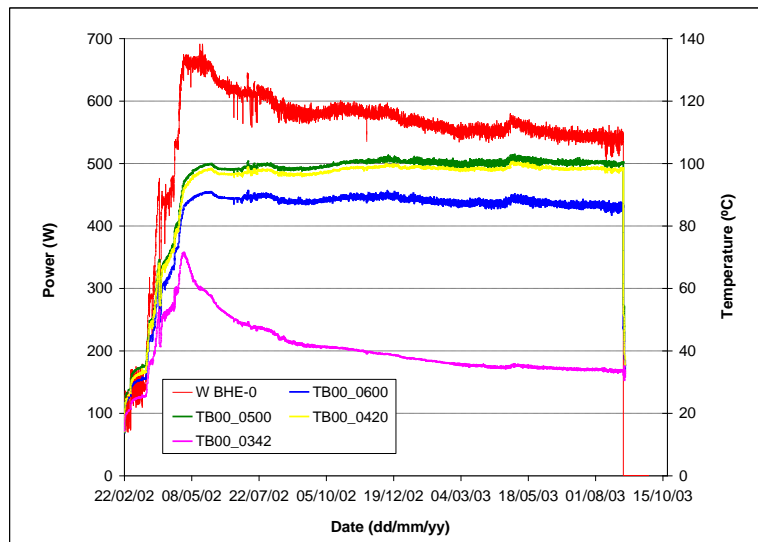


Figure 5.16: Evolution of applied power (W BHE-0) and temperatures in BHE-0 versus time (numbers indicate depth of sensor in the vertical borehole, e. g. 0500 meaning 5 m)

Monitoring results

The electric power needed to maintain a constant temperature of 100 °C at the heater decreased with time, the most likely reason being a decrease in the thermal conductivity of the bentonite, probably caused by drying (Figure 5.16). Eight months after the start of heating, a constant temperature profile had developed at a distance of 1 to 2 m from the heater. In more peripheral regions, it took until the end of the heating phase to develop an approximately steady temperature state.

The pore pressure sensors show a pressure build-up at the beginning of heating, followed by a slow decrease and then a sharp pressure drop after heating stopped (Figure 5.17). The curves also differ in the size of their maxima, etc. Measurements of relative humidity (capacity sensors) showed no conclusive results and were probably perturbed by the heating.

The angle variations registered by the inclinometers were very small (Figure 5.18). According to these data, there was a progressive displacement from the heater, clearer in those inclinometers installed at depths closer to the heater (4.5 m, 5.5 m, and 6.5 m). The trend was maintained until the end of the heating phase (see the lines corresponding to June 1999 and August 2003). The maximum displacement registered was about 5.5 mm, measured a few days after the end of heating, and in the inclinometer placed at 4.50 m depth. Beginning with the end of the heating phase, the displacements decreased slightly. The measured values are more than one order of magnitude larger than the results of the computer simulations.

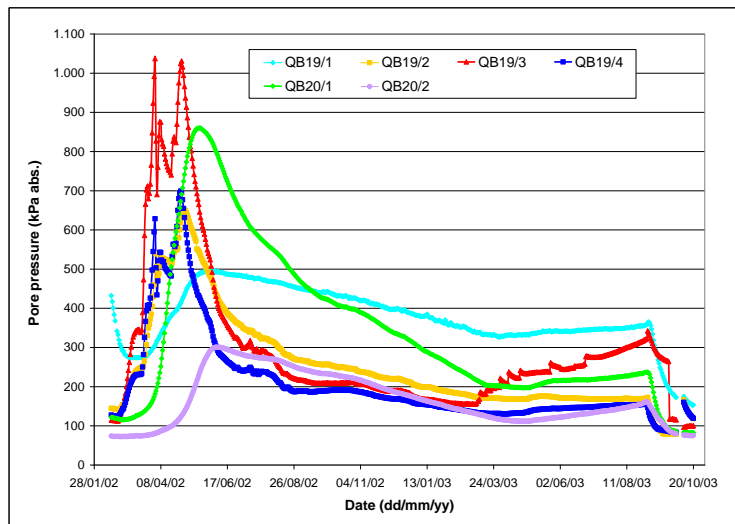


Figure 5.17: Evolution of pressure in boreholes BHE-19 and BHE-20. Depth of sensors: /1 = 3.5 m, /2 = 5 m = mid-heater, /3 = 6.5 m, /4 = 8 m)

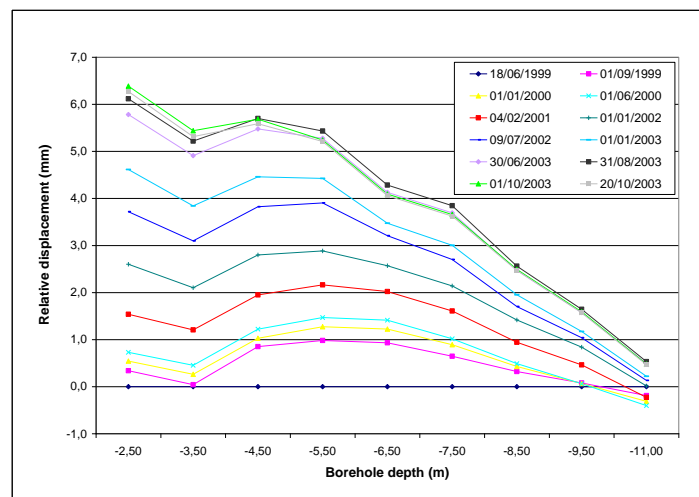


Figure 5.18: Temporal evolution of accumulated displacements

Hydraulic conductivities were measured before and after the heating period in boreholes close to the heater borehole (Bühler *et al.*, 2006). Figure 5.19 shows the results for the conductivity of Opalinus Clay as a function of depth. The post-heating saturated hydraulic conductivity is estimated to be $K_s = 5 \cdot 10^{-11}$ m/s. Assuming saturated conditions in the deeper parts of the borehole the pre-heating hydraulic conductivity is $K_s = 1 \cdot 10^{-12}$ m/s although there is no strong indicator that the hydraulic conductivity really has changed due to the heating because there is no indication of a decrease in saturation and the temperatures at a distance of 0.65 cm from the heater borehole did not exceed 50 °C. In comparison, Gaucher *et al.* (2003) report hydraulic conductivities in the Opalinus Clay of

Matrix rock: $1 \cdot 10^{-13}$ to $5 \cdot 10^{-13}$ m/s
 EDZ: $4 \cdot 10^{-12}$ to $8 \cdot 10^{-8}$ m/s

This indicates that the conductivities measured in the boreholes are similar to values for the EDZ. There is a slight indication that the heating may have influenced the hydraulic conductivity.

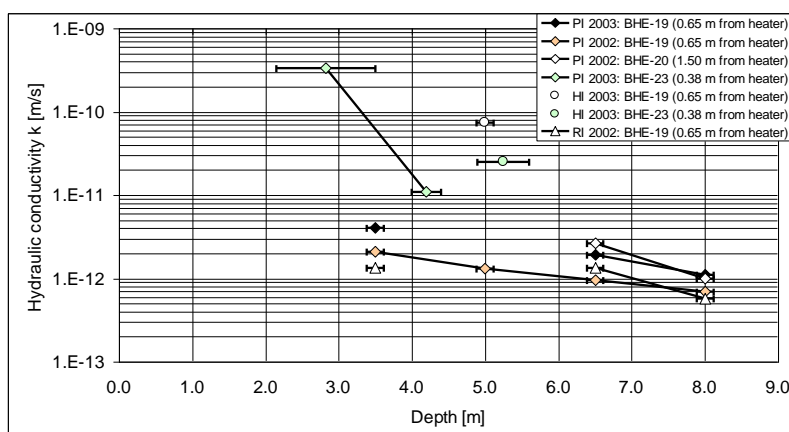


Figure 5.19: Hydraulic conductivity close to the heater borehole. Results of in situ tests: PI: Pulse injection test, HI: Constant head injection test, RI: Constant rate injection test (injection period)

Dismantling analysis – host rock

The dismantling was done by excavating a vertical shaft, with sensors and samples being collected as planned after each meter of progress.

The mineralogical and chemical properties of the Opalinus Clay were determined in laboratory experiments. With regard to heat-induced changes in Opalinus Clay, no conclusive answers could be found because, for the temperatures were too low (Kaufhold & Emmerich, 2006). From temperature sensors which monitored the experiment throughout the heating phase, it can be concluded that the Opalinus Clay located close to the engineered barrier was heated up to about 40 °C, which is insignificant compared with the geological history of this clay. Regarding heat-induced changes in bentonite and, particularly in Opalinus Clay, future heater experiments should consider the use of a different test configuration to get more representative repository conditions, meaning higher temperatures on clay.

Modelling of the HE experiment at Mont Terri

The **near-field model** comprises the most important technical features of the engineered barrier. It includes all sequences in the history of the test, beginning with the excavation of the HE niche. Modelling the initial phases of the experiment is of vital importance, since they control the initial stress state and the pore pressure for the subsequent phases. The **far-field model** deals with the THM interactions in the host rock only.

HE-Experiment: Near-field modelling

The initial model for the nearfield of the HE experiment was axisymmetric.

The mechanical behaviour of the host rock has been modeled by means of the mechanical constitutive law proposed by Vaunat & Gens (2003). Opalinus Clay is considered as a composite material made of a clay matrix interlocked by bonds. The bond response is modeled by a damage model proposed by Carol *et al.* (2001), while the clay matrix can be represented by any model usually used to characterize a clay soil. In the case of Opalinus Clay, which has a low porosity (13.7 %), a Hoek-Brown criterion associated with a linear-elastic law was used. Applying the compatibility and equilibrium equations between bond, matrix and external strains and stresses, the material response was derived. It is governed by the equations and parameters shown in Table 5.6, where E , E_M , and E_b are Young's modulus of, respectively, the composite material, the clay matrix

and the bonds, ν is Poisson's ratio, R_c and R_{cM} are uniaxial compression shear strengths of, respectively, the composite material and the clay matrix and m is a parameter determining the shape of the yield locus. The parameter χ is related to the amount of bonding. It takes the value χ_0 when bonds are intact (undamaged rock) and progressively degrades as damage proceeds (measured by the damage variable L). L appears to be related to the degradation of the Young's modulus of the bond only, following the expression $L = \ln(E_0/E)$, where E_0 and E are the undamaged and damaged Young's modulus of the bond, respectively.

Comparison with monitoring results shows that the evolution of stress state and pore pressure during niche excavation and borehole drilling could be reproduced well. During the hydration phase, the high initial suction of bentonite induced an unsaturated state in the surrounding rock, reaching a maximum at a radial distance of 0.70 m. The desaturation and subsequent resaturation took place in approximately 200 days. The hydration of the bentonite generated high swelling pressures, reaching a maximum value of 14 MPa in the rock close to the interface.

Table 5.6: Equations defining the constitutive law of Opalinus Clay. For explanation of symbols see text

Law	Equation	Parameters
Elastic	Linear elasticity	$E = (1 + \chi)E_M(1 + \chi) + \chi E_b \chi$ $\nu = \text{Constant}$
Yield surface	Hoek-Brown criterion	$R_c = (1 + \chi) \cdot R_{cM}$ $m = \text{Constant}$
Flow rule	Associated	
Degradation law		$\chi = \chi_0 e^{-L/2}$

Table 5.7: Mechanical properties of the Opalinus Clay for the axisymmetric nearfield model

Properties	Value
E (Young's modulus)	6000.0 MPa
ν (Poisson's ratio)	0.27
UCS (unconfined compressive strength)	16.0 MPa
UTS (unconfined tensile strength)	2.0 MPa
m	8.0
χ	2.0

Table 5.8: Hydraulic properties of the Opalinus Clay for the axisymmetric nearfield model

Properties	Value
Intrinsic permeability, k (Kozeny model)	$k = k_0 \frac{\phi^3 (1-\phi_0)^2}{(1-\phi)^2 \phi_0^3}$ ϕ_0 : reference porosity (0.137) k_0 : intrinsic permeability for matrix ($3.50 \cdot 10^{-19}$) [m ²]
Water retention curve (modified Van Genuchten model)	$S_e = \frac{S_l - S_{rl}}{S_{ls} - S_{rl}} = \left(1 + \left(\frac{P_s - P_l}{P} \right)^{\frac{1}{1-\lambda}} \right)^{-\lambda}$ S_e : Effective saturation ($0 \leq S_e \leq 1$) P : Material parameter (3.90) [MPa] P_s : Material parameter (700.00) [MPa] λ : Shape function for retention curve (0.128) λ_s : Material parameter (2.73) S_{rl} : Residual saturation (0.00) S_{ls} : Maximum saturation (1.00)
Relative permeability, k_{rl} (Van Genuchten model)	$k_{rl} = \sqrt{S_e} \left(1 - \left(1 - S_e^{1/\lambda} \right)^\lambda \right)^2$ S_e : Effective saturation ($0 \leq S_e \leq 1$) λ : Power (0.29) S_{rl} : Residual saturation (0.00) S_{ls} : Maximum saturation (1.00)
Porosity, n	(0.137)

Table 5.9: Thermal properties of the Opalinus Clay for the axisymmetric nearfield model

Properties	Value
Thermal conductivity	(2.10) [W/m/K]
Linear thermal expansion coefficient, b_s	($1.00 \cdot 10^{-5}$) [°C ⁻¹]
Specific heat, C_s	(874.00) [J kg ⁻¹ K ⁻¹]

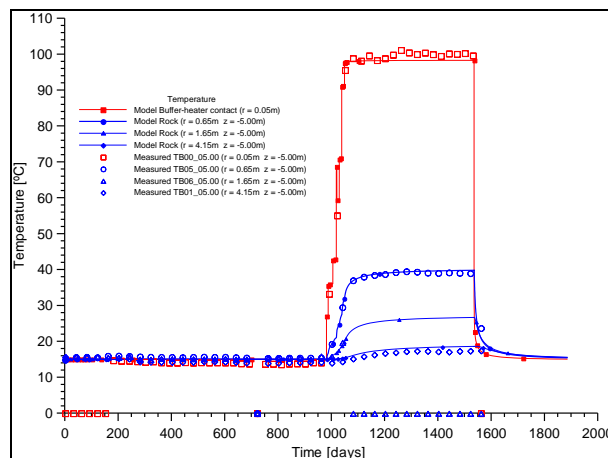


Figure 5.20: Axisymmetric model: Time evolution of temperatures calculated and measured during the hydration, heating and cooling phases, in points located in bentonite and rock

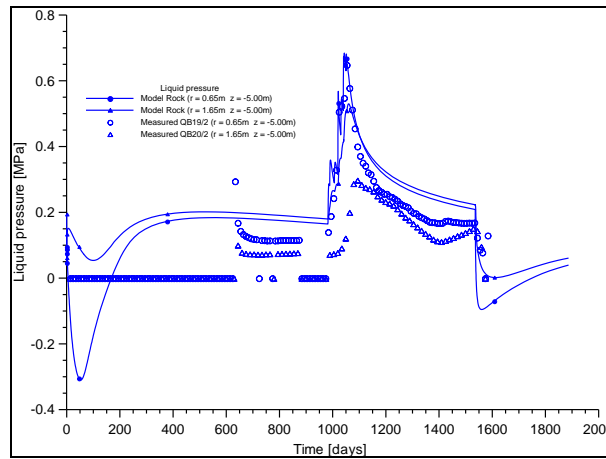


Figure 5.21: Time evolution of liquid pressure in points located in rock during hydration, heating and cooling phase

The bentonite swelling pressure produced significant changes in the stress state in the surrounding rock, affecting a zone of 1 m diameter. Plastic strains were produced in a narrow zone of the rock (thickness of 0.05 m) adjacent to the bentonite-rock interface. The post-dismantling analysis showed that the in situ behaviour was different (see section on bentonite).

Modelled temperatures during the heating phase are close to the measured values. The area with increased temperature extends to a maximum radial distance of 5.0 m. The increase in the pore pressure and the subsequent dissipation measured during heating are well reproduced by the model. The positive pore pressure generated by temperature increases causes a drop in the effective stress, which implies a certain loss of rock strength. The magnitude of pore pressure increase is controlled by the rate of temperature increase, the rock permeability, the rock porosity, the rock stiffness, and the geometry of the experiment. The heating phase generates a transient change in the total and effective stresses. Successive heating extends the annular zone of plastic strain to a maximum thickness of 0.08 m. The latter could not be confirmed in situ.

The cooling phase induces a reduction in pore pressure, the magnitude of which depends on the rate of the temperature decrease. The pore pressure reaches a stable state after approximately 250 days of cooling. Cooling implies a transient change in total and effective stresses. On the long term, steady state stresses do not seem to be affected by the heating and cooling phases.

To better represent the mechanical behaviour of the Opalinus Clay, an anisotropic elasto-viscoplastic model was applied. A significant proportion of the material parameters were taken from tests performed on the Opalinus Clay as part of the HE experiment (Table 5.10).

All the construction and testing phases of the HE experiment were modelled including the niche excavation and borehole drilling. The latter control the initial stress state and pore pressure for the subsequent phases.

Table 5.10: Mechanical parameters of the Opalinus Clay used in the 3D model

Deformation parameters of transverse rock model	
Tangent modulus $E_{X'-X'} = E_{Y'-Y'}$ (<i>//</i> bedding planes) [MPa]	3000
Tangent modulus $E_{Z'-Z'}$ (<i>⊥</i> bedding planes) [MPa]	1500
Poisson's ratio. ν_{XY}	0.33
Poisson's ratio. $\nu_{ZX} = \nu_{ZY}$	0.24
Shear modulus $G_{ZX} = G_{ZY}$ [MPa]	650
$\alpha =$ angle of strike ($0^\circ < \alpha < 180^\circ$), with respect to	60.0

Y axis	[°]	
Dip angle ($0^\circ < \beta < 90^\circ$)	[°]	35.0
Viscous parameters		
$\Gamma_M = \Gamma_J$	[1/s]	10^{-5}
$N_M = N_J$	-	3
F_{0M}	[MPa]	12.0
F_{0J}	[MPa]	1.0
Strength parameters of matrix		
Uniaxial compressive strength UCS \perp - UCS \parallel	[MPa]	12.0
Uniaxial tensile strength UTS \perp - UTS \parallel (χ)	[MPa]	5.0
Cohesion (c)	[MPa]	6.0
Friction angle (ϕ)	[°]	30.0
Residual friction angle (ϕ_R)	[°]	15.0
Dilatancy angle (ψ)	[°]	25.0
Strength parameters of the joint		
Tensile strength (χ_{joint})	[MPa]	2.0
Cohesion (c_{joint})	[MPa]	2.0
Friction angle (ϕ_{joint})	[°]	23.0
Residual friction angle (ϕ_R)	[°]	15.0
Dilatancy angle (ψ)	[°]	20.0

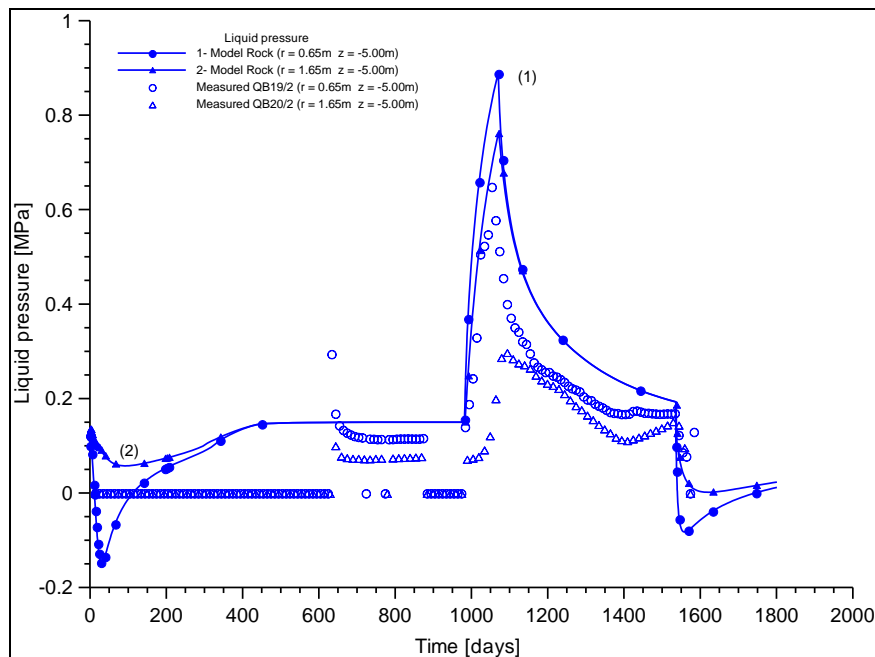


Figure 5.22: Anisotropic nearfield model: Modelled and measured evolution of fluid pressure with time at points located in rock during the excavation, hydration, heating and cooling phases

Significant differences between the isotropic and the anisotropic models have been found in the

- direction and intensity of displacements;
- stress distribution;
- plastic zone developed.

Points located at the same radial distance from the HE borehole axis but at different positions in the circumferential direction, show significantly different responses. Particularly sensitive are the calculated radial displacements caused by borehole heating (Figure 5.23).

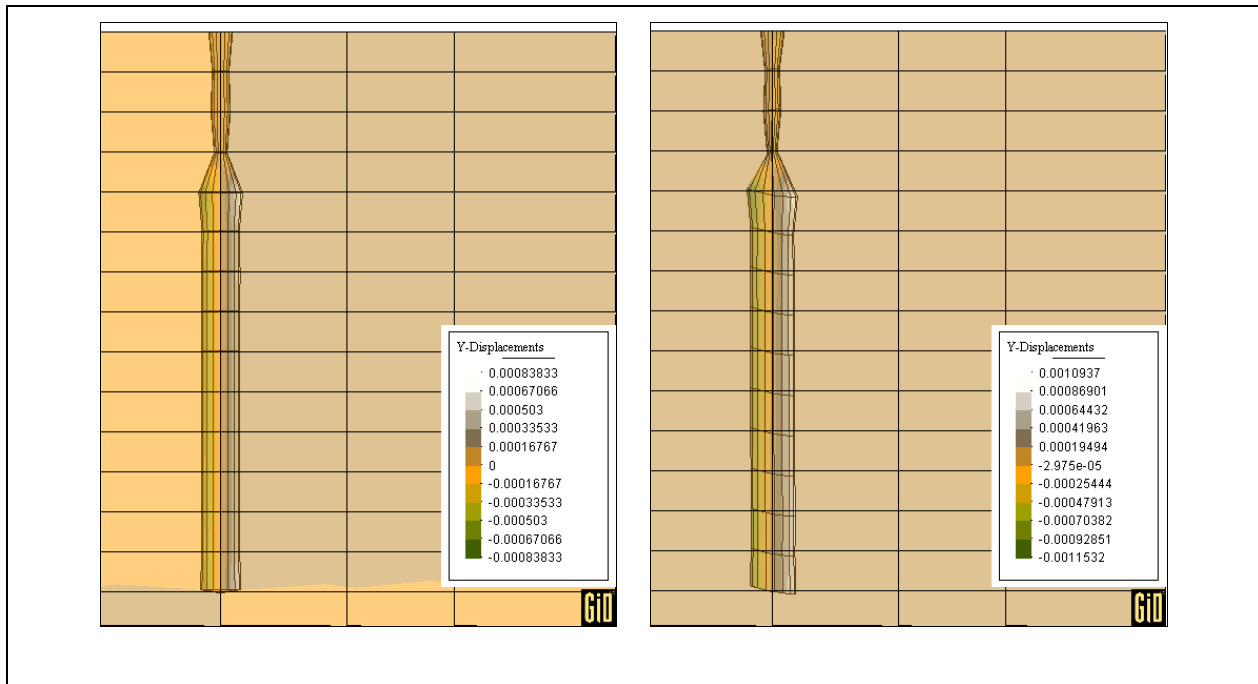


Figure 5.23: HE-Experiment: Displacement in Y direction. Isotropic model (left) and anisotropic model (right) during heating phase, $t = 1070$ days

HE-Experiment: Far-field model

A THM-version of the MEHRLIN code was developed by adding the thermal reaction. Verification and testing showed that the overall observed behaviour of the measurements with respect to TH-processes could be well reproduced by an axisymmetric model. The thermal parameters obtained by numerical fitting to in situ observations correspond well with the values measured on samples in the laboratory. Based on the data available, the work was not conclusive with regard to the simulation of mechanical effects: it was found that the volume of rock undergoing a rise in temperature by more than a few degrees was relatively small. The pore-water pressure rise due to heating was important, as expected in the low-permeability Opalinus Clay. The induced changes in effective stress are equally important and can, at least for low effective stress conditions, clearly not be ignored, both for mechanical stability (where applicable) and for changes in volumetric rock deformation and/or damage with the consequences for rock permeability and the creation of preferential features (fractures) and the integrity of the barrier. This aspect would be of key importance for design purposes, i.e. the back-fill material and geometry, as well as the maximum permissible heat load.

Table 5.11: Far field model parameters (HE-Experiment)

Parameter	Rock
Grain density	2710 kg/m ³
Porosity	0.16
Residual saturation	0 %
Intrinsic permeability	5 10 ⁻¹⁹ m ²
Heat capacity	920 J/kg/K
Thermal conductivity	1.8 - 3.2 W/m/K

Thermal expansion coefficient	$3.5 \cdot 10^{-5} \text{ 1/K}$
Van Genuchten P_0	$1.7 \cdot 10^7 \text{ Pa}$
Van Genuchten m	0.4
Young's modulus	$6.8 \cdot 10^9 \text{ Pa}$
Poisson's ratio	0.27

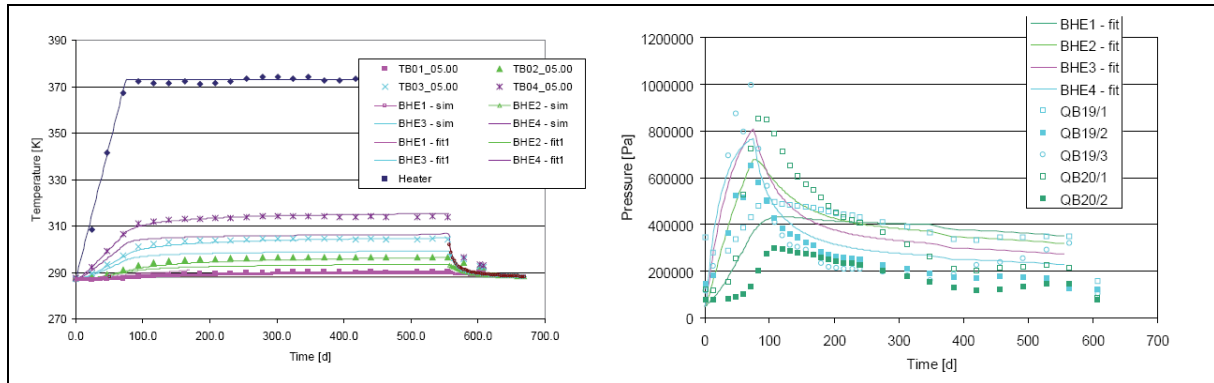


Figure 5.24: Heating and cooling phase temperature results – comparison between simulation (lines) and measurements (markers) in Borehole BHE-3

A reasonable fit with the measured temperature curves could be obtained, with differences between measured and calculated values of a few 1/10 K with the following parameters for the Opalinus Clay:

Intrinsic permeability	$8 \cdot 10^{-19} \text{ m}^2$
Thermal conductivity	2.1 W/m/K
Heat capacity	920 J/kg/K

and by assuming isotropic conditions. These values represent a best guess which lies within an acceptable range of values presented in the literature.

The calculated pressure level is very sensitive not only to the rock permeability but also to the thermal parameters of the rock. A reasonable fit (Figure 5.24) could be achieved using a standard thermal expansion coefficient and a permeability of $8 \cdot 10^{-19} \text{ m}^2$. Compared to undisturbed values for the Opalinus Clay (less than $2 \cdot 10^{-20} \text{ m}^2$), this value is very large, which can be interpreted as an indication that the swelling of the bentonite buffer might have induced fractures in the Opalinus Clay during the resaturation of the bentonite. It is worth noting that this value is only slightly higher than the fitted value obtained by means of hydraulic tests in boreholes BHE-19 and BHE-20 (less than $2 \cdot 10^{-19} \text{ m}^2$, see monitoring section). Therefore, the Opalinus Clay formation might be disturbed within this area.

The porewater pressures were, according to the calculations, significantly influenced by the heating, with considerable pore pressures developing even in regions that were only slightly affected by the rise in temperature. After the temperature reached a steady state, the overpressures dissipated due to flow within the Opalinus Clay. However, the porewater

pressures did not drop back to their original level during the heater test duration, but levelled off to a more or less constant value. The early pore pressure increases reach up to 10 MPa and the rock permeability is a major parameter influencing the level of overpressure reached through the heating as well as the porewater pressure dissipation.

Based on the results obtained, it seems that changes in effective stress due to pore pressure rise are the dominant mechanical effect, with changes in mechanical properties due to temperature effects or thermal plastification probably being very limited. Local changes in the stress field reach several MPa. As the effective stress reduction due to pressure variations is isotropic, this could potentially

lead to strong mechanical effects and classic plastification under conditions which are characterized by a very anisotropic in-situ stress field and/or in cases of a generally low effective stress level compared to pore pressure changes. No direct comparison between displacements measured and simulated could be made within this study, as the displacement measurements started (at least) at the beginning of the hydration process of the bentonite, prior to the heating phase, and no change in the evolution could be observed when the heater was switched on. In any case, displacements related to heating seem to be small and less than one millimetre, which is supported by the simulations.

HE-D experiment

At Mont Terri Andra (France) in cooperation with GRS (Germany) and supported by DBE (Germany) and CEA (France) performed the in-situ experiment HE-D in which the THM coupled behaviour of the Opalinus Clay was to be investigated.

The aims of the HE-D experiment have been summarized as follows (Wileveau *et al.*, 2005)

- To ensure the capability of the heater to provide a temperature of 100 °C for a period of one year (and ultimately) at 150 °C with a pressure of 1-MPa at the interface with the rock;
- To test new sensor technologies, such as pore-water-pressure sensors suitable for clay formations with very low permeability and a heated environment, or optic-fibre sensors for measuring temperature and deformations;
- To determine the thermal and thermomechanical properties of Opalinus clay on the basis of *in-situ* observations and tests on samples;
- To determine the impact of temperature on the hydromechanical behaviour of Opalinus clay on the basis of the *in-situ* test and test on samples;
- To study the scale effect.

The HE-D experiment was carried out in the homogenous shaly facies in the gallery 98 close to the MI niche in order to have access from two sides to the main experimental region (Figure 5.13 and Figure 5.14).

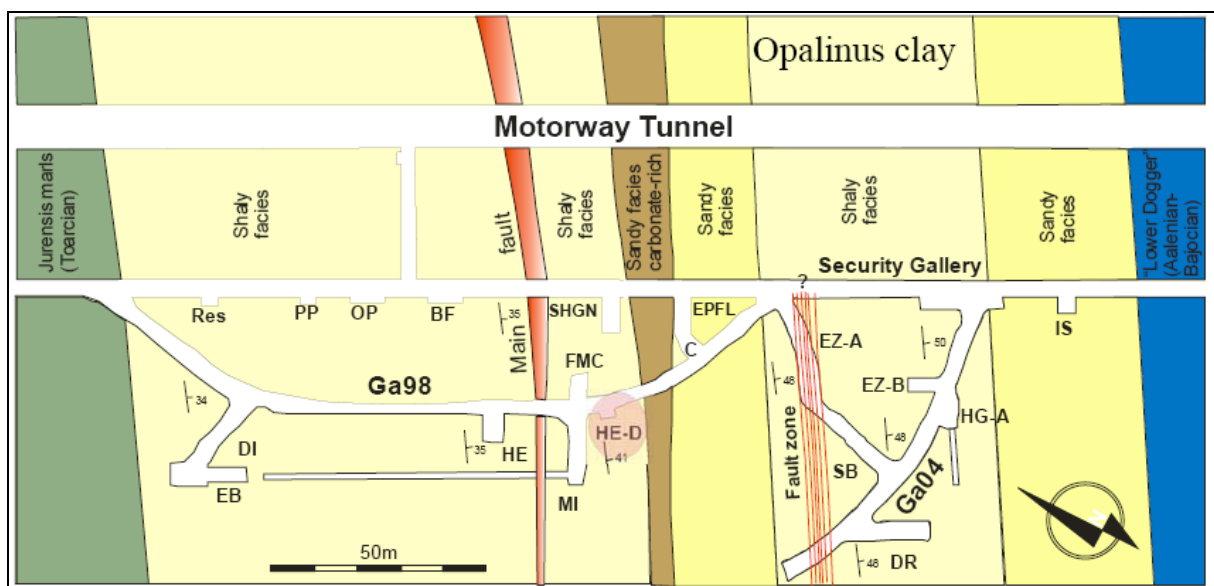


Figure 5.25: Position of the HE-D experiment in the Mont Terri URL

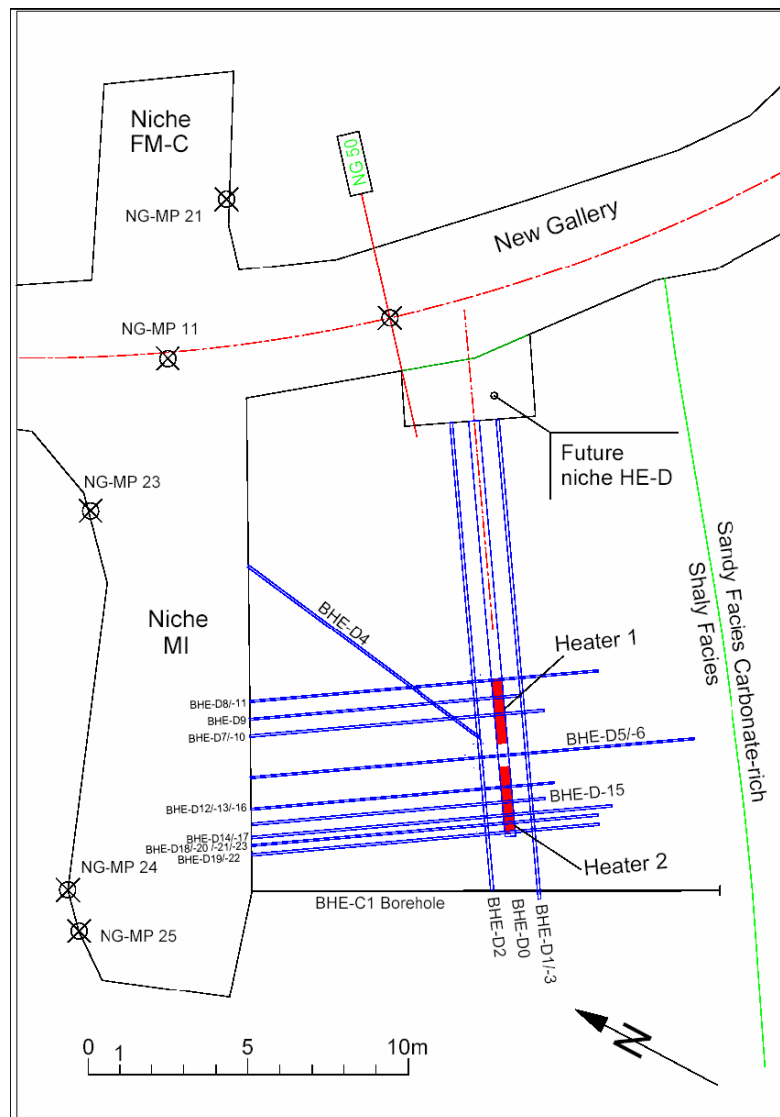


Figure 5.26: Top view of the HE-D test showing the overall borehole layout (Wileveau *et al.*, 2005)

Test procedure

A two element heated packer system was placed in the centre of the experiment. The heater elements were in direct contact with the host rock. Their diameter was 30 cm and each system included a 2 m long packer element. The total length of the system was 6.2 m. The heat output and the pressure onto the rock were fully controlled. 24 peripheral boreholes were drilled and instrumented with 110 sensors to record the reaction of the rock-water system to the heating.

Packer installation and sensor installation was followed by one month of stand-by time to allow pore pressures to equilibrate. Heating started on 6th April 2004 and lasted for over 8 months. After the increase of the heating power to 1950 W, the packer no. 2 failed on the 21st July 2004 and could not be re-inflated, the test was continued with only one packer under pressure. Approximately 60 liters of oil leaked into the heater borehole. Another disturbance of the heating phase was encountered on the 17th December 2004 when the power supply failed. After heater shut down on the 16th March 2005 monitoring continued for another 7 months during cooling of the experiment. The system was dismantled starting from the 1st November 2005. The heater could not be retrieved and was lost.

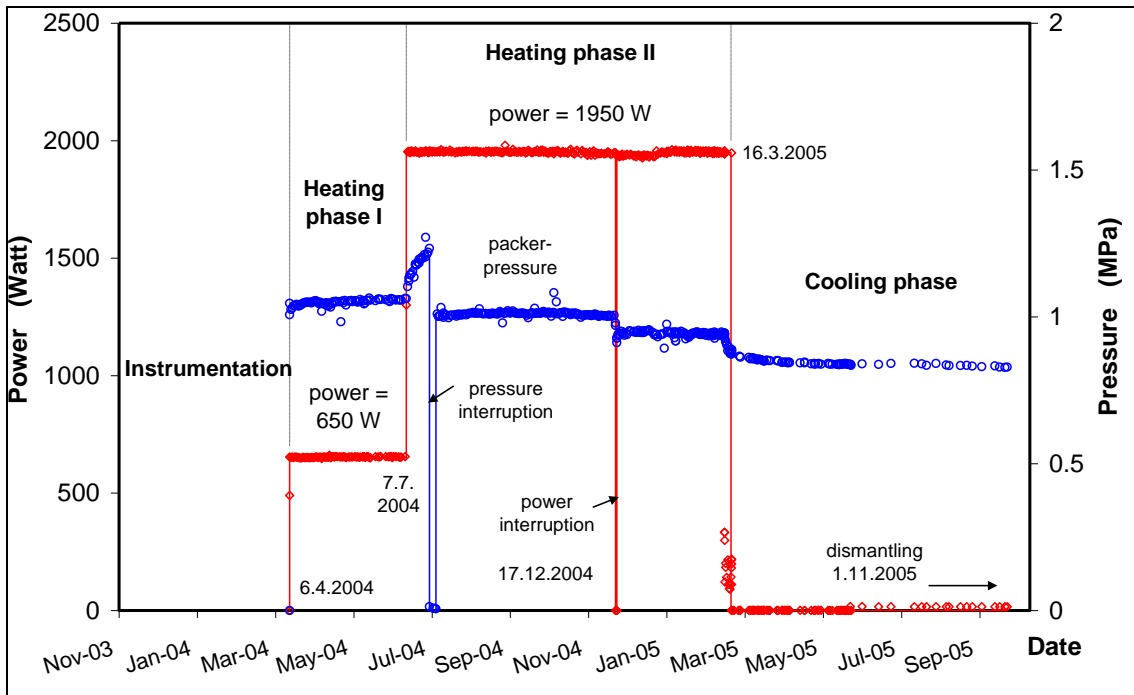


Figure 5.27: Heating power and pressure of packer no. 1 after start of HE-D experiment on April, 6th 2004 (Zhang *et al.*, in prep.)

Results

Temperature recordings are depicted in Figure 5.28 and Figure 5.29 along with the radial distance of the sensors to the heater system.

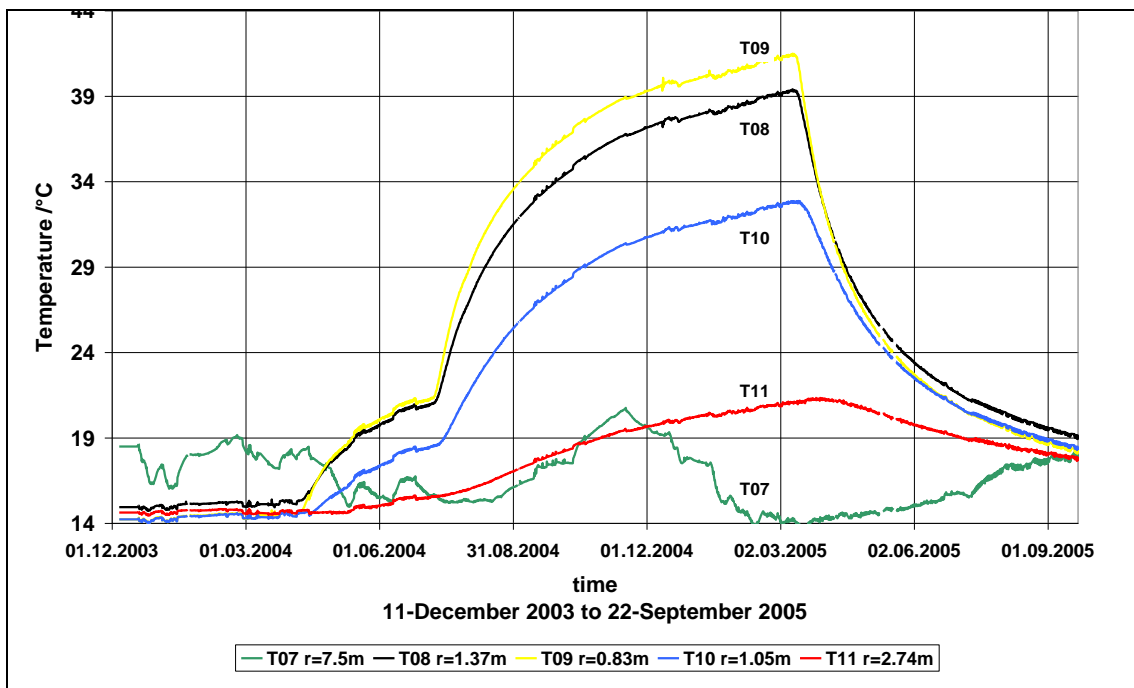


Figure 5.28: Temperatures above the heater number 1

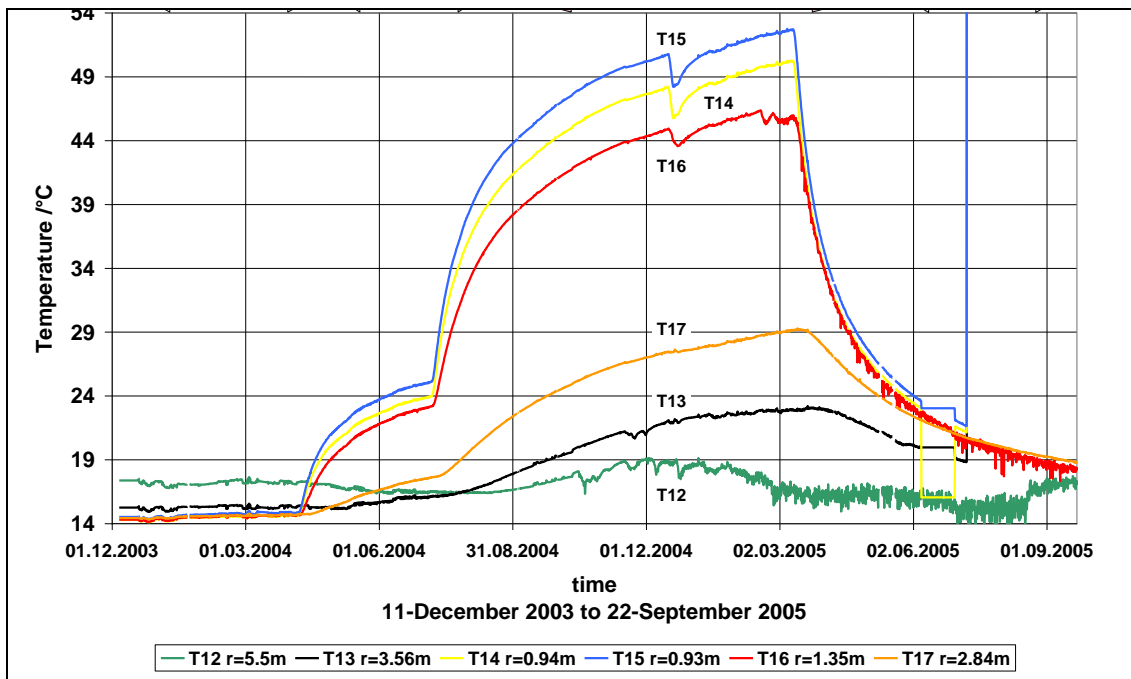


Figure 5.29: Temperatures below the heater number 2

Prior to heating the rock temperature was between 14 and 19 °C, clearly showing higher values close to the MI niche. Temperature variations in the rock showed correlations with the temperature variations in the Niche up to 7 m into the rock. These variations were also discernable in the pore pressure measurements.

During the first heating phase the observed differences between the arrays above heater 1 (up to 21 °C) and below heater 2 (up to 25 °C) can possibly be attributed to the anisotropy of the rock. A similar explanation may hold for the curves of heating phase two where the maximum temperatures for the arrays above heater 1 and below heater 2 were 41 °C and 53 °C, respectively.

The power interruption in December 2004 did only decrease the temperatures in the sensors below heater number 2. The other sensors remained largely unaffected.

Pore pressure measurements are shown in Figure 5.31 and Figure 5.33. During the pre-heating phase the pore pressures remained low in the array above heater number 1. In the second array below heater 2 the pore pressure equilibrated to approximately 0.8 to 1.2 MPa. These were also affected by the drilling of the heater borehole. In the closest borehole D14 a slight increase before the passing of the borehole face and a sharp overpressure peak of around 150 kPa is followed by a steep drop of 450 kPa. Subsequently the pressure slowly recovered. The reactions of the more distant boreholes are similar but the magnitudes are smaller possibly also on their relative position to the central heater borehole.

Upon the start of heating the pore pressure decreased in sensors D8, D14 and D15. However, it re-increased soon afterwards and surpassed initial values within a few hours. The reason for the initial decrease of pressures remains unclear. All other sensors showed increases upon pressurization and start of heating of the two central packers.

Temporary pressure drops in D08, D15 and D16 at the beginning of phase 2 remain unexplained while pressure drops in D14 and D15 on July 24, 2004 are related to the loss of heater packer pressure. Close to the MI niche (D07, D13; data of D12 are unreliable) the pressure were only slightly changed by the heating.

After the end of the heated phase on 13th March 2005 brief peaks were observed in the pressure sensors D08, D09, D15, D16 and D17, similar to the power failure event on 15th December 2004.

This was followed by a smooth decrease in all pressure sensors to almost atmospheric pressures except for the sensors D11 and D17 which were situated far away from the surrounding galleries.

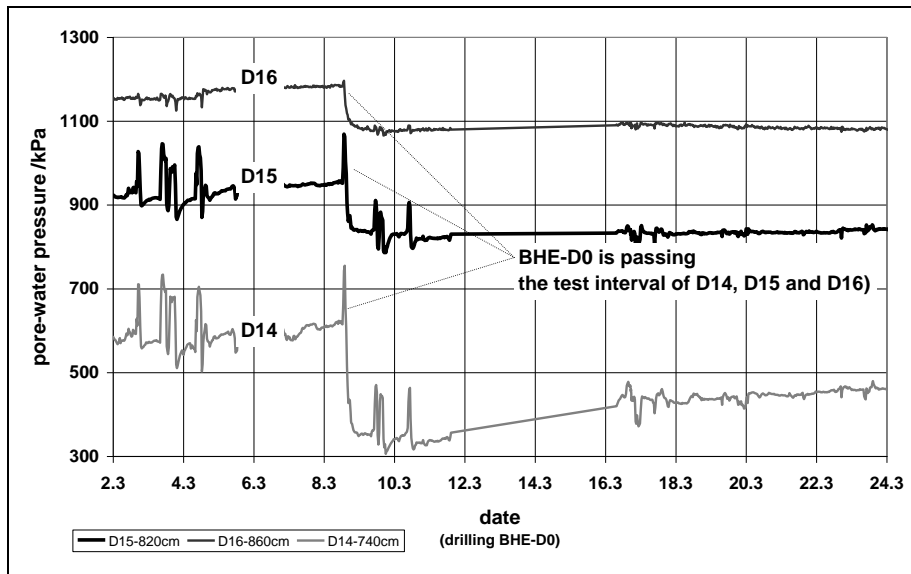


Figure 5.30: Pore pressure changes during drilling of the central heater borehole. Note short overpressure pulse prior to the drop. The distance to the heater borehole is smallest for D14 and largest for D16, lateral positions are identical.

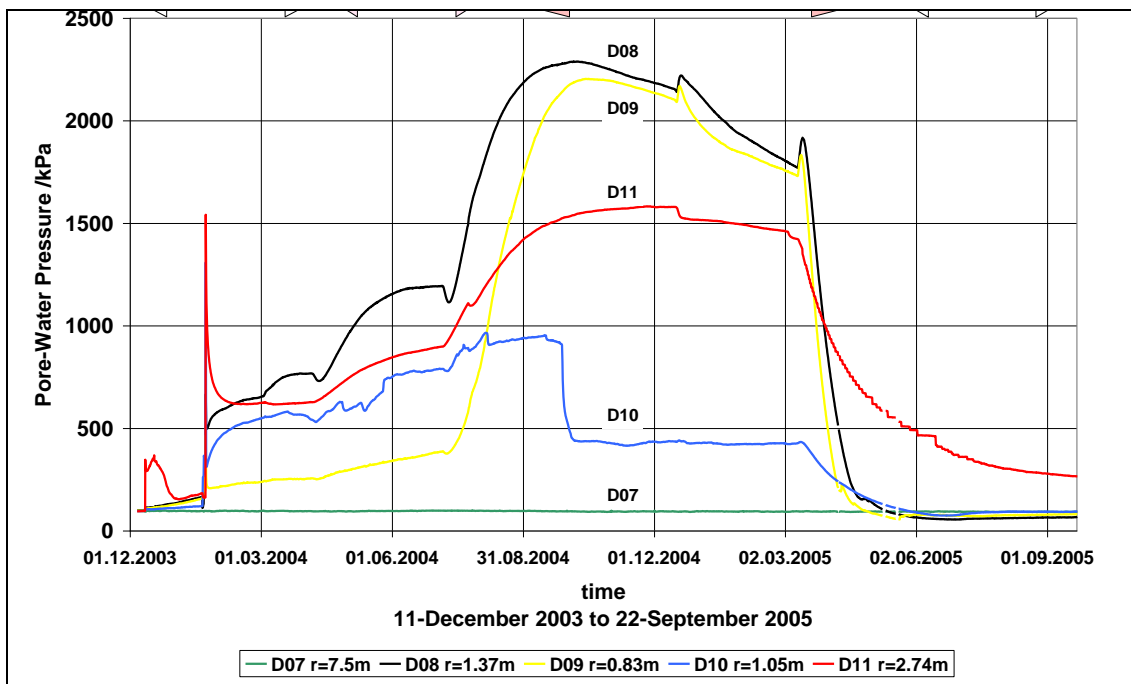


Figure 5.31: Pore pressure values in the sensors above heater number 1

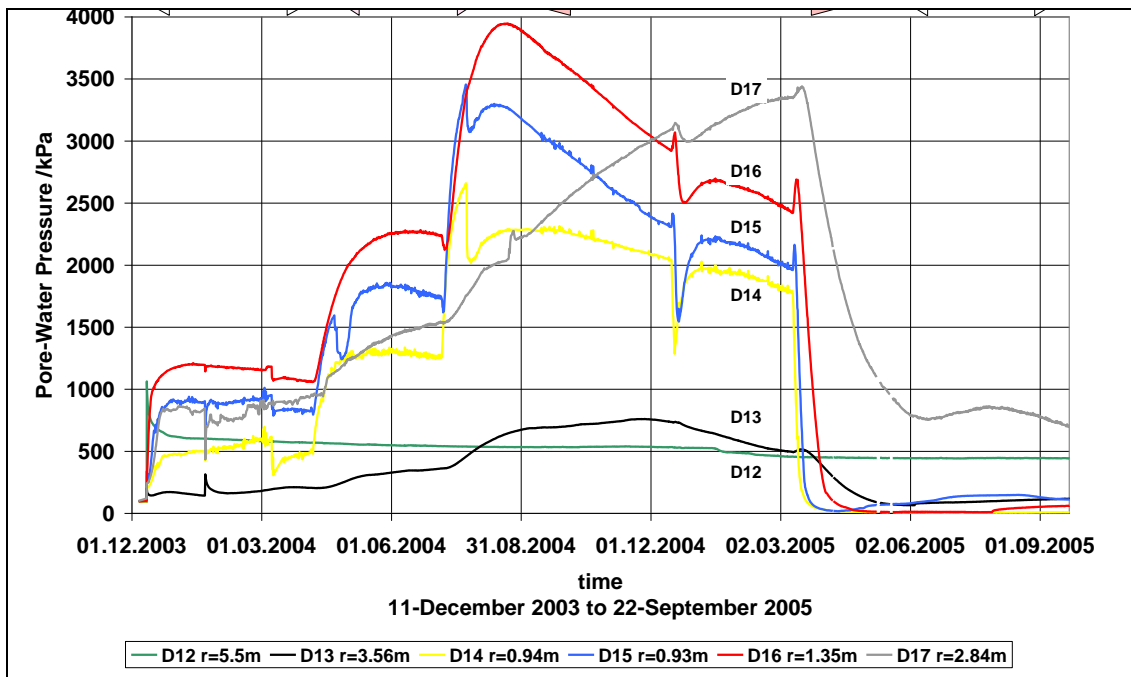


Figure 5.32: Pore pressure values in the sensors below heater number 2

Deformation of the rock mass surrounding the heater borehole was measured as axial extension in three subhorizontal or horizontal boreholes: normal to the heater, towards the centre (BHE-D6, Figure 5.35), normal to the heater but passing slightly below its centre (BHE-D5, Figure 5.34) and finally oblique towards the centre (BHE-D4, Figure 5.33).

The deformation time-series for the 3 extensometers are plotted as the difference between the fixed heads in the adjacent galleries and the base points in the rock. The oblique extensometer BHE-D4 records contractional deformation increments immediately after each increase in heating power, while later its axial direction keeps extending.

In the borehole BHE-D5 that passed below the heater only extension was measured. The deformation rates increased during at the beginning of the two heating steps. After heater shut down the deformations were reversed. Close to the heater contraction surpassed the initial state.

Deformations in the borehole BHE-D6 were much larger than in the other boreholes, and it has been speculated that the shotcrete layer bearing the headplate has detached from the rock during the experiment. This is in line with the observation that visible cracks opened in the MI niche during the excavation of the gallery 04 that took place at the end of the first heating phase (Wileveau, 2005).

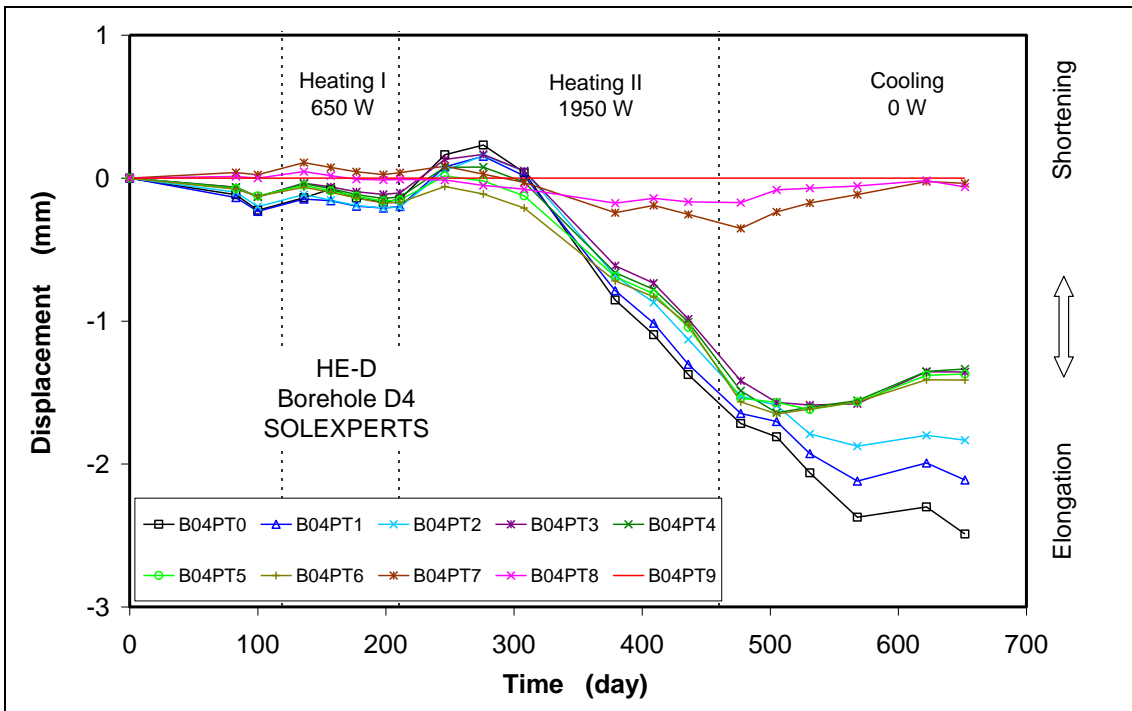


Figure 5.33: Axial deformation between the headplate and fixed points in the borehole BHE-D4

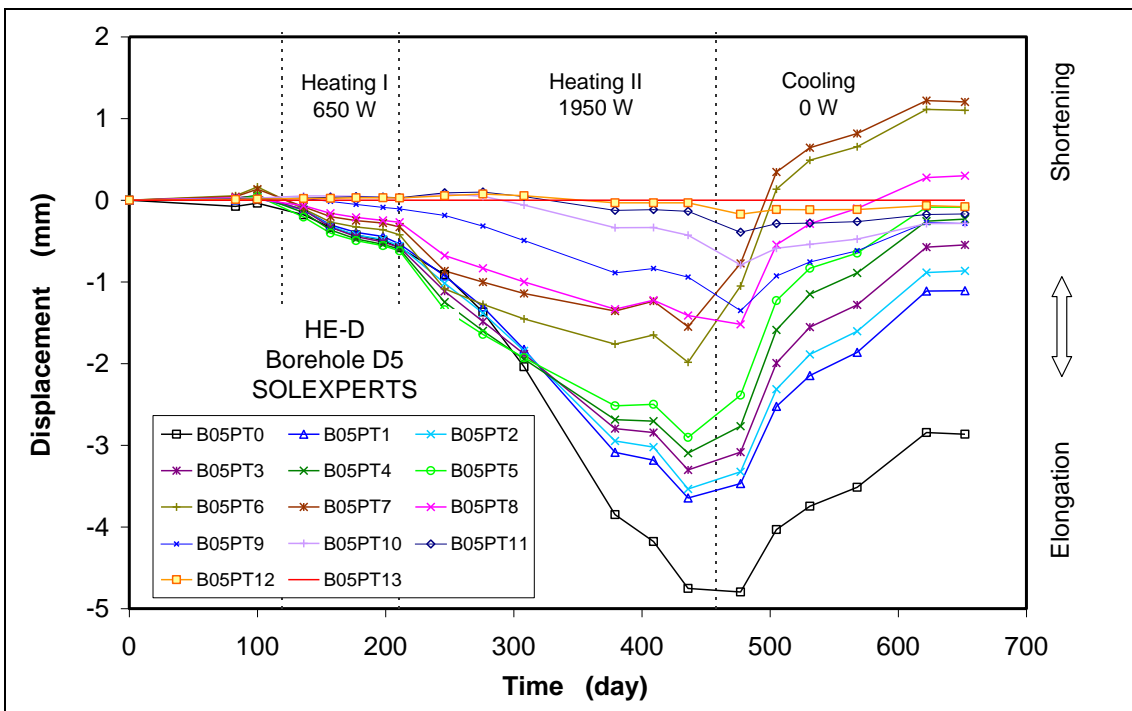


Figure 5.34: Axial deformation between the headplate and fixed points in the borehole BHE-D5

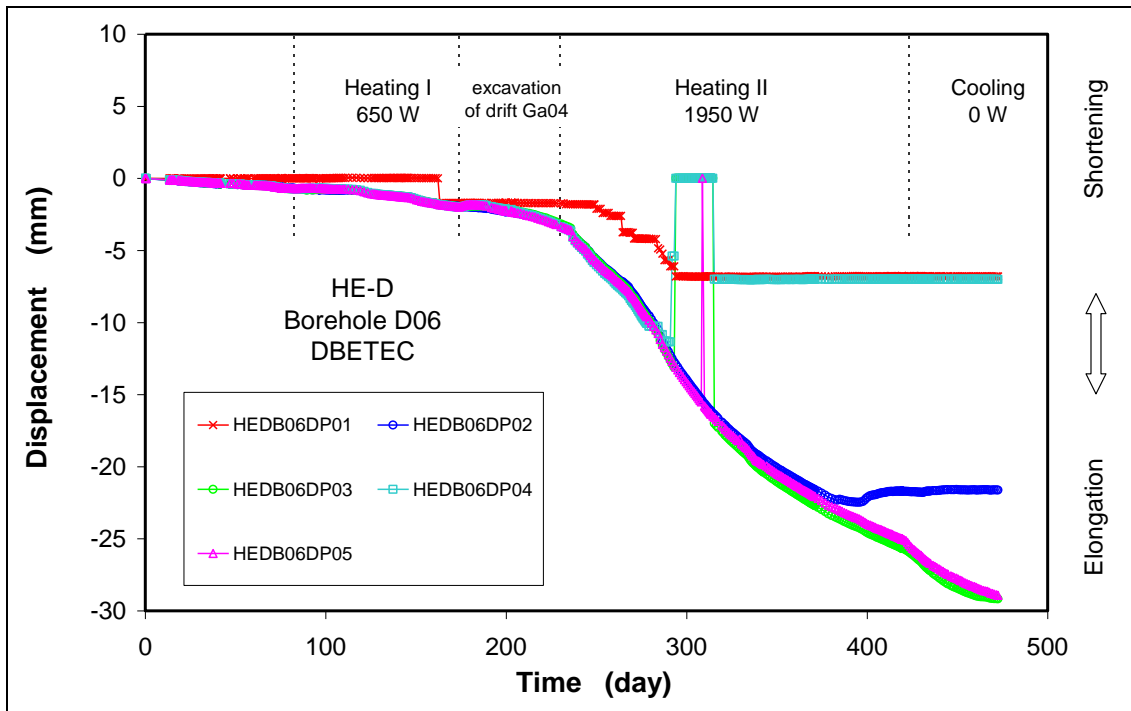


Figure 5.35: Axial deformation between the headplate and fixed points in the borehole BHE-D6

Pulse injection tests performed with mini packer systems after the end of the HE-D experiment were to investigate whether heating affects the permeability of the Opalinus Clay. It shows that the hydraulic conductivities are in the range of the undisturbed rock. However no test results are reported from the time prior to heating. Hence, these results require verification (Andra in prep.).

Modelling of the HE-D experiment at Mont Terri

The multitude of data that resulted from the HE-D test was analysed using various kinds of models. The results are reported in the modelling section. It shows that even with even heavily instrumented tests like the HE-D depend on modelling technology, modelling skills and modelling assumptions. All of which have some inherent range and / or uncertainty.

Thermal modelling of the HE-D experiment

CEA constructed a 3D thermal model of the niche including the temperature sensors. The comparison of model outcome and measured temperature evolution during the first 3 months of phase 1 were used to predict the heating power that was required to reach 100 °C at the rock/heater interface in phase 2. For that purpose the thermal properties of the Opalinus Clay were determined by back-analysis. It was assumed that Opalinus clay is an orthotropic rock with a 40° dip. The mechanical impact of the borehole (disturbance) is not taken into account and clay is considered to be fully saturated with water.

It showed that another parameter (called α) to account for a lower effective heat output of the heaters was required to fit the overall thermal behaviour of the experiment. At the current stage, that corrective coefficient does not have a well-identified physical sense

Subsequent sensitivity analysis showed that there is no unique selection to α and the values for the thermal conductivity of the Opalinus Clay. During the parameter-optimisation phase through the inversion method, both verification models ($\lambda_l = 2,03 \text{ W/m}\cdot\text{K}$, $\lambda_t = 1,03 \text{ W/m}\cdot\text{K}$, $\alpha = 0,77$ for the first, and $\lambda_l = 2,74 \text{ W/m}\cdot\text{K}$, $\lambda_t = 1,29 \text{ W/m}\cdot\text{K}$, $\alpha = 0,99$ for the second) fully reproduce the entire set of *in-situ* temperature measurements (Figure 5.37).

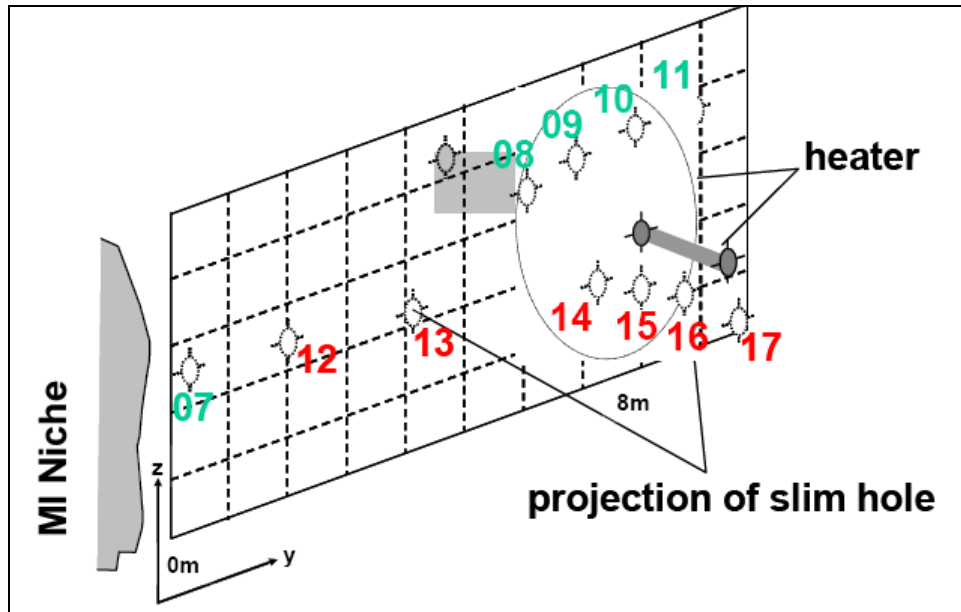


Figure 5.36: Location of pressure and temperature measurement points in GRS boreholes BHE-D7 to BHE-D17

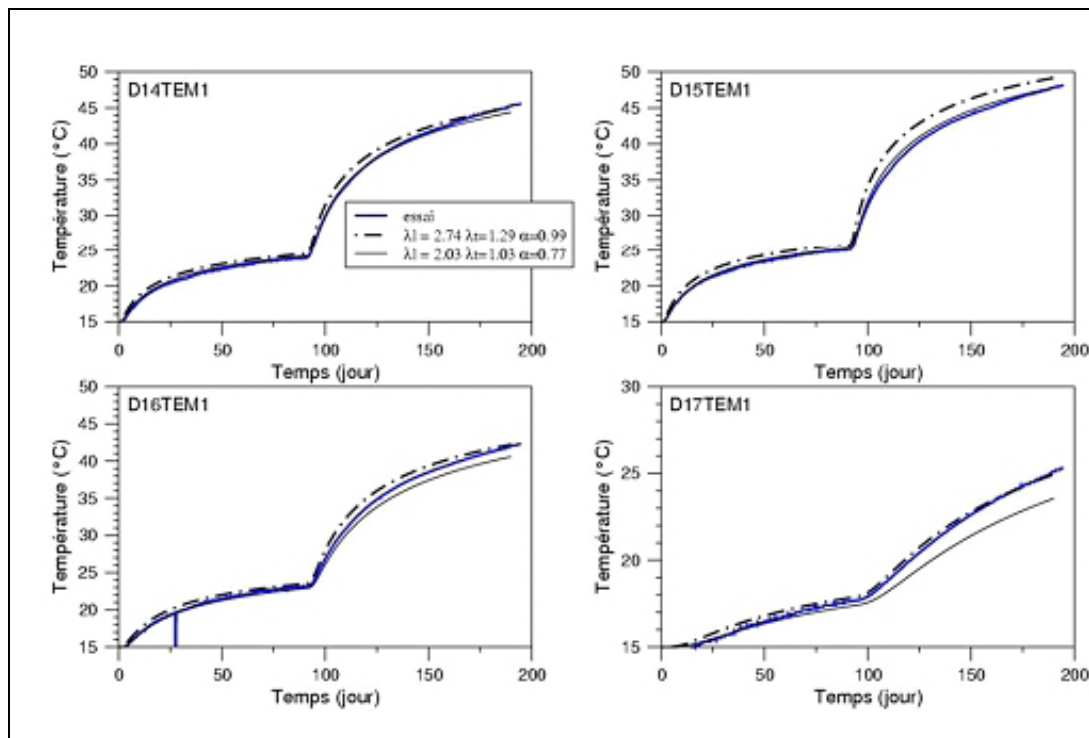


Figure 5.37: Model/data comparison for sensors D14, D15, D16 and D17 sensors for the two end-member data sets for thermal conductivity and effective heat output factor α

Coupled THM modeling of the HE-D experiment by DBE, GRS and UPC

Various modeling approaches were used in a first interpretation stage of the HE-D experiment to model the system behavior over the initial 200 days (Wileveau, 2005). The modeling approaches by GRS, DBE and UPS are summarized in Table 5.12.

The comparison of the model results with the measured data (Figure 5.38 to Figure 5.43) shows that the coupled models were able to reproduce quite accurately the thermal field of the experiment including the anisotropy of the rock properties. However, it proved more difficult to match the hydraulics and even more so the mechanical response of the system.

Table 5.12: Summary of model approaches for the HE-D experiment by GRS, UPC and DBE

Team	Code	Digital Model	Assumptions
UPC	CODE BRIGHT	Axissymmetric 2D geometry	<ul style="list-style-type: none"> Saturated THM Model Elastic Elasticity $E=6.3$ GPa and permeability $K=5E-13$m/s adjusted to results of drilling operations BHE-D0 No thermal or mechanical anisotropy Initial pressures adjusted to measured values: 0.9 MPa 20% decrease in heating power Average thermal conductivity $\lambda = 1.5 \text{ Wm}^{-1}\text{K}^{-1}$ Average thermal expansion $\alpha = 2.6 \text{ E-}5 \text{ }^\circ\text{C}^{-1}$ Solid grain expansion coefficient $\alpha_s = 9.6 \text{ E-}6 \text{ }^\circ\text{C}^{-1}$ Thermal expansion coefficient of water $\alpha_w = 3.4 \text{ E-}4 \text{ }^\circ\text{C}^{-1}$
GRS	CODE BRIGHT	Plane 2-D and axissymmetric 2-D geometry	<ul style="list-style-type: none"> Saturated THM Model Elastoplastic model, $E = 3.4$ GPa No thermal or mechanical anisotropy Initial pressures before drilling of heater borehole adjusted to 2D calculation: 1 MPa Average thermal conductivity $\lambda = 1.7 \text{ Wm}^{-1}\text{K}^{-1}$ Average thermal expansion $\alpha = 2.0 \text{ E-}5 \text{ }^\circ\text{C}^{-1}$ Solid grains linear expansion coefficient $\alpha_s = 2.0 \text{ E-}6 \text{ }^\circ\text{C}^{-1}$ Fitted thermal expansion coefficient of water $\alpha_w = 2.0 \text{ E-}4 \text{ }^\circ\text{C}^{-1}$
DBE	FLAC3D	3-D model	<ul style="list-style-type: none"> Saturated THM Model Elastoplastic model (Drucker-Prager) Thermal anisotropy No mechanical anisotropy Fitted thermal parameters: $\lambda_{//} = 1.7 \text{ Wm}^{-1}\text{K}^{-1}$, $\lambda_t = 0.8 \text{ Wm}^{-1}\text{K}^{-1}$ Adjusted permeability $K=5E-13$m/s with initial pressure distribution Thermal expansion coefficient of the matrix $\alpha = 1.5E-5 \text{ }^\circ\text{C}^{-1}$ Thermal expansion of solid grains $\alpha_s = 9.0 \text{ E-}6 \text{ }^\circ\text{C}^{-1}$

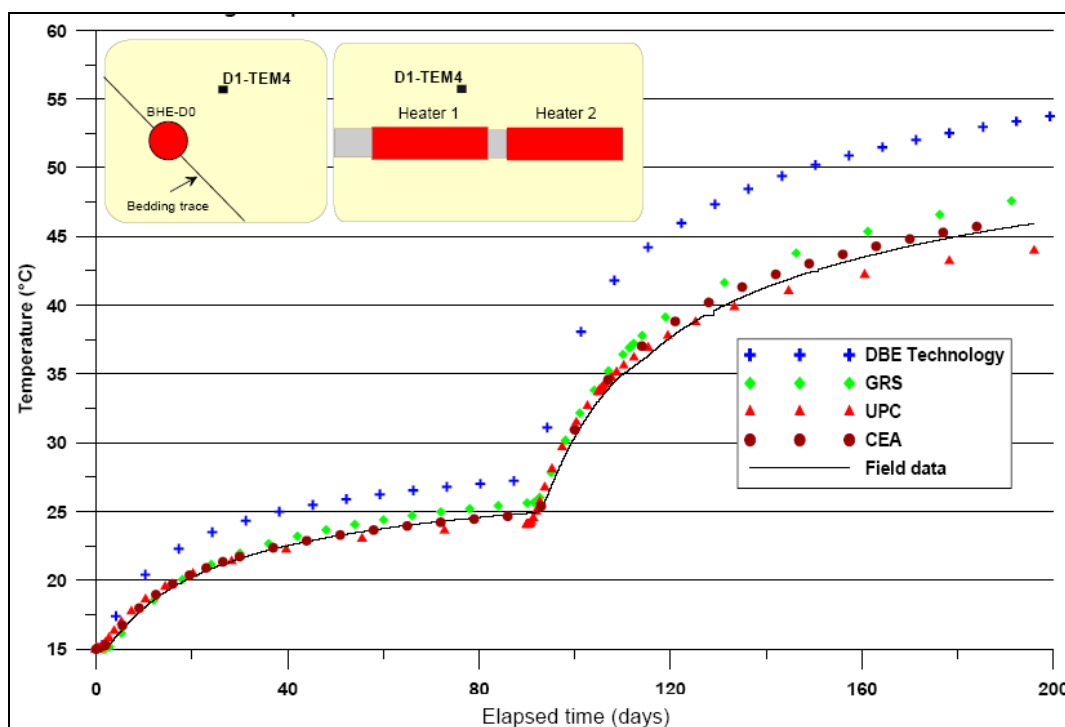


Figure 5.38: Model – field data comparison for sensor BHE-D1

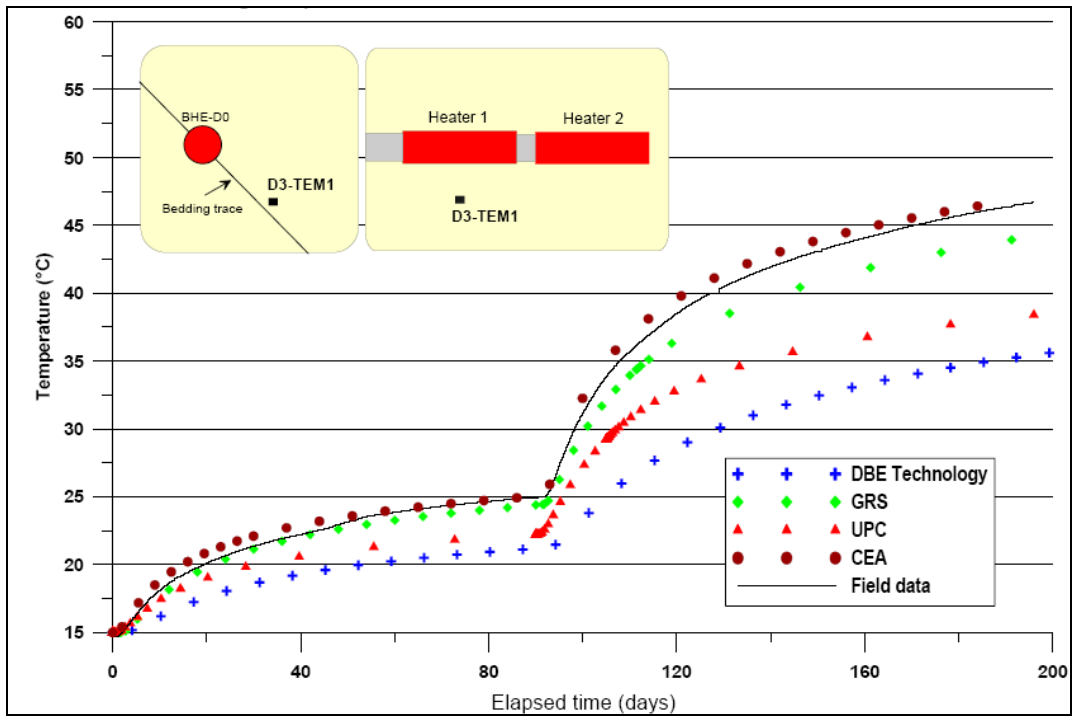


Figure 5.39: Model – field data comparison for sensor BHE-D3

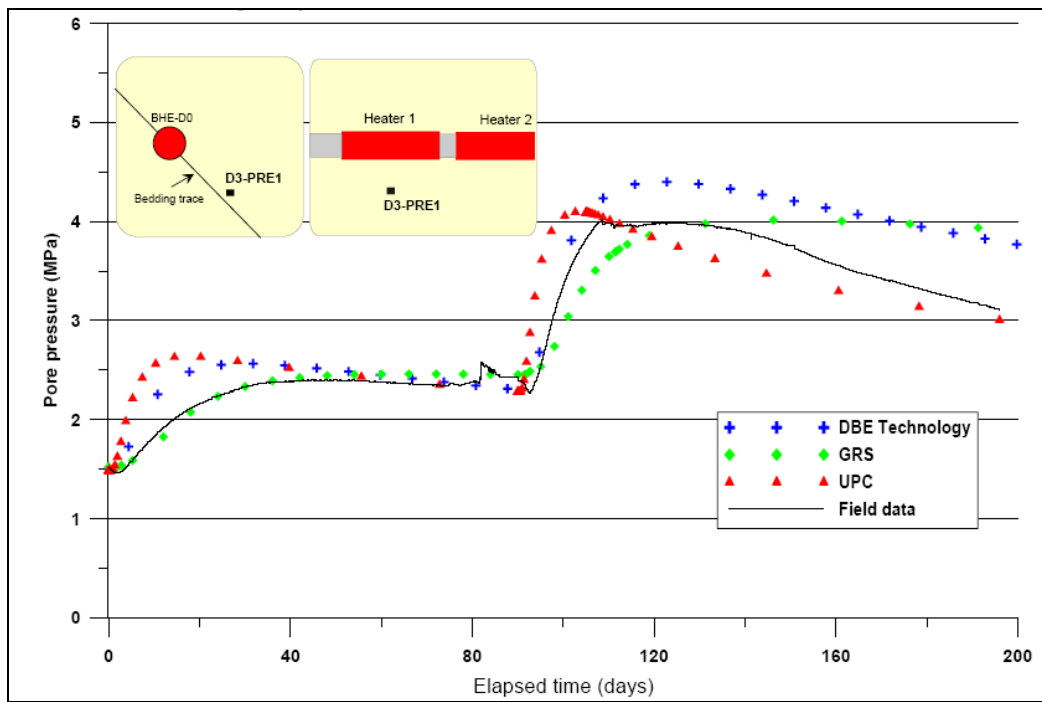


Figure 5.40: Model – field data comparison for pore pressure sensor BHE-D3-Pre 1

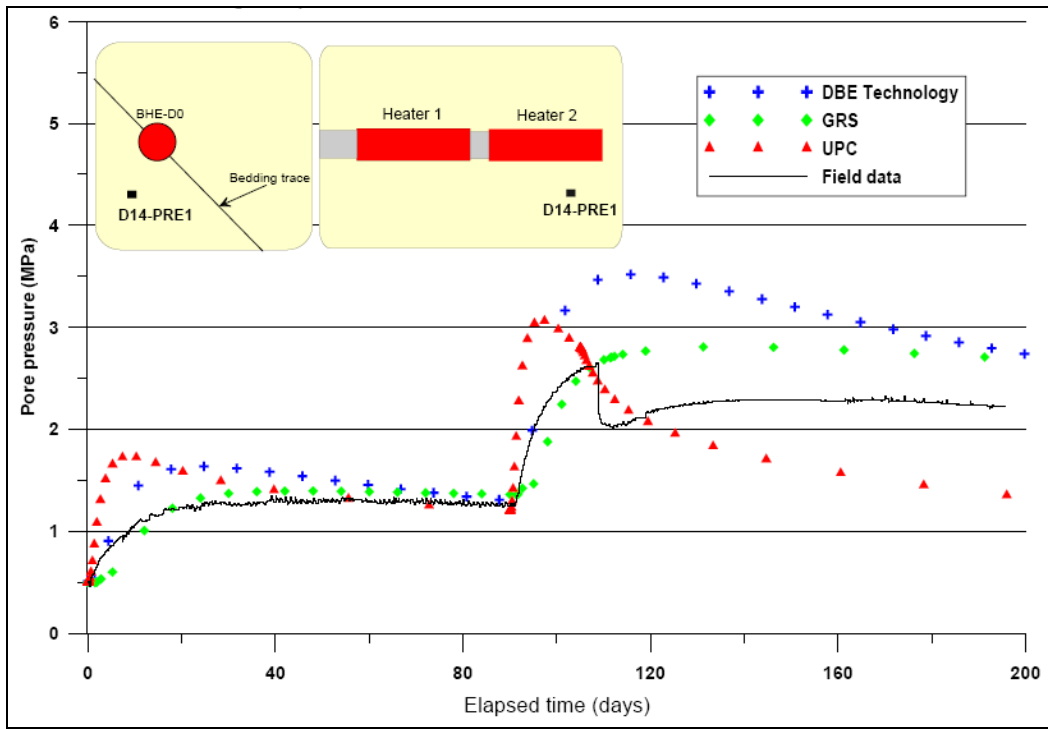


Figure 5.41: Model – field data comparison for pore pressure sensor BHE-D14-Pre 1.

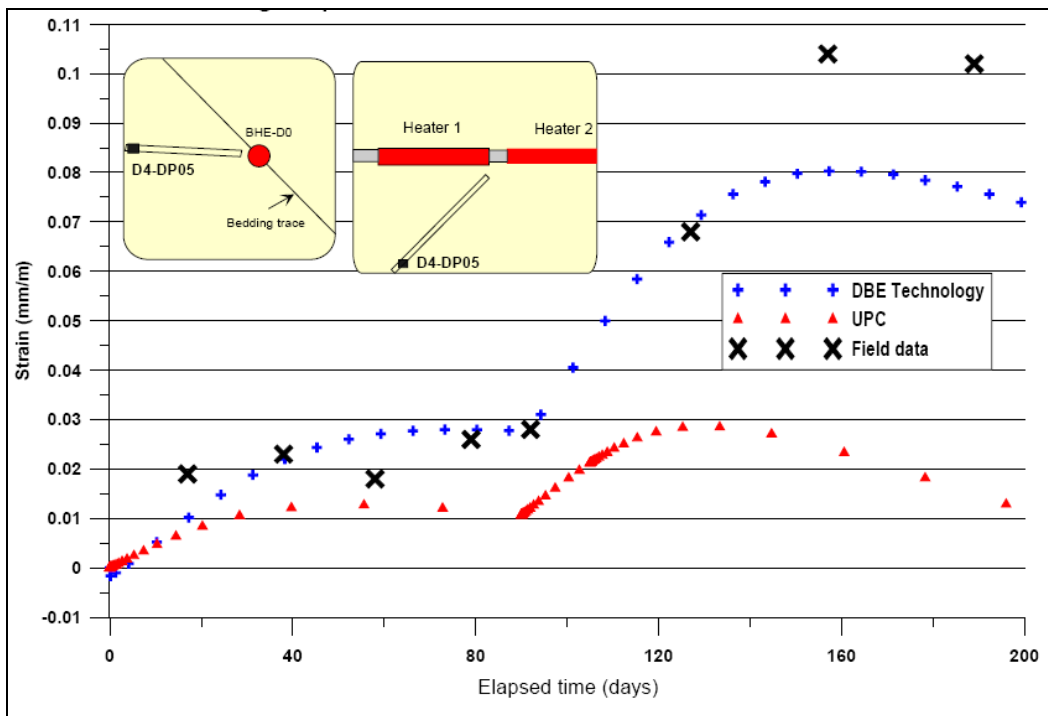


Figure 5.42: Model – field data comparison for extensometer BHE-D4-PT5

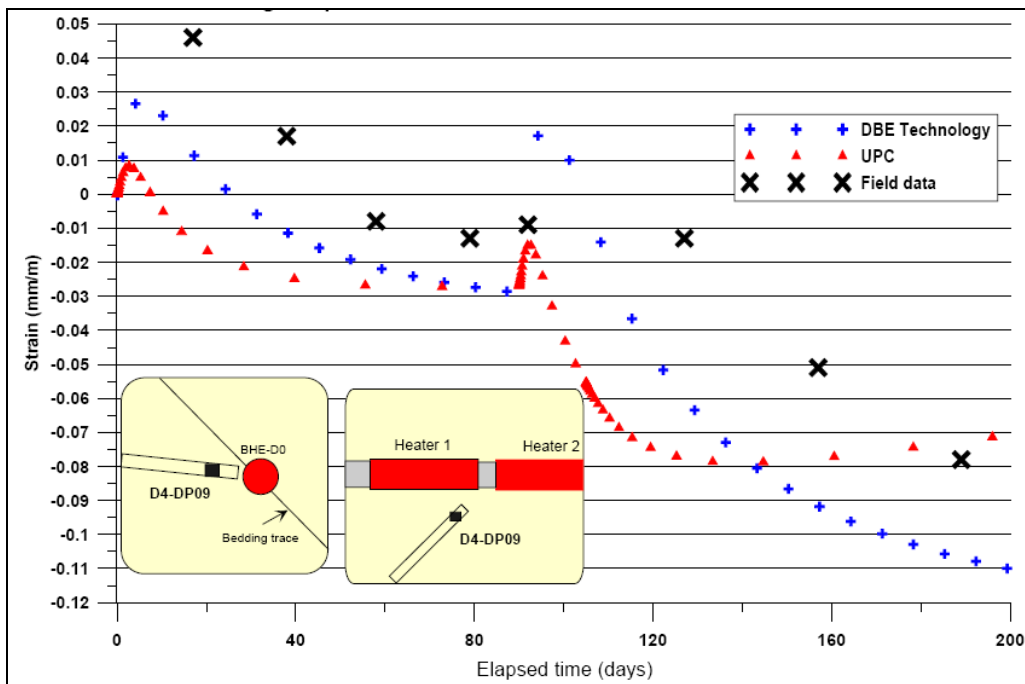


Figure 5.43: Model – field data comparison for extensometer BHE-D4-PT5

However preliminary conclusions of the modelling efforts have been presented by Wilevau (2005):

Temperature

The fit of the temperature curves with the observation data from the heater- rock interface is good (H1T1 and H2T2), except for the UPC model in which the temperatures are moderately overestimated. However, UPC only used a 2-D model. The rock temperatures predicted away from the heater are also in fairly good agreement with the data. The overestimates in a perpendicular direction (D1 TEM4) and the underestimates parallel to the bedding (D3- TEM1) by DBE suggests that their thermal anisotropy needs adjustment. Both 2D and 3D models are able to reproduce the thermal data by adjusting the thermal properties. However, only the 3-D anisotropic thermal model used by the CEA is able to fit the data at some distance from the heater. That model uses the power-decrease coefficient α , otherwise it requires a set of thermal conductivities significantly higher than those achieved on the argillite samples collected at Mont Terri. The reason for the power loss that α accounts for may be in the heater system itself or in the EDZ, but remains unclear at the moment. A reasonable combination of parameters for the thermal modelling appears to be $\lambda_{\text{normal}} = 2.1 \text{ W/m}\cdot\text{K}$;

$\lambda_{\text{parallel}} = 1.2 \text{ W/m}\cdot\text{K}$, $C_p = 860 \text{ J/kg}\cdot\text{K}$ at dry state and $20 \text{ }^\circ\text{C}$.

Hydraulic pressure

Pore-water pressures are adjusted to the hydraulic-pressure values measured at each point at the beginning of the heating process. The modelling results by the four teams are qualitatively correct. An overpressure phase is followed by a decrease of pressure. The peak values are correctly matched in BHE-D3 at around 4 MPa. UPC and DBE were able to reproduce the kinetics concerning the evolution of pore-water pressure, including its rise, its peak and its decrease. From that point of view, the results confirm the relative consistency of the THM-coupling parameters, such as permeability, thermal-expansion coefficient, Biot's coefficient, etc.

Deformation

For the points under study, the observed axial deformation trend of the installed extensometers is reproduced by the models: a compression phase followed by an extension phase occurring more or less rapidly according to the remoteness of the heat source. It should be noted that the data are consistent with the DBE model, that uses a ten times higher thermal expansion than the LAEGO model. Generally speaking, deformations appear not to be consistent with the lab determinations of thermal expansion. This may indicate that the geometry and mechanical boundary conditions of the HE-D experiment with the presence of access drifts and the MI niche are not well represented in the model. The thermomechanical deformations of the massif are affected by those structures and are difficult to model through simplified models.

5.4 Chemical aspects related to heating of the host rock

Significant chemical effects of heating in the host rock are not to be expected. Possible effects of heating are listed in the following table. An in-depth literature study of natural analogues and experimental data shows that neither of these effects is rapid enough to produce measurable effects within the thermal phase of the waste that spans a few hundred years (Mazurek, 2002). For instance the maturation of organic material is mainly controlled by the Temperature-Time-Interval (TTI) that the rock experiences Elie & Landais (2000). A brief comparison shows that the TTI of the thermal phase of the waste is 40 to 80 times smaller than the TTI of the geological burial. Hence the effect can be neglected. Similar reasoning applies for the illitization of the smectite layers. It has been pointed out in the basin analysis by Leu *et al.* (2001) that the Opalinus Clay has experienced 85° for at least 20 Ma in NE Switzerland. Investigations of the clay minerals show that smectite is still present in the rock (Mazurek 1998). This confirms numerical modelling results which show that the kinetics of the smectite-illite transformation are very slow and significant effects require Millions of years of heating.

Table 5.13: Possible chemical effects of heating on the host rock (Mazurek, 2002)

<i>Process</i>	<i>Possible Consequences</i>
Maturation of organic material	Production of gas, modification of pore water chemistry
Transformation of smectite to illite in composite clay minerals, cementation with SiO ₂	Loss of swelling capacity, embrittlement
Acceleration of oxidation	Mineral reactions, Modification of porosity and pore water chemistry
Re-adjustment of geochemical equilibrium reactions	Modification of porosity and pore water chemistry

5.5 Discussion

Uncertainty

Generally, large uncertainty accompanies the experimentally derived parameters for the rock. For example, the anisotropy factor for thermal expansion varies between 1 and 10. Due to the small number of samples it is not always clear whether the large range of parameters represent natural

variability, differences in test procedures or sample quality (sample disturbance by drilling, storage, subsampling, testing).

Modelling of the HE-D shows that the 3D models can be fitted to the observed temperature field by reducing the heat output to 80 % and by adjusting the two parameters for the thermal conductivity normal and parallel to bedding. This is the case because thermal properties in intact rock are only weakly dependent on the mechanical and hydraulic state (pore pressures) of the model.

However, modelling of strongly coupled processes involve larger uncertainties. Pore pressures generally show poorer fit to the observed values and deformations are still worse. The reasons for this observation may be manifold. The values applied for THM coupling may be incorrect or they may have systematic spatial variations which are not accounted for in the models e.g. an EDZ has not been implemented. Moreover, the real boundary conditions may not be well represented in the model and finally the concepts for THM coupling may be inadequate. For example the HM coupling in the fractured EDZ may be different from the continuum of the intact rock. This highlights the need for parameters from the damaged region around excavations that can be used for modelling. However, such experiments will have to keep in mind fracture network properties, scale and homogenisation issues both in experiments and models.

More tests with thoughtful chosen boundary conditions are needed. As one simple example, thermal expansion could be tested at different heating rates under drained boundary conditions.

Delineate the most important temperature-dependent material properties

Some important parameters of the rock appear to be strongly temperature dependent. For example the temperature dependence of strength is significant. However, the nature of the temperature dependence is little understood. It is not clear if lower strength and the moderately higher creep rates at higher temperatures result from temperature sensitive deformation processes (e.g. crack growth) or from increased pore pressures and consequently reduced effective stresses.

Define the most important coupled processes and parameters,

In the intact rock the temperature induced pore pressure rise (thermal diffusivity vs. hydraulic diffusivity) has to be considered. However, the data base for modelling such phenomena is insufficient and more experiments are required. Specifically tests are required that study the dependence of pore pressure on heating rate.

Furthermore temperature dependent strength is an important issue. It is desirable to have more data on creep rates and strength limits at elevated temperatures and to investigate the influence of temperature on the properties of existing faults.

Long term evolution of the tunnel nearfield will be controlled by the complex interaction of resaturation, backfill behaviour (swelling) and time-dependent deformation mechanisms in the host rock. All of these may be sensitive to elevated temperatures during the thermal phase of the radioactive waste. Important issues in the host rock EDZ appear to be the time and temperature dependence of fracture self sealing and the thermally induced growth of fractures. It should be noted however, that experimental test layouts should respect repository concepts. For example, during most of the thermal phase the nearfield will be desaturated. Hence, the properties of the desaturated material should be determined under the influence of heat.

Assess the effect of discrete fractures and fracture connectivity on the effective hydraulic properties

The major changes in the hydraulic properties of the host rock in the nearfield of excavations in the Opalinus Clay (Martin and Lanyon *et al.*, 2004; Marschall, 2004) are mostly a result of localized deformation i.e. the formation of fractures. Hence, the importance of the fractures, namely their geometry, their distribution and their interconnectedness cannot be overemphasized.

In contrast, for the intact rock fractures play a small roll. The hydraulic properties of tectonic faults have been shown to be indistinguishable from the intact rock. So within the host rock they can even be neglected in terms of hydraulic properties.

Importance of chemical impact

For the Opalinus Clay chemical effects of heating can be neglected. All possible effects are too slow to have significant impact in the host rock.

Derive the most appropriate conceptual models and evaluate the most appropriate numerical code

Beyond the EDZ in the intact rock, the continuum assumption holds and any anisotropic elastic FE code will be able to model the coupled processes quite adequately. The HE-D experiment shows that elastic modelling as done by UPC (Wileveau, 2005) can account for the general deformation trends. Things may be different in the vicinity of excavations. Here, fracture generation due to strain localisation have a large impact on properties and thus need to be included into modelling. Continuum models have a poor record of doing so. Hence, scale issues need to be taken into account.

6 Thermo-hydro-mechanical behaviour of Callovo-Oxfordian argillite

6.1 Main characteristics

6.1.1 Geological setting

The Meuse / Haute-Marne site is located in Eastern France, on the boundary between the Meuse and Haute-Marne departments. Geologically, it is part of the eastern region of the Paris Basin (Figure 6.1).



Figure 6.1: Geological location of the Meuse / Haute-Marne site within the Paris Basin

In this region, the Paris Basin is composed of alternating sedimentary layers (predominantly argillaceous) and limestone layers, deposited in a stable marine environment during the Jurassic, between 165 and 135 million years ago. These layers have a simple and regular geometric structure, slightly dipping towards the northwest (1.5 to 2 degrees) in accordance with the general structure of the Paris Basin (bowl-shaped structured centred in the Paris area).

Within the sedimentary sequence, the Callovo-Oxfordian layer has been selected for the repository feasibility study (Figure 6.2). It is surrounded by two geological formations (underlying Dogger and overlying carbonated Oxfordian) containing water-bearing sedimentary horizons with low permeabilities and slow runoff (approximately one kilometre per hundred thousand years for the Darcy water velocity)

The structural framework is stable, with natural stresses oriented in a stable manner for the past 20 million years. The site is located apart from large regional faults such as the Marne fault towards the southwest (Figure 6.2).

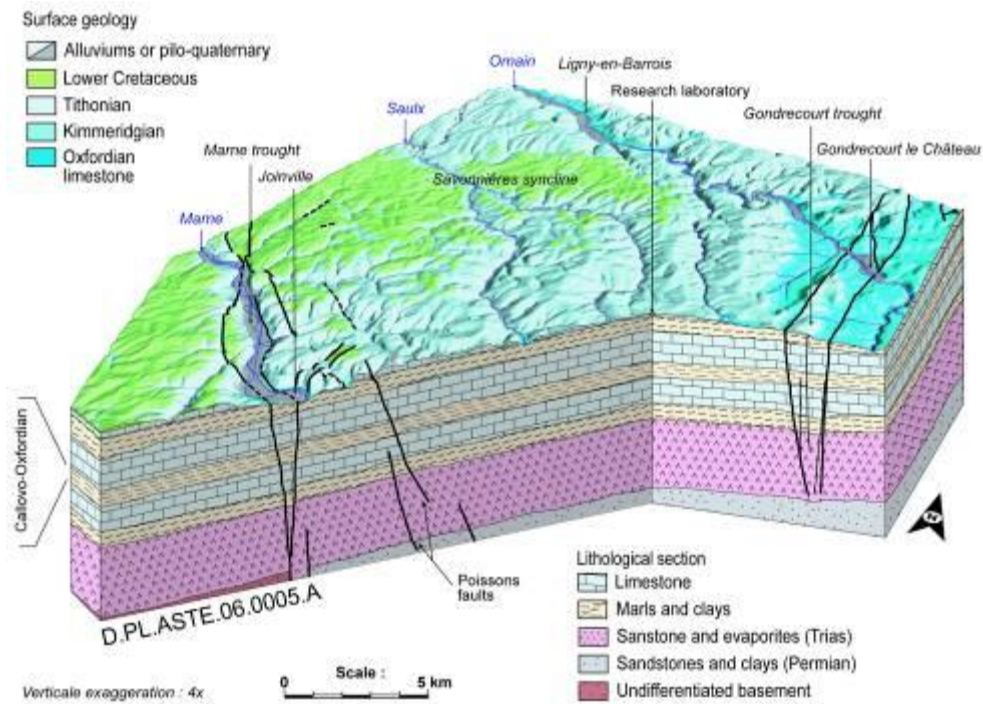


Figure 6.2: 3D geological block diagram of the Meuse / Haute-Marne site

From a seismotectonics perspective, the Paris Basin is a stable zone with very low seismicity, remote from active zones such as the Rhine Graben towards the east, the Alps (southeast), the Massif Central (south) and the Armorican Massif (west). There is no detectable neotectonic activity or significant local seismic activity through the Meuse / Haute-Marne site.

The Callovo-Oxfordian formation is at least 130 meters thick. It consists of clay mineral representing up to 60 % of its mass, as well as silts (fine quartzes) and carbonates, and is laterally homogeneous. The 3D seismic data obtained on the URL site show no fault with a vertical throw exceeding 2 meters within the layer. Directional boreholes confirm the absence of secondary (subseismic) faults. Moreover, only a few microfissures, stable and not affecting water flow, have been observed in over 4 km of core samples, and some of them are sealed with sulphates (celestine), which is indicative of a precociously tight formation during the compaction of deposits.

The characteristics of the Callovo-Oxfordian layer have been acquired shortly after its deposition. The layer has subsequently remained undisturbed, as indicated by Sr and $\delta^{13}\text{C}$ isotopic markers, geological thermometers (maximum palaeotemperature of approximately 40 °C) and the near absence of minerals formed at a later date (beyond 10 million years).

6.1.2 Mineralogy and porewater chemistry of the Callovo-Oxfordian argillites

Vertically, the proportions of the main mineralogical phases vary and are structured into three sedimentary sequences. The upper sequence is characterised by higher carbonate content. The Callovo-Oxfordian argillite resembles tectosilicates (essentially quartz) and carbonates (essentially calcite) embedded in a fine matrix formed out of swelling and non-swelling phyllosilicates (clay minerals) that contain a small quantity of organic matter and sulphides (0.5 to 1% each). The morphology of the minerals is representative of two distinct origins:

- detrital minerals settled by marine sedimentation (quartz, carbonated bioclasts, clay minerals),
- calcite precipitated on site in the sea or remobilized after deposition.

The clay minerals constituting the matrix consist of illite, interstratified illite/smectite, chlorite and from kaolinite. They are assembled in the form of aggregates a few microns in size. The lower part

of the Callovo-Oxfordian is marked predominantly by R1 interstratified illite/smectite (ordered I/S with 20 to 40 % of swelling smectic layers). An abrupt transition was systematically identified in all boreholes towards the upper part of the argillites with a predominance of R0 interstratified illite/smectite (disordered I/S, with 50 to 70 % of swelling smectic layers).

The total porosity of the argillites is around 15 to 18 %. The pores have an average size of 50 nm, what implies that half the porosity is occupied by bound water.

Owing to these textural properties, permeability of the argillites is low within all the formation. Based on the various measurements carried out on samples and in situ, permeability ranges from 5.10^{-14} to 5.10^{-13} m/s.

The diffusion coefficient values are also low, particularly for anions, which undergo an electrostatic repulsion within the smaller pores due to the existence of negative charges on the clay mineral surfaces. The effective diffusion (D_e) coefficient values have been assessed at:

- $D_e = 5.10^{-12}$ m²/s for an accessible porosity value of 5% in the case of anions,
- $D_e = 2.5.10^{-10}$ m²/s for an accessible porosity value of 18 % in the case of cations.

The natural tracer profiles (³⁷Cl, ¹¹B, ⁴He) and the marked differences in chloride concentration between the base of the carbonated Oxfordian and the roof of the Callovo-Oxfordian confirm the presence of slow solute transport processes.

The argillaceous mineralogical composition of the argillites gives the Callovo-Oxfordian formation high retention capabilities for cations.

Different water salinities have been observed in the Callovo-Oxfordian and surrounding formations, 3 to 4 g/l in the argillite porewater (see Table 6.1:most probable water composition (and plausible alternative) of Callovo-Oxfordian argillites at the Bure URL), around 4 g/l in the Dogger, and 0.9 g/l in the calcareous Oxfordian. High salinity of the interstitial water in the Callovo-Oxfordian indicates an absence of hydraulic exchanges with water-bearing formations. It confirms the low permeability of the argillites and the very slow displacement of ions in solution.

Table 6.1:most probable water composition (and plausible alternative) of Callovo-Oxfordian argillites at the Bure URL

parameters	reference	alternative
Eh (mV)	-156	-180
pH	7,0	7,3
ionic force (mol/l)	0,12	0,09
Alkalinity (meq/l)	$2,5. 10^{-3}$	$1,4. 10^{-3}$
Cl (mol/l)	$3,0. 10^{-2}$	$1,5. 10^{-2}$
S(VI) (mol/l)	$3,4. 10^{-2}$	$3,1. 10^{-2}$
Na (mol/l)	$3,2. 10^{-2}$	$2,6. 10^{-2}$
K (mol/l)	$7,1. 10^{-3}$	$6,2. 10^{-3}$
Ca (mol/l)	$1,5. 10^{-2}$	$1,1. 10^{-2}$
Mg (mol/l)	$1,4. 10^{-2}$	$1,1. 10^{-2}$
Fe (mol/l)	$3,3. 10^{-4}$	$7,1. 10^{-5}$
Si(aq) (mol/l)	$9,4. 10^{-5}$	$9,4. 10^{-5}$

6.1.3 Mechanical properties of the Callovo-Oxfordian argillites

Finally, the argillites have mechanical properties favouring the feasibility of underground engineered structures at the depth of the Callovo-Oxfordian layer in the transposition zone (simple compression resistance > 21 MPa) and also significant thermal properties (thermal conductivity of between 1.4 and 2,7 W.m-1.K-1, depending on the stratigraphy).

Based on the position of the underground research laboratory, one defines a transposition zone within which the Callovo-Oxfordian layer has physical and chemical properties similar to those observed at the laboratory (Figure 6.3). Its surface area is approximately 250 km². The depth of the Callovo-Oxfordian roof varies from 420 m at the underground research laboratory to over 600 m along the dip direction, and the thickness of the layer varies from 130 m at the laboratory to 160 m towards the north.

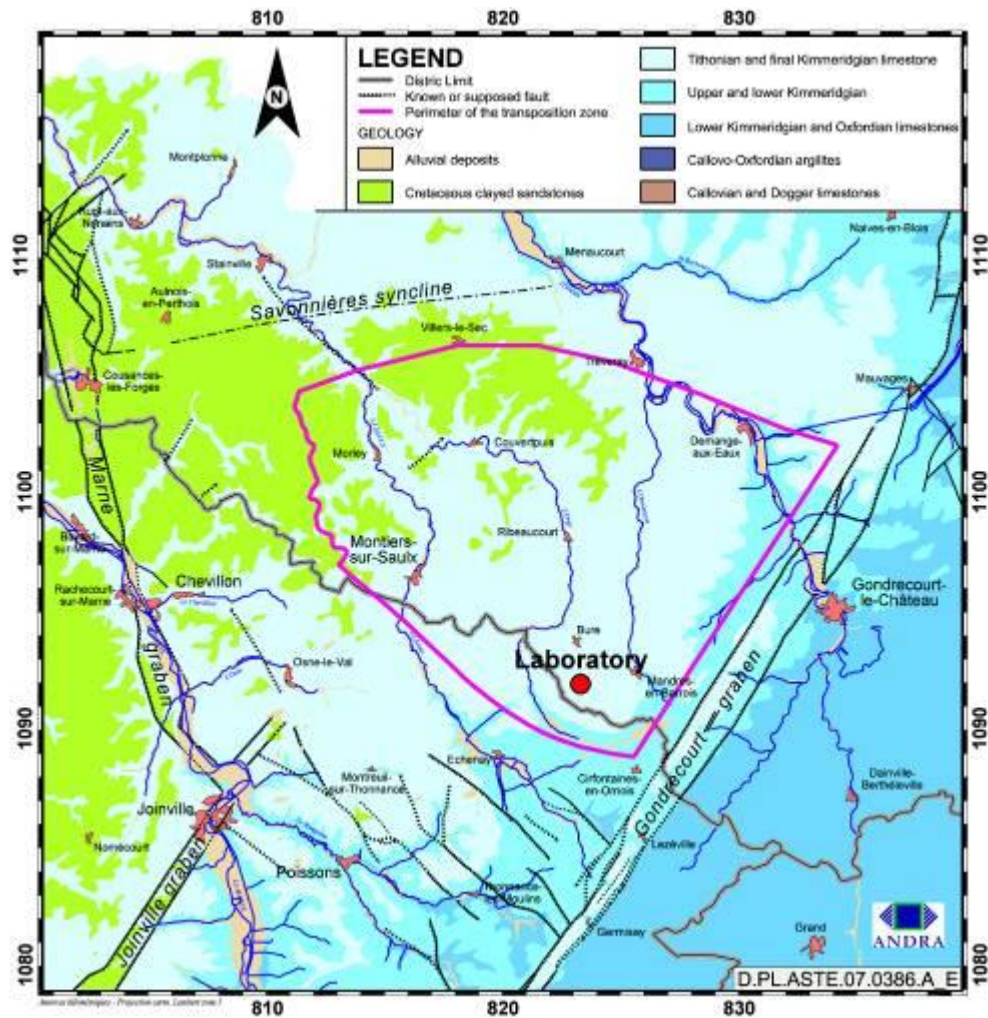


Figure 6.3: Perimeter of the transposition zone around the Meuse / Haute-Marne site

6.1.4 Thermal conductivity

Thermal conductivities of argillites have been either calculated on the basis of the thermal-diffusivity measurements taken on cores from boreholes EST104 and HTM102 through the “flash” method (Homand, 1998) or measured directly through the “divided-bar” method (GdR ForPro, 2002).

Results show an obvious correlation between thermal conductivity, porosity and mineralogical composition. For this reason, there are significant differences in thermal conductivity of the Callovo-Oxfordian argillites within the formation (Su, 2002a), as follows (Figure 6.4 and Figure 6.5).

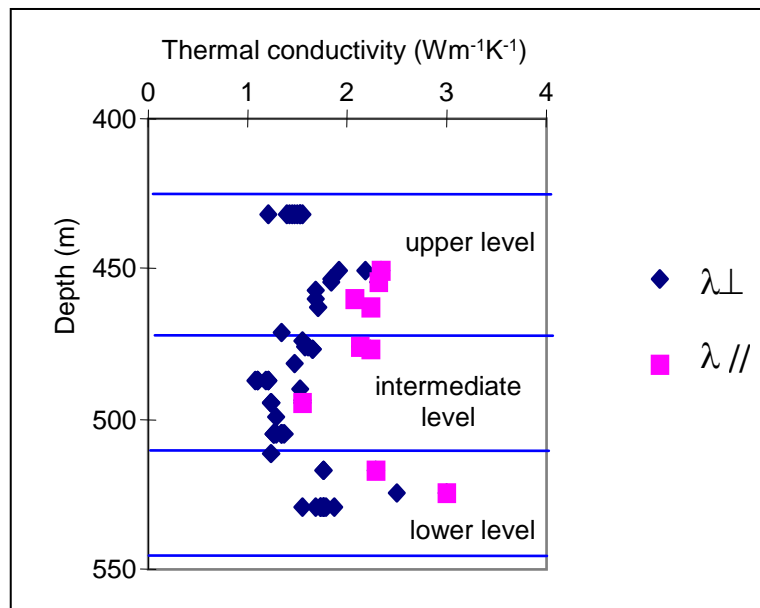


Figure 6.4: Vertical evolution of thermal conductivity as measured on samples from boreholes EST104 and HTM102 (François, 1998)

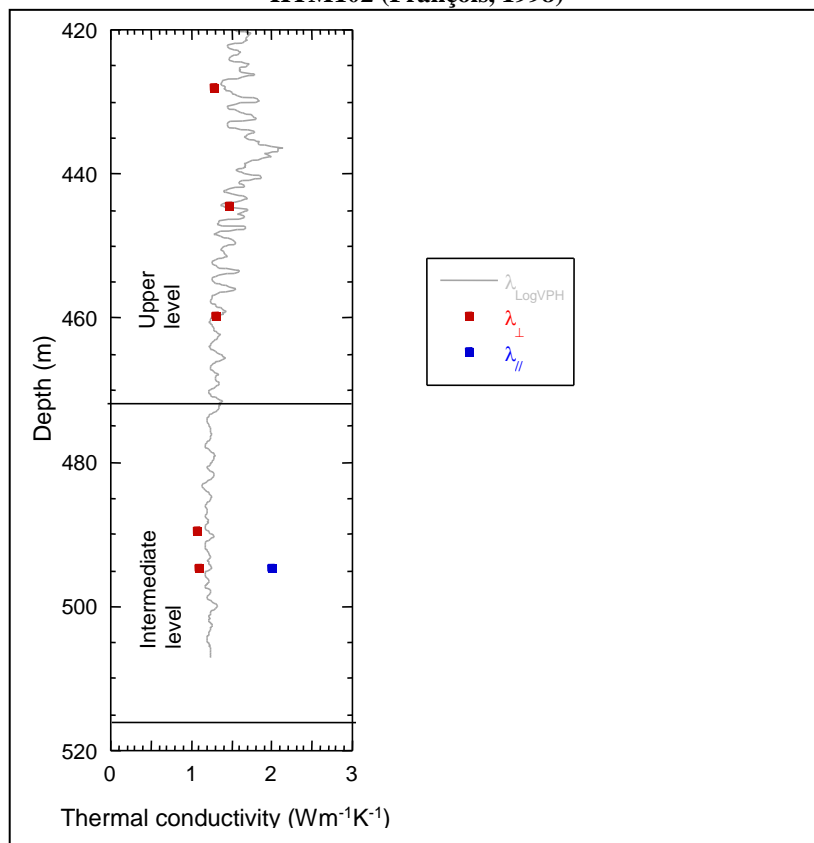


Figure 6.5: Vertical evolution of thermal conductivity of Callovo-Oxfordian argillites as measured on samples from borehole EST205 (GdR ForPro, 2002)

All upper horizons are siltier (maximum quartz concentration: 38 %) and more carbonated (maximum calcite concentration: 38 %): their thermal conductivity is very high. Those values result from the thermal conductivity of quartz, which is twice as high as pure calcite, considering the fact that the thermal conductivity of the latter is already double that of clay minerals. Furthermore, the porosity of that zone is less significant, thus causing an increase in thermal conductivity. The average parallel and perpendicular thermal conductivities to the stratification amount to 2.2 and 1.6 W/m/K, respectively.

The central horizon corresponds to the maximum-clayiness zone. It is characterised by the lowest conductivity values of the host formation. The homogeneity of the resulting thermal conductivities demonstrates the homogeneity of the silto-carbonated argillites of that unit (Su & Yven, 2003). Parallel and perpendicular conductivities to the stratification amount to 1.9 W/m/K and 1.3 W/m/K, respectively.

All lower horizons of the Callovo-Oxfordian formation show the highest conductivity values. They include a thin carbonated episode of several metres in thickness, which induces a lower average porosity and, consequently, a higher thermal conductivity.

6.1.5 Specific heat

The specific-heat of argillites was measured on samples from borehole EST104 (François, 1998). The specific heat of saturated argillites varies only slightly with depth.

At 20 °C, it reaches an average of 1,096 J/kg/K. The highest values are found in the carbonated beds (i.e., 515-527 m for borehole EST104).

At 100 °C results are more dispersed. The dispersion coefficient (standard deviation/average) reaches 10 to 15 %. The variability on clay and carbonate concentrations between the different horizons may explain in part such dispersion.

6.2 Thermohydrromechanical characterisation in laboratory

6.2.1 Observation of temperature impact on samples

Impact of temperature on the mechanical behaviour over the short term

The impact of temperature on the short-term mechanical behaviour was studied through uniaxial-compression tests (three tests at ambient temperature and eight tests at higher temperatures) and triaxial-compression tests (nine tests at ambient temperature and 35 tests at higher temperatures) with temperatures as high as 100 °C.

Test results do not indicate any impact of temperature on the strain modulus of the Callovo-Oxfordian argillites, within the spectrum of tested temperatures ($T < 100$ °C) (Figure 6.6) (Bauer, 1997).

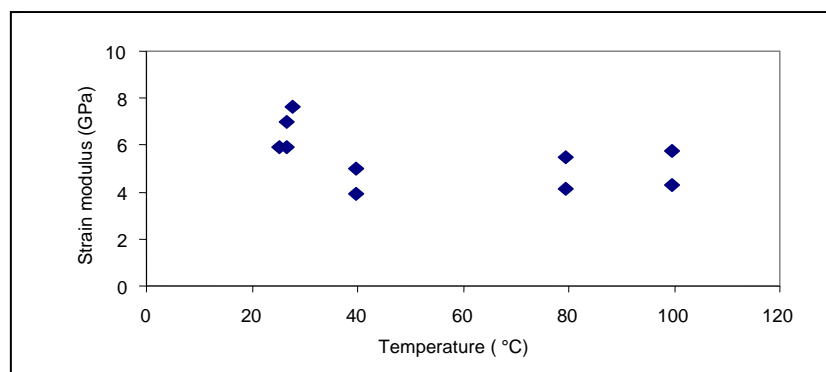


Figure 6.6: Evolution of the deformation modulus in relation to temperature as obtained under uniaxial compression (Bauer, 1997).

The rise in temperature can lead to a reduction of argillite strength. UCS is 30 % less when temperature reaches 80-100 °C (Figure 6.7), but no net reduction is visible under triaxial compression (Figure 6.8). Those results must be put in perspective with the small number of tests and their broad dispersion.

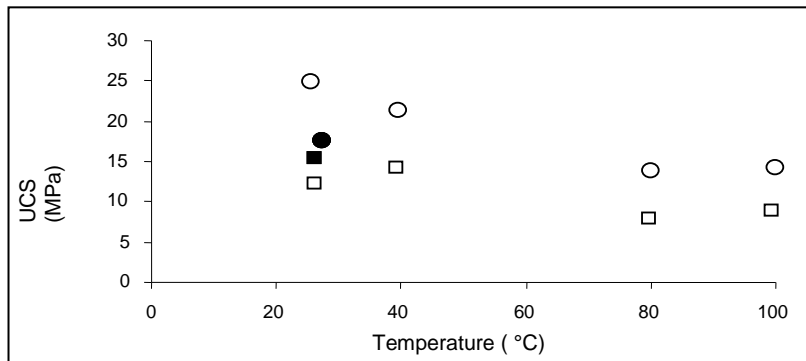


Figure 6.7: Evolution of resistance to uniaxial compression in relation to temperature (samples from borehole ST104, depth: ○ - 472-474 m; □ - 502-505 m; ● ■, pre-heated samples at 100 °C) (Bauer, 1997).

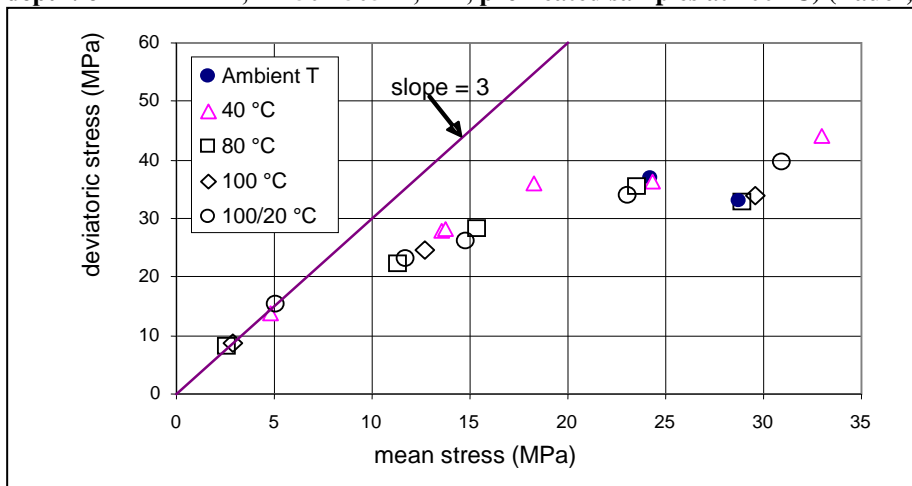


Figure 6.8: Evolution of resistance to triaxial compression in relation to temperature (samples from borehole EST104, depth: 502-505 m) (Bauer, 1997)

Beyond the rupture the argillites behave as more ductile during triaxial tests when the temperature reaches 80-100 °C.

The influence of a thermal cycle was analysed by mean of 15 triaxial tests carried out at ambient temperature on pre-dried samples at 100 °C. Results show that:

- moduli of dried samples tend to be slightly higher than those measured on non-dried samples when the water content of argillite is above 6.2 %. No net tendency was noticeable on other samples;
- no influence of temperature on rupture and damage characteristics was detected.

In conclusion, no study carried out until now has ever detected any significant impact of temperatures up to 100 °C on the mechanical characteristics of deformability, strength or damage. Either that impact, if it exists, is low enough to be obliterated by the dispersion of results, or the number of available tests is not sufficient to reach a sound conclusion (as in the case of the reduction of strength at 80-100 °C).

Impact of temperature on the mechanical behaviour over the long term

Since 1994, Antéa and G3S-LMS have conducted several creep-test campaigns under specific temperature conditions (Antea 1999 ; Gasc 2002; Gasc & Malinsky 2002 ; Chanchole 2004). Those campaigns include uniaxial, triaxial, mono-stage and multi-stage tests.

The key result is that the creep rate increases with temperature (Figure 6.9 and Figure 6.10). It is practically multiplied by a factor of 1.5 when temperature increases by 30 °C (from 20 °C to 50 °C) and by a factor of about 3, on average, when temperature increases by 60 °C (from 20 to 80 °C) (Figure 6.10b, Gasc 2002).

Multi-stage tests at a constant temperature of 80 °C show that the creep rate varies between $3.5 \cdot 10^{-11}$ and $3.5 \cdot 10^{-10} \text{ s}^{-1}$ depending on the value of the deviator and on the timescale. However, as shown in Figure 6.7a, even under these temperature conditions the creep rate is progressively cancelled over time for deviator values less than or equal to 10 MPa, but remains at a value of about 10^{-10} s^{-1} for a 15 MPa deviatoric stress.

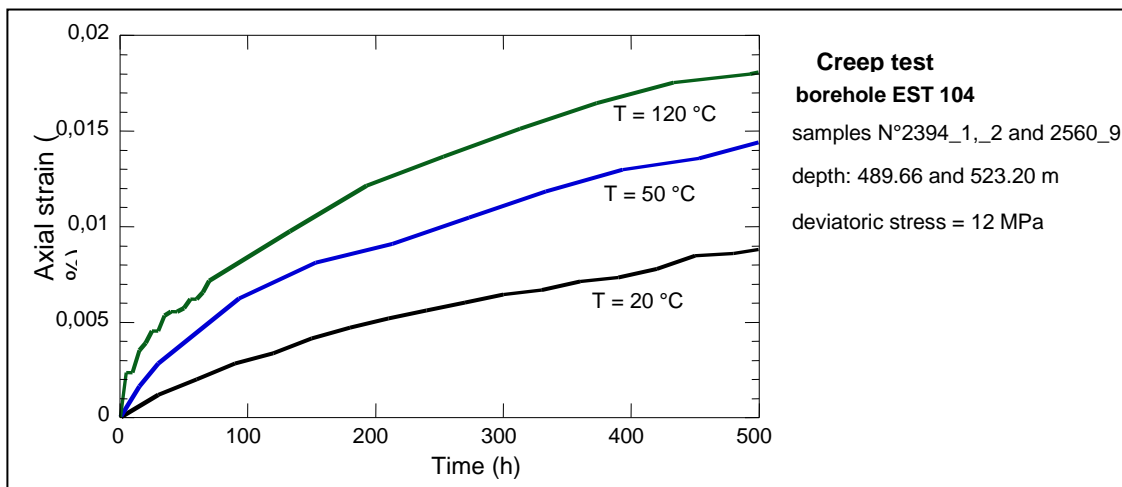


Figure 6.9: Impact of temperature on creep tests with a 12-MPa deviator, (borehole EST104, geomechanical units C and E (Gasc, 1999))

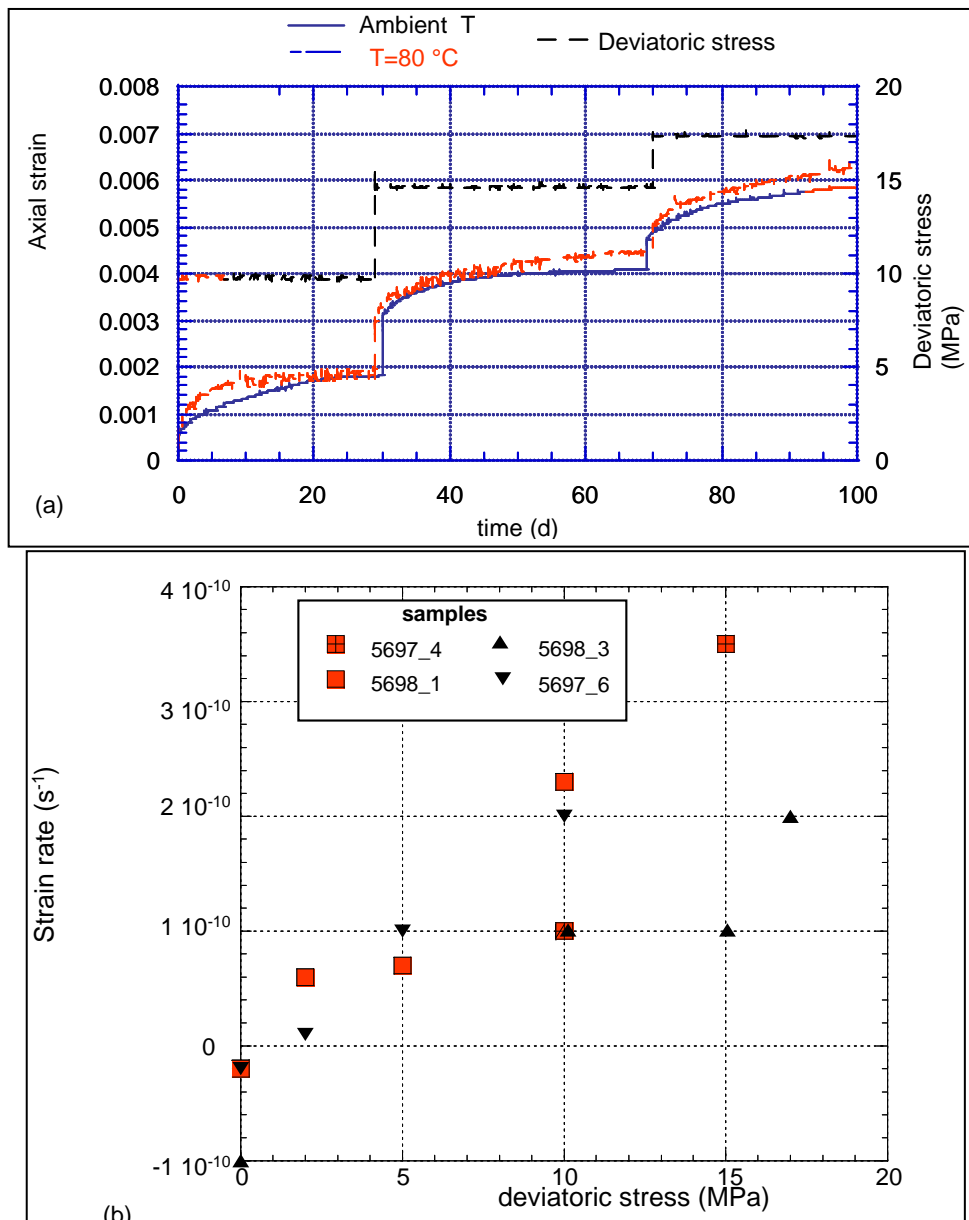


Figure 6.10: Impact of temperature on creep – a) axial deformation over time for three deviators at ambient temperature and at 80 °C; b) synthesis of strain rates versus deviatoric stress at two temperatures (black triangles : ambient, red squares: 80 °C), (borehole EST205, geomechanical unit C)

Whatever the temperature, all the creep tests can be interpreted by a Lemaître model. The impact of the temperature on the creep rate is taken into account by the mean of the Arrhenius law, which is frequently used for viscoplastic rocks.

Pore overpressure induced by thermo-hydrromechanical coupling

Generally speaking a temperature increase within a slightly permeable porous medium induces a pore overpressure. In order to magnify that coupling effect, a fracturing test by thermal overpressure was performed on argillite samples (Su & Bounenni, 1998).

The test consisted in placing a cylindrical 24-mm diameter and high argillite sample in a microwave oven in order to raise the temperature evenly and rapidly throughout the sample. The sample surfaces are free to strain. The sample temperature is monitored by an infrared camera.

Tests show that rupture by overpressure is brutal, and even explosive, under such test conditions. The heating time before rupture is about 2 s with a heating power of 700 W (full power of the microwave oven being used).

Coupled analytical thermal and THM calculations (Su & Bounenni, 1998) show that the temperature of the sample after 2 s of heating in the microwave oven is about 70 °C, and the pore pressure induced at that time is about 2.1 MPa. Calculations using Biot poro-mechanical coupling parameters lead to an effective tensile stress of 1.3 MPa (for $b = 0,6$), which corresponds to the tensile strength of the argillites.

The test shows that fracturing by overpressure resulting from a THM coupling is possible in argillites under certain thermal, hydraulic and mechanical conditions.

Thermomechanical and thermohydraulic-coupling parameters in argillites

In porous-media mechanics, the key parameters characterising thermomechanical (TM) and THM couplings are:

- the drained linear thermal dilatation coefficient, α_0 ;
- the differential thermal dilatation coefficient, α_m ;
- hydro-mechanical coupling parameters: Biot coefficient (b) and Biot modulus (M).

The thermal-dilatation coefficients were measured by two different methods (i) with an automatic dilatometer (Homand, 1998), (ii) with a heating-bath system (Antéa, 2001).

In an automatic dilatometer samples measure 10 mm in diameter and about 30 mm in length. The used heating rate was 5 °C/min. Measurements were taken in different directions for three different initial saturation levels (100 %, 95 % and 85 %) and over a temperature spectrum ranging from 40 to 150 °C.

The heating-bath system needs samples measuring 30 mm in diameter and 80 mm in height. The temperature was increased by 10 °C increments. Each incremental phase lasted between 30 and 60 min.

Due to the diameter of the sample and the heating rate, the sample was also considered to be under pseudo-undrained conditions for both methods. Consequently, both series of measurements provide an estimation of the thermal-dilatation coefficient under pseudo-undrained conditions (α). An example of test-result curves provided by the dilatometer (deformation in relation to temperature) is shown in Figure 6.11, where the curves at various saturation levels are grouped according to their orientation. Those curves show the existence of a quasi-linear dilatation phase up to 90 °C. Subsequently, in the case of all samples, when pore water begins to vaporize a disturbance appears in the curves between 100 °C and 130 °C, as reflected by a specific phase during which the material shrinks. That disturbance is proportional to the saturation rate of the sample. Lastly, under the highest temperatures, the behaviour varies according to the orientation and initial saturation rate of the samples.

The non-linearity of the thermal dilatation may be explained by the beginning of the pore water vaporisation above 100 °C. The sample dehydration induces consequently capillary forces within the rock. Those capillary forces tend to make the rock shrink more, and then they compete with the thermal dilatation of the solid matrix.

The mean values of the thermal-dilatation coefficient obtained by dilatometer for samples from borehole EST104 (Homand, 1998) and by a heating-bath system from borehole EST205 (Antéa, 2001), as measured between 40 and 90 °C, are shown in Table 6.2, in relation to the saturation rate and the orientation of the sample.

Table 6.2: Linear thermal dilatation coefficient (in $10^{-6} K^{-1}$) between 40 and 90 °C (samples from boreholes EST104 and EST205) (average value and standard deviation)

Borehole					Average
		Parallel	At 45°	Perpendicular	
EST104 (dilatometer)	Sr = 100 %	6.8 ± 2.1	6.7 ± 4.6	12.6 ± 6.7	8.7 ± 5.2
	Sr = 95 %	8.2 ± 2.2	8.6 ± 1.5	11.1 ± 2.8	9.3 ± 2.4
	Sr = 85 %	8.7 ± 2.4	10.7 ± 0.7	12.6 ± 3.0	10.7 ± 2.6
Average		7.9 ± 2.2	8.6 ± 3.1	12.1 ± 4.2	9.5 ± 3.7
EST205 (heating bath)	Sr = 100 %	12.2 ± 4.4		18.7 ± 6.4	15.4 ± 6.2

The main conclusions are as follows:

The thermal-dilatation coefficient under pseudo-undrained conditions ranges between:

- 0.8 and $1.2 \cdot 10^{-5} K^{-1}$, in a direction parallel to the stratification;
- 1.2 and $1.9 \cdot 10^{-5} K^{-1}$, in a direction perpendicular to the stratification.

Cores from borehole EST104 are more damaged than the ones from EST205, what can explain a part of the discrepancy between the results for the saturated samples.

The thermal dilatation of the rock is linear up to 90 °C (see Figure 6.11). Above that temperature, significant behaviour non-linearities appear and may induce the material to shrink between 100 and 130 °C.

Desaturation seems to increase the thermal-dilatation coefficient, but exceptions exist.

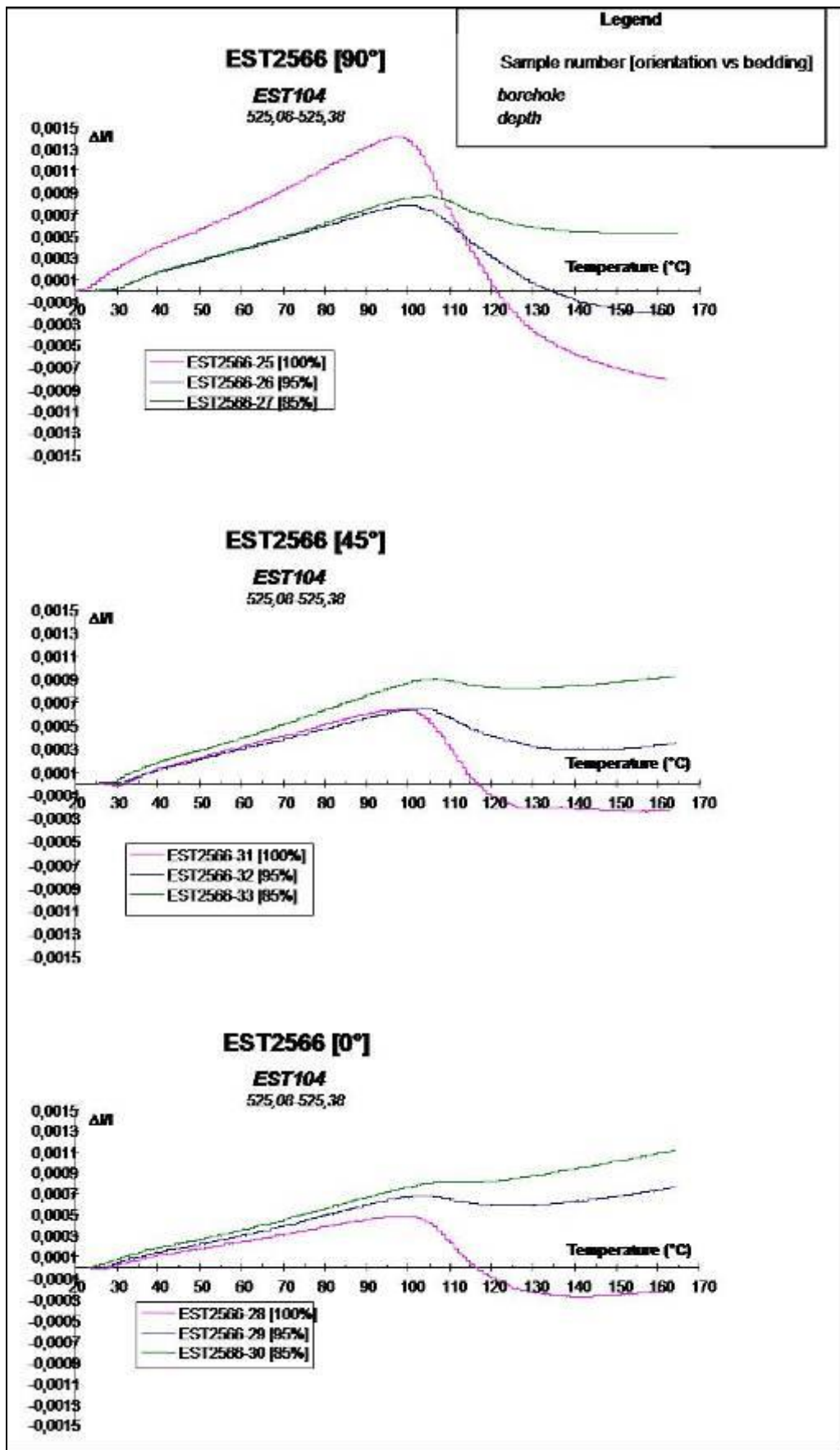


Figure 6.11: Examples of thermal-dilatation curves for argillites (Homand, 1998)

Reference values under pseudo-undrained conditions:

Average linear thermal-dilatation coefficient:

isotropy hypothesis: $\alpha_{average} = 1.28 \cdot 10^{-5} \text{ K}^{-1}$;anisotropy hypothesis: $\alpha_{//} = 1.0 \cdot 10^{-5} \text{ K}^{-1}$; $\alpha_{\perp} = 1.55 \cdot 10^{-5} \text{ K}^{-1}$.

The differential thermal-dilatation coefficient, α_m , is also called the “isochoric drained thermal fluid mass contribution coefficient”. Currently, there is no available method to measure it directly. However, there is a theoretical model capable of determining it on the basis of the drained thermal-dilatation coefficient and of the porosity of the material, as follows:

$$\alpha_m = (b - \Phi) \alpha_0 + \Phi \alpha_{fl} \quad (6.1)$$

where b is the Biot coefficient, Φ the porosity, and α_{fl} the linear thermal-dilatation coefficient of water.

Reference values for argillites, such as $b = 0.6$; $\Phi = 15 \%$, $\alpha_0 = 1 \cdot 10^{-5} \text{ K}^{-1}$ (hypothesis) and $\alpha_{fl} = 1.0 \cdot 10^{-4} \text{ K}^{-1}$, give:

$$\alpha_m = 1.95 \cdot 10^{-5} \text{ K}^{-1}.$$

It should be noted that such a figure constitutes a theoretical value. The uncertainty about α_m depends on uncertainties concerning Biot coefficient, porosity and the drained thermal-dilatation coefficient.

6.3 In-situ thermo-hydromechanical characterisation

6.3.1 Monitoring of thermal disturbance during the REP experiment

The REP experiment is a vertical mine by test equipped with hydromechanical sensors (Armand 2006). Pore pressure measurements are associated with a temperature recording in the same chamber of the instrumented borehole. During the lining of this zone (concrete pouring), the concrete curing created a temperature increase at the shaft rock wall face and the thermal effect has been observed in the rock mass on temperature, pore pressure and deformation sensors (Figure 6.12 and Figure 6.13).

The amplitude of maximal temperature variation is decreasing with the distance to the wall of the main shaft. At 5 meters, the maximal variation is less than $0.5 \text{ }^\circ\text{C}$ which confirms the low effect of the concrete lining on the rock mass. Figure 6.12 shows also that the temperature diffusion around the shaft is nearly isotropic and not affected by stress anisotropy. The thermal conductivity is isotropic in the bedding plane (close to horizontal).

Figure 6.10 gives the overpressure created by the temperature increasing during the curing phase of the lining (and the reverse effect during the cooling phase). The coefficient of pore pressure variation with temperature ranges from $0.225 \text{ MPa/ }^\circ\text{C}$ to $0.29 \text{ MPa/ }^\circ\text{C}$, depending on the chamber and borehole considered (Figure 6.13 is showing only recording in borehole REP2103). This pore pressure reaction confirms that the argillite is a porous media with some important THM coupling.

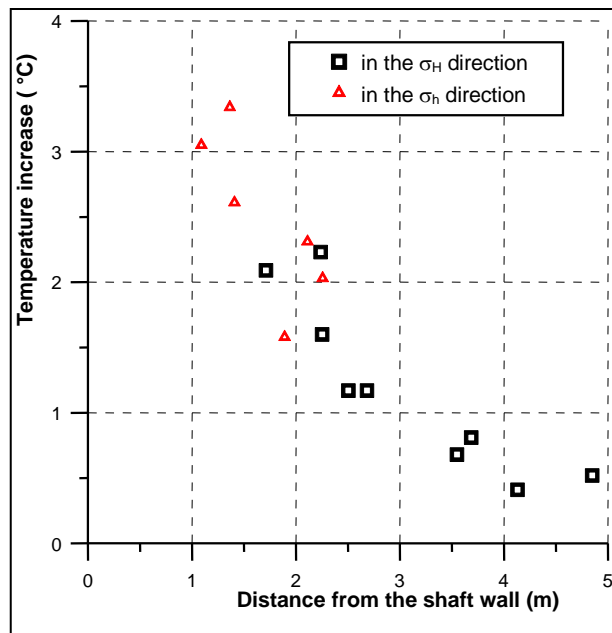


Figure 6.12: Maximum temperature variation observed versus distance from the shaft wall

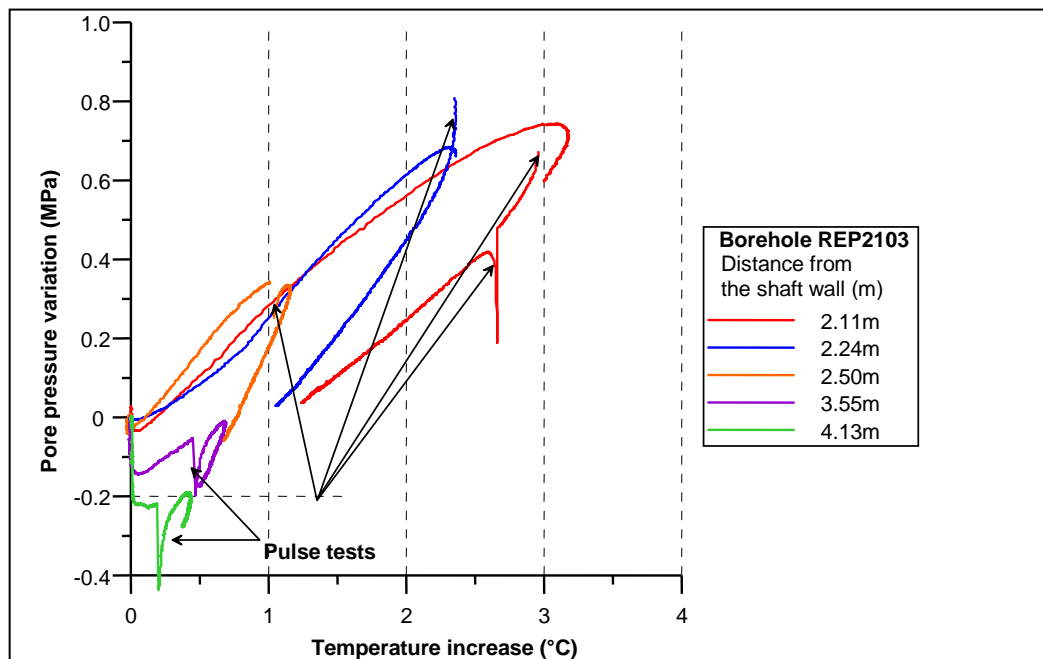


Figure 6.13: Pressure and temperature variation at a distance between 2.1 and 4.1 from the shaft wall

6.3.2 The TER experiment

Objectives

In order to identify the thermal properties, as well as to enhance the knowledge about the THM processes in the argillites, an in situ heating experiment has been performed since early 2006. The concept of the in situ heating experiment was designed to heat the clay formation in an undisturbed zone by using an electric heater packer.

The main objective of the heating experiment (TER) is to determine the thermal properties of argillites in its natural state. The second objective of the heating test is to provide the first knowledge on *in situ* THM processes in saturated argillites. The scientific program includes also sample testing

to compare the results at different scale. The thermal effect on the damaged zone is studied in this experiment by permeability measurement tests before and after the thermal loading.

Instrumental layout

The TER experiment is located at the main level of URL (490m deep) near the GEX drift. This location was chosen in order to set up some extensometers radial to the heater borehole and to better estimate the thermally-induced deformation (Figure 6.14). Notice that the TER design is quite similar to the HE-D design (experiment carried out in the Mont Terri Rock Laboratory, see § 5.3) which is also located at the corner of two drifts/niches.

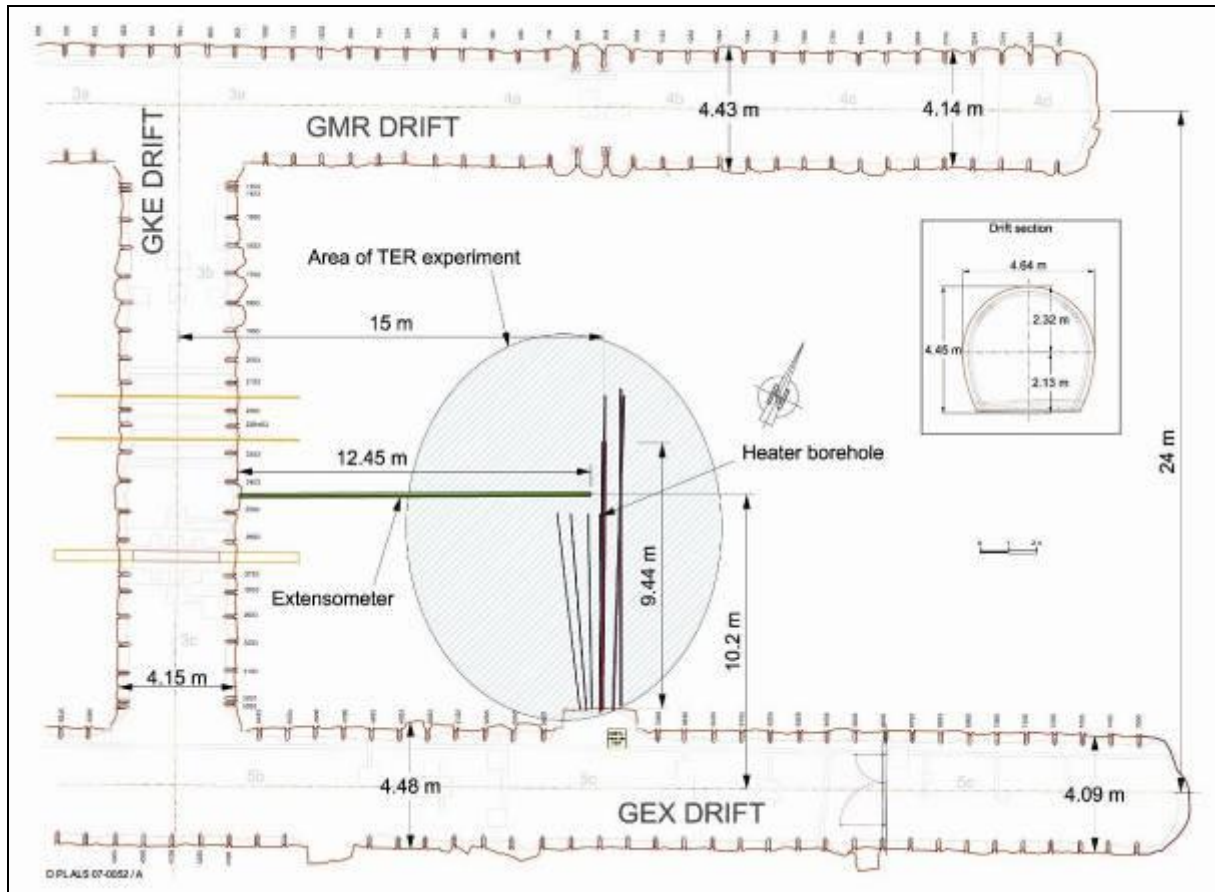


Figure 6.14: Location of the TER experiment and its neighbour drifts

The heated area is located approximately 6 m far from the wall of the GEX drift in order to avoid the damaged or desaturated zone around this drift.

The heating device consists of a heating packer capable to develop a pressure exceeding 10 MPa, if installed in a 300-mm-diameter borehole and to withstand temperatures up to 150 °C (Figure 6.15). Thermal power and pressure of the heating device are regulated from the drift. The device is equipped with temperature sensors in order to control the homogeneity of the temperature field inside it. A tubing (plastic and steel in the heated zone) was added to protect the borehole debris falls.

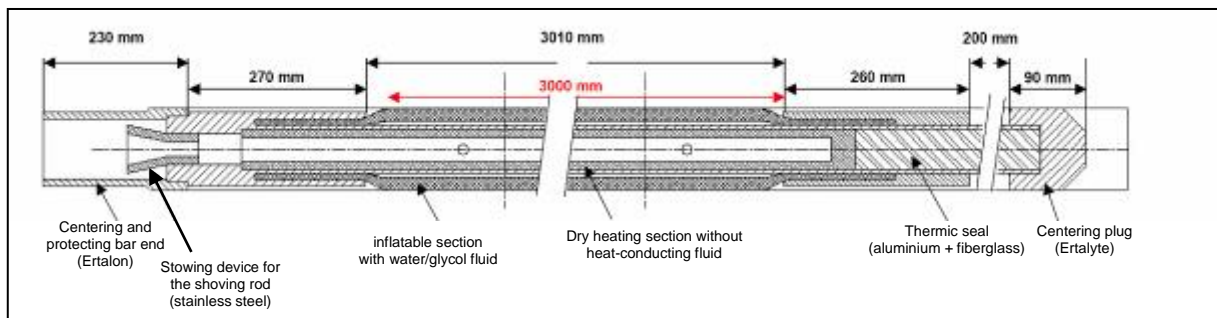


Figure 6.15: Detailed layout of the TER heater device

Two kinds of extensometers have been installed. TER1301 is a non permanent acquisition system, developed by Solexperts (« Sliding Micrometer »), which monitors the strain between metallic rings at each meter in the borehole. The other one (TER1302) is an automatic classical extensometer (less accurate) which is installed at 50 cm up to the TER1301 in order to record all the transient period when the thermal loading is modified (Figure 6.15).

Pore pressure is measured around the heating borehole between 0.5 m and 1.5 m. The sensors have been provided by GRS with a similar design as in the HE-D experiment (Figure 6.16). Both pore pressure and temperature can be monitored in each chamber. The chambers give also the possibility to connect a hydraulic system to carry out some pulse tests in it (permeability characterization).



Figure 6.16: Pore pressure and temperature sensors in slim holes (TER1401 to TER1405) as in Mont Terri HE-D experiment

Three boreholes are dedicated to monitor the temperature around the heater in 3 directions (normal, parallel, and at 45° of the bedding plane). They are 0.6 m to 1.8 m far from the heater (Figure 6.17).

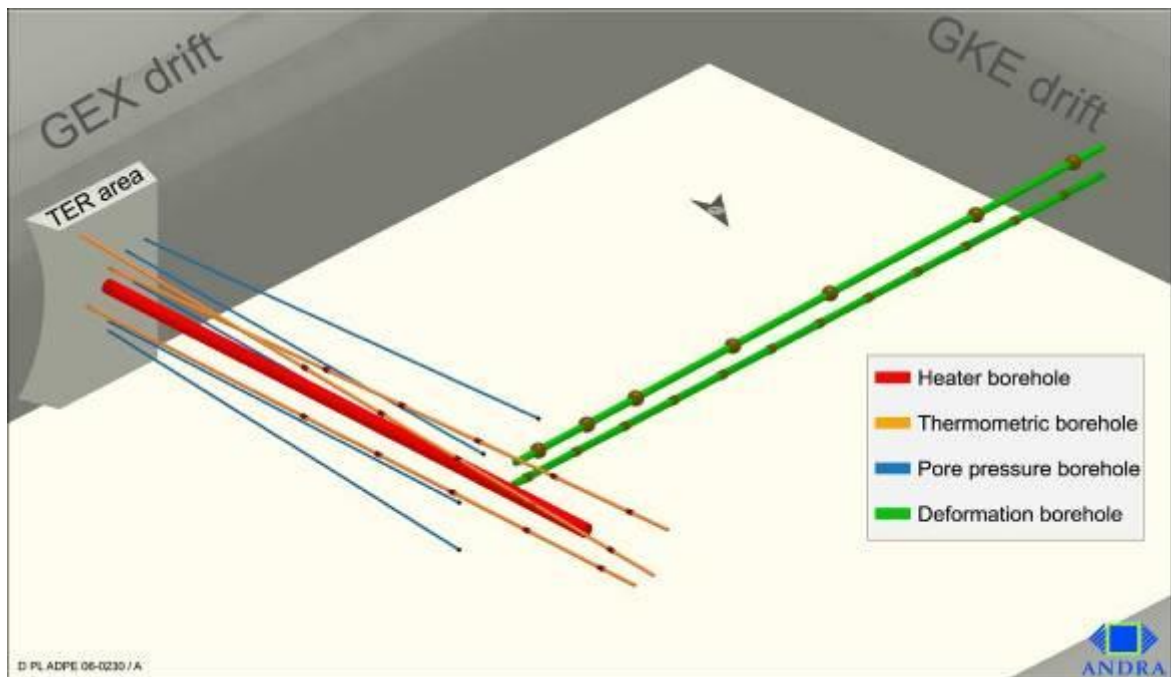


Figure 6.17: 3D view of the TER experiment instrumental layout

The entire instrumentation of surrounding boreholes took place in second semester 2005. Early December, the coring and installation of heating device was carried out. The first heating phase was switched on 11 January 2006. This heating was voluntarily switched off in February 2006 because the packer membrane failed.

After having fully checked the heating device, it was found that the real power injected during this first heating period was 85 % higher than expected (Figure 6.18).

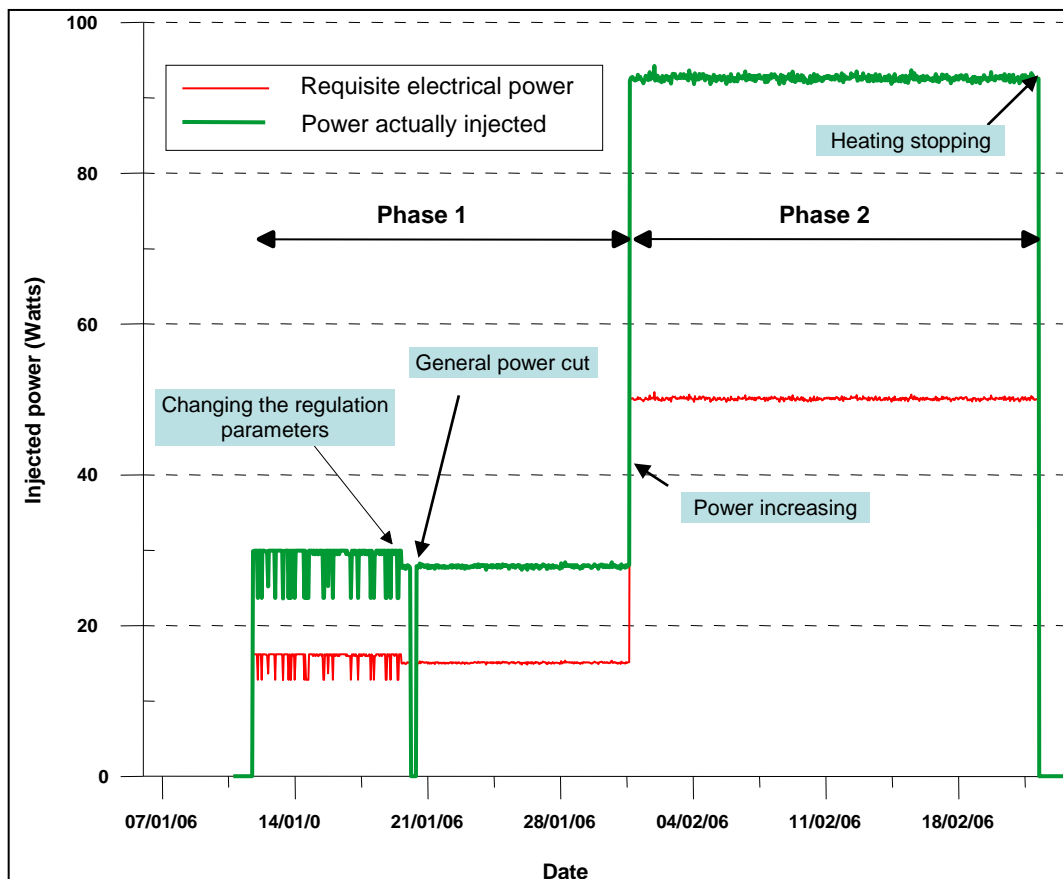


Figure 6.18: Power injected in TER experiment during the first heating phase

Acquired data

Figure 6.19 shows the evolution over time of overpressures (pore pressures increase) throughout the heating and cooling phases.

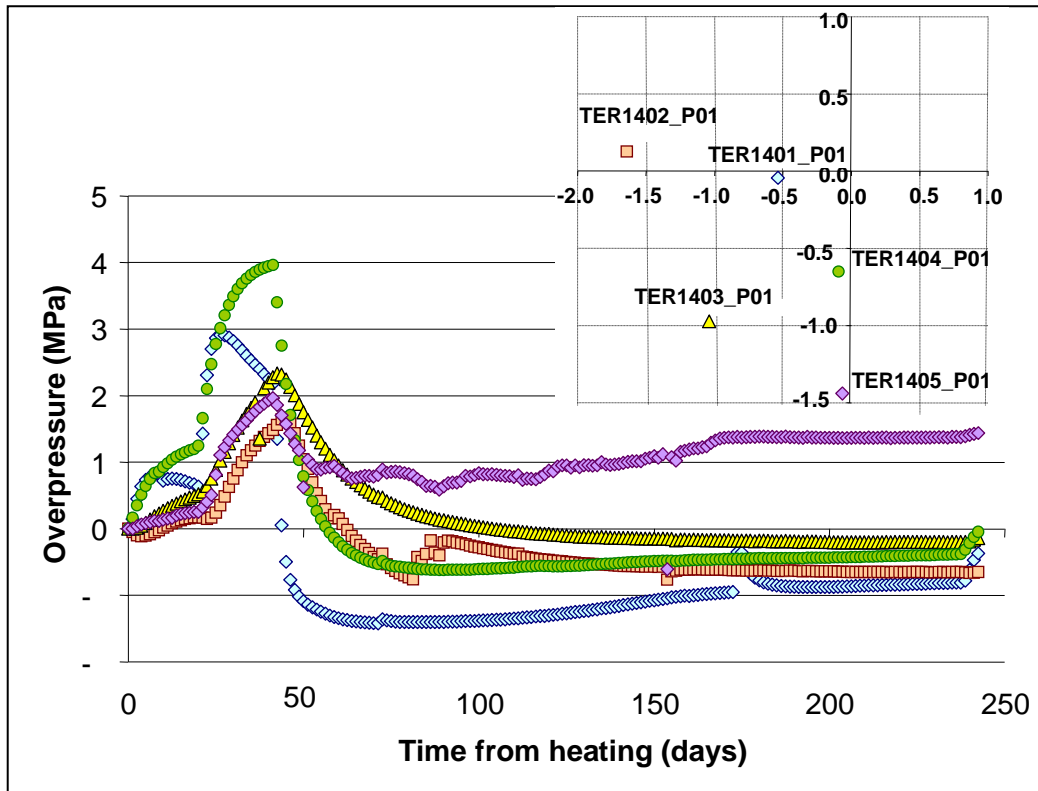


Figure 6.19: Evolution over time of pore overpressures generated during the heating phase

The two pore pressure peaks recorded on sensor TER1401 suggest a partly-drained response of the argillite. Even after a 200-day cooling period, the pore pressures did not resume their initial state on 11 January, before the beginning of the heating phase. The other sensors show a continual increase of pore pressures with temperature, thus indicating that, due to their position, thermo-consolidation is not sufficient to absorb the pressure increase by thermal expansion.

Figure 6.20 shows deformation measurements for a period including the cooling phase.

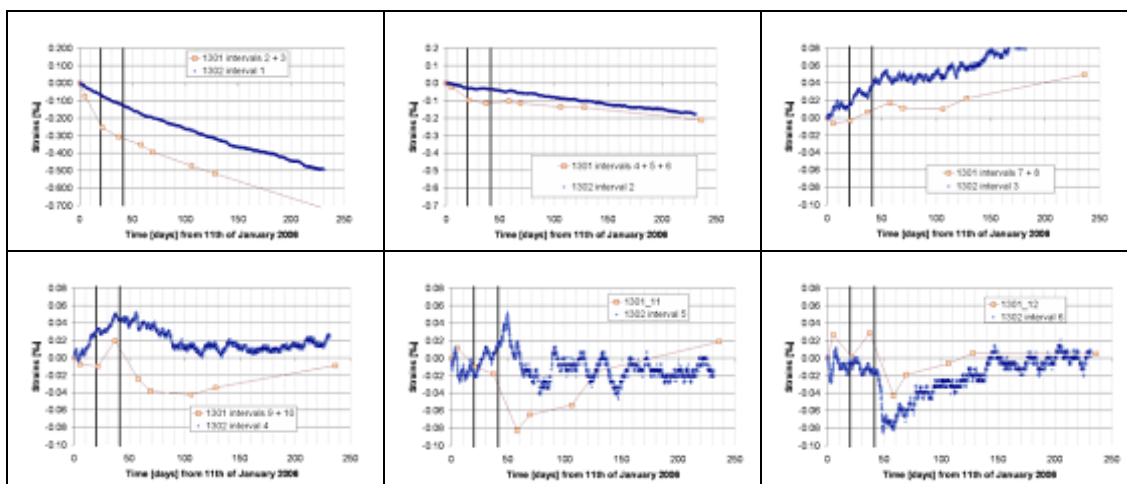


Figure 6.20: Evolution over time of the measurements recorded manually on extensometer TER1301, compared to automatic measurements in borehole TER1302

6.4 Related chemical aspects

Callovo-Oxfordian argillites contain interstratified illite/smectite clay minerals: R1-type at the base of the formation and R0 type in the upper half. The smectitic portion is likely to be modified due to the rise in temperature induced by the introduction of certain exothermal waste in the geological environment. Two complementary approaches, experimentation and modelling, were used to identify and quantify possible mineralogical transformations.

6.4.1 Experimental characterisation of mineralogical transformations

Introduction

The mineralogical transformations of smectites have been widely investigated in the case of the burial of sediments within a sedimentary basin where pressure increase and temperature rise are significant. Experimentations (Cathelineau *et al.*, 1999), conducted at temperatures ranging often between 200 and 500 °C, show that:

the illitisation process involves transformation mechanisms at the solid state by cationic substitutions and dissolution/recrystallisation phenomena;

besides pressure and temperature, many physico-chemical parameters may play a role in that transformation: initial chemical composition of the smectite, flake-closing mechanisms during the transformation, nature of the other minerals contained in the rock, etc.

In the literature, the temperature is the determining factor for the transformation of smectite into illite. However, clay determinations rely only on X-ray diagrams that are only able to show the closing of the flakes and not their chemical alteration.

For homoionic poles of smectites, significant differences in behaviour were observed. Potassic smectites, for example, react rapidly to a rise in temperature with a readily dehydration due to the high charge of the flake (Cathelineau *et al.*, 1999) and/or to the low affinity of potassium for water. On the other hand, cations with high hydration energy, such as Na⁺ and Mg²⁺, retard that charge increase and slow down the dehydration of the flake. The result is that the calcic pole remains remarkably stable in temperature and that the sodic smectite has an intermediary behaviour between the potassic and calcitic poles. Similarly, the presence of Na⁺, Mg²⁺ and Ca²⁺ cations in the water retards the transformation of smectites at moderate temperatures (200 °C).

The bibliography on the subject shows a broad variability in the behaviour of the smectitic homoionic poles in relation to the experimental conditions, even though some key orientations may be drawn. Furthermore, the stability of the smectites under conditions close to those of a repository (low temperature and pressure) has been rarely investigated in depth.

Therefore Andra undertook laboratory experiments on pure clay poles and on natural sediments (Ruck, 1996 a).

Experiments performed in the Callovo-Oxfordian formation

Experiment protocol

Experiments were conducted: (i) on three pure-smectite poles in order to examine the behaviour of each of those minerals in relation to temperature, (ii) on Callovo-Oxfordian argillites in order to establish behaviour forecasts.

In the first case, three homoionic smectites (K, Na, Ca) prepared from Wyoming bentonite (SWy-1) were tested with a view to identifying the impact of different physico-chemical parameters:

- the initial interlayer chemical composition of the smectites;
- the cation-exchange capacity of those minerals;
- the closing mechanisms of clay flakes during transformation and the nature of the close flakes;
- the activation and kinetic energies of the transformation of smectite into mica or illite;
- the impact of the presence of other minerals on the reactivity of smectites.

In the second case, the following aspects were investigated on Callovo-Oxfordian argillites:

- the overall evolution of the rock or of its fine portion;
- the crystallo-chemical evolution of each mineral phase;
- the impact of the water/rock ratio on reactions;
- the transformation of associated phases.

Close to 200 tests were carried out by heating samples in autoclaves, according to the experiment protocol presented in Figure 6.18. The three following types of autoclave were used:

- a fast-quenching oven: both pressure and temperature are controlled at ± 0.5 MPa and ± 1 °C respectively ; a few milligrams of clay and a few microlitres of solution are placed in a closed capsule made of gold; the reaction is set at the end of the experiment by using a fast-quenching system;
- a high temperature-sealing oven: both pressure and temperature are controlled at ± 0.5 MPa and ± 1 °C respectively ; the cavity, lined with gold or Teflon, is more important (18 ml) ; cooling is slow;
- a sampling oven: thanks to a special valve system, it is possible not only to collect some of the solid/solution mixture together with gas, but also to inject some gas.

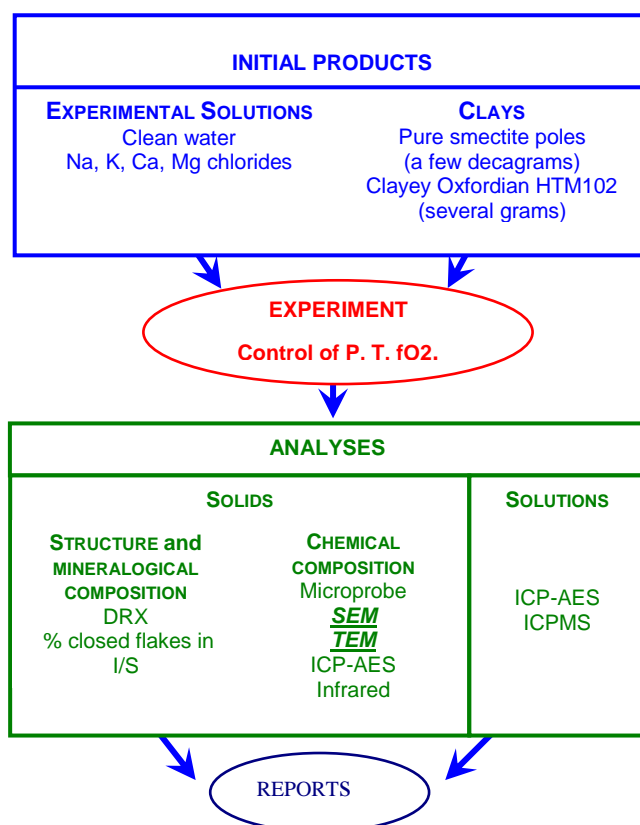


Figure 6.21: Experimental protocol for the thermal treatment of clay, under conditions close to repository conditions (Ruck R, 1996a, simplified).

Samples were heated at a temperature of 300 °C and at a pressure of 10 MPa, in mixed NaCl + KCl solutions with variable concentration (K: 100-300 ppm; Na: 0-17,638 ppm) or in deionised water. A few series of experiments were performed at lower temperatures (50-120 °C, or 150-250 °C). The liquid/solid ratio stood generally at 10/1; a few tests were carried out with liquid/solid ratios of 100/1, 2/1, and even 1/10, the latter type being closer to the water content of Callovo-Oxfordian argillites.

Analytical protocol

The resulting mineralogical composition at the end of the heating experiments (clay minerals and other phases – siliceous products, in particular) was determined by using the following multidisciplinary approach:

- X-ray diffraction, in order to determine the different mineral phases and, especially, clay minerals (types of interstratified minerals, flake closing rate);
- a routinely-used electronic microprobe, in order to obtain average analyses of a few tens of cubic micrometers or for particle spot analyses with an average diameter varying between 2 µm and a few micrometers;
- transmission electron microscopy (TEM) and scanning electron microscopy (SEM) for textural observation, especially dissolution/recrystallisation figures, and for semi-quantitative analyses at the particle scale;
- ICP-AES for an average analysis of clays;
- Fourier-transformation infrared spectroscopy, in order to measure indirectly the cation-exchange capacity of smectitic flakes.

In the case of experimental solutions with a higher volume than 0.5 mL, major and trace elements were analysed by ICP-AES (inductive coupled plasma - atomic emission spectroscopy) and ICPMS (inductively coupled plasma mass spectroscopy), respectively.

The use of those complementary techniques helped to calculate a mass balance and to estimate the variations of the global properties of the materials.

Main results

Results for pure smectite poles

Results obtained by X-ray diffraction, especially with regard to the percentages of closed flakes, were calculated on the basis of the Reynolds model.

Most experiments were conducted at 300 °C in order to detect the reactions of the different smectites. At that temperature, potassic smectite proves to be more reactive in relation to the sodic and calcic poles. The products resulting from Na and Ca smectites often remained unchanged compared to their initial states. At the very most, they result in disorderly illite/smectite interstratified minerals (I/S R0) with 70 % swelling flakes. On the other hand, potassic smectite evolves towards disorderly illite/smectite interstratified minerals, followed by orderly R1 and R2 types, and the occurrence of by-products, such as quartz (Figure 6.22) and cristobalite in neomineralised phase (Ruck, 1996-a).

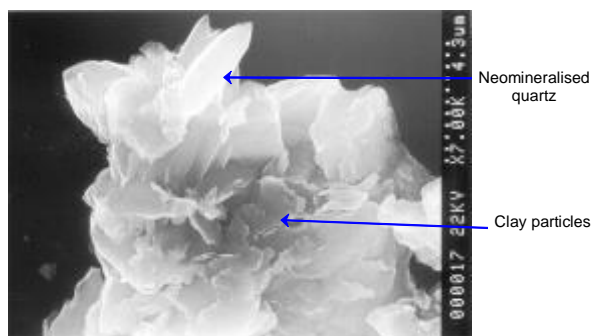


Figure 6.22: Neomineralised quartz within accumulated clay (SEM observation)

With TEM, the neomineralised interstratified minerals form a crystal fabric with a hexagonal weft and a different morphology from the veil shape of the initial smectites (Mosser-Ruck *et al.*, 1999). However, that type of result is only generated for experiments with a timescale ranging from 28 to 112 days, with aqueous solution (liquid/solid ratio of 10/1) containing only potassium (Mosser-Ruck, 1999).

When potassic smectite is placed in a mixed solution of NaCl and KCl, the presence of sodium inhibits partly the transformation of the smectite, without stopping it however. Analyses carried out with an electronic microprobe show that the evolution of potassic smectite towards interstratified mineral is correlated with a decrease in the Si(IV) concentration and an increase of the interlayer charge, whereas the octahedral composition in magnesium and iron remains relatively constant.

When potassic smectite is placed in a solution containing 0.5 mol/L of KCl, the variations in composition are significant in the different crystallo-chemical sites, but they remain insignificant: in most cases, the silicon concentration of tetrahedral sites ranges from 3.75 to 3.8 for the most evolved products. According to the microprobe and infrared spectroscopy, the transformation into interstratified mineral is less significant than what the sole interpretation of X-ray diffraction would suggest: see *Table 6.3*, excerpt from Mosser-Ruck *et al.* (2001).

Under such conditions, part of the closed flakes would have been submitted only to dehydration and would have undergone a chemical illite-type transformation.

Table 6.3 Percentages of flake types in I/S-production experiments generated by different analytical methods

Experiment time (weeks)	RX diffraction % of closed flakes	Infrared spectroscopy % of flakes without NH ₄ +exchange	Electronic microscopy % of illite flakes	Electronic microscopy + DRX % of closed illite flakes
1	42	36	13	29
2	42	37	13	29
4	65	53	11	54
8	68	53	29	39
16	70	-	17	53
24	73	59	20	53

Preliminary conclusion

Consequently, it appears that potassic smectite appears to be quite reactive at 300 °C. Its transformation into interstratified mineral follows probably several processes (Cathelineau *et al.*, 1999):

- short-term transient phenomena with dissolution and/or early hydrolysis of a few flakes;
- after one week of treatment, crystallisation of interstratified minerals with a lesser silicon content and a higher interlayer charge (silicon being replaced by Al³⁺).

However, according to the sole observation of X-rays, part of the closed flakes corresponds only to dehydration without any chemical alteration.

As for sodic and calcic smectites, they are more stable and the partial closure of the flakes corresponds only to variable hydration states. Those dehydrations do not constitute irreversible phenomena.

The two main parameters that increase the transformation rate of smectite into illite are temperature and time. However, it is difficult to extrapolate at low temperatures the test results achieved at higher temperatures: is it possible to use test results at 300 °C over three months to extrapolate subsequent mineralogical transformations at temperatures in the order of 80-150 °C over timescales of about 1,000 years?

Experiments conducted at 50, 80 and 120 °C on calcic and sodic smectites placed in NaCl and KCl solutions (liquid/solid ratio of 10/1) show that the structure of those minerals does not evolve. Under X-rays, the slight movement of the main reflections indicates a small variation in the hydration state, but no definitively-closed flakes were detected: the minerals maintain their swelling capacity with ethylene glycol and no neomineralised phase is observed. According to the results of the ICPES (inductively coupled plasma emission spectrometry) analyses on minerals, the chemical variations in the tetrahedral and octahedral sites are negligible in relation to their initial composition (Ruck, 1996b).

The interlayer site is the only one to be concerned by the partial substitutions of ions that occur mainly by exchange, with the dissolution phenomena being practically negligible. In general, the K/Na exchange is favourable to potassium, whereas K/Ca and Na/Ca exchanges are favourable to calcium, thus confirming the high stability of calcic smectites. The K/Ca exchange seems to be more sensitive to temperature (Figure 6.23), contrary to the Na/Ca exchange. Those exchange reactions result in a higher proportion of dehydrated flakes as shown through X-rays.

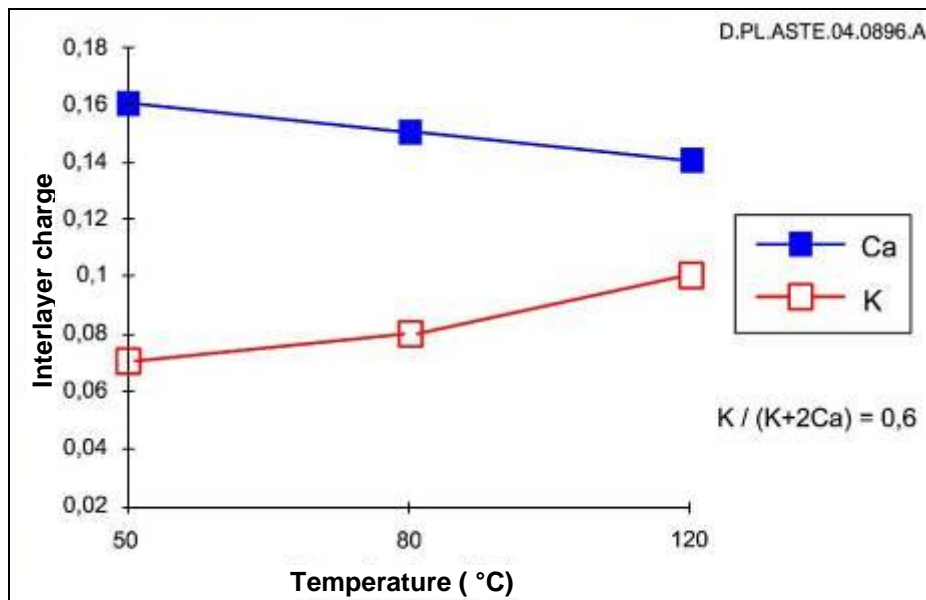


Figure 6.23: Evolution of a Ca-smectite interlayer charge depending on K/Ca exchange at different temperatures, in the case of a solution with $K/(K+2Ca) = 0,6$ (Ruck, 1996 b).

Results for Oxfordian argillites

Experiments were carried out on a Callovo-Oxfordian argillite sample collected in borehole HTM102, at a depth of approximately 405 m, i.e., in the part of the formation containing R0-type interstratified clay minerals. According to the X-ray spectrum of the fine fraction ($< 40 \mu\text{m}$), these minerals contain only 30 % of closed flakes (Ruck, 1996b).

Heating was applied for 112 days at a temperature of $200 \text{ }^\circ\text{C}$ to two different granulometric fractions:

- The finest fraction of the sample ($< 40 \mu\text{m}$), was dispersed in water (high liquid/solid ratio);
- A coarser fraction ($40\text{-}80 \mu\text{m}$) with a lower liquid/solid ratio, since particles were well settled at the bottom of the Teflon reactor;

Results achieved with X-ray spectra, microprobe analyses as well as TEM and SEM observations, show a very different behaviour between both granulometric populations, as follows:

- **the fine fraction** was very reactive with a progressive dissolution of potassic smectites, illite/smectite interstratified minerals, as well as calcite, quartz and pyrite. At the end of the experiment, some potassic smectites remained, but the most important fraction consisted of ferriferous chlorites and lath-shaped illite. Neomineralised quartz, calcite, aluminium hydroxides and calcic silicate complete that fraction whose cation-exchange capacity amounts to $50.48 \text{ meq}/100 \text{ g}$, compared to $95.36 \text{ meq}/100 \text{ g}$ initially;
- **the coarser fraction** shows no major mineralogical or crystallo-chemical evolution.

Hence, it appears that the reactivity of minerals depends on the liquid/solid ratio, with the dissolution of swelling clays and the formation of new phases being commensurate with the significance of that ratio.

Experiments show mineralogical transformations for temperatures that are often high, but those transformations are not associated with those expected within a potential repository. However, the question remains about the reactivity of clay materials at lower temperatures, i.e., less than $100 \text{ }^\circ\text{C}$ with regard to argillite in the context of a repository. Experimentally speaking, no transformation was observed at low temperatures. In order to verify if the same conclusion applies to longer

timescales than those of the actual experiments, thermal-disturbance models were built for the water/argillite system.

6.4.2 Modelling of the geochemical evolution under temperature conditions

Principle

Modelling relies on the same equilibrium hypotheses than at 25 °C. The solubility equilibriums of certain constitutive mineral phases of the argillite and the chemical equilibriums between the solution and the sorbed cationic population on the exchange sites of the rock are considered simultaneously. In order to describe those equilibriums at variable temperatures, a Van't Hoff approximation was applied in order to limit the number of parameters to be introduced in the models, since only reaction enthalpies are actually necessary.

Considering the temperature spectrum to be explored (25-80 °C), a Van't Hoff approximation is applicable and proves particularly useful when describing the temperature dependency of cation-exchange reactions. Indeed, if the dependency of the solubility of mineral phases is well known thanks to the thermodynamic database, without relying on a Van't Hoff approximation, it is not the case for ionic-exchange reactions and very few studies have been conducted on this topic until now (Martin & Laudelout, 1963 ; Laudelout *et al.*, 1968 ; Gast, 1969 ; Talibudeen & Goulding, 1983 in Gaucher & Blanc 2004). Those investigations provide enthalpy values for cation-exchange reactions on smectites (Table 6.4).

Table 6.4: Enthalpies of cation-exchange reactions & cation exchange constants (LogK) considered in the modelling of the chemical composition of Callovo-Oxfordian pore water (Gaucher & Blanc, 2004)

Exchange	ΔH (kJ/mol)	LogK at 25 °C
Na-Mg	4.20	0.38
Na-Ca	3.78	0.50
Na-Sr	0.35	0.68
Na-K	-4.52	0.44

On the basis of the enthalpies of each cationic-exchange reaction it is possible to assess the value of each exchange constant at different temperatures (Gaucher & Blanc, 2004) (Table 6.4).

Table 6.5: Influence of temperature on cation-exchange constants (log(K)) applicable to Callovo-Oxfordian argillite

T (°C)	Na-Mg	Na-Ca	Na-Sr	Na-K
25	0.38	0.50	0.68	0.44
40	0.45	0.56	0.69	0.36
60	0.53	0.64	0.69	0.27
80	0.61	0.70	0.70	0.19
100	0.67	0.76	0.70	0.12

Results

Table 6.6 presents the chemical composition of the pore water in Callovo-Oxfordian argillite, as calculated at different temperatures. It is composed of three parts (i) the chemical parameters of the pore water, the cations on the exchange sites and the saturation indices of the closest minerals to the

solubility limit for each calculated composition. The constitutive minerals of the argillite appear in bold, among which, those in thermodynamic equilibrium with the pore water are highlighted in red.

As temperature rises, the solubility of calcite and of dolomite decrease and cause the total concentration of inorganic carbon in solution to decrease. The reduction of the bicarbonate ion concentration is proportional, with the pH of the solution being constant in general over the modelled temperature spectrum. In the argillite pore water, alkalinity is essentially associated with the activity of the bicarbonate ion in solution (HCO_3^-), representing approximately 80 % of the total inorganic carbon in solution. Hence, a reduction of the alkalinity of the solution is observed as temperature increases.

Table 6.6: Calculated chemical composition of Callovo-Oxfordian pore water at different temperatures

Temperature (°C)	20	25	40	60	80
pH	7.00	7.00	7.00	7.01	7.03
Eh (mV)	-151	-155	-168	-183	-196
Alkalinity (eq.kg _w ⁻¹)	2.92E-03	2.40E-03	1.42E-03	7.93E-04	4.96E-04
Ionic Force (M)	1.21E-01	1.18E-01	1.09E-01	9.61E-02	8.37E-02
Cl (M)	3.01E-02	3.01E-02	3.01E-02	3.01E-02	3.01E-02
S (M)	3.29E-02	3.19E-02	2.91E-02	2.49E-02	2.04E-02
Na (M)	3.21E-02	3.20E-02	3.14E-02	3.02E-02	2.85E-02
K (M)	6.96E-03	7.14E-03	7.63E-03	8.07E-03	8.30E-03
Ca (M)	1.49E-02	1.52E-02	1.53E-02	1.40E-02	1.20E-02
Mg (M)	1.34E-02	1.21E-02	8.95E-03	6.20E-03	4.56E-03
Sr (M)	1.12E-03	1.11E-03	1.06E-03	9.26E-04	7.63E-04
Si (M)	7.43E-05	9.40E-05	1.75E-04	3.40E-04	5.77E-04
Al (M)	4.83E-09	6.72E-09	1.82E-08	6.39E-08	1.98E-07
Fe (M)	4.67E-04	2.85E-04	7.06E-05	1.29E-05	2.83E-06
CIT (M)	3.33E-03	2.72E-03	1.59E-03	8.74E-04	5.34E-04
<u>SrOx2</u>	4 %	4 %	4 %	4 %	4 %
<u>KOx</u>	8 %	8 %	8 %	8 %	8 %
<u>NaOx</u>	14 %	14 %	14 %	14 %	14 %
<u>MgOx2</u>	30 %	28 %	23 %	19 %	17 %
<u>CaOx2</u>	43 %	45 %	51 %	55 %	58 %
Log(Q/K) Strontianite	1.04	0.97	0.78	0.57	0.40
Log(Q/K) Microcline	0.50	0.51	0.53	0.55	0.57
Log(Q/K) Illite	0,00	0,00	0,00	0,00	0,00
Log(Q/K) Calcite	0,00	0,00	0,00	0,00	0,00
Log(Q/K) Dolomite	0,00	0,00	0,00	0,00	0,00
Log(Q/K) Quartz	0,00	0,00	0,00	0,00	0,00
Log(Q/K) Pyrite	0,00	0,00	0,00	0,00	0,00
Log(Q/K) Celestite	0,00	0,00	0,00	0,00	0,00
Log(Q/K) <u>Montmor-Ca</u>	-0.25	-0.20	-0.03	0.16	0.33
Log(Q/K) <u>Chlorite-14A</u>	0,00	0,00	0,00	0,00	0,00
Log(Q/K) CO ₂ (g)	-1.92	-1.96	-2.08	-2.22	-2.32
Log(Q/K) <u>Daphnite-14A</u>	0,00	0,00	0,00	0,00	0,00
Log(Q/K) <u>Clinochlorine-14A</u>	-7.62	-6.49	-3.30	0.53	3.96
Log(Q/K) Gypsum	0,00	0,00	-0.01	-0.05	-0.10
Log(Q/K) <u>Beidellite-Mg</u>	-0.77	-0.79	-0.83	-0.88	-0.92
Log(Q/K) <u>Beidellite-Ca</u>	-0.80	-0.81	-0.86	-0.91	-0.97
Log(Q/K) <u>Beidellite-K</u>	-0.85	-0.90	-1.03	-1.19	-1.33
Log(Q/K) <u>Beidellite-Na</u>	-0.98	-1.01	-1.12	-1.24	-1.36
Log(Q/K) <u>Saponite-Mg</u>	-2.63	-1.93	0.07	2.48	4.65
Log(Q/K) <u>Saponite-Ca</u>	-2.66	-1.95	0.04	2.45	4.60
Log(Q/K) <u>Saponite-K</u>	-2.71	-2.04	-0.13	2.17	4.24
Log(Q/K) <u>Saponite-Na</u>	-2.84	-2.15	-0.21	2.12	4.22

Saturation index, Log(Q/K) is positive when a mineral is oversaturated (tendency to precipitation), it is neutral when a mineral is at equilibrium and is negative when a mineral is undersaturated (tendency to dissolve).

Similarly, as temperature increases, the total sulphur concentration in solution decreases correlatively with the strontium concentration due to the decrease in the solubility of celestite.

An increase in the silica and aluminium concentration is observed in relation with the general increase in the solubility of aluminosilicates with temperature, thus resulting in a significant evolution towards the oversaturation of saponites (trioctahedral smectites with an initial tetrahedral charge). That oversaturation indicates a potential transformation of smectites. Beaufort *et al.* (2001) show experimentally that, before the smectite/illite transformation is observed, alterations occur in the nature of the smectites.

The increase in the potassium concentration in solution is induced by the increase of the illite solubility with temperature, what is applied at the thermodynamic equilibrium with calculated solutions. That means that without any additional source of potassium, illitisation is impossible. In addition, it was observed that for the temperature spectrum involved in this case (25-80 °C), microcline remains oversaturated and is unable to constitute a potassium source, although it was present initially in the constituting mineralogical fabric of the argillite.

Conclusions of experiments and models

Experiments conducted on pure poles of smectite confirm the data mentioned in the literature for temperatures in the order of 300 °C. However, analyses supplementing X-ray diffraction (chemical, microprobe, etc.) show that part of the closed flakes resulting from those experiments corresponds only to dehydration and not to an irreversible chemical transformation of those flakes.

As soon as temperatures are below 120 °C, smectites remain stable. Only interlayer sites are affected by cation exchanges and it is possible to detect a change in the location of the charge within smectites in relation with the temperature.

All detected transformations depend highly on the physico-chemical parameters concerned. Besides temperature, it is necessary to take into account the initial chemical composition of the smectite, the chemical composition of the fluid and the liquid/solid ratio.

Similarly, it seems that the presence of organic matter may play a role in the kinetics of the transformations of clay materials (Michel, 2006). In fact, a physical phenomenon of preferential adsorption of the organic matter on the clay surfaces appears during the pyrolysis experiments in a confined environment under increasing temperatures (200 to 365 °C). According to X-ray diffraction on the resulting products, no natural interlayer insertion (and, indeed, the potential microscopic swelling of smectites) of maturation-induced organic molecules is observed, which suggests that the presence of organic matter would tend to slow down the mineralogical transformation of clays.

Callovo-Oxfordian clays remain very stable at temperatures close to 200 °C, provided that particles are larger than 40 µm in diameter and that the liquid/solid ratio decreases, even though it remains higher than those in the natural environment.

It may therefore be possible to conclude that the mineralogical transformations of Callovo-Oxfordian interstratified clay minerals due to a radwaste repository will be minor because the argillite water content is lower than 10 % and the temperature will be always below 100 °C in the argillite, what is much below than the 200 °C of the experiment.

It is impossible for increasing the argillite temperature from 25 to 80 °C to result in a phenomenon of illitisation without any additional source of potassium. Over the temperature spectrum under investigation, the only constitutive potassium-bearing phase of the argillite is oversaturated and is unable, consequently, to constitute the required source of potassium for the illitisation process to occur.

6.5 THM modelling

Accompanying the conception and the result analysis of THM *in situ* experiments, different kinds of modelling have been carried out on the Callovo-Oxfordian argillites.

6.5.1 Analytical and numerical thermal calculations

The analytical solution for a linear thermal source (Su, 2001) shows that, irrespective of the applied thermal flux, the rate of temperature rise is very fast during the first months of the heating phase, then it decreases. The same phenomenon is observed for the cooling of the rock (Figure 6.24). The required cooling time for the massif to resume its initial temperature is much longer than the heating time. With $Q = 350 \text{ W/m}$, for example, the temperature on the borehole wall remains at $35 \text{ }^\circ\text{C}$ after two years of cooling ($t = 1,100 \text{ days}$), i.e., $5 \text{ }^\circ\text{C}$ above the initial temperature.

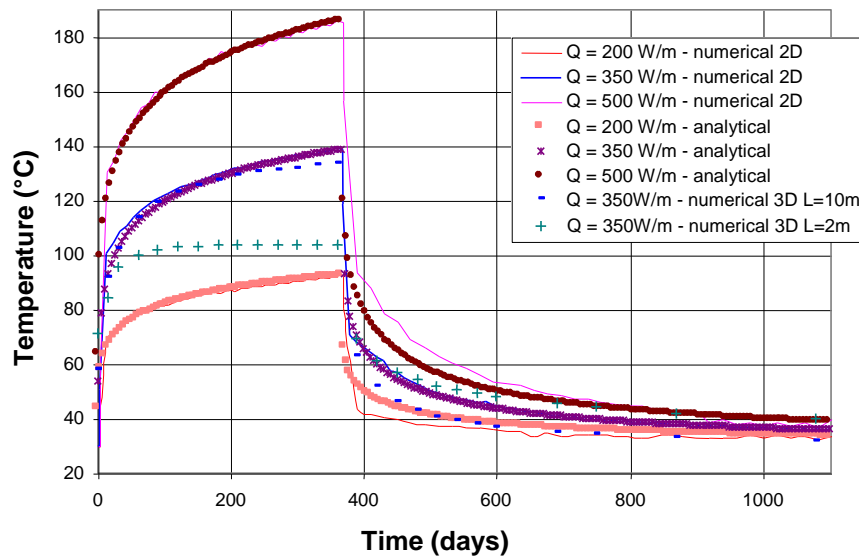


Figure 6.24: Evolution of temperature on the borehole wall in relation to time – Comparison between analytical calculations and numerical modelling with CASTEM (Su, 2001).

The maximum temperature of the borehole wall depends on the applied thermal flux: after 12 months of heating, it reaches $186 \text{ }^\circ\text{C}$, $140 \text{ }^\circ\text{C}$ and $92 \text{ }^\circ\text{C}$ for 500 , 350 and 200 W/m , respectively. The evolution over time of the thermal-disturbance radius is shown in Table 6.7 on the basis of three temperature-variation criteria in relation to the initial temperature (0.5 , 1 and $2 \text{ }^\circ\text{C}$).

Table 6.7: Extension of temperature, deformation/stress and hydraulic disturbances (Su, 2001)

Criteria	Extension of: Thermal disturbances*		
	After drilling of borehole	After 12 months (end of heating)	After 36 months (after 24 months of cooling)
$\Delta T > 2\text{ }^{\circ}\text{C}$	–	12 m	18 m
$\Delta T > 1\text{ }^{\circ}\text{C}$	–	14 m	23 m
$\Delta T > 0.5\text{ }^{\circ}\text{C}$	–	16 m	27 m
	Mechanical disturbances		
$\Delta\sigma_d > 0.5\text{ MPa}$	1.2 m	3,0 m	6 m
$\Delta\sigma_d > 0.2\text{ MPa}$	2 m	21 m	9 m
$\Delta\varepsilon^v > 1\cdot 10^{-4}$	0.3 m	7 m	1 m
$\Delta\varepsilon^v > 0.5\cdot 10^{-4}$	0.4 m	11 m	2 m
	Hydraulic disturbances		
$\Delta P > 0.25\text{ MPa}$	0	11 m	14 m

* It should be noted that the disturbance extension depends on the selected criterion: the stricter the criterion, the broader the extension.

At the end of the heating phase (one year), the thermal-disturbance radius for temperature variation of a half-degree is 16 m and reaches 27 m after three years. The extension of the thermal disturbance depends on the adopted value for the temperature-variation criterion.

Impact on the fractured and excavation-disturbed zone (EDZ)

Fractured or damaged argillites around the borehole (EDZ) have a lower thermal conductivity than sound argillites due to their fissuration and their desaturation. On the basis of measurements taken on samples and of empirical relationships, a conductivity-decrease function is proposed on the Figure 6.25 for the EDZ (Su, 2002 b).

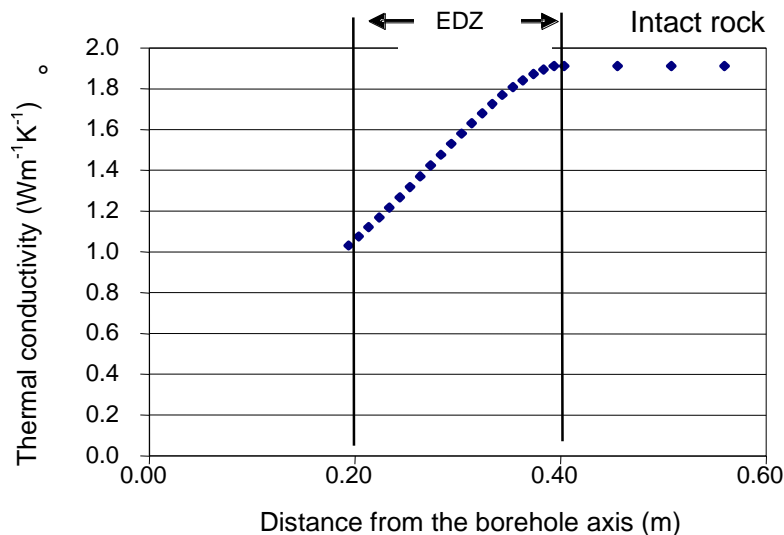


Figure 6.25: Thermal-conductivity variation in the EDZ (Su, 2002b)

The comparison between calculations taking into account or not the impact of the EDZ on thermal conductivity shows that the temperature difference on the wall of the heating borehole of the thermal experiment is approximately 7.5 °C. The impact of the EDZ is slightly lower than that established with a 10 % margin of uncertainty on the thermal conductivity of the overall argillite layer (Calculations 2 in Figure 6.26). More precisely, it is equivalent to an 8 % uncertainty on the thermal conductivity of the argillites.

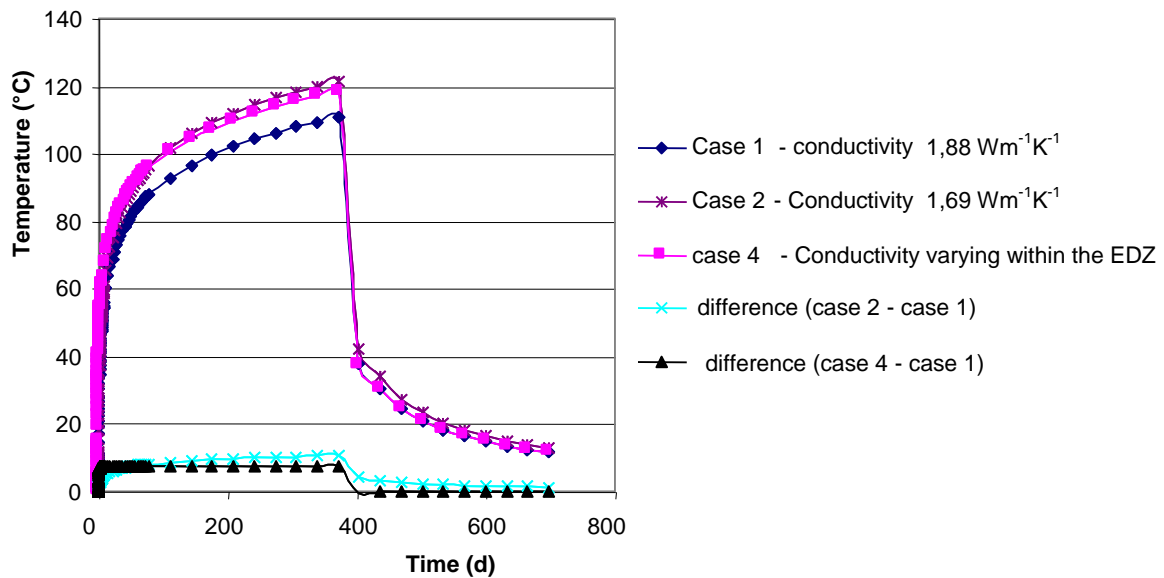


Figure 6.26: Temperatures on the borehole wall vs argillite thermal conductivity (Su, 2002b)

6.5.2 Numerical modelling of the REP experiment

Two thermo-mechanical modelling (Figure 6.27) have been performed in order to compare the values to the in situ observation. This modelling does not take into account THM coupling and is based on a hypothesis of global elastic behaviour. The values considered for the different parameters are:

- Young modulus: $E = 9000 \text{ MPa}$ (from in situ dilatometer tests),
- Poisson coefficient : $\nu = 0.3$,
- linear thermal expansion (assumed isotropic) : $\alpha = 1.28 \cdot 10^{-5} \text{ K}^{-1}$
- thermal conductivity: $\lambda_{//} = 2.2 \text{ W/m/K}$ (in the horizontal plane) and $\lambda_{\perp} = 1.6 \text{ W/m/K}$,
- heat capacity: $C_p = 935 \text{ J/kg/K}$.

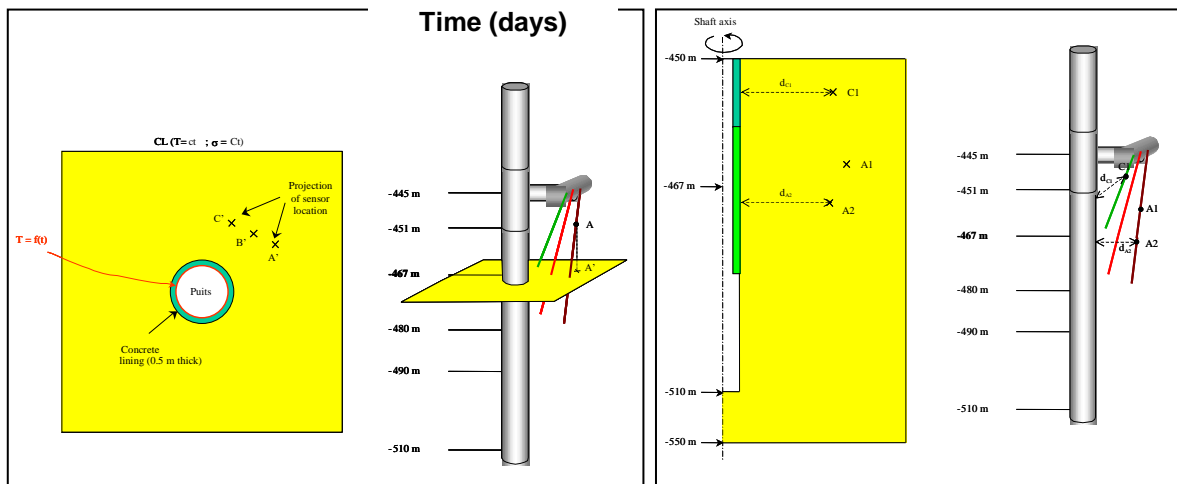


Figure 6.27: Geometry and location of observed point in the thermo-mechanical model carried out in 2D plane strain (on the left) and in axisymmetric condition (on the right)

The thermal loading is induced by exothermic cure reaction within the concrete mass of the lining, but to simplify the model, the boundary condition imposed at the rock wall is the temperature history measured inside the lining (Figure 6.28) without taking into account the concrete.

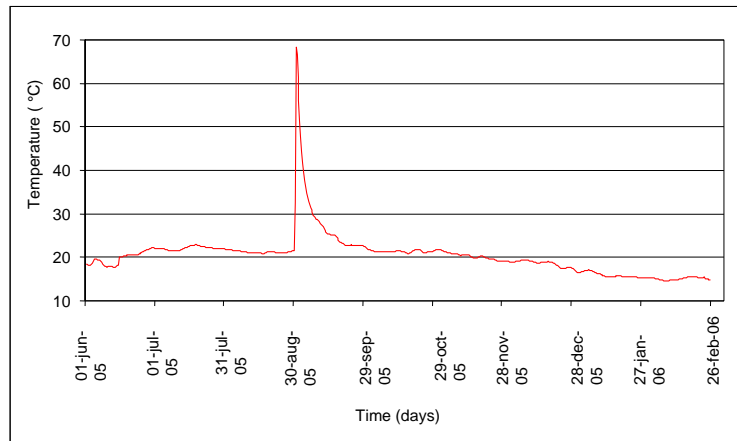


Figure 6.28: Temperature history measured inside the concrete lining of the shaft

The temperature evolution obtained for the two modellings (2D plane and 2D axisymmetric) at different distances are depicted on Figure 6.29. It can be observed that results are very similar (differences are less than 0.1 °C).

Temperature evolution at different distances from the shaft wall is well predicted by the modelling, but amplitudes of the temperature peak are over estimated due to the used simplified boundary condition. There is actually a temperature gradient across the lining that is why temperature at the rock wall face is smaller than in the concrete.

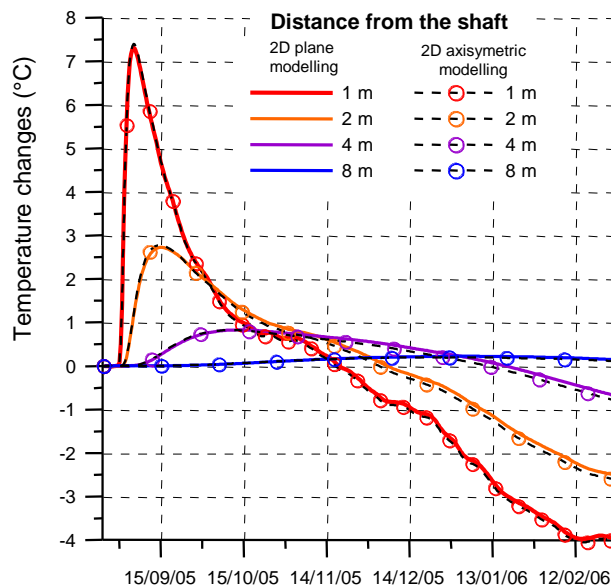


Figure 6.29: Comparison of temperature evolution calculated by both models (depth -467 m)

These models highlight the fact that the pouring of rings of concrete between -459 m to -465 m depth in the shaft does not significantly affect the temperature profile at 467 m (Armand, 2006). This confirms that the horizontal thermal conductivity of argillite is rather predominant.

This elastic model is not able to reproduce the strains observed in the shaft (Figure 6.30). Whereas the temperature is decreasing with the concrete cure, the displacements observed with extensometers continue to increase which is mainly due to the long term behaviour of the rock mass around the shaft. On the other hand, we have observed strong pressure reaction associated to lining effect. For further modelling program, it will be interesting to integrate the effect of lower permeability of argillite at the vicinity of the shaft wall (as it was measured in situ by permeability tests) and to realize a THM numerical modelling.

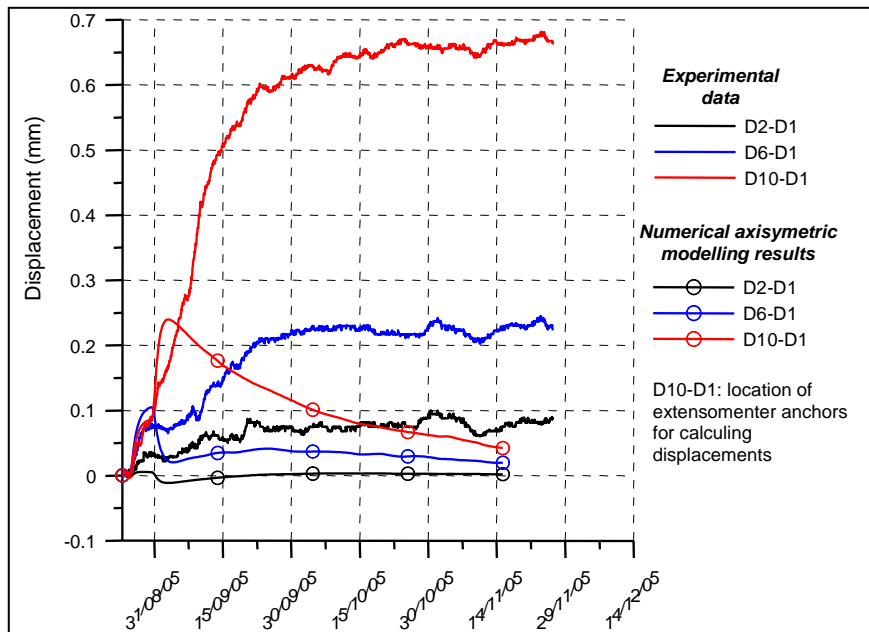


Figure 6.30: Displacements measured on extensometer REP2202 compared with axisymmetric numerical model

6.5.3 Numerical modelling of the TER experiment

Thermal analysis

The experiment was followed by two numerical models. The first one was entrusted upon CEA (DM2S Department – System and Structure Modelling) in order to compare the results of direct calculations to those of *in-situ* measurements (Filippi, 2006), while the second was drawn by UPC and aimed at identifying thermal parameters by minimising a cost function on the base of a 3-D model (Olivella, 1996).

Direct thermal modelling by CEA

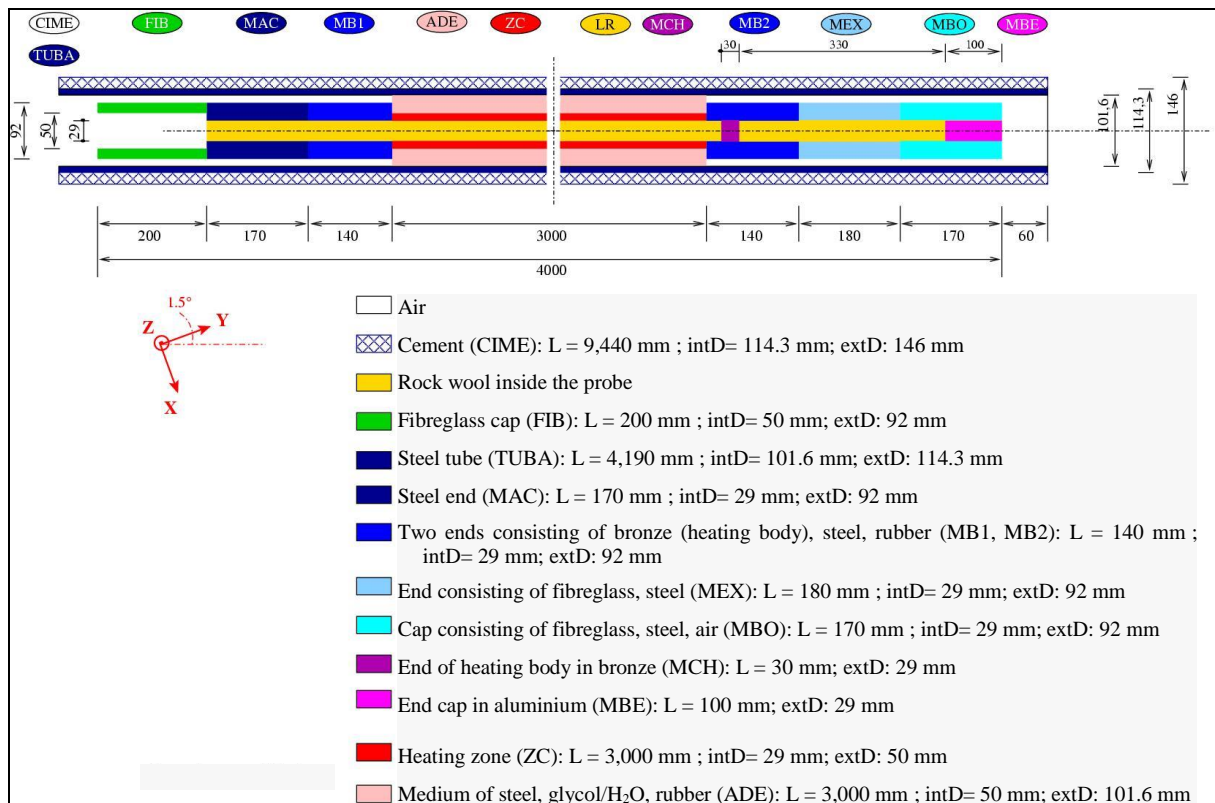
The thermal analysis is conducted by using the heat equation (Fourier's law) in transient regime. A 3-D model was considered in order to simulate the overall test with a side extension in the order of 20 m. Eleven materials are covered in the calculations; their characteristics are mentioned in Table 6.7 and in Figure 6.31. Certain zones consist of several materials and must be taken into account by homogenisation. All materials contained in the heating probe are assumed isotropic.

Table 6.8: Thermal characteristics of the materials

	Thermal conductivity	Specific heat	Specific gravity
	$\lambda [W \cdot m^{-1} \cdot K^{-1}]$	$C_p [J/(kg \cdot K)]$	$\rho [kg/m^3]$
Material, heating probe			
Air	0.0214	1,010	1.292
Steel	52.5	440	7,850
Bronze	83	410	8,670
Aluminium	227.6	896	2708
Fibre glass	1.05	824.5	2,630
Pressurised fluid (gly.)	0.412	3,544	1,080
Rubber, membrane	5	2,000	1,100
Rock wool	0.04	1,000	70
External material			
PVC	0.16	1,210	1,550
Cement mortar	1	830	1,600
Argillite	$\lambda_{\parallel}^a = 1.9$ $\lambda_{\perp}^a = 1.3$	1,064	2,390

For the argillites, the selected parameters are:

- specific heat of the saturated rock: $C_p = 1,000 J \cdot kg^{-1} \cdot K^{-1}$,
- anisotropic thermal conductivity: three cases around the parameters measured on samples
 - Case 1, $\lambda_{\parallel} = 2.2 W \cdot m^{-1} \cdot K^{-1}$; $\lambda_{\perp} = 1.48 W \cdot m^{-1} \cdot K^{-1}$;
 - Case 2, $\lambda_{\parallel} = 1.9 W \cdot m^{-1} \cdot K^{-1}$; $\lambda_{\perp} = 1.3 W \cdot m^{-1} \cdot K^{-1}$ (reference parameters);
 - Case 3, $\lambda_{\parallel} = 2.0 W \cdot m^{-1} \cdot K^{-1}$; $\lambda_{\perp} = 1.25 W \cdot m^{-1} \cdot K^{-1}$.



The thermal power were taken into account in the modelling is the actual injected power in the formation, i.e. 277 W and 925 W during Phases 1 and 2, respectively (see Figure 6.18).

The overall results show that the 3-D thermal model reproduces satisfactorily the test and that the thermal-diffusion process is well understood, as in the case of the HE-D experiment at Mont Terri.

The comparison between the different cases calls for the following observations:

Experimental data are always higher than the temperature calculated in and on the surface of the heating probe, but the thermal parameters of the different elements of the heating probe must be adjusted. However, that has no impact on the results within the argillite, since the heat flux is the key factor in that zone.

It is difficult to detect the best set of parameters from this (Figure 6.32).

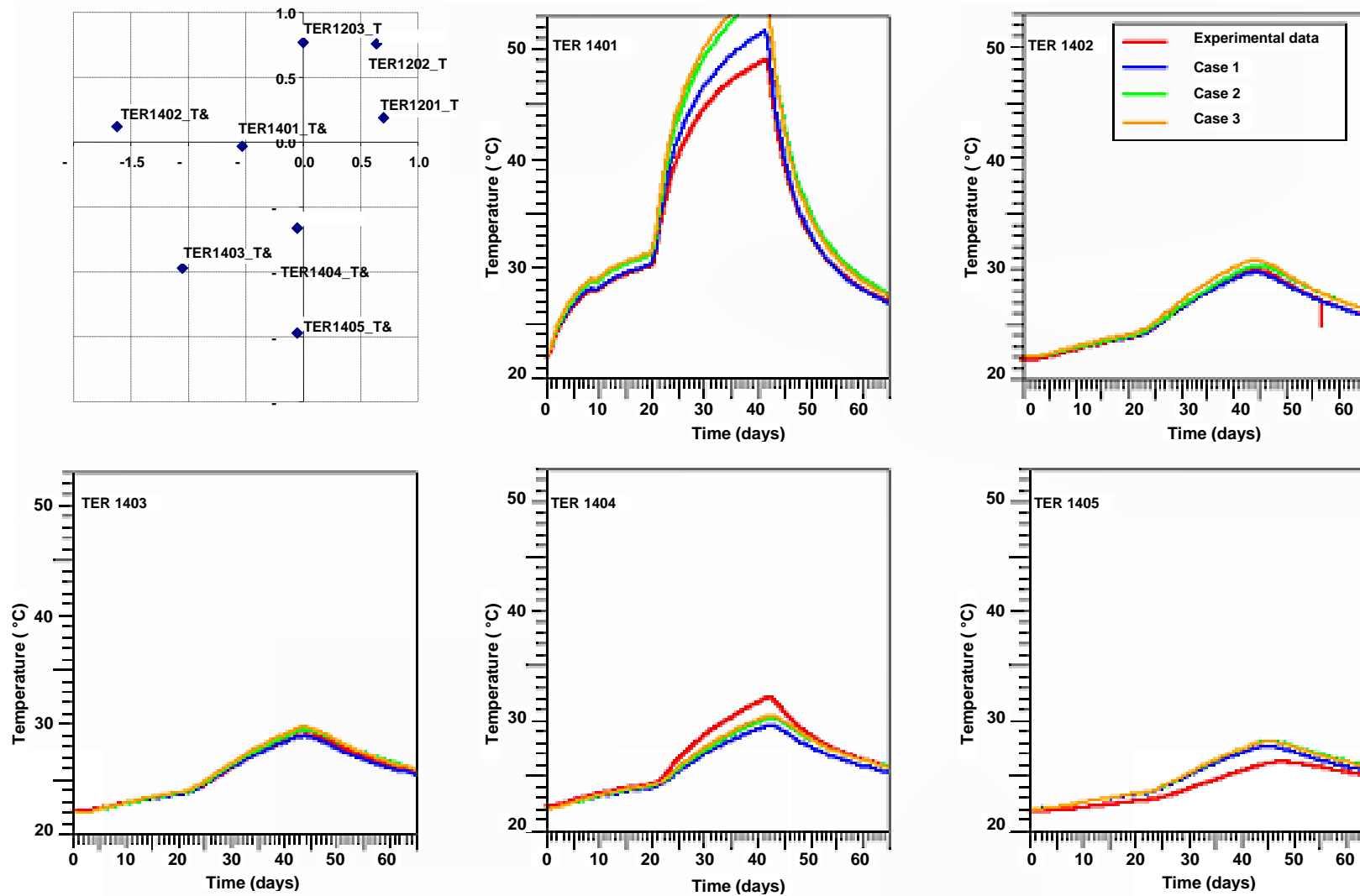


Figure 6.32: Location of temperature sensors and comparison of temperatures from experimental data and modelling

Determination of thermal parameters by inverse modelling by UPC

The purpose of inverse modelling is to estimate the specific heat of the rock, C_p , as well as thermal-conductivity parameter, λ , considered isotropic, on the basis of the temperature field measured *in situ*.

The resolved equation is the one for energy-conservation. A single phase is considered as an equivalent porous medium. Thermal conductivity and specific heat are considered to be constant. Their value is the result of inverse modelling.

The purpose of the analysis is to minimise the error between measurements and calculation results, by repeating the calculations for different pairs of thermal-conductivity and specific-heat values. The error is calculated as follows:

$$\varepsilon = \frac{\sum_{i=1}^{n_{MP}} \left[\sum_{j=1}^{n_T} \left((T_{real}(j) - T_{sim}(j))^2 \cdot \frac{\Delta t(j)}{t_{heat}} \right) \right]}{n_{MP}} \quad (6.2)$$

where:

$T_{real}(j)$ represents the temperature measurements achieved *in situ* and $T_{sim}(j)$, the calculation results during the corresponding time, j ;

$\Delta t(j)$, the time interval between two temperature measurements;

t_{heat} , the time during which measurements are analysed (47 days);

n_T , the number of time intervals involved;

n_{MP} , the number of comparison points, i.e., the number of temperature sensors.

Two kinds of modelling are performed: an axisymmetric modelling in which the medium is assumed isotropic and a 3D modelling in which the medium is anisotropic.

In the first case, the axisymmetric portion measuring 23.4 m in height and 12.7 m in width is discretised into 3,300 triangles (Figure 6.33). On the symmetry axis and on the borehole wall, no flux is applied. On the lower, right and upper boundaries, a temperature of 22 °C is applied, corresponding to the initial temperature of the massif.

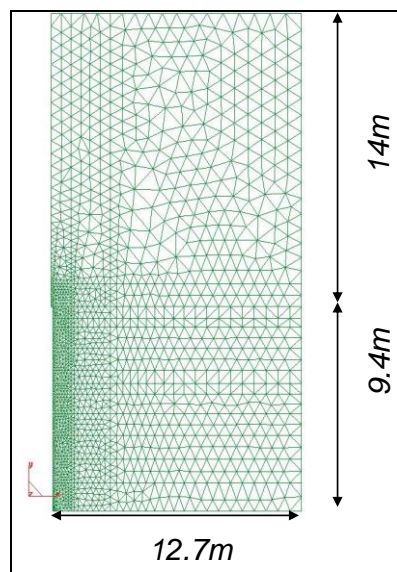


Figure 6.33: Mesh used for the inverse modelling of TER experiment

The heating element is not explicitly discretised. Heating is simulated by an applied flux on the borehole wall (277 and 925 W during heating phases 1 and 2). The initial temperature is set at 22°C.

A total of 110 variations of axisymmetric calculations were performed for thermal-conductivity values ranging from 1.2 to 2 W·m⁻¹·K⁻¹ and for specific-heat values ranging from 800 to 1,200 J·kg⁻¹·K⁻¹. The error, calculated over all temperature sensors, is shown in Figure 6.34. The minimum error is obtained with $\lambda = 1.75 \text{ W}\cdot\text{m}^{-1}\cdot\text{K}^{-1}$ and $C_p = 1,005 \text{ J}\cdot\text{kg}^{-1}\cdot\text{K}^{-1}$. The quasi-verticality of iso-error lines shows a high dependency of the thermal field to thermal conductivity and a low dependency to specific heat.

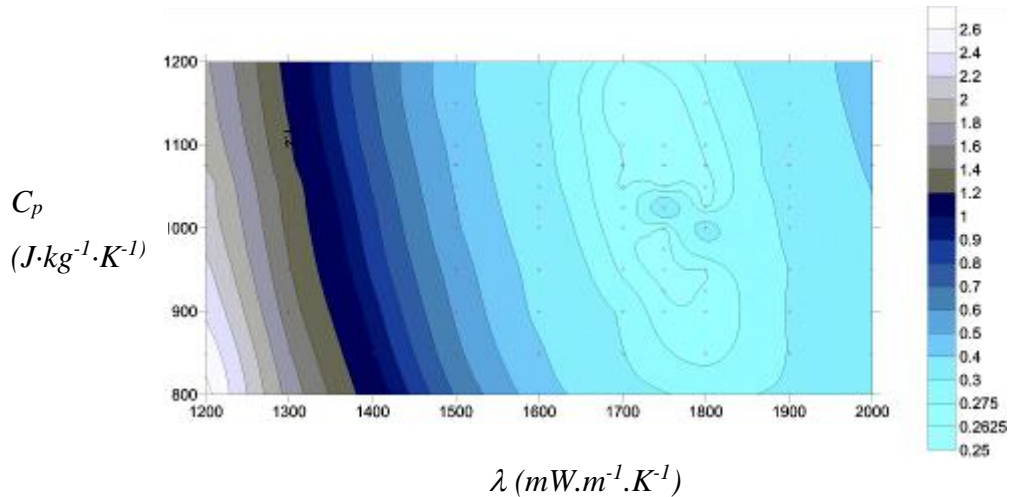


Figure 6.34: Axisymmetric thermal calculations: error map generated on the basis of axisymmetric thermal calculations by varying thermal conductivity and specific heat

Figure 6.35 provides a comparison between measurements and simulations related to the direction. In the direction parallel to the bedding, measured temperatures are higher than those simulated by axisymmetric modelling. In the vertical direction, calculations overestimate the temperature.

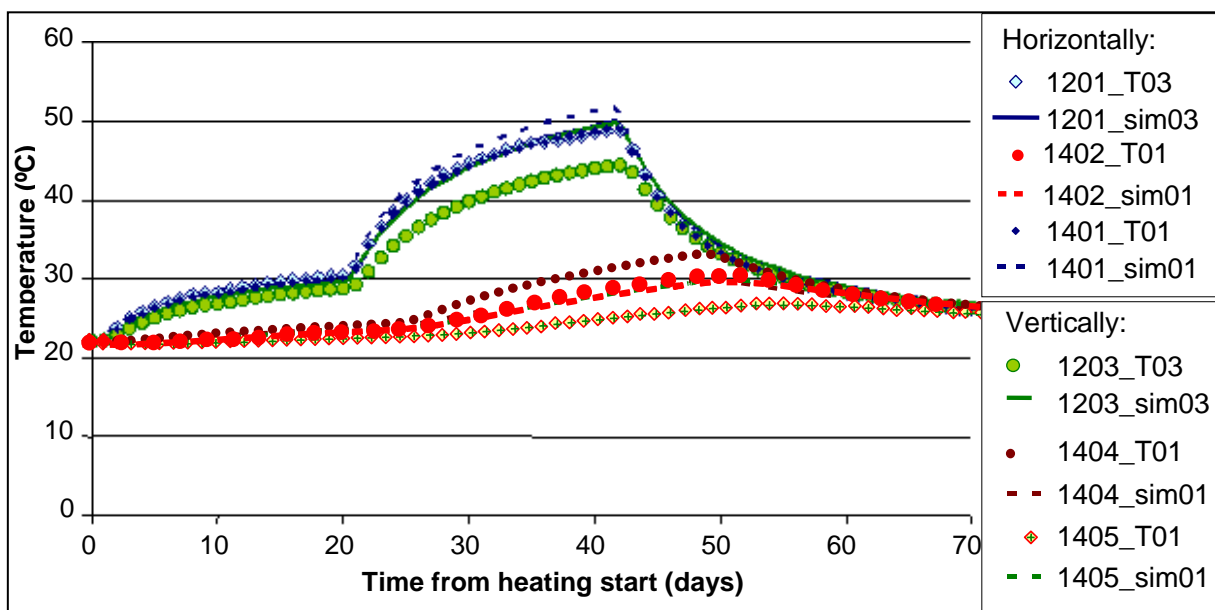


Figure 6.35: Axisymmetric thermal calculations: Comparison between measured and calculated temperatures in directions parallel and perpendicular to the bedding (precise location of the sensors is given by Figure 6.29)

Particularly, sensors 1201_T03, 1203_T03 and 1401_T01 located at the same distance from the centre of the probe, but in different directions, confirm the incapability of an isotropic model to reproduce the temperature differences measured in the different anisotropy directions. That observation leads us to consider the anisotropy of thermal conductivity in order to reproduce better the thermal field being measured.

In the second case, the purpose of 3-D thermal analysis is to estimate both thermal-conductivity parameters, λ_{\perp} and λ_{\parallel} , of argillites, with λ_{\perp} representing the vertical thermal conductivity and λ_{\parallel} , the horizontal thermal conductivity containing the borehole. The estimated value of the specific heat by the axisymmetrical analysis ($C_p = 1,005 \text{ J}\cdot\text{kg}^{-1}\cdot\text{K}^{-1}$) is used for those calculations.

A domain measuring 24 m square and 12 m in height was discretised into 23,000 hexahedra (Figure 6.36). A temperature equal to 22°C was applied on the lateral sides and on the opposite side to the TER niche. On the side of the TER niche, no flux was applied. The initial temperature was equal to 22°C.

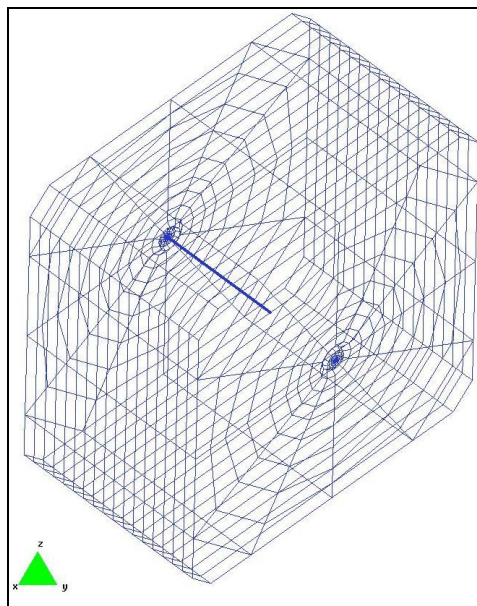


Figure 6.36: 3-D thermal calculations: Geometry and spatial discretisation

A total of 315 calculations were performed. The resulting error map is shown in Figure 6.37. The minimum error corresponds to the values of $2 \text{ W}\cdot\text{m}^{-1}\cdot\text{K}^{-1}$ and $1.3 \text{ W}\cdot\text{m}^{-1}\cdot\text{K}^{-1}$ for λ_{\parallel} and λ_{\perp} respectively. Since that minimum error has the same value as the one calculated from the axisymmetric calculations, it is possible to assume that the overall quality of the reproduction of the thermal field on the basis of 3-D thermal calculations did not improve significantly.

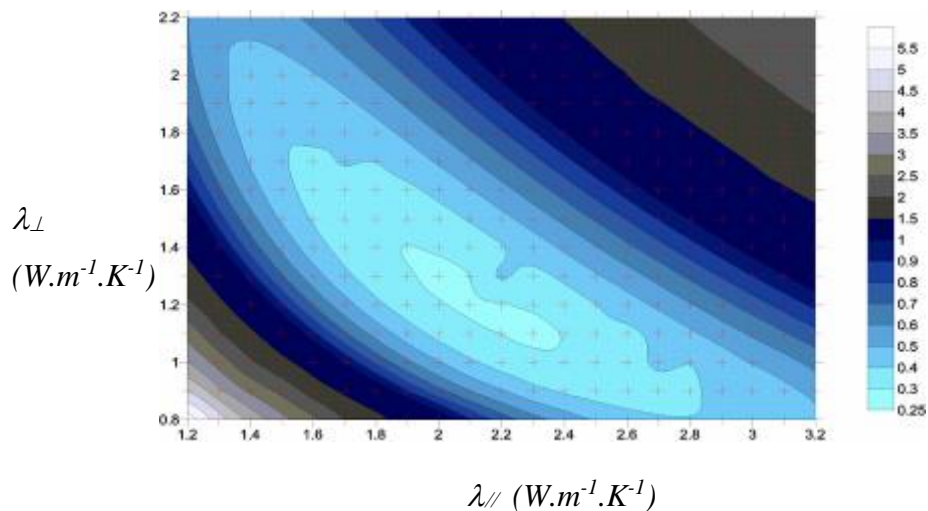


Figure 6.37: Error map generated on the basis of 3-D thermal calculations by varying thermal conductivity in the parallel vertical and horizontal planes to the borehole axis.

To take into account the thermal conductivity anisotropy, while keeping the same mean thermal conductivity ($\lambda = (\lambda_{\parallel} + \lambda_{\perp})/2 = 1.75$) as used by axisymmetric simulation, leads to the following consequences comparing to the axisymmetric simulation (Figure 6.38):

- The temperatures increase in a direction parallel to the bedding;
- The same temperatures are found in the intermediate direction;
- The temperatures decrease in a direction perpendicular to the bedding.

In the case of 3-D thermal calculations, when calculating the temperatures at a same distance from the probe, the temperatures in a direction parallel to the bedding are higher than the others.

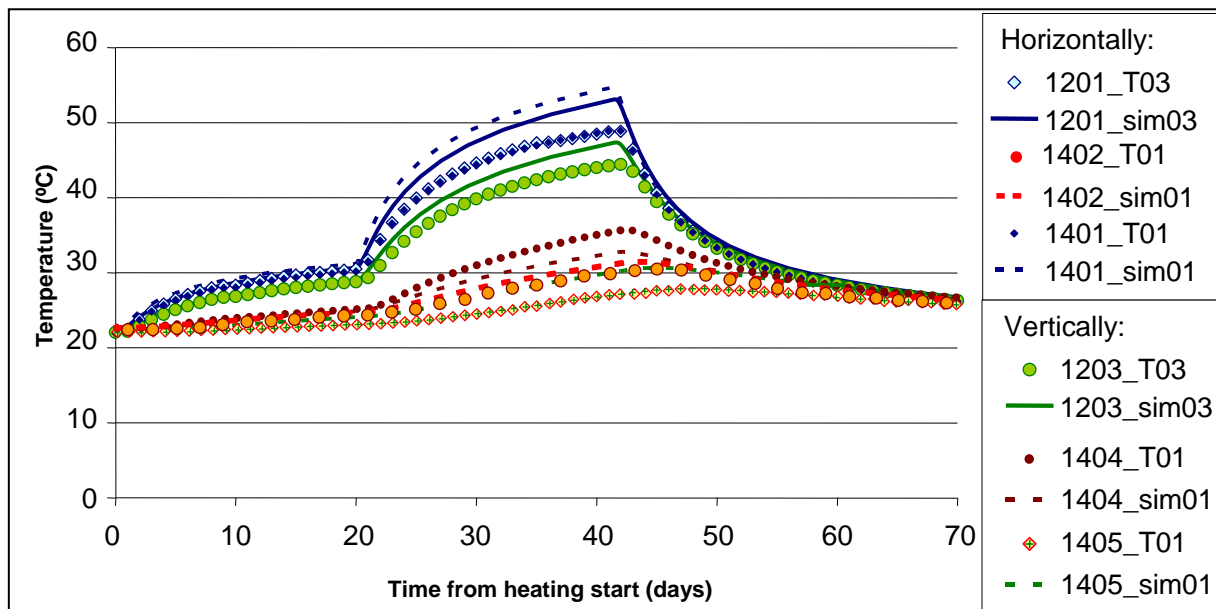


Figure 6.38: 3-D thermal calculations: Comparison between measured and calculated temperatures in directions parallel and perpendicular to the bedding (precise location of the sensors is given by Figure 6.27)

The 3-D thermal calculations brings some improvement, which also helps to refine the results analysis of the sensors that had already been confirmed as consistent by comparison of the thermal field measured with the results of the isotropic simulation. However it is difficult to dissociate the

uncertainties concerning the experimental phase n°2 from the problems linked to the incorrect programming of the power regulator. Since September 2006, new temperature cycles should improve the reproduction of the *in-situ* test.

At the current stage of the analysis and following the two interpretative models developed by the CEA and UPC, the following preliminary conclusions may be drawn:

- Both 3-D calculations are consistent with each other, as well as with test data;
- Phase 2 of the heating process (31 January-20 February 2006) seems to be less consistent with the involved power of 975 W. A slight error in the calibration of the sensors or a disturbance in the power injection at the time of the incident on the membrane should not be excluded. Other thermal cycles should help to determine if such divergence recur;
- A systematic discrepancy between measurements and simulations for sensors located at the level of the heater front remains unexplained by the thermal anisotropy. Measured data are always higher than those of calculations. A possible explanation might be a non-homogeneous heating along the probe;
- A specific heat for the rock equal to $1,005 \text{ J}\cdot\text{kg}^{-1}\cdot\text{K}^{-1}$ (i.e., $800 \text{ J}\cdot\text{kg}^{-1}\cdot\text{K}^{-1}$ for the solid phase, with a 15 % porosity) is determined by the backward thermal calculations made by the UPC. The error map presented in Figure 6.34 also shows that the specific-heat parameter is very dependent on thermal conductivity;
- Thermal conductivities determined through inverse modelling (3-D calculations by UPC) for $\lambda_{//}$ and λ_{\perp} are in the order of $2 \text{ W}\cdot\text{m}^{-1}\cdot\text{K}^{-1}$ and $1.3 \text{ W}\cdot\text{m}^{-1}\cdot\text{K}^{-1}$, respectively. Those values are close to the values measured on samples (1.9 and 1.3 W/m/K parallel and perpendicular to the bedding, respectively).

Figure 6.39 represents the average temperature difference as calculated by UPC between the pairs of sensors installed symmetrically on both sides of middle plane the of the heating element).

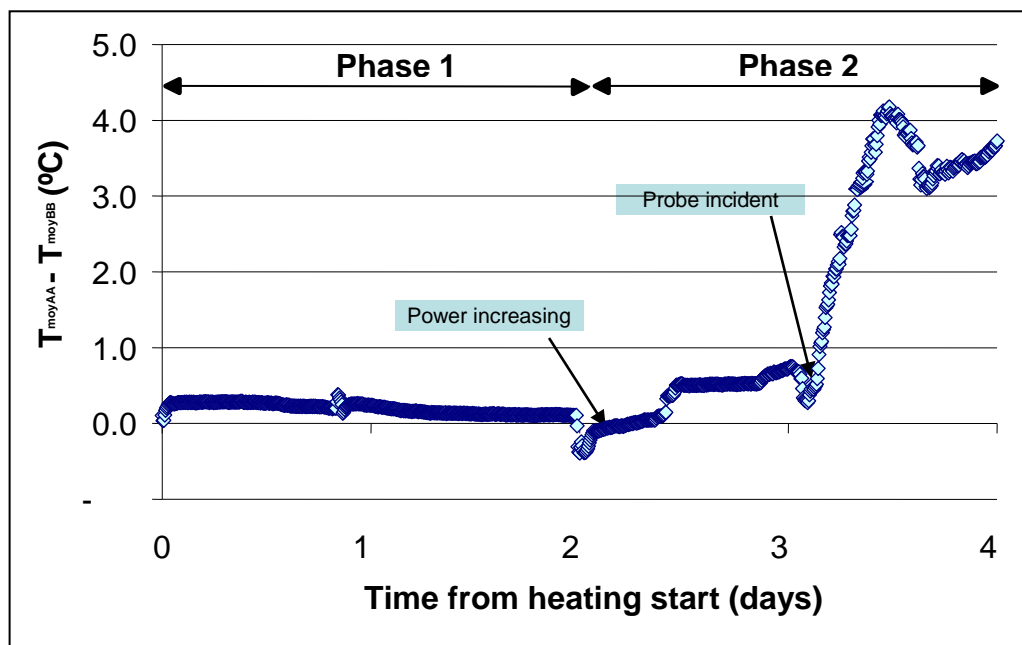


Figure 6.39: Differences of the average temperatures between the pairs of sensors installed symmetrically on both sides of middle plane the of the heating element).

(from UPC 3D modelling)

The difference remains small during phases 1 and 2 before the incident, thus confirming the symmetry of the temperature field. After the incident, it increases sharply and is likely associated with a heat loss on the side where the oil leak occurred.

Thermo-hydro-mechanical coupling analysis

The purpose of the THM-coupling analysis is to understand the evolution of pore pressures and of deformation during the different thermal phases (heating and cooling). UPC was responsible for carrying out this modelling with Code_bright, the numerical THM code developed by them (Olivella, 1996).

The method used is to estimate the permeability and thermal expansion of the porous medium by performing an inverse analysis of pore-pressure and deformation fields. It is similar to that developed for the thermal field analysis. It should be noted that those parameters have a direct impact on pore pressures and deformations of a porous medium during the heating process.

Resolved equations and parameters taken into consideration for the argillite

A linear elastic law was considered for the argillite. The reference parameters were used except for thermal conductivity, the value of which results from the above-mentioned inverse isotropic model ($\lambda_{\text{mean}} = 1.75 \text{ W/m/K}$). The purpose is to minimise the error between the measured pressure and deformation fields and those resulting from the THM calculations. In order to achieve that goal, different calculations are performed by considering a pair of intrinsic-permeability and thermal-expansion values for each of them. The error is calculated by replacing T in Equation 6.2 by pore pressure, p_w , for the hydraulic field and by deformation standard, ε , for the kinematic field. The intrinsic-permeability values being used range between 10^{-21} and 10^{-18} m^2 . In the case of the linear thermal expansion, values vary between 10^{-8} and $10^{-4} \text{ }^\circ\text{C}^{-1}$. The values for the thermal expansion of the solid grain and of the skeleton are considered to be equal, assuming that the heating process does not induce any structural alteration.

The temperature field has already been described above and is not affected by the interstitial-pressure and deformation fields.

Geometry, initial conditions and boundary conditions

An axisymmetric domain measuring 23.4 m in height and 12.7 m in width is discretised in 3,333 triangles. The applied boundary conditions are given by the Figure 6.40.

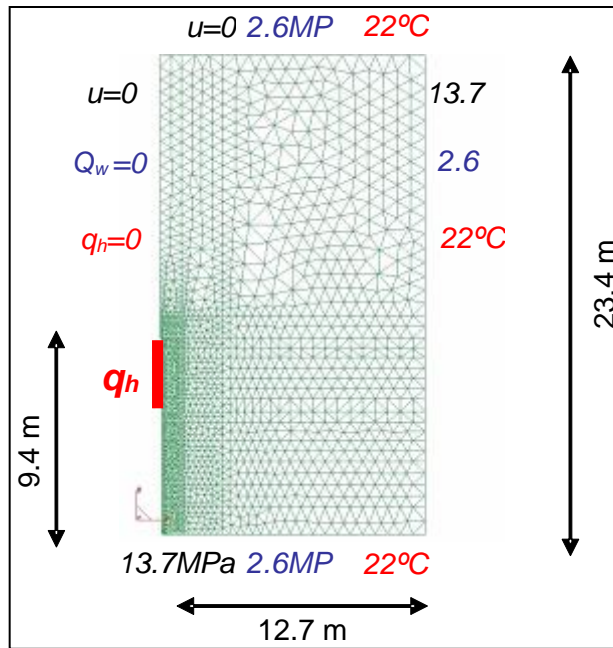


Figure 6.40: HM modelling: geometry, spatial discretisation and boundary conditions

The heating element is not explicitly discretised. Heating is simulated by a flux being applied to the borehole wall (277 and 925 W during phases 1 and 2, respectively).

Analysis of results

A total of 1,320 calculations were performed. The error representation for each of those calculations for the pore-pressure and the deformation fields is shown in Figure 6.41(a) and (b), respectively.

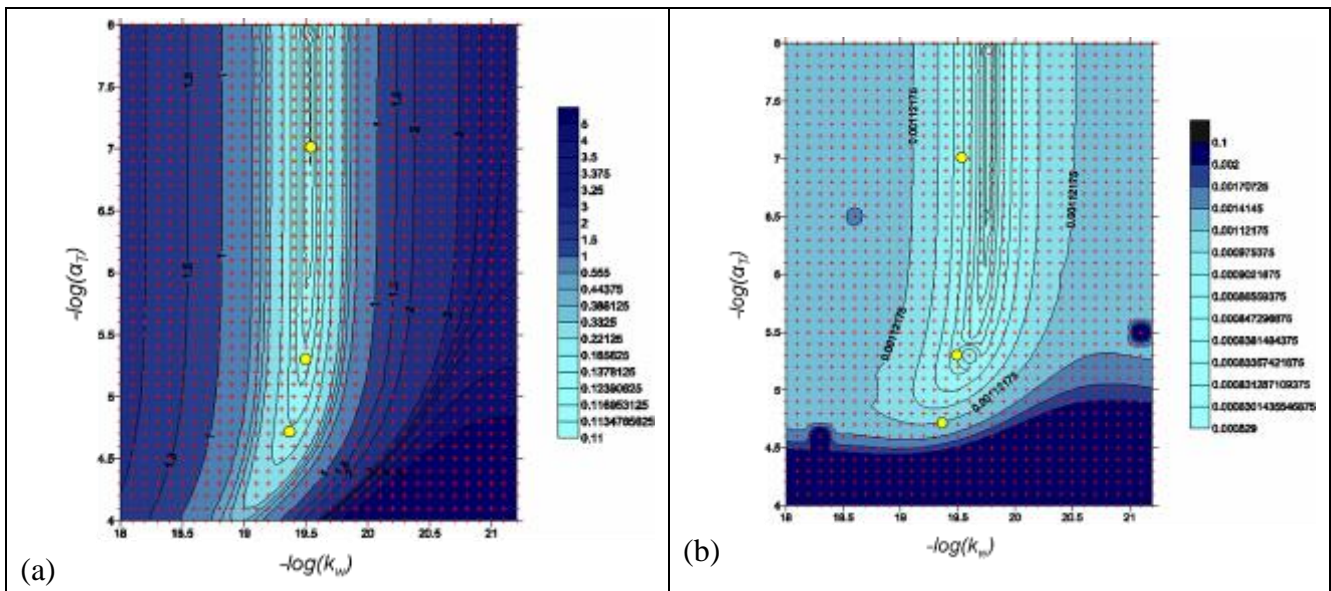


Figure 6.41: Error maps generated by comparing pressure fields (a) and deformation fields (b) to THM calculation variations

The error is dissociated from the value of the coefficient for linear thermal expansion, when the latter is lower than $10^{-5} \text{ }^\circ\text{C}^{-1}$ and becomes negligible in comparison to the coefficient for the thermal expansion of water ($1.13 \cdot 10^{-4} \text{ }^\circ\text{C}^{-1}$). Consequently, the pore pressure is only controlled through the intrinsic permeability of the argillite. In that case, the deformation mechanism of the medium follows the principle of effective stress.

The error concerning the deformation field increases rapidly with the value for the linear thermal expansion of the solid, when that value exceeds $10^{-4.7} \text{ }^\circ\text{C}^{-1}$. As that value increases, the deformation field appears to be controlled more and more by the thermal-expansion coefficient of the solid.

As the permeability of the argillite increases, the error concerning the pore-pressure becomes more stable, which seems to be logical since no pore pressure is generated once a certain permeability level has been reached. On the contrary, when permeability decreases, both the induced pore pressures and the error increase.

The *de minimis* zone of the error map for pore pressures ($k_w = 10^{-19.5} \text{ m}^2$) is offset compared to the error map for deformations ($k_w = 10^{-19.75} \text{ m}^2$). It is possible to grant a higher level of confidence to the former than to the latter, since deformations evolve within a range of very low values that are close to the measurement thresholds of the instruments being used.

In order to display better the error between calculations and data, it was decided to compare measurements recorded by sensors and calculations results for three sets of different parameters taken in the *de minimis* zone of the error map for pore pressures. The values of the selected parameters and the errors associated with each of the calculations are summarised in Table 6.9.

Table 6.9: Variations in THM-calculation parameters and associated errors

	$k_w [m^2]$	$-\log(k_w)$	$\alpha_T [K^{-1}]$	$-\log(\alpha_T)$	ε (pressure)	ε (deformation)
THM-I.2.A	$2.8 \cdot 10^{-20}$	19.55	$1 \cdot 10^{-7}$	7	0.113	$8.9 \cdot 10^{-4}$
THM-I.2.B	$3.16 \cdot 10^{-20}$	19.5	$5 \cdot 10^{-6}$	5.3	0.131	$8.9 \cdot 10^{-4}$
THM-I.2.C	$4.46 \cdot 10^{-20}$	19.35	$2 \cdot 10^{-5}$	4.7	0.166	$11 \cdot 10^{-4}$

The intrinsic permeability assessed by this method (2.8 to $4.5 \cdot 10^{-20} \text{ m}^2$) is very close to the one measured in situ ($5 \cdot 10^{-21}$ to $5 \cdot 10^{-20} \text{ m}^2$). THM-I.2.A corresponds to the area where the thermal-expansion coefficient is very low in comparison to that of water, THM-I.2.B to the area where the error is minimised on both the pore-pressure and deformation map (area consistent with reference values). THM-I.2.C corresponds to a thermal expansion coefficient of $2 \cdot 10^{-5} \text{ }^\circ\text{C}^{-1}$, which is the upper limit of experimental data.

Figure 6.42 compares the results of the three cases with the experimental pore pressure data.

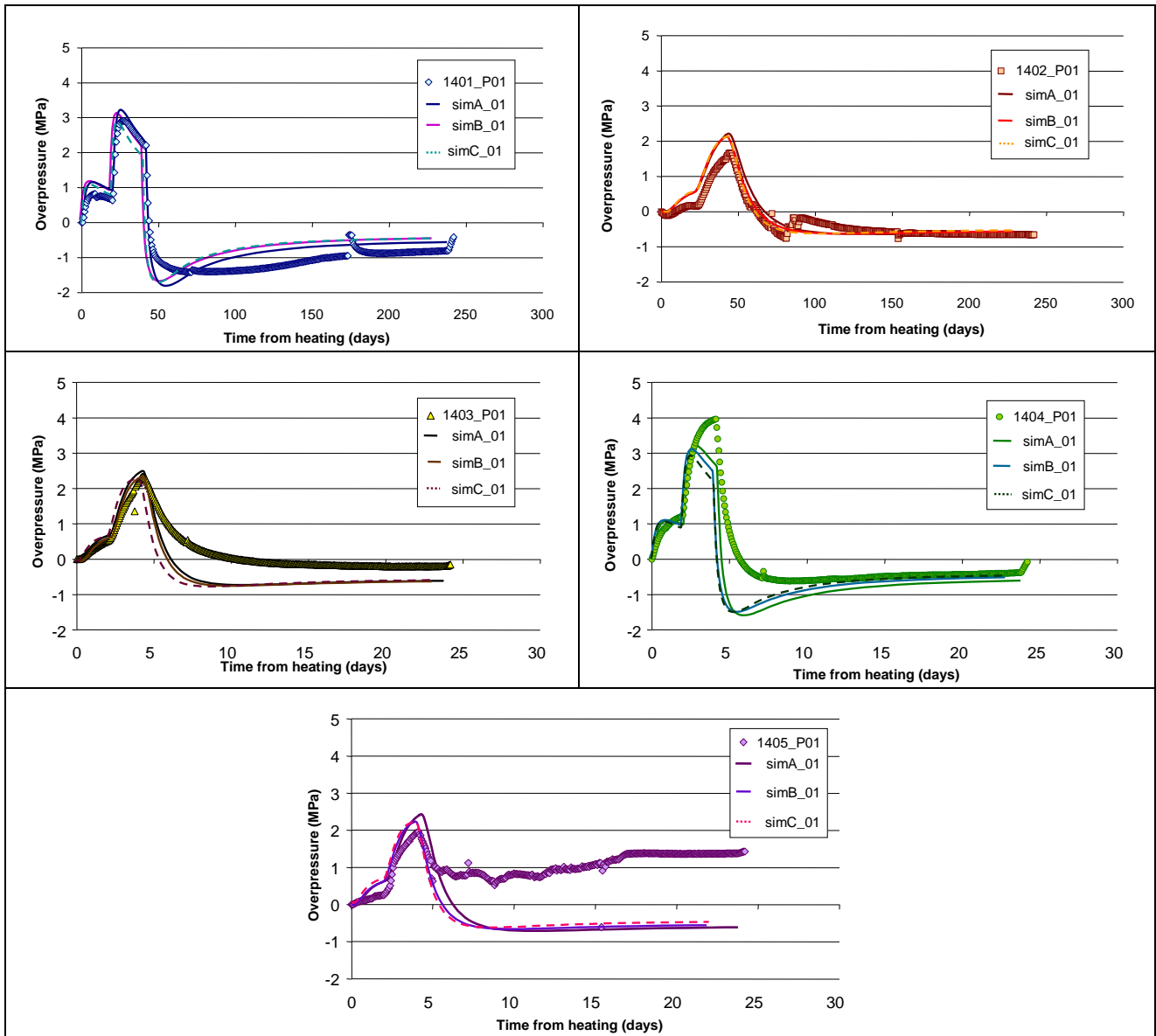


Figure 6.42: Comparison between the tree results of modelling and measured pore pressures

In general, it should be noted that the three cases gives very close results. Pore pressure is overestimated for chamber TER1401 and underestimated for chamber TER1404. That observation could be correlated with a small anisotropy in the permeability of the argillite, although it was not detected by hydraulic tests in boreholes. Simulations suggest that pore pressures, at the end of the cooling period, do not resume their initial state before heating. The behaviour of sensor TER1405 during cooling is unexplained.

Figure 6.43 compares the results of the three cases with the experimental deformation data.

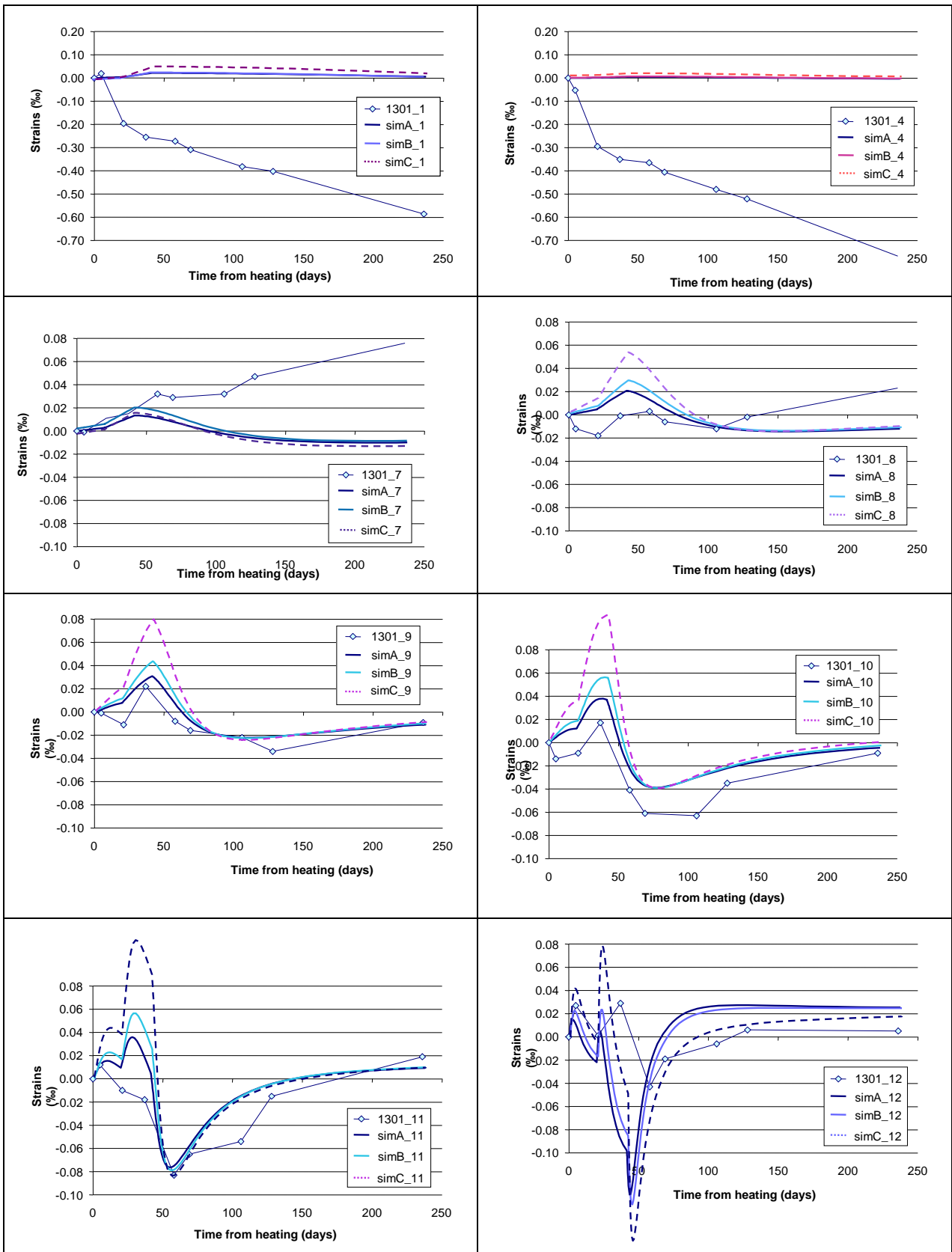


Figure 6.43: Comparison between the three modelling results and deformations measured inside extensometer TER1301

The deformations forecasted by the three simulations are quite inconsistent with measurements of intervals 1 to 4 in extensometer TER1301. In fact the convergence of the KEY drift, which is not

taken into account in the modelling, is much larger (4 to $5 \cdot 10^{-4}$) than the compression due to heating ($5 \cdot 10^{-6}$ to $3 \cdot 10^{-5}$).

For intervals 5 to 8 the three simulations indicate a monotonous compression during the heating, corresponding relatively well to *in-situ* measurements. The extended compression measured during the cooling phase (deferred in the interval 8) is neither explained by modelling. It is obviously due also to the convergence of the drifts delineating the TER zone.

With regard to intervals 9 to 12, the slope inversion between phases 1 and 2 and the compression-extension cycle associated with the heating-cooling period is well reproduced by modelling. However, the initial extension phase as measured *in situ* for intervals 8 to 10 does not exist in the numerical simulations. It is therefore possible to assume that measurements are incorrect due to their low value.

It is important to note that the deformation mechanism of the porous medium in simulation A (THM-I.2.A) is only associated with the pore pressure development. The very good reproduction of measurements for a negligible value of the solid thermal expansion, except in interval 12, seems to indicate that the actual value of the thermal-expansion coefficient is close to the inflection point of the valley of the error map of the pressure field (Figure 6.41a), i.e., the moment when the solid thermal expansion starts to have an impact.

At the opposite, the simulation C (THM-I.2.C) results for the intervals located close to the heating probe suggest that the value of the solid thermal-expansion coefficient is too high: those high values would have been reproduced by measurements, the precision of which keeps improving for more significant deformations.

Simulation B (THM-I.2.B) results fit best to *in-situ* data and seems to provide the best estimate in terms of error on pore pressures and deformations.

It is not clear if extension could have led to fracturing. The only visible fractures appeared on the wall of the GEX drift during the phase 2 (Figure 6.44). They are to be related to the non-homogeneous heating along the probe.



Figure 6.44: Radial fractures occurred around the heater borehole on the GEX drift wall

7 References

References for Boom Clay

- Adenot, F., Maxoin, C., Tognazzi, C., Bredy, P., Bourbon, X., Bloem, P. J. C., Fachinger, J., Abdou, L., Sneyers, A., Labat, S., Van Iseghem, P., Marx, G., Altenhein-Haese, C., Bischoff, H., Brodersen, K., Cowper, M., Glasser, F. P., Paul, M., Dickson, C. L., Reed, D., and Tyrer, M. (2001) Barrier performance of cements and concretes in nuclear waste repositories, Final report, EUR 19780 EN.
- Alheid H.J., Aranyosy J.F., Blumling P., Hoteit N., Van Geet M. (2007) EDZ development and evolution – State of the art. NF-PRO. Contract Number F16W-CT-2003-02389
- Alonso E.E., Gens A. and Josa A., (1990) A constitutive model for partially saturated soils. *Géotechnique*, 40(3), p. 405-430
- Alonso E.E., Alcoverro J. (2000) Calculation and testing of the behaviour of unsaturated clay as a barrier in radioactive waste repositories ('Catsius clay' project), Final report, EUR 19141
- Altaner S.P. & Ylagan R. F. (1997) Comparison of structural models of mixed-layer illite/smectite and reaction mechanisms of smectite illitization. *Clays and Clay Minerals*, 45, 517 - 532.
- Awwiller D.N. (1993) Illite-smectite formation and potassium mass transfer during burial diagenesis of mudrocks: a study from the Texas Gulf Coast Paleocene-Eocene. *J. Sediment. Petrol.* 63, 501-512.
- Baldi G., Borsetto, M., Hueckel, T., (1987) Calibration of mathematical models for simulation of thermal , seepage and mechanical behaviour of Boom clay, Final report, EUR 10924 EN
- Baldi G., Hueckel T., Peano A. Pellegrini R., (1991) Developments in modeling of thermo-hydro-geomechanical behaviour of Boom clay and clay-based buffer materials, Final report EUR 13365 EN
- Bastiaens, W., Bernier, F., Buyens, M., Demarche, M., Li, X.L., Linotte, J.M., Verstricht, J. (2003) The Connecting Gallery. Euridice report 03-294
- Bastiaens W., Bernier F., and Li X.L. (2006) An Overview of Long-Term HM Measurements around HADES URF. Symp., Liège, 2006, May 9-12, 15-26.
- Bastiaens, W., Bernier, F., Li, X.L., 2007. SELFRAC: Experiments and conclusions on fracturing, self-healing and self-sealing processes in clays. *Physics and Chemistry of the Earth, Parts A/B/C*, Volume 32, Issues 8-14, Pages 600-615, Elsevier.
- Bernier, F., Li, X.L., Verstricht, J., Barnichon, J.D., Labiouse, V., Bastiaens, W., Palut, J.M., Ben Slimane, J.K., Ghoreychi, M., Gaombalet, J., Huertas, F., Galera, J.M., Merrien, K. and Elorza, F.J. (2003) Clipex: Clay instrumentation programme for the extension of an underground research laboratory. Report EUR 20619 EN. European Commission, Luxembourg, 141 pp

- Bernier F. (2004) SELFRAC: Fractures and self-healing within the excavation disturbed zone in clays. Geological Disposal of Radioactive Wastes produced by Nuclear Power. European Commission Report EUR21224.
- Bernier F., Li X.L., Bastiaens W., Ortiz L., Van Geet M., Wouters L., Frieg B., Blümling P., Desrues J., Viaggiani G., Coll C., Chanchole S., De Greef V., Hamza R., Malinsky L., Vervoort A., Vanbrabant Y., Debecker B., Verstraelen J., Govaerts A., Wevers M., Labiouse V., Escoffier S., Mathier J.-F., Gastaldo L., Bühler Ch. SELFRAC: Fractures And Self-Healing Within The Excavation Disturbed Zone In Clays- Final report, European Commission, CORDIS Web Site, EUR 22585, 2006
- Bernier F., Li X.L. and Bastiaens W. (2007) Twenty-five years' geotechnical observation and testing in the Tertiary Boom Clay formation, Thomas Telford, *Géotechnique* 57, N°2, 229-237
- Bouchet A., Meunier A., Velde B. (1988) Hydrothermal mineral assemblages containing two discrete illite-smectite minerals. *Bull. Min.* 111, 587-599.
- Bouchet A., Lajudie A., Rassineux F., Meunier A., Atabek R. (1992) Mineralogy and kinetics of alteration of a mixed-layer kaolinite/smectite in nuclear waste disposal simulation experiment (Stripa site, Sweden). *Appl. Clay Sci.* 7, 113-123.
- Chapman N.A. (1994) The geologist's dilemma predicting the future behaviour of buried radioactive waste. *Terra Nova* 6, No. 1.
- Coll C., Escoffier S., Hamza R.W., Vervoort A., Blümling P., Frieg B., Bastiaens W., Berest P., Bazargan B., Desrues J., Viaggiani G., Labiouse V., Dehandschutter B., Wouters L., Vanbrabant Y., Mertens J., Li X.L., Bernier F. (2004) EC SELFRAC Project – FIKW-CT-2001-00182, Deliverable 1: State of the art on Fracturation and Sealing-Healing Processes and Characterisation, EURIDICE
- Coll C. (2005) Endommagement des Roches Argileuses et Perméabilité Induite au Voisinage d'Ouvrages Souterrains, PhD Thesis, Université Joseph Fourier, Grenoble
- C. Coll, F. Collin, J.P. Radu, P. Illing, Ch. Schroeder & R. Charlier (2007), Long term behaviour of Boom Clay- Influence of clay viscosity on the far field pore pressure distribution, Final report, research convention EURIDICE-ULg
- De Bruyn D. (1999) Influence d'une élévation de température sur le comportement physique et mécanique de l'argile de Boom dans le cadre de la problématique de galeries d'enfouissement de déchets radioactifs. PhD Thesis, UCL, Belgium
- De Bruyn D., Labat S. (2002): The second phase of ATLAS: the continuation of a running THM test in the HADES underground research facility at Mol. In: *Engineering Geology* 64, 309 - 316
- De Craen M., Wang L. and Weetjens E. (2004) Natural evidence on the long-term behaviour of trace elements and radionuclides in the Boom Clay. SCK•CEN Final report to NIRAS/ONDRAF for the period 2000-2003, Contract CCHO 2000-773/00/00, KNT 90 01 1467. R-3926, Mol, Belgium.

- De Craen M. (2005) Geochemical characterisation of specific Boom Clay intervals. SCK-CEN Technical Report to NIRAS/ONDRAF for the year 2004. Contract CCHO 2004-2470/00/00, CO 90 01 1467.01, R-4080, Mol, Belgium.
- De Craen M., Wemaere, I., Labat S. and Van Geet M. (2006) Geochemical analyses of Boom Clay pore water and underlying aquifers in the Essen-1 borehole. External report of the Belgian Nuclear Research Centre. SCK-CEN-ER-19, 24 pp. Mol, Belgium.
- Delage P., Sultan N. and Cui Y-J. (2000) On the thermal consolidation of Boom clays. *Canadian Geotechnical Journal*, 37, pp 343-354
- Delage P., Cui Y.J., Sultan N. (2004) On the thermal behaviour of Boom clay. *Proceedings Eurosafe 2004 Conference, Berlin, CD Rom*, 8 p.
- Deniau I., Derenne S., Beaucaire C., Pitsch H. and Largeau C. (2001) Morphological and chemical features of a kerogen from the underground Mol laboratory (Boom Clay Formation, Oligocene, Belgium): structure, source organisms and formation pathways. *Organic Geochemistry* 32, 1343-1356.
- Deniau I., Derenne S., Beaucaire C., Pitsch H. and Largeau C. (2004) Occurrence and nature of thermolabile compounds in the Boom Clay kerogen (Oligocene, underground mol laboratory, Belgium). *Organic Geochemistry* 35, 91-108.
- Deniau I., Derenne S., Beaucaire C., Pitsch H. and Largeau C. (2005a) Simulation of thermal stress influence on the Boom Clay kerogen (Oligocene, Belgium) in relation with long-term storage of high activity nuclear waste. I – Study of generated soluble compounds. *Applied Geochemistry* 20, 587-597.
- Deniau I., Behar F., Largeau C., De Cannière P., Beaucaire C. and Pitsch H. (2005b) Determination of kinetic parameters and simulation of early CO₂ production from the Boom Clay kerogen under low thermal stress. *Applied Geochemistry* 20, 2097-2107.
- Djeran I., Bazargan B., Giraud A., Rousset G. (1994) Etude experimental du comportement Thermo-Hydro-Mecanique de l'argile de Boom, Rapport final, Rapport n° 94-002
- ECOCLAY II (2005) ECOCLAY II : Effects of Cement on Clay Barrier Performance - Phase II. Final Report, EC project n°FIKW-CT-2000-00028 ; Andra report n°CRPASCM04-0009, 381 p.
- Horseman S.T., Winter M.G. and Entwistle D.C. (1987) Geotechnical characterization of Boom Clay in relation to the disposal of radioactive waste, Commission of the European Communities, Report EUR 10987
- Horton D. G. (1985) Mixed-layer illite/smectite as a paleotemperature indicator in the Amethyst vein system, Creede district, Colorado, USA. *Contrib. Min. Petrol.* 91, 171-179.
- Hueckel T., Baldi G., (1990) Thermoplastic Behavior of Saturated Clays: an Experimental Constitutive Study. *Journal of Geotechnique Engineering*, Vol. 116, N° 12, pp. 1778-1796
- Hueckel T., Borsetto M. (1990) Thermoplasticity of saturated soils and shales: constitutive equations. *Journal of Geotechnique Engineering*, Vol. 116, N° 12, pp. 1765-1777

- Inoue A., Velde B., Meunier A., Touchard G. 1988: Mechanism of illite formation during smectite to illite conversion in a hydrothermal system. *Amer. Mineralogist* 73, 1325-1334.
- Inoue A., Utada M., Wakita K. (1992) Smectite-to-illite conversion in natural hydrothermal systems. *Appl. Clay Sci.* 7, 131-145.
- Jefferies, R.M., (1995) Intercaly II project. A coordinated benchmark exercise on the rheology of clays. Report on stages 2 and 3. CEC Rep., Luxembourg, EUR 16204 EN
- Kolaříková I., Příkryl R., Hanus R., Jelínek E. (2005) Thermal loading of smectite-rich rocks: Natural processes vs. laboratory experiments. *Appl. Clay Sci.* 29, 215-223.
- Li X.L. (2004): Research on THM behaviour of Boom clay - State of the art & Proposal for future research, EURIDICE 04-251
- Mair R.J., Taylor R.N., Clarke B.G. (1992): Repository tunnel construction in deep clay formations, Final report. EUR 13964 EN, Luxembourg: Commission of the European Communities
- Nadeau P. H. & Reynolds R. C. (1981) Burial and contact metamorphism in the Mancos shale. *Clays and Clay Minerals*, 29, 249 - 259.
- Noynaert L., Volckaert G., De Cannière P., Meynendonck P., Labat S., Beaufays R., Put M., Aertsens M., Fonteyne A., Vandervoot F. (1998): The CERBERUS project – Demonstration test to study the near-field effects of an HLW canister in argillaceous formation. Final Report. EUR 18151 EN
- Noynaert L., De Cannière P., De Bruyn D., Volckaert G., Put M., Kursten B., Sneyers A., Van Iseghem P., Beaucaire C., Pitsch H., Bouchet A., Parneix J.C., Samper J., Delgado J., Navarro V., Montenegroz L. and Zhang G. (2000): Heat and radiation effects on the near field of a HLW or spent fuel repository in a clay formation (CERBERUS project), EC report, EUR 19125 EN, 157 pp.
- ONDRAF/NIRAS (2001): Safety and Feasibility interim Report, SAFIR-2 report, NIROND 2001-05, December 2001
- P.A.G.I.S. (1988) Performance Assessment of Geological Isolation System for Radioactive Waste, Commission of the European Community, EUR 11775 EN.
- Perry E. and Hower J. (1970) Burial diagenesis in Gulf Coast pelitic sediments. *Clays and Clay Miner.* 18, 165-177.
- Picard J.M. (1994): Ecrouissage thermique des argiles saturées : application au stockage de déchets radioactifs. PhD Thesis, École Nationale des Ponts et Chaussées, Paris, 283 p.
- Poinssot C., Goffé, B., Magonthier M.C., Toulhoat, P. (1996) Hydrothermal alteration of a simulated nuclear waste glass : effects of a thermal gradient and of a chemical barrier. *Eur. J. Min.* 8, 533-548.
- Pusch R. Karnland O., Lajudie A. and Decarreau A. (1993) MX80 clay exposed to high temperatures and gamma radiation. SKB Technical Report 93-03.

- Pushkareva R., Kalinichenko E., Lytovchenko A., Pushkarev A., kadochnikov V. and Plastynina M. (2002) Irradiation effect on physico-chemical properties of clay minerals. *Appl. Clay Sci.* 21, 117-123.
- Read, D., Glasser, F. P., Ayora, C., Guardiola, M. T., and Sneyers, A. (2001) Mineralogical and microstructural changes accompanying the interaction of Boom Clay with ordinary portland cement, *Advances in Cement Research*, 13, 175-183.
- Robinet J.C., Pasquiou A., Palut J.M., Noynaert L. (1998) Etudes des transferts hydriques entre le massif argileux et les excavations dans un laboratoire souterrain pour le stockage de déchets radioactifs – Essai Phebus. Rapport final. EUR 17792, Eurooffice
- Rousset G. (1988) Comportement mécanique des argiles profondes – Application au stockage de déchets radioactifs. PhD Thesis, Ecole Nationale des Ponts et Chaussées, Paris, 435 pp
- Rousset G., Bazargan B., Ouvry J.F., Bouilleau M., (1993) Etude du comportement différé des argiles profondes, Rapport final, EUR 14438 FR
- Sillen X. and Marivoet J. (2002) Spent fuel performance assessment for a hypothetical repository in Boom Clay at the Mol site (Belgium). SCK•CEN Report BLG-877.
- Smellie, J.A.T., 1998. Maqarin natural analogue study: phase III. SKB Technical Report, TR 98-04, SKB, Stockholm, Sweden.
- Sneyers, A., Paul, M., Tyrer, M., Glasser, F. P., Fays, F., and Van Iseghem, P. (2001) In-Situ interaction between cement and clay: Implications for geological disposal, *Mat.Res.Soc.Symp.Proc.*, 663, 123-129.
- Środoń J., Elsass F., McHardy W. J., Morgan D. J. (1992) Chemistry of illite-smectite inferred from TEM measurements of fundamental particles. *Clay Miner.* 27, 137-158.
- Sucha V., Kraus I., Gerthofferova H., Petes J., Serekova M; (1993) Smectite to illite conversion in bentonites and shales of the East Slovak Basin. *Clay Min.* 28, 243-253.
- Sultan N., (1997) Etude du comportement Thermo-HydroMécanique de l'argile de Boom, expérimentation et modélisation. PhD Thesis, École Nationale des Ponts et Chaussées, Paris, 310 p.
- Techer I., Lancelot J., Clauer N., Liotard, J.M., Advocat, T. (2001) Alteration of a basaltic glass in an argillaceous medium: The Salagou dike of the Lodeve Permian basin (France): Analogy with an underground nuclear waste repository. *Geochim.Cosmochim. Acta* 65, 1071-1086.
- Techer I., Rousset D., Clauer N., Lancelot J., Boisson J-Y. (2006) Chemical and isotopic characterization of water-rock interactions in shales induced by the intrusion of a basaltic dike: A natural analogue for radioactive waste disposal. *Applied Geochemistry* 21, 203-222.
- Trentesaux C. (1997) Modelling of thermo-hydro-mechanical behaviour of the Boom clay – 'Cactus test'. EUR 17558
- Van Geet, M., Bastiaens, W., Volckaert, G., Vallejan, B. and Gens, A. (2003) Reconnaissance Study of EDZ Around a Large Scale Shaft Sealing Demonstration Test (RESEAL). Proceedings of a European Commission CLUSTER Conference on Impact of the Excavation Disturbed or

Damaged Zone (EDZ) on the Performance of Radioactive Waste Geological Repositories, Luxembourg 3-5 November 2003, pp. 134-142

Van Geet M., De Craen M., Weetjens E. and Sillen X. (2006) Extent of oxidising conditions in the host formation. Experimental data and scoping calculations. External Report. SCK-CEN-ER-05. 21 pp. Mol, Belgium.

Velde B. and Vasseur G. (1992) Estimation of the diagenetic smectite to illite transformation in time-temperature space. *Am. Mineral.* 77, 967-976.

Vervoort A., Bastiaens W., Bernier F., Chanchole S., Coll C., Debecker B., De Greef V., Desrues J., Escoffier S., Gastaldo L., Govaerts A., Hamza R., Labiouse V., Li X.L., Malinsky L., Mathier J.-F., Ortiz L., Vanbrabant Y., Van Geet M., Verstraelen J., Viaggiani G., Wevers M. (2006) EC SELFRAC Project – FIKW-CT-2001-00182, Deliverable 2, Fractures and sealing/healing within the excavation disturbed zone in clays: Laboratory tests, EURIDICE

Volckaert G., Bernier F., Dardaine M. (1996) Demonstration of the in situ application of an industrial clay-based backfill material (Bacchus 2), Final report EUR 16860 EN/FR

Volckaert, G., Dereeper, B., Put, M., Ortiz, L., Gens, A., Vaunat, J., Villar, M.V., Martin, P.L., Imbert, C., Lassabatère, T., Mouche, E. and Cany, F., (2000) A large-scale in situ demonstration test for repository sealing in an argillaceous host rock. RESEAL project – Phase I. European Commission, Luxembourg, EUR 19612, 273pp

Wang L., De Cannière P., Jacques D., Moors H., Van Gompel M., Aertens M. (2004) Experimental and modelling studies of Boom Clay exposed to an alkaline perturbation. Final Report to NIRAS/ONDRAF, DS 2.13 (2002-2003). SCK•CEN report R-4019.

Wang L., Jacques D., De Cannière P. (2007) Effects of an alkaline plume on the Boom Clay as a potential host formation for geological disposal of radioactive waste. First full draft, Restricted Contract Report, SCK•CEN-ER-28, 182 pp., Mol, Belgium.

Weetjens E., Sillen X., SCK-CEN (2005): Thermal analysis of the supercontainer Concept, SCK-CEN report R-4277, December 2005

References for Opalinus Clay

Bock H. (2001): RA Experiment. Rock mechanics analysis and synthesis: Data report on rock mechanics. - Mont Terri Project, Technical Report TR 2000-02.

Carol I., Rizzi E., & William K. (2001): On the formulation of anisotropic elastic degradation. I. Theory based on a pseudo-logarithmic damage tensor rate. - *Int. J. Solids and Struct.* 38(4): 91-518.

Delacre et al. (2000)

Elie M. & Landais P. (2000): Facies and thermal reactivity of the organic matter from samples of Opalinus clay and Posidonia shale - Evaluation of paleotemperature by experimental maturation. Nagra Internal Report.

- Gens A. (2000): HE Experiment: Complementary rock laboratory tests. Laboratory Interim Report Phase 3. Mont Terri Technical Note TN 2000-47. Mont Terri Project, Saint Ursanne, Switzerland, 12p.
- Göbel I., Alheid H.J., Jockwer N., Mayor J.C., García-Siñeriz J.L., Alonso E., Weber H., Ploetze M., Klubertanz G., Rothpletz C.A., (2006): Heater Experiment: Rock and bentonite Thermo-Hydro-Mechanical (THM) processes in the near-field of a thermal source for development of deep underground high level radioactive waste repositories (HE), Final Report. Contract No: FIKW-CT-2001-00132. Euratom, Directorate-General for Research, 122p.
- Gaucher, E.C., Fernandez, A.M., & Waber, H.N. (2003): Annex 9: Rock and Mineral Characterization of the Opalinus Clay Formation. - Reports of the FOWG, Geology Series, No. 5, Bern.
- Zhang C.L., Rothfuchs T., Jockwer N., Wieczorek K., Dittrich J., Müller J., Hartwig L., Komischke M. (in prep.) Thermal Effects on the Opalinus Clay – A Joint Heating Experiment of ANDRA and GRS at the Mont Terri URL (HE-D Project) Final Report. Gesellschaft für Anlagen- und Reaktorsicherheit (GRS) mbH, Braunschweig, Germany.
- Martin, D. and Lanyon, G. (2004): EDZ in Clay Shale: Mont Terri. Technical Report TR 2001-01. Mont Terri Project, Saint Ursanne, Switzerland.
- Mazurek M. (2002): Geochemische Effekte des vom radioaktiven Abfall ausgehenden Wärmepulses auf den Opalinuston. Nagra Internal Report.
- Nagra (2002a): Project Opalinus Clay: Safety Report. Nagra Technischer Bericht NTB 02-05, 360p.
- Nagra (2002b): Calculations of the Temperature Evolution of a Repository for Spent Fuel, vitrified high-Level Waste and Intermediate Level Waste in Opalinus Clay. Nagra Technischer Bericht NTB 01-04, 28p.

References for the Callovo-Oxfordian Clay

- Andra (2005) Dossier 2005 - Référentiel de connaissance et modèle d'inventaire des colis de déchets à haute activité et à vie longue. Rapport Andra n° C.RP.AHVL.04.0006.
- Antea (1999) Site Est. Comportement thermohydromécanique différé des argilites de l'Oxfordien inférieur. Rapport Andra n° D.RP.0ANT.99.07
- Antea (2001) Lot 3. Forages d'investigation géologique complémentaire. Rapport de synthèse. Rapport Andra n° B.RP.0ANT.01.022
- Armand G. (2006) Expérimentation REP - Analyse des mesures 1 an après le fonçage du puits d'accès – document Andra – D RP ADPE 06 0308A
- Bauer C. (1997) Propriétés thermo-mécaniques des argilites silto-carbonatées de l'Est. Rapport Andra n° B.RP.0G3S.97.001.A
- Bauer C. (2005) La charge thermique d'un stockage - Site de Meuse / Haute-Marne. Rapport Andra n° C.NT.ASIT.03.118.

- Bond K.A., Heath T.G. & Tweed C.J. (1997) A referenced thermodynamic database for chemical equilibrium studies. *Nirex report NSS/R379*
- Cathelineau M. *et al.* (1999) Interactions fluides / argiles en conditions de stockage profond des déchets nucléaires. *Acte des journées scientifiques Andra*. Nancy, 7 au 9 décembre 1999
- Chancholle S. (2004) Etude expérimentale du comportement différé des argilites de l'Est à l'aide des essais sur échantillons de longue durée. Rapport Andra n° D.RP.0G3S.2004.01.A
- Chivot J. (2004) Thermodynamique des produits de corrosion: fonctions thermodynamiques, diagrammes de solubilité, diagrammes Eh - pH des systèmes Fe-H₂O, Fe-CO₂, Fe-S-H₂O, Cr-H₂O, Ni-H₂O en fonction de la température. *Andra (Ed.)*, Châtenay-Malabry, 141 p
- Coelho D. (2005) La thermo-convection dans la couche du Callovo-Oxfordien et les formations géologiques encaissantes sous l'effet de la charge thermique d'un stockage - Site de Meuse / Haute-Marne. Rapport Andra n° C.NT.ASTR.03.105.
- Filippi M. (2006), « Modélisation thermique directe de l'expérimentation TER et première étude de sensibilité », Rapport Andra D RP 21 CEA 06 001.
- François O. (1998) Propriétés thermiques et thermomécaniques des argilites silto-carbonatées de l'Est. Rapport Andra n° D.RP.AGEM.98.081
- Gasc-Barbier M. (2002) Etude des mécanismes de déformation de roches argileuses profondes : apport de la microstructure et des analyses pétrophysiques. Thèse de l'Université de Paris VI
- Gasc M., Malinsky L. (2002) Elaboration d'un ou de plusieurs modèles de comportement différé des argilites de l'Est. Rapport Andra n° D.RP.0G3S.02.04.B
- Gast R.G. (1969) Standard free energies of exchange for alkali metal cations on Wyoming bentonite. *Oil Sci. soc. Amer. Proc.*, Vol. 33, p. 37-41
- Gaucher E. & Blanc P. (2004) Influence de la température sur les modélisations de la chimie des eaux du Callovo-Oxfordien. Note technique du BRGM : EPI/EG/824
- GdR Forpro (2002) Etude en laboratoire des propriétés physiques des échantillons du forage EST 205 du site de la Meuse. Rapport final des actions 2000.III-2002-I
- Homand F. (1998) Mesures thermiques sur le site Est. Rapport Andra n° B.RP.0ENG.98.009
- Hummel W., Berner U., Curti E., Pearson F.J. & Thoenen T. (2002) Nagra /PSI chemical thermodynamic database 01/01. *Universal Publishers (Ed.)*, 600 p
- Laudelout H., Van Bladel R., Bolt G.H. & Page A.L. (1968) Thermodynamic of heterovalent cation exchange reactions in a montmorillonite clay. *JCS Trans. Faraday Society*, 64, p.1477-1488
- Martin H. & Laudelout H. (1963) Thermodynamique de l'échange des cations alcalins dans les argiles. *J. Chim. Phys.*, 60, p. 1086-1097
- Michau N. (2005) L'évolution chimique des ouvrages d'un stockage à base d'argile gonflante : alvéoles de stockage de déchets C et combustibles usés et scellements de galeries et de puits. Site de Meuse / Haute-Marne. Rapport Andra n° C.NT.ASCM.03.043.

- Michel P. (2006) Etude expérimentale des interactions organo-minérales de roches argilo-carbonatées : application au Callovo-Oxfordien de la Meuse. Thèse de l'Université Louis Pasteur de Strasbourg.
- Mosser-Ruck R. *et al.* (1999) Hydrothermal reactivity of K-smectite at 300°C and 100 bars: dissolution – crystallization process and non-expandable dehydrated smectite formation. *Clay Minerals* (1999) 34, p. 275-290
- Mosser-Ruck R. *et al.* (2001) Experimental illitisation of smectite in a K-rich solution – *Eur. J. Mineral.* 2001, 13, p. 829-840.
- Olivella, S., A. Gens, J. Carrera, E. E. Alonso, (1996) “Numerical Formulation for a Simulator (CODE_BRIGHT) for the Coupled Analysis of Saline Media”, *Engineering Computations*, Vol. 13, No. 7, p. 87-112.
- Ruck R. (1996 a) Etude de la stabilité thermique des argiles. Synthèse des données acquises depuis 1989. Rapport final. Rapport Andra n° B.RP.0CRE.96-004/A.
- Ruck R. (1996 b) Etude expérimentale des propriétés d'échange des smectites et des interactions entre fluides et sédiments naturels. Rapport Andra n° B.RP.0CRE.96.001.A
- Su K. & Bounenni A. (1998) Couplage entre la perméabilité et l'endommagement dans les matériaux des sites du Gard, de l'Est et de la Vienne. Rapport Andra n° B.RP.0G3S.98.021.A
- Su K. (2001) Modélisations thermohydromécaniques de l'expérimentation TER pour élaboration du cahier des charges de l'expérimentation. Rapport Andra n° D.NT.AGEM 01.021
- Su. K. (2002a) Propriétés thermiques des éléments de stockage. Rapport Andra n° C.RP.ASMG.02.079
- Su K. (2002b) Effet des perturbations mécaniques et hydriques sur la conductivité thermique des argilites. Bilan des études et travaux de l'Andra 2001, p. 137-142
- Su K. & Yven B. (2003) Modèle conceptuel de distribution des propriétés thermiques dans les formations géologiques du site de Meuse/Haute Marne. Rapport Andra n° C.RP.ASMG.03.014
- Su K. & Barnichon J.D. (2005) Le comportement mécanique d'alvéoles de stockage de déchets C et de combustibles usés dans le temps - Site de Meuse / Haute-Marne. Rapport Andra n° C.RP.ASMG.03.0109.
- Talibudeen O. & Goulding K.W.T. (1983) Charge heterogeneity in smectites. *Clays and clay minerals*, 31, p. 37-42